Politecnico di Bari

LIBERATORIA PER L'ARCHIVIAZIONE DELLA TESI DI DOTTORATO

Al Magnifico Rettore
del Politecnico di Bari

Il sottoscritto CALO' GIUSEPPE nato a WIESBADEN (GERMANIA) il 28/12/1985

residente a ORIA in via VICO GUALBERTO DE MARZO, 2, e-mail gpp.calo@pec.it

iscritto al 3° anno di Corso di Dottorato di Ricerca in INGEGNERIA MECCANICA E GESTIONALE ciclo XXXV

ed essendo stato ammesso a sostenere l'esame finale con la prevista discussione della tesi dal titolo:

"Lubricant Oil influence on the Combustion Process of Conventional and Innovative Internal Combustion Engines"

DICHIARA

1) di essere consapevole che, ai sensi del D.P.R. n. 445 del 28.12.2000, le dichiarazioni mendaci, la falsità negli atti e l'uso di atti falsi sono puniti ai sensi del codice penale e delle Leggi speciali in materia, e che nel caso ricorressero dette ipotesi, decade fin dall'inizio e senza necessità di nessuna formalità dai benefici conseguenti al provvedimento emanato sulla base di tali dichiarazioni;
2) di essere iscritto al Corso di Dottorato di ricerca in INGEGNERIA MECCANICA E GESTIONALE (DRIMEG) ciclo XXXV, corso attivato ai sensi del "*Regolamento dei Corsi di Dottorato di ricerca del Politecnico di Bari*", emanato con D.R. n.286 del 01.07.2013;
3) di essere pienamente a conoscenza delle disposizioni contenute nel predetto Regolamento in merito alla procedura di deposito, pubblicazione e auto archiviazione della tesi di dottorato nell'Archivio Istituzionale ad accesso aperto alla letteratura scientifica;
4) di essere consapevole che attraverso l'auto archiviazione delle tesi nell'Archivio Istituzionale ad accesso aperto alla letteratura scientifica del Politecnico di Bari (IRIS-POLIBA), l'Ateneo archivierà e renderà consultabile in rete (nel rispetto della Policy di Ateneo di cui al D.R. 642 del 13.11.2015) il testo completo della tesi di dottorato, fatta salva la possibilità di sottoscrizione di apposite licenze per le relative condizioni di utilizzo (di cui al sito http://www.creativecommons.it/Licenze), e fatte salve, altresì, le eventuali esigenze di "embargo", legate a strette considerazioni sulla tutelabilità e sfruttamento industriale/commerciale dei contenuti della tesi, da rappresentarsi mediante compilazione e sottoscrizione del modulo in calce (Richiesta di embargo);
5) che la tesi da depositare in IRIS-POLIBA, in formato digitale (PDF/A) sarà del tutto identica a quelle **consegnate**/inviate/da inviarsi ai componenti della commissione per l'esame finale e a qualsiasi altra copia depositata presso gli Uffici del Politecnico di Bari in forma cartacea o digitale, ovvero a quella da discutere in sede di esame finale, a quella da depositare, a cura dell'Ateneo, presso le Biblioteche Nazionali Centrali di Roma e Firenze e presso tutti gli Uffici competenti per legge al momento del deposito stesso, e che di conseguenza va esclusa qualsiasi responsabilità del Politecnico di Bari per quanto riguarda eventuali errori, imprecisioni o omissioni nei contenuti della tesi;
6) che il contenuto e l'organizzazione della tesi è opera originale realizzata dal sottoscritto e non compromette in alcun modo i diritti di terzi, ivi compresi quelli relativi alla sicurezza dei dati personali; che pertanto il Politecnico di Bari ed i suoi funzionari sono in ogni caso esenti da responsabilità di qualsivoglia natura: civile, amministrativa e penale e saranno dal sottoscritto tenuti indenni da qualsiasi richiesta o rivendicazione da parte di terzi;
7) che il contenuto della tesi non infrange in alcun modo il diritto d'Autore né gli obblighi connessi alla salvaguardia di diritti morali od economici di altri autori o di altri aventi diritto, sia per testi, immagini, foto, tabelle, o altre parti di cui la tesi è composta.

Luogo e data BARI, 30/05/2023 Firma Giuseppe Calò

Il/La sottoscritto, con l'auto archiviazione della propria tesi di dottorato nell'Archivio Istituzionale ad accesso aperto del Politecnico di Bari (POLIBA-IRIS), pur mantenendo su di essa tutti i diritti d'autore, morali ed economici, ai sensi della normativa vigente (Legge 633/1941 e ss.mm.ii.),

CONCEDE

- al Politecnico di Bari il permesso di trasferire l'opera su qualsiasi supporto e di convertirla in qualsiasi formato al fine di una corretta conservazione nel tempo. Il Politecnico di Bari garantisce che non verrà effettuata alcuna modifica al contenuto e alla struttura dell'opera.
- al Politecnico di Bari la possibilità di riprodurre l'opera in più di una copia per fini di sicurezza, back-up e conservazione.

Luogo e data BARI, 30/05/2023 Firma Giuseppe Calò

Politecnico di Bari

Department of Mechanics, Mathematics and Management

MECHANICAL AND MANAGEMENT ENGINEERING Ph.D. PROGRAM

SSD: ING-IND/08 – FLUID MACHINERY

Final Dissertation

Lubricant Oil influence on the Combustion Process of Conventional and Innovative Internal Combustion Engines

by

CALO' GIUSEPPE

Referees:

Prof. Ing. A. P. Carlucci

Prof. Ing. E. Mancaruso

Supervisors:

Prof. Ing. R. Amirante

Prof. Ing. E. Distaso

Coordinator of Ph.D. Program:

Prof. Ing. G. P. Demelio

Course n° 35, 21/11/2019 – 20/02/2023

Abstract

The negative impacts of climate change are mounting very fast and bold actions are required, so that significant efforts are needed to improve the current technologies for mobility because of the competitive marketplace as well as of the ever-tightening regulations concerning emissions and fuel economy. In this scenario, internal combustion engines (ICEs) need radical modifications to be still considered a sustainable option for the future.

The motivation for the proposed research stems from evidence reported in the literature, which suggests that lubricant oil droplets are the primary inducer of abnormal combustion modes. Additionally, lubricant oil can represent a major source of very fine soot particles emitted from engines. These adverse effects severely hinder the further development of efficient and cleaner internal combustion engines.

However, the influence of lubricant oil on the combustion process is not yet fully understood as it is often neglected in numerical simulations, due to the assumption that the amount of lubricant oil reaching the combustion chamber is negligible. Thus, there is a need to fill the knowledge lack of lubricant-oil-related auto-ignition processes in engines. In this scenario, the accurate chemical modelling of the fuel-lubricant interaction represents an essential aspect for enabling the further development of the internal combustion engine for providing information difficult or impossible to obtain solely through experiments.

The present work tries to shed light on the criticalities arising from the interaction between fuel and lubricant oil in modern internal combustion engines, through rigorous numerical investigations. A variety of fuels, including traditional fossil fuels (gasoline) as well as carbon-free alternatives (hydrogen), were considered. As a first step a way for considering the presence of trace amounts of lubricant in the combustion chamber was defined, by selecting proper lubricant oil surrogate species. Consequently, several detailed chemical models were developed and validated to isolate the lubricant oil's contribution to abnormal combustion events. However, it is well known that CFD numerical simulations employing detailed chemical models are computationally expensive. In light of this, the detailed chemical models were reduced for the purpose of conducting Three-Dimensional (3D) CFD numerical simulations, in order to reproduce experimental data involving lubricant oil combustion. With the aim to further reduced computational costs, a practical and simple analytical correlation able to predict variations of gasoline ignition delay induced by the presence of lubricant oil, at different temperatures, is presented. Such a correlation was developed by considering both experimental data available in the literature and numerical simulations.

The urgent need to reduce both the environmental impact of mobility and the dependence on fossil fuels has re-ignited the interest toward Hydrogen Internal Combustion Engines (HICEs). However, there are still criticalities that need to be assessed for accelerating the development of this technology. The undesired but unavoidable participation of lubricant oil to the combustion process is considered at the basis of the criticalities that affect the development of a reliable and efficient HICEs. In order to investigate and highlight the role of lubricant oil in the development of HICEs a specific reduced chemical model was developed and validated. The newly developed chemical model was employed in Zero-Dimensional (0D) simulations with the aim to quantify the effects that lubricant oil can have on hydrogen ignition delay time (IDT) in engine-like conditions.

Contents

List of Figures

List of Tables

List of Abbreviations

AMR	Adaptive Mesh Resolution
CID	Chemical Ignition Delay
CI	Compression Ignition
CFD	Computational Fluid Dynamic
DRGEP	Directed Relation Graph method with Error Propagation
DRG	Directed Relation Graph
DISI	Direct Injection Spark Ignition
FSSA	Full Species Sensitivity Analysis
GCI	Gasoline Compression Ignition
HTHR	High Temperature Heat Release
HCCI	Homogeneous Charge Compression Ignition
HRR	Heat Release Rate
ICEs	Internal Combustion Engines
IQT	Ignition Quality Tester
ITHR	Intermediate Temperature Heat Release
KH-RT	Kelvin-Helmholtz and Rayleigh-Taylor
LTC	Low Temperature Combustion
LSPI	Low Speed Pre-Ignition
LTHR	Low Temperature Heat Release
NTC	Negative Temperature Coefficient
PRF	Primary Reference Fuel
HICEs	Hydrogen Internal Combustion Engines
SACI	Spark Assisted Compression Ignition
SMD	Sauter Mean Diameter
TID	Total Ignition Delay
0D	Zero-Dimensional
3D	Three-Dimensional
HCS	Half Compressione Stroke
BDC	Bottom Dead Center
TDC	Top Dead Center
CAD	Crank Angle Degree
BEVs	Battery Electric Vehicles
FEVs	Fuel Cell Vehicles
GHG	Greenhouse Gas
HTP	Human Toxicity Potential
GCI	Gasoline Compression Ignition
RCCI	Reactivity Controlled Compression Ignition
GDI	Gasoline Direct Injection
PAH	Polycyclic aromatic hydrocarbon
CCD	Combustion Chamber Deposit
VI	Viscosity Index
API	American Petroleum Institute
PRP	Pressure Recovery Point
PoI	Point of Inflection
PID	Physical Ignition Delay
RANS	Reynolds-Averaged Navier-Stokes
TRF	Toluene Reference Fuel
PRF	Primary Reference Fuel
$\Delta\tau_R$	Relative change of Chemical Ignition Delay
SI	Spark-Ignition
SOInj	Start of Injection
SOIgn	Start of Ignition
PISO	Pressure-Implicit with Splitting of Operators
DCN	Derivative Cetane Number

Lubricant Oil influence on the Combustion Process of Conventional and Innovative Internal Combustion Engines

Introduction and Motivations

Automotive is an essential component that allows people not only to connect with each other, but also to progress. The advent of the Internal Combustion Engine (ICE) in the late 19th century revolutionized the world, providing unprecedented levels of freedom and access. The ICE succeeded for many of the same reasons it remains popular now: its high-power density, long range, low cost, and convenience.

However, the growing demand for more efficient and cleaner transport systems must necessarily intersect with respect for the environment, requiring the constant development of new technologies [1,2]. Greenhouse Gas (GHG) emissions from transport are major contributors to both climate change and air pollution, so that significant efforts are needed to improve the current technologies for mobility. Carbon dioxide (CO_2) emissions are the primary driver of global climate change. It is widely recognized that to avoid the worst impacts of climate change, the world needs to urgently reduce emissions [3]. But how this responsibility is shared between regions, countries, and individuals has been an endless point of contention in international discussions.

The globally hoped transition from fossil fuel-powered to fully electric mobility requires massive investments in infrastructure and technology, without any certainty regarding timing and methods. Achieving a successful transition to electric mobility requires a shared global vision to ensure sustainability from environmental, social, and economic perspectives. Such change is unlikely to happen in the near future, especially considering that the economic growth of the poorest countries is based on the use of fossil fuels. These emerging economies, unable to handle immediate and massive investments, would see their chances of rapid development reduced, with negative social and economic consequences.

Nowadays, the electrification of the mobility is presented as the only obvious remedy to counteract the environmental impact caused by the emissions from internal combustion engines (ICEs). Battery electric vehicles (BEVs) and hydrogen fuel cell vehicles (FCVs) have attracted significant attention as they do not generate harmful emissions during the operational phase [4].

In fact, not being equipped with a tailpipe, there are no exhaust emissions nor GHGs coming from the vehicle. However, the operational phase is only part of the life cycle, therefore the source used to produce the energy needed to build all the components the environmental impact of vehicle disposal processes should be evaluated. Analyzing the entire life cycle, namely "from the cradle to the grave", although they do not directly emit CO_2 during operation, the processes of production and disposal/recycling of the batteries have consequences harmful consequence on the environment in terms of acidification and human toxicity [5–7]. However, the energy source that drives the BEVs must be produced and supplied. Today, in much of the world, about 67% of electricity is generated by fossil fuels [8]. In addition, a significant source of GHG emission in BEVs derives from battery production. It was highlighted that GHG emission are about 50% higher for a BEV compared to an ICEV [9–11]. Regarding human toxicity potential (HTP), it was shown that BEVs could have a significantly greater impact on human toxicity, eutrophication, and metal depletion impacts than ICEVs [12–15]. Add to this range anxiety, charge time, infrastructure, battery decommissioning, and the need to mine rare materials, and it becomes apparent that BEVs are far from the single solution to our transportation problem.

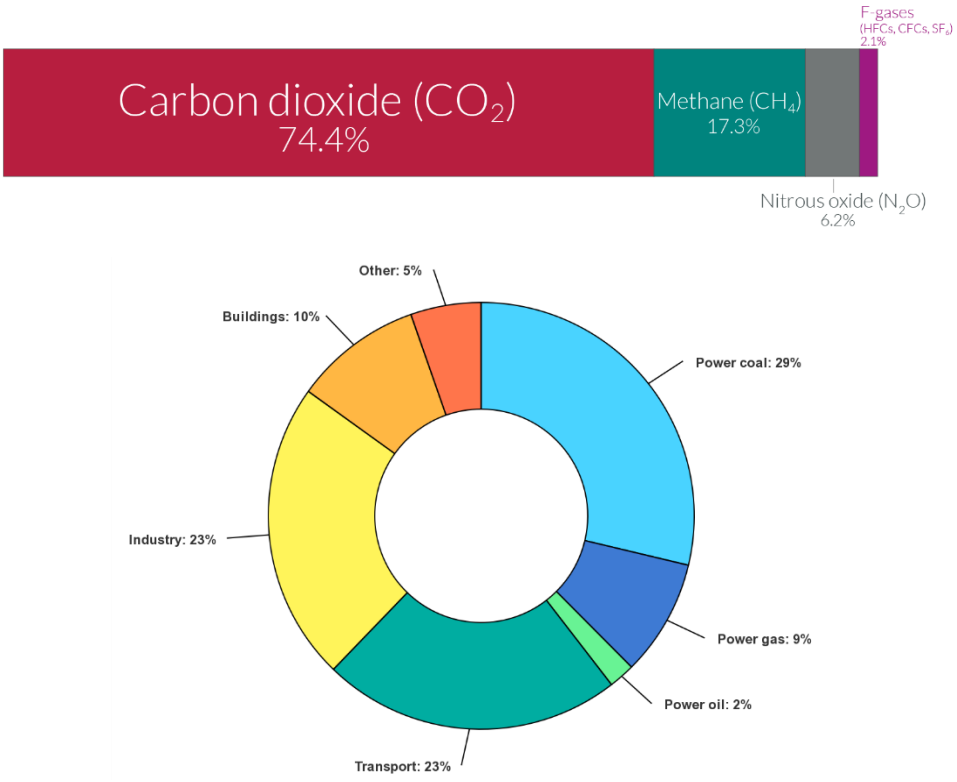

Figure 0.1. Greenhouse Gas composition and Global energy-related CO2 emissions by sector (International Energy Agency IEA – iea.org – 2022)

While this change occurs, all currently available technologies must be employed, and it would be extremely short-sighted to discourage further development of ICEs. Banning the sale of new ICEs, as some countries propose to do, will stop needed research and development well before the deadline for such a ban and this could limit available options. Thus, research and development in ICEs should

continue because there is still scope for significant improvements in reducing fuel consumption and emissions.

Significant progress has been made in the development of cleaner and more efficient engines over the past 50 years [16–18]. This was due to the combination of government regulations and technology innovation. However, world governments are ready to enact even stricter regulations [19–21]. Therefore there is a need to continue with the efforts in the research and development of ICEVs in order to meet future regulations, by employing emerging strategies [22–26], implementing more accurate and cost-effective sensors [27–29] and using low-carbon fuels [30–32].

Technology development trends in ICEs have exploited high boosting, downsizing and direct injection strategies as common practice to enhance power density and reduce fuel consumption [33–35]. However, there are significant untapped potential in advanced ICE concepts. For example, Gasoline Compression Ignition (GCI) engines [36–38], Spark-Assisted Compression Ignition (SACI) [39–41], Reactivity Controlled Compression Ignition (RCCI) [42–44], Homogeneous Charge Compression Ignition (HCCI) [45–48], have gained increasing attention over the last decades, due to the potential of achieving diesel-like thermal efficiencies with significantly reduced NO_x and soot emissions [49–51]. The classical dichotomy between SI and CI might be soon blurred as Low Temperature Combustion (LTC) technologies are developed, and engines with the ability to seamlessly transition between different operating modes become feasible [52–54], and this could lead these new engine concepts to effective global market penetration.

Although the majority of today's engines are fueled from fossil-derived sources, there is the alternative represented by fuels that are carbon free or with lower carbon than fossil-derived fuels. In addition to being characterized by a low or zero carbon fraction, these fuels have the advantage of being able to be used in existing fleets, replacing fossil-derived fuels. These new concepts of fuels hold great potential for decarbonizing future mobility, with the potential to reduce CO_2 emissions. Among these alternative fuels, there are biofuels, natural gas, hydrogen, synthetic fuels, electro-fuels, liquid petroleum gas (LPG) and methanol [55–58]. In addition, there are synergistic benefits to the use of oxygenate components in gasoline, notwithstanding the potential renewable nature of these components [59–61].

In this scenario of global transition, the hybridization of mobility, characterized by a combination of different propulsion technologies, could provide a promising solution for reducing the environmental impact, avoiding the need for massive technological and infrastructural investments. Moreover, this would allow an ever-increasing quantity of liquids from renewable sources to be added to the fuel, further reducing the environmental impact and dependence on petroleum fuels. This would involve the abatement of particulate and CO_2 emissions [62]. In confirmation of this, in a recent analysis three scenarios to meet an EU target of 85% CO_2 reduction by 2050 were explored. In conclusion, it was stated that in order to reach the set targets faster, the use of different propulsion technologies and

low-carbon fuels were essential [63]. And this was also the message of the analysis conducted by Senecal et al. [64], Lešnik et al. [65] and Leach et al. [66], all of whom argued that a mix of propulsion technologies is the way forward for the future fleet.

Thus, research in the field of internal combustion engines cannot be hindered by the rush and anxiety to reduce the environmental impact of transport. If the goal is to achieve a hybridization of mobility, the combustion engine will need to evolve to further improve their efficiency and meet upcoming stringent emissions regulations, playing an important role for future mobility, especially in the perspective to mixing new propulsion technologies. Indeed, it is still possible to push further the limits of modern internal combustion.

Automotive research is currently facing an obstacle that limits the further development of modern Internal Combustion engines. This is represented by abnormal combustion induced by trace amounts of lubricant oil within the engine combustion chamber, preventing these engines from achieving optimized combustion phasing and higher boost pressures and compression ratios [67–69]. Several studies have been conducted to investigate abnormal combustion, and it is generally accepted that this phenomenon is triggered by local pre-ignition events most likely related to lubricant-fuel interactions within the combustion chamber [70–74]. The auto-ignition tendency of engine lubricant oil received little attention in the past, because it was commonly assumed that engine lubricant effects on knock could be considered negligible due to the low amounts of lubricant oil that reach the combustion chamber. However, with modern DISI engines being developed to operate at higher loads and closer to knock limits, the reactivity of engine lubricants can significantly impact the knock behavior. However, there is still a lack of experimental data concerning fundamental characteristics of lubricant oil auto-ignition. Usually pre-ignition may be triggered by several inducements, namely hot surface [75–78], carbon deposits that fluctuate inside the cylinder [79–83], lubricant oil droplets or oil-fuel droplets [84–88], fuel properties and fuel decomposition by boiling behavior of individual components [89–93]. In Highly boosted Direct Injection Spark-Ignition (DISI) engines fueled with gasoline, lubricant oil contamination could induced the onset of a particularly violent detonation phenomenon, known as super-knock or Low-Speed Pre-Ignition (LSPI) [94–96]. Also engines fueled with hydrogen are not exempted from abnormal combustion, such as back-fire, premature auto-ignition of the charge and engine knock [97–101], preventing these engines from penetrate the marketplace [102,103]. These undesired events were initially ascribed to the presence of richer regions in the chamber. This might be the case for the Direct Injection (DI) mode, for which the achievement of a proper mixing is a really challenging tasks, but it appears unlikely for port fuel injection mode, for which a much better mixing is expected. Presumably, the explanation for the occurrence of premature autoignitions should be sought elsewhere. Hydrogen has a higher auto-ignition temperature compared to petroleum fuels [104], thus its resistance to knocking is expectedly higher. However, its lower ignition energy (one tenth that of gasoline) makes hydrogen easily

ignitable by hot spots or residues in combustion chamber. Many recent works have linked the onset of abnormal combustions in HICEs to the presence of "sensitive spots" and lubricant oil, with an extremely low auto-ignition resistance can play a primary role in their generation [97,105,106].

It must be also considered that oil contamination within the combustion chamber can represent a non-negligible source for soot particle generation, as highlighted by recent literature findings [107–112]. The presence of hydrocarbons with longer chains during the combustion event can enhance soot precursor formation in the reaction zone [113,114], including C_2 species, such as the ethyl radical (C_2H_5) and acetylene (C_2H_2), which are the most abundant gaseous hydrocarbon species in regions where soot is formed [59,115]. These findings are of significant relevance, because even in the case of using fuels with zero or low carbon content, the contribution of the lubricant oil becomes predominant in the emissions of very fine soot [111,116–120]. Indeed, the presence of engine oil in the combustion chamber can lead to production of sub-micrometer exhaust particles (lower than 30 nm) [121–125], affecting air quality and human exposure to particulate pollution, especially in urban environments [126–129]. Due to their small size, reaching only a few nanometers, these particles penetrate deep into the alveolar region and induce health effects through interactions at the cellular or subcellular level [129–132]. The inhalation of ultrafine particles of mixed heavy metal elements has adverse human health effects [133–138]. In addition, a strict correlation between soot levels and the occurrence frequency of super-knock has been observed [81,83,94,139–143]. Carbonaceous deposits and floating soot particles within the combustion chamber can serve as high temperature spots able to prematurely ignite the mixture. This points out a possible secondary way by which lubricant oil can promote pre-ignition phenomena.

Therefore, to push further the development of modern Internal Combustion Engines it is essential to shed light on the role played by lubricant oil in affecting the combustion process, both through experimental campaigns and numerical investigations. Unfortunately, in the literature, there is an evident lack of dedicated research on autoignition delay times of lubricant oils. To meet this aim, it is necessary to investigate the reaction paths of the lubricant oil, and this to provide innovative tools, useful for improving the control of combustion process and for a better understanding of the mechanisms involved in the abnormal combustion. In this scenario, the accurate chemical modelling of the fuel-lubricant interaction can represent an essential aspect for providing information difficult or impossible to obtain solely through experiments.

Aim and Outlook

The aim of this work it to provide evidence and guidance in understanding the mechanism involved in abnormal combustion induced by lubricant oil, by means of the development of several reaction mechanisms employed in rigorous numerical investigations, to isolate the contribute of lubricant oil in promoting such undesired event. Following the experimental evidence available in the literature, numerical simulations were performed as useful additional tool to unravel and highlight the role played by trace amount of lubricant oil in affecting the fuel reactivity and, thus, in promoting the premature auto-ignition of the charge.

In the first three Chapter a brief overview on lubricant oil induced abnormal combustion is presented, in order to provide to the reader an essential background on the topic of this work. Thus, the reader can be introduced into the main discussion concerning the results obtained and presented in the following chapter.

Chapter 1 provides a brief overview of the possible routes followed by lubricant oil to contaminate the combustion chamber. Evidence about the release mechanism of oil droplets and their influence on undesired pre-ignition is reported. However, oil droplets are not the only inducement of pre-ignition. Floating solid particles in the combustion chamber also have a close connection with pre-ignition. Thus, the formation of solid deposits due to the lubricant oil and the role played in terms of pre-ignition are provided. Finally, evidence on the influence of lubricant oil degradation on premature auto-ignition of the charge is provided.

Chapter 2 reports a brief description of the components that compose the lubricant oil, i.e. base oil and additive package. Firstly, an analysis focusing on the influence of base oils on pre-ignition is provided. However, the base oil is not the only inducement of undesired abnormal combustion, but also the additives could play an important role. Thus, after a brief description of the functionality of the additives on the lubrication performance, evidence on the influence on pre-ignition of these important elements are provided. However, due to the current poor knowledge there is no consensus on some additives and their influence on abnormal combustion events. The last part of the chapter focuses on providing an overview about these additives and the ambiguity of their influence.

Chapter 3 contains a brief overview on research experimental directions and efforts in formulating innovative lubricant oil with the aim to reduce the frequency of abnormal combustion. The second part of the chapter reports an overview on numerical efforts for enclosing lubricant oil combustion in numerical simulation.

Chapter 4 shows a way for taking into account lubricant oil presence within an engine's combustion chamber was defined. Based on experimental data, hydrocarbons species suitable for reproducing oil's chemical reactivity were first identified. Then, a detailed reaction mechanism, suitable for simulating the lubricant oil influence on the combustion process of gasoline-like fuels, was developed and validated. Zero-Dimensional numerical simulations were conducted to reproduce experimental measurements available in the literature, aimed at quantifying the effect of lubricant oils on the ignition delay of iso-octane (selected as surrogate for commercial gasoline). Furthermore, by means of the numerical analysis, it was possible to determine a surrogate hydrocarbon mixture that could averagely reproduce the reactivity of both base oils and a fully formulated lubricant oil.

Chapter 5 reports the development and validation of a reduced chemical model, including essential lubricant oil pathways. This step was necessary to conduct practical 3D CFD motor simulations at low computational cost. Experimental studies were reproduced in which iso-Octane (i-C_8H_{18}) was blended with different percentages of either fully formulated lubricant oil (SAE 20W50) or base oils or n-Hexadecane (n-$C_{16}H_{34}$) and injected in an Ignition Quality Tester (IQT). Finally, a thorough analysis of the 3D numerical results, with a particular focus on the study of the pressure traces and of the Heat Release Rate (HRR), is used to explain the role of lubricant oil on the reduction of the TID time of the mixture.

Chapter 6 provides a simple analytical correlation is presented and proposed to predict variations of gasoline ignition delay induced by the presence of lubricant oil, at different temperatures. Such a correlation was developed by taking into account both experimental data available in the literature and numerical simulations employing the "GasLube" reaction mechanism. The proposed correlation makes possible to accurately derive the ignition delay of gasoline/lubricant oil mixtures directly from the values related to pure iso-Octane (gasoline surrogate), avoiding the use of dedicated reaction mechanisms, and thus saving computational time.

Chapter 7 presents a characterization of the effects caused by the interaction of hydrogen with lubricant oil in the combustion chamber of Hydrogen Internal Combustion Engines. The analysis aims at ascertaining whether lubricant oil can vary the charge reactivity in a significant way so that it can promote its premature ignition. To unravel the role of lubricant oil in altering hydrogen auto-ignition tendency a reduced reaction mechanism was developed. By employing the reduced kinetic model, Zero-Dimensional numerical simulations were performed to quantify the variation of hydrogen ignition delay time induced by different amounts of lubricant oil.

A summary of the work and some recommendations for future research are given in *Summary and Outlook.*

Chapter 1

In this opening Chapter a brief overview on lubricant oil induced pre-ignition in modern engines is provided. The aim is to highlight the possible routes of lubricant oil entrainment within the combustion chamber and how this contamination could promote abnormal combustion.

1.1. Lubricant Oil Routes

Lubricant oil can enter the combustion chamber as liquid, gas, or as a mist, namely in the form of an aerosol formed by small oil droplets suspended in and transported by a gas flow, which can be air or a fresh or burned air-fuel mixture or a combination of these components. Depending on the physical state, the relative amounts, the in-cylinder conditions and the available time, lubricant oil can produce very different effects on the combustion process [107,144]. Figure 1 schematically summarizes all the possible routes of lubricant oil entrainment identifiable in a modern internal combustion engine. The most direct link between the crankcase and the combustion chamber is represented by the piston ring pack. A sufficient lubrication needs to be provided to the piston rings sliding along the cylinder liner in order to minimize friction and wear, as well as for thermal reasons. Therefore, some oil is unescapably transported and released into the combustion chamber. In addition, the unavoidable clearances existing between the moving parts of the piston-rings-liner system represent direct ways for flow exchanges between the crankcase and combustion chamber of an engine. Perhaps the dominating contributions to lubricant oil transport come from the piston-rings-liner system [145], but it does not represent the solely route for oil entertainment. Another contribution can come from the blow-by gas flow recirculation. Namely, by means of the crankcase ventilation system a multiphase flow, composed of polydisperse oil droplets suspended in a gaseous mixture of oil vapors and exhaust gases (usually referred as "oil mist"), are recirculated to the intake manifold. Oil droplets can be released from the valve stem seals directly into the combustion chamber or drugged in by the entering flows. Oil leakages from the turbocharger seals can reach the combustion chamber through both the intake and the exhaust port (internal gas recirculation). Moreover, in DI engines, the high-pressure jet will inevitably impact the cylinder walls [146], entraining oil droplets, and this might be the case not only of liquid fuels but also of gaseous fuel, such as in the case of HICEs [103]. In HICEs, oil contaminations can also originate from the injector lubrication system. In addition, lubricant-based low-ignition delay components being carried into the combustion chamber could survive to become a pre-ignition origin in a subsequent cycle [147,148].

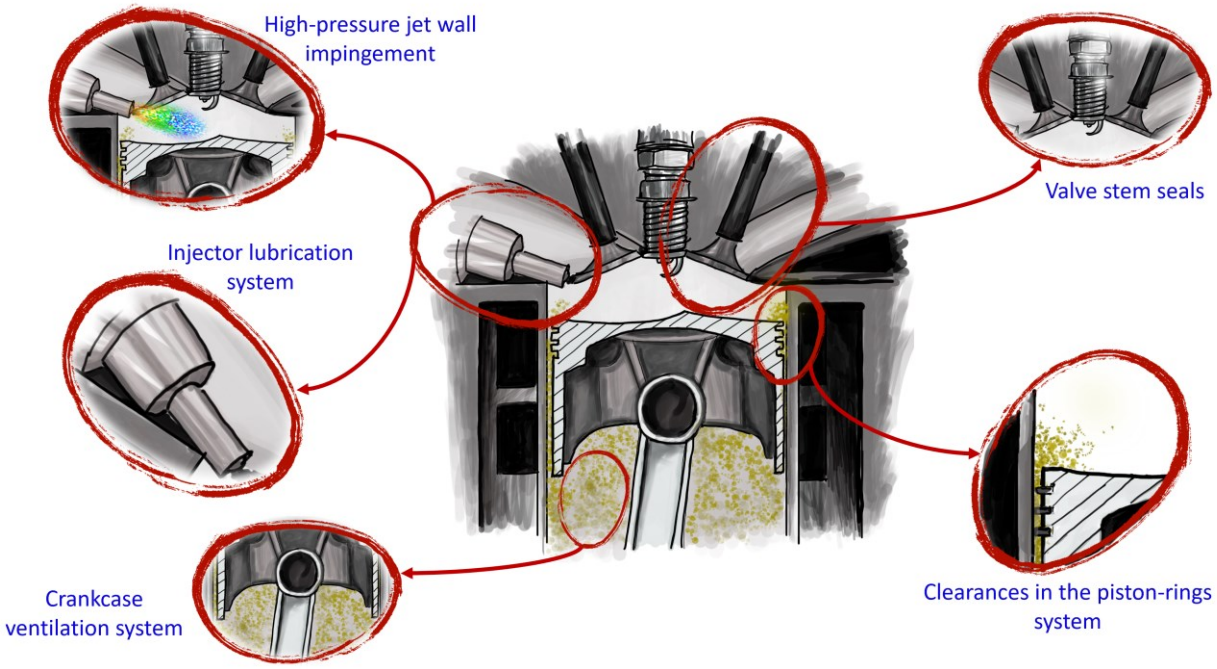

Figure 1.1. Possible routes of lubricant oil entrainment identifiable in a modern internal combustion engine.

1.2. Lubricant Oil Droplets

Dahnz et al. [145] first proposed the mechanism of lubricant oil droplet release from the cylinder liner, which was considered the most probable explanation for the occurrence of pre-ignition. The mechanism for auto-ignition of oil droplets from a piston crevice is shown in Figure 1.2. Due to the spray impingement on the wall, the oil film that lubricates the walls undergoes a variation in viscosity and surface tension. This leads to the accumulation of oil droplets in the piston crevice, which are subsequently released into the combustion chamber, where the evaporation process takes place [149]. The process from an oil drop to the formation of a combustible mixture around an oil drop is illustrated in Figure 1.3. When the evaporation phase takes place, a mixture of combustible gas is formed around the droplet and, once the suitable thermodynamic conditions are reached, pre-ignition occurs.

Dahnz and Dingle et al. [145,150] further pointed out that the auto-ignition of lubricating oil droplets induced pre-ignition firstly and then super-knock occurs. When oil droplets are released, a gaseous mixture of oil and fuel can form and react with the available air. The following ignition of a lubricant oil droplet will increase local temperature of surrounding pre-mixed mixture and additives. The subsequent gas-phase reaction may be accelerated by temperature and additive catalytic effects and finally pre-ignition can occur which is strong enough to start flame propagation [147,151]. Thus, due to the low auto-ignition temperature of lubricant oils, vaporized oil in a gas layer around an oil droplet

can auto-ignite and oxidize [149,152]. The heat release from this reaction might initiate combustion of the surrounding air-fuel mixture. Such a pre-ignition event can be accompanied by a knocking combustion with significant higher-pressure amplitudes compared to a normal knocking combustion.

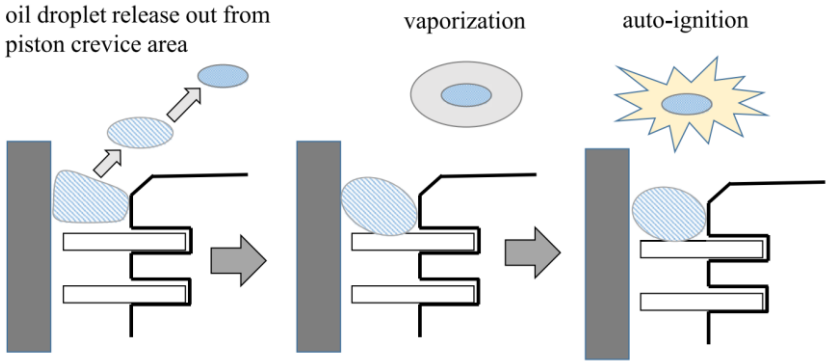

Figure 1.2. Mechanism for auto-ignition of oil droplet from piston crevice [adapted from [149].]

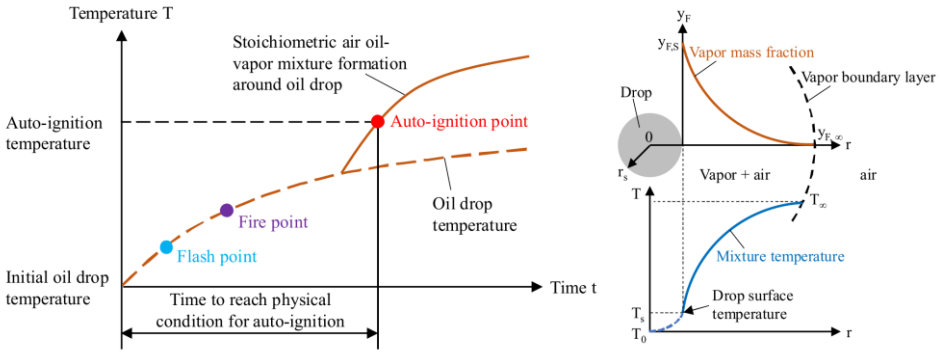

Figure 1.3. Process for an oil drop in cylinder to ignite the mixture [adapted from [153].]

However, some authors proposed that the oil droplet itself did not cause the ignition [149,152,154–156]. Due to oil intrusion into combustion chamber and subsequent interaction with the fuel, species not initially present in the fuel or oil could be generated, triggering pre-ignition [157–162]. The direct evaporation products of the lubricant oil droplet are not able to initiate pre-ignition, but they can promote the generation of stable and highly reactive intermediate radicals that are formed during the low temperature hydrocarbon oxidation process [163].

However, analyzing how an oil droplet can promote pre-ignition events is not trivial. This is because, this complex phenomenon is influenced by several factors. Several authors have investigated the influence of parameter such as location, size and temperature of the oil droplet on the onset of pre-ignition. Zaccardi et al. [164] observed that pre-ignition could start at two possible locations: the bridge of the exhaust valves and around the spark plug on the combustion chamber roof. Heiss and Lauer et al. [165,166] and Gunther et al. [167] noticed that pre-ignition was most possibly started in the hot area on the combustion chamber roof between the spark plug and exhaust valves. Dahnz and Spicher [96] reported that pre-ignition was often started in the gasket gap between the cylinder head and the engine block. Some investigators also proposed that the area of the piston top land could be a location for pre-ignition to be ignited [145,149,152]. Qi et al. and Ohtomo et al. [87,88] found that the oil intruded into the cylinder before Top Dead Center (TDC) could result in pre-ignition and the

ignition timing induced by the oil droplet became shorter as the droplet diameter decreased and the temperature increased [168].

Kuboyama et al. [142] in order to clarify the mechanism of pre-ignition employed direct photography and light induced fluorescence imaging of lubricant oil droplets during pre-ignition cycles. They found that, in the pre-ignition cycles, luminous flame could be observed around the piston crevice area during expansion stroke. This implies that the lubricant oil or mixture of oil and liquid fuel is accumulated in the piston crevice area. It was stated that the oil droplets released from the crevice area, by the piston motion, could be heated during the combustion process and maintain their heated state till the next cycle, and these droplets were thought to be the possible inducer of ignition and abnormal combustion [96,145,149,152,169]. In the work by Long et al. [170], was found that pre-ignition may be possible if oil droplets are present in the combustion chamber close to TDC. The effects of droplet size on the lubricating oil droplet behavior greatly depend on the ambient conditions. Under low temperature and pressure conditions, the smallest oil droplet has the shortest heating period. This is because the high internal heat transfer rate in the small droplet enhances the heating rate when the external heat conduction flux is low. However, in the opposite conditions, the larger droplet increases the heating area and improves the droplet heating rate. Accordingly, the heating period of lubricating oil droplet is prolonged as the droplet size increases [171,172]. In the work by Ohtomo et al. [168,173], was established that the ignition delay of a single oil droplet decreases with decreasing size and increasing temperature. Similar conclusions were presented in the work by Deng et al. [174]. In the work by Huang et al. [175], was found that the ignition delay time for the mixture can reach a minimum when the oil droplet size is appropriately selected. More specifically, the ignition delay time for the air/fuel mixture first decreases and then increases with an increase of the lubricant oil droplet diameter. An increase in the temperature of the lubricant oil droplet, and the temperature and pressure of the gas mixture will also help shorten the ignition delay time for the air/fuel mixture and thus induce pre-ignition. The ignition delay also decreases with the increase in temperature because the amount of evaporation increases [173].They also concluded that most likely the cause of the pre-ignition is not to be attributed solely to the oil droplet, but rather to the generation of stable and highly reactive intermediate radicals that are formed during the low temperature hydrocarbon oxidation process, which accumulate after several cycles. reaching a concentration such as to induce pre-ignition in turbocharged DISI engines. Similarly, in the work by Kassai et al. [176], was highlighted that the effect of oil droplet can presumably be explained by the elementary reactions in the low temperature oxidation region. Ignition of a lubricant oil droplet will increase local temperature of surrounding pre-mixed mixture and additives. The subsequent gas phase reaction may be accelerated by temperature and additive catalytic effects and finally pre-ignition can occur which is strong enough to start flame propagation [151].

In the work by Feng et al. [177], pre-ignition was investigated through the controlled injection of lubricant directly into the combustion chamber of a single-cylinder engine with a full-bore optical access. Simultaneous thermodynamics analysis and high-speed combustion imaging were employed to study the pre-ignition sites, flame propagation, and knocking combustion. They found that pre-

ignition sites were observed consistently from where the lubricant was directly injected. The pre-ignited flame-front induced by the lubricant propagated faster than the normal spark-ignited flame-front, which was mainly attributed to the initial higher heat release from multiple oil droplets. Then, pre-ignition can result in non-knock and knocking combustion with different knock intensities. Occurrence of knocking combustion either close to pre-ignited flame front or near cylinder wall generated high-frequency pressure oscillation. High frequency of pressure oscillation led to the ejection of oil droplets from the piston ring crevice, which was observed by the presence of oil droplets or soot burning in the subsequent cycle of pre-ignition.

The ambient conditions have significant effects both on the behavior of lubricant oil droplet and on the distribution of oil vapor on the droplet surface [171,172]. Under low temperature and pressure conditions, the smallest oil droplet has the shortest heating period. This is because the high internal heat transfer rate in the small droplet enhances the heating rate when the external heat conduction flux is low. In the opposite conditions, the larger droplet increases the heating area and improves the droplet heating rate. Accordingly, the heating period of lubricating oil droplet is prolonged as the droplet size increases. The oil vapor mass fraction on the droplet surface decreases with the increase of ambient pressure under low temperature conditions, because the high ambient pressure causes the lower evaporation rate under low ambient temperature conditions. Oppositely, the ambient pressure has little effect on the oil vapor distribution on the droplet surface under high ambient temperature conditions.

1.3. Solid Deposits

Oil droplets are not the only inducement of pre-ignition. Floating solid particles in the combustion chamber also have a close connection with pre-ignition [178]. It was observed that higher in-cylinder particles increase the frequency occurrence of pre-ignition and super-knock cycles in gasoline direct injection engines [139–141]. The deposit formation and their growth is considerably influenced by engine design, its characteristics and operating conditions, fuel composition, fuel additives and lubricating oil [179–185]. These particles can stay in the combustion chamber and serve as high temperature spots able to ignite the mixture. This is because as the surface temperature increases the deposits can be heated up by combustion, forming hot-spots which can host reactive species, leading to pre-ignition events and consequently support knocking combustion [186–188]. In extreme cases strong deposits increase knocking by increasing the effective compression ratio, due to the thermal insulation of the combustion chamber the gas temperature and hence the ignition timing changes [189]. Palaveev et al. [190] and Schünemann et al. [191], showed that these glowing particles could induced pre-ignition in the next cycle if they remain in the cylinder after the exhaust stroke. They stated that if such a particle does not leave the cylinder during the exhaust stroke and is large enough to maintain its temperature, it may react with the oxygen present in the fresh charge and its temperature may increase further during the intake and compression strokes.

Figure 1.4 shows the mechanism that leads to pre-ignition caused by the presence of deposits. Deposits formed by cylinder liner wall wetting (A) and deposits formed at low engine loads over extended periods of time (B) peel off and float in the combustion chamber space (C). Deposits exposed to combustion are burned and increase in temperature (D). However, although the flame is extinguished between the expansion and exhaust strokes (E), gradual surface reactions with unburned oxygen continue. High-temperature deposits in the residual gases that remain in the next cycle are exposed to new oxygen in the intake stroke of the next cycle. The high-pressure and high temperature of the compression stroke combine with the internal heat to accelerate the surface oxidizing reactions, creating the glowing particles that were observed (F). When the energy required for ignition of the surrounding mixture is discharged, the mixture starts to combust (i.e., flame propagation occurs) (G). In the work by et al. Kuboyama [142], was observed by direct photography that some of the particles generated during first preignition cycle are not scavenged and remain inside the cylinder. The residual particles are heated during the subsequent combustion cycle and induce a second event of pre-ignition. Preignition event continues until the residual particles are consumed.

Kalghatgi and coworkers have published a number of studies on combustion deposit flaking, in which they reported that deposit flaking depends on the temperature regime under which they are formed [192–194]. Indeed, temperature plays a crucial role in the deposits formation [177,195–205]. At high temperatures oxidation reactions take place involving a series of liquid oxidation reactions of alkyl radicals generating hydroperoxides and other oxidized products which are believed to be responsible for solid deposit formation.

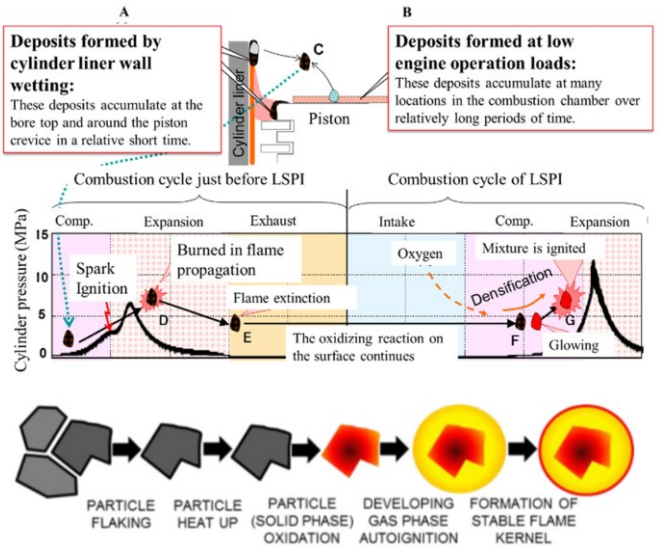

Figure 1.4. Schematic Mechanism of deposit-induced pre-ignition (adapted from [82]).

At high temperatures the formation of deposits can occur in two different ways, namely by decomposition of hydrocarbons to elemental carbon and hydrogen or polymerization/condensation of hydrocarbon species to larger polynuclear aromatic hydrocarbons (PAHs) which then nucleate and grow to become carbonaceous deposit. In some researches the main process for which deposits are formed is polymerization of fuel and to some extend oil which is attached to hot surfaces [206–211].

These two modalities could lead to the formation of catalytic or non-catalytic carbon deposit. The formation of catalytic or non-catalytic carbon deposit depends on the characteristics of the substrate surface. A non-catalytic surface may affect the heat/mass transfer in the system and act as an inert substrate to collect the carbon deposit the formation of which is thermally initiated in the fluid phase. In contrast, a catalytic surface could, in addition, interact with the reactive species and accelerate the deposit formation [211].

Recently, research focused on the influence of lubricant oil on deposit formation. Several publications have in common that the cause of the formation of deposits could be attributed to the partial oxidation and/or combustion of the fuel and lubricant oil, due to the chemical reactions of fluid mixtures of different C–H molecules and other components. Ahrenfeldt et al. [212] generated deposits on a 0.48 l single cylinder high compression ratio Spark-Ignition (SI) engine fueled by synthetic gas. The results of the experiment indicate that the deposits were derived from the lubricating oil. Zerda et al. [213] suggested that the main cause of deposits formed in engines was the incomplete combustion of fuel and thermal cracking of the lubricant oil. In the work by Weidenlener et al. [214], the oil influence on combustion chamber deposit formation was assessed using energy-dispersive X-ray spectroscopy. They found typical engine oil additives such as Mg, Ca or Zn in the deposits. Moreover, comparing the deposits in the cylinder head with the piston top ones, was found that combustion chamber deposit on the piston top have higher concentrations of these elements, suggesting that oil plays a bigger role in forming piston deposits.

Shimizu et al. [215] conducted an investigation to assess the influence of Ca-based additives on abnormal combustion by means of in-cylinder visualization and absorption spectroscopic measurements. An increased presence of deposits in the cylinder was observed when the neutral Ca-based additives were used. From this observation, it was inferred that auto-ignition was influenced not merely by the additives, but also deposits had an effect on promoting ignition. It was assumed that this influence may be due to the fact that as the deposits increase, the temperature increases, leading to differences in auto-ignition behavior.

In the work by Smith et al. [216], a detailed micro characterization of piston deposits generated in a single-cylinder test bench engine showed that the formation is initiated by adsorption of a thin lubricant layer on the piston surface during start-up. Oil-soluble additive degradation products within this thin lubricant layer react with surface oxides to form a phosphate-rich layer. With increasing engine run time, degraded lubricant additive species react with fuel combustion acids to form inorganic sulphates and phosphates that become embedded in a gum-like matrix of non-volatile hydrocarbon residues and partial oxidation products. Extended running times result in the build-up of a concentration of crystalline species near the deposit/substrate interface as a result of agglomeration and annealing. The layer structure was completed by deposition of further lubricant additive material during over-run on completion of the engine test. Haji-Sulaiman and Mat-Isa found that gasoline doped with a trace amount of used engine oil exhibited a high intake-valve deposit-forming tendency in their simulated study [217].

Dearn et al. [218] that the deposits were composed by fuel- and oil-derived, such as C, O, Na, Mg, Si, P, S, K, Ca, Mg and Zn, with four dominating elements (C, S, Ca and O). This is because, the deposits that are formed have a remarkable surface activity, capable of trapping the decomposition products of the lubricating oil and fuel [219]. Diaby et al. [220] showed that the deposits of the first ring grooves are mainly carbonaceous and results principally from the lubricant degradation, inducing polymerizations reactions. Hoang and coworkers [221] used SEM to visualize fouling over the course of an engine testing cycle, showing growth of deposits as lubricating oil degraded over time. Carlisle et al. [222] showed the presence of elements sourced from lubricating oil in the deposit itself such as calcium and phosphorus. Other elements such as sulphur, sourced from lubricating oil, have also been found in injectors via EDS analysis by Von Bacho et al. [223], and later by Trobaugh et al. [224].

Stępień et al. [181] claimed that the most important lubricating oil component for deposit formation is the base oil, in particular increasing the high molecular weight and low volatility content of the oil increases deposit formation. In the work by Caceres et al. [225] chemical analysis techniques were applied to the combustion chamber deposits, and was found that the deposits consist primarily of polynuclear aromatic compounds and unsaturated hydrocarbons. In particular, the presence of the ash residues, the fractions of inorganic materials, and the type of hydrocarbons found are suggestive that oil sources are the primary contributor to combustion chamber deposits. Owrang et al. [226], showed that up to 50% of the deposits consist of volatiles and that the composition of the deposits was strongly related to the composition of the engine oil. Fukui et al. [227] studied the influence of fuel and lubricant oil components on the combustion chamber deposit (CCD) formation. The results showed that the influence of lubricant oil on CCD formation was greater than that of the fuel and most CCD was formed from the detergent dispersant added to the lubricant oil. In particular, the metallic detergent formed a larger amount of CCD than the ashless dispersant.

Anomalous combustion events are also influenced by the size of the deposits, this is because as the size increases, the energy released when they burn increases. This leads to a higher frequency and severity of abnormal combustion [80,83,228]. Therefore, there is a correlation between deposit size and temperature. This suggests that agglomerates of soot particles or deposits in the combustion chamber with higher temperature and larger size detached from piston bowl surface could be one of the inducements of pre-ignition and super-knock events [75,83,229,230].

In the work by Magar et al. [143], was found that pre-ignition is initiated in the immediate vicinity of glowing solid particles. The particles are either a result of the flaking of deposits or of contamination of the combustion chamber. As shown in Figure 1.5, there is also a correlation between soot emissions and super-knock. Higher in-cylinder soot emission correlated well with the frequency of pre-ignition and super-knock cycles. To validate the hypothesis of soot particle-induced pre-ignition, carbon particles with different temperatures and sizes were introduced into the combustion chamber to trigger pre-ignition and super-knock. The results indicate that large-diameter carbon particles directly lead to pre-ignition and super-knock phenomena. This can be explained by the fact that the bigger carbon particles could form an ignition kernel and be more prone to be the source of heat imbalances. The experimental data suggest that agglomerated soot particles with higher

temperatures and larger sizes could be one of the inducements of pre-ignition and super-knock. In addition to deposits and soot, sulphated ash [231] and wear metals such as Fe and Cu [152], also contribute to increased pre-ignition frequency due to catalytic effects.

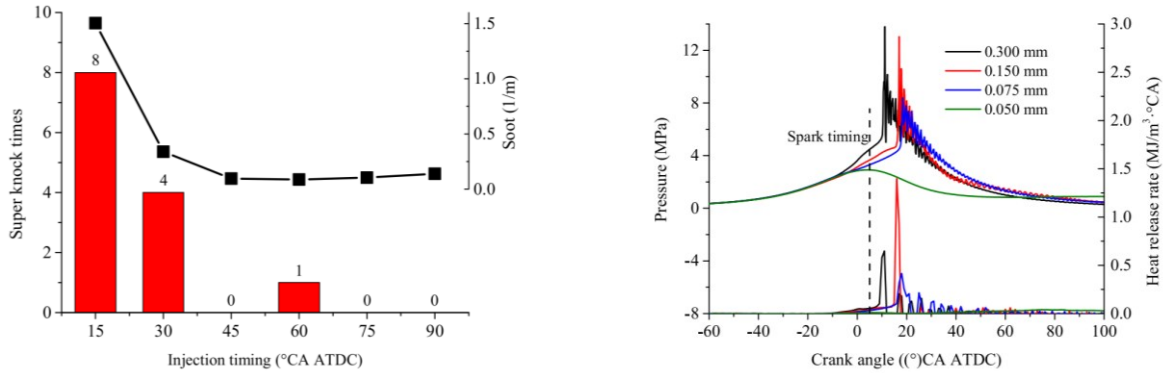

a. Super-knock frequency and soot emission (adapted from [81])

b. Pre-ignition with carbon particles addition (adapted from [75])

Figure 1.5. Mechanism of carbon particle induced the pre-ignition.

In the work by Wang et al. [75], a 4-cylinder turbocharged Gasoline Direct Injection (GDI) engine was used to analyze the correlation between soot emissions and super-knock frequency, a single cylinder research engine was utilized to validate the hypothesis that super-knock is triggered by carbon particles under high temperature and high pressure conditions. They found that super-knock frequency has close relationship with soot emissions in high boosted gasoline direct injection engine. The higher soot emission level in cylinder can result in more pre-ignition and super-knock cycles. Super-knock intensity tends to increase with the increasing particle diameter and temperature. Finally, they suggested that the agglomerated soot particles/combustion chamber deposit with higher temperature and larger size detached from the piston bowl surface could be one of the inducements of pre-ignition and super-knock. These results are in line with the work by Gupta et al. [82], in which was found that only larger particles surviving the gas exchange process or rebreathed into the combustion chamber are sufficiently hot enough to induce pre-ignition.

1.4. Lubricant Oil Degradation

Engine oil degradation also plays a fundamental role in triggering LSPI phenomena. The majority of the modern hydrocarbon base fluids used in diesel and gasoline engines is prone to oxidative degradation [232–234]. When engine oil is used in engine, it degrades gradually and changes its physical and chemical properties. These changes can affect the vaporization and oxidation tendency of the engine oil, which in turn can negatively affect the LSPI frequency.

Michlberger et al. [235], Hirano et al. [152] and Zhang et al. [236], highlighted that LSPI propensity changes as a function of engine oil age and engine age. Perryman et al. [237] stated that the wear metal-catalyzed oxidation of the lubricants could be responsible for the formation of sludge deposits in the used oils during which metals act as radical scavengers at the initial stage of the reaction but would catalyze the oxidation for the rest of the ageing process.

Lubricant oil degradation ca be accelerated by fuel dilution [235,238,239], resulting in changes of the oil properties, such as viscosity, surface tension and volatility [240–242], making it more prone to the release of droplets to the combustion chamber [243,244]. A mainstream view is that in super-knock cycle the occurrence of pre-ignition is related with the dilution of the cylinder oil [244–246]. This was confirmed also by Dahnz et al. [145] who systematically conducted numerical and experimental investigations to find the source of the pre-ignition. As a result, they pointed out that the ignition of the droplets of lubricant oil diluted by the fuel is the most possible source of the LSPI, because oil dilution greatly affects the amount of oil droplets released. This can be caused because the fuel inside the lubricant may react with some oil additives, leading in a thinner oil film and more volatile. Moreover, a depletion of oxidation inhibitors could occur, leading in a considerable carbon deposits on the piston lands as well as on the oil ring of the piston [247–252]. Contamination via fuel dilution could also occurs while the blow-by gas is passing through the ring pack of a piston [253–255].

Several studies have investigated the effects of fuel contamination in lubricant oil, identifying "limits" within which the properties of the oil are stable or altered due to fuel contamination. According to the published results, oil films should be stable up to 10 wt% of fuel dilutions [256]. Some authors followed certain specific parameters of oils in the case of dilution with fuel [240]: mineral oils even at 1% of fuel dilution lose their properties considerably and at 7% dilution they lose their properties of wear protection totally. In the same experiment synthetic oils showed better stability resistance, but also with 7% of dilution with fuel they lose most of their lubrication properties. Other authors observed that for gasoline-fueled engines the maximal level of oil dilution is 4% [257], but some of them give general warnings, e.g. amount of fuel in engine oil of 5% is high enough to lower considerably the flash point or to weaken considerably the oil film stability [250]. For engines using fuel of lower viscosity compared to the engine oil, fuel dilution causes a reduction of viscosity [247]. The adverse effects of fuel dilution on the properties and performance of the lubricant has been studied by Ljubas et al. [258], who found that viscosity, flash points and fire points of oils decrease with amounts of added gasoline fuel.

Thus, the oil film adhering to the cylinder walls could be diluted by the fuel, and this would determine a mixture of hydrocarbons with a higher cetane number than that of gasoline, which can be released as droplets, entering the combustion chamber, could potentially cause a pre-ignition event in the subsequent cycle [259–261]. The higher cetane number of the evaporating mixture would cause a lower ignition delay time compared to gasoline [262]. Under these conditions, the processes that govern the evolution of the lubricating oil/fuel mixture are oxidation and evaporation of the mixture [68,70,149]. When having a closer look at ignition in the surrounding sphere of droplets, several papers report on the dependency of the pre-ignition rate of the fuel-oil interaction [263–265].

Moreover, due to fuel dilution, oil properties such as viscosity, volatility, oxidation resistance and thermal stability have influence on the occurrence of pre-ignition [147,152].

These variations lead to the detachment of the droplets, the causes of which are most likely the result of the reduction of the viscosity and the surface tension. Surface tension was found to be the main factor influencing droplet release from the oil wiped off form the crank case liner during the compression stroke [139,142,168,266]. This is because the surface tension and viscosity of the droplets decreases, thus accelerating the process of droplet breakup and shortening the time required for droplet evaporation. This leads to greater ease in the conversion of droplets from the liquid phase to the gas phase, promoting the oxidation reactions of the surrounding gas mixture. As the temperature of the gas mixture rises, the ignition delay time gradually decreases because the increasing temperature can accelerate the evaporation of the lubricant oil droplet, thus promoting the interaction between the evaporation product of the lubricant oil droplet and the air/fuel mixture. This has been confirmed by several studies, in which was found that that properties of oil particles entered the engine cylinder were affected significantly by fuel dilution [88,147,148,248].

As mentioned above, one of the parameters that can be most influenced by degradation is viscosity. The viscosity of engine oil can drop for reasons of fuel dilution or because of high water content and/or shearing of the VI (Viscosity Index) improver. Viscosity can increase because of heavy contamination of the oil by soot, polymerization, vaporization losses, and emulsions due to water contamination and/or oxidation of the oil [267–272]. Change in viscosity will strongly depend on the formulation of oil by the manufacturer [273–275].

The degradation of synthetic lubricating oils involves polymerization that can produce high molecular weight material [276,277]. When this molecular weight gets too high, the material may become insoluble, leading to its precipitation. This degradation mechanism was observed by Santos et al. [278,279], in synthetic lubricating oils. Viscosity variation, as well as rheological behavior, may be related to the polymerization followed by precipitation of these products. This precipitation is very deleterious, as these products are harmful to machines. Recently, some new functionalities of the additives are introduced in order to modify copolymers and improve their thermal and mechanical stability [280–282]. Copolymers containing alkyl methacrylate structural units are some of the most widely used additives for lubricating mineral oils [283–285]. They improve the viscosity-temperature behavior and at the same time, lower significantly the pour point of base oils.

Several studies have shown that the change in viscosity is able to influence the frequency of LSPI events. For example, in the work by Fan et al. [260], eleven different types of base stock lubricant oil were tested. Results showed that oil with higher kinematic viscosity had a higher ignition delay. The possible reason is that high viscosity makes worse atomization of the lubricant, which is unfavorable for combustion and lengthens the ignition delay. This is consistent with others work in which was found that the auto-ignition frequency decreased with increasing viscosity, which is related to the physical property of the additives [147,286].

Several studies pointed out that if there is an effect of viscosity grade or oil volatility on LSPI, this could be related to the theory of lower viscosity giving lower surface tension and higher droplet release in the combustion zone [83,156,168]. But disagree with the work by Andrews et al. [287], in which was reported that engine oils formulated with higher viscosity produced the highest frequency of LSPI events, and of the various physical and chemical properties, viscosity had the highest correlation with pre-ignition events. They justified these results by stating that higher viscosity lubricants produce thicker films, which could lead to a larger number of fuel-oil droplets produced when injected fuel impinges on the walls. The study of Andrews et al. [287] agree with the paper by Chapman et al. [228], in which was pointed out that the increase in viscosity can be correlated with increased abnormal fuel/lubricant derivative ignition tendency. Moreover, an increase in oil volatility was shown to trend with increasing abnormal fuel/lubricant derivative ignition [228].

In the study developed by Kocsis et al. [288], although the amount of oil droplets release was not measured, occurrence of LSPI events was correlated to the oil viscosity by means of analysis of variance (ANOVA). This analysis showed a connection between this property and lower LSPI rates when the low viscosity formulation had magnesium (Mg) instead of calcium (Ca), otherwise, no conclusive results were observed for the oil viscosity. Spicher et al. [289] found a decrease in the LSPI rate, of about 35%, using an oil formulation of higher viscosity. On the contrary, in the work by Tormos et al. [290], was found that oil viscosity did not have a determining effect on the oil amount reaching the combustion chamber, while engine speed greatly increases this phenomenon. Takeuchi and Luef [149,166] found that low viscosities and high calcium content benefit the pre-ignition rate.

In addition, the evaporative characteristics are also affected since fuel and lubricant oil have different physical-chemical properties. Undiluted fuel has a lower boiling point than undiluted lubricating oil. As a result, the evaporative process for undiluted fuel requires a lower temperature than in the case of undiluted oil. On the other hand, the lubricating oil has a lower auto-ignition temperature than that of the fuel, due to the long-chain lubricating oil components [77,146]. Therefore, mixing lubricant oil with gasoline will result a reduction of the boiling point, volatility and minimum auto-ignition temperature. As a result, the presence of gasoline increases the evaporation rate of the mixture, but the time to ignition of the oil/gasoline mixture is shorter than that of gasoline. Thus, the vapor of the mixture then mixed with the hot ambient air, formed a combustible mixture from which the ignition of the droplet is triggered [248]. Qian et al. [291] investigated the evaporation characteristics of lubricating oil/gasoline blended droplet at different ambient temperature. They pointed out that the evaporation process of lubricating oil/gasoline blended droplet exhibit three-period evaporation characteristics, which is depended on T_{amb} and gasoline content. Moreover, they observed several phenomena, such as bubble generation and rupture, puffing and micro-explosion evaporation process of lubricating oil/gasoline blended droplet. They concluded that gasoline dilution plays an important role in determining the occurrence of puffing and micro explosion for blended droplet. With the increase of gasoline content, lubricating oil/gasoline blended droplet evaporation behavior becomes more violent. More important is that evaporation, puffing and micro-explosion of droplet can generate a large number of small droplets, influencing engine performances [292–294].

Sequence of experimental images of bubble generation, puffing and micro-explosion are reported in Figure 1.6. Lubricating oil/gasoline blended droplet is a multi-component blends with different volatilities, which may produce puffing or micro-explosion during evaporation process based on the previous literatures [295–298].

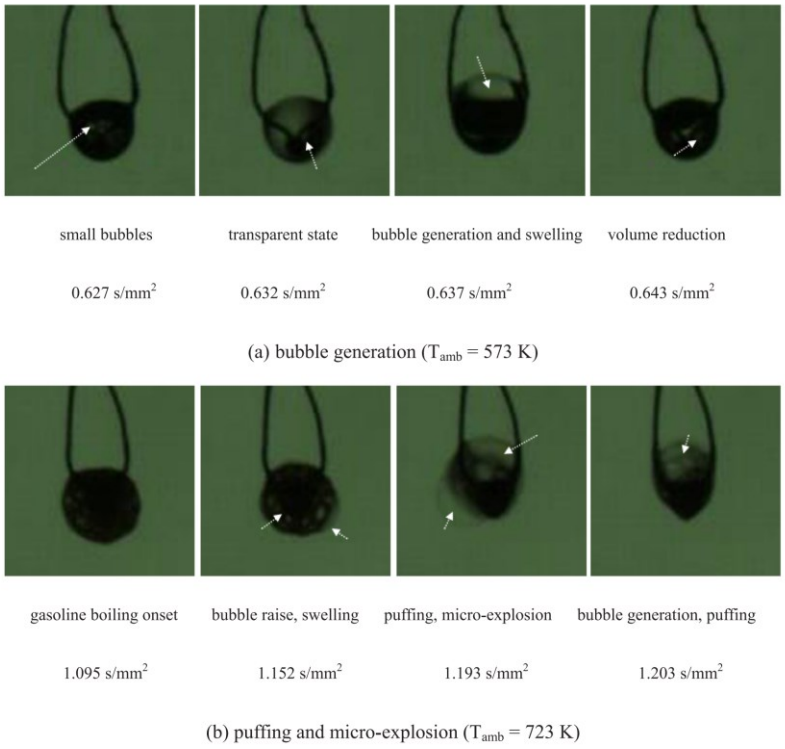

Figure 1.6. Sequence photographs of bubble generation, puffing and micro-explosion of lubricant oil (80% Lubricant oil and 20% gasoline) [adapted from [291].]

Chapter 2

This chapter deals with the analysis of the components that compose the lubricant oil, i.e. base oil and additive package. The aim is to provide a deeper insight into the influence of base oils and additives on abnormal combustion. The purpose of the base oils and the additive package is to guarantee the lubricating performance over time, guaranteeing the thermo-oxidative stability of the oil. To meet this is aim careful balance between base oil and additives is needed. Unfortunately, the oil undergoes to an oxidative process, essentially due to the interaction with the fuel. This oxidative process severely compromises the performance of the oil and negatively affects the additive package. Fuel dilution can dilute the concentration of additives, causing them to separate from the oil. This side effect could negatively affect the frequency of abnormal combustion (LSPI).

2.1. Base Oils Classification and Reactivity

The formulation of the engine oil is extremely complex, as it consists of base oil and additives such as antioxidant, corrosion inhibitor, detergents and dispersants. All Chemical analyses indicate that base oils are mainly composed of C_{15}–C_{34} normal alkanes (n-paraffins) combined with other iso-alkanes and cycloalkanes [261,299].

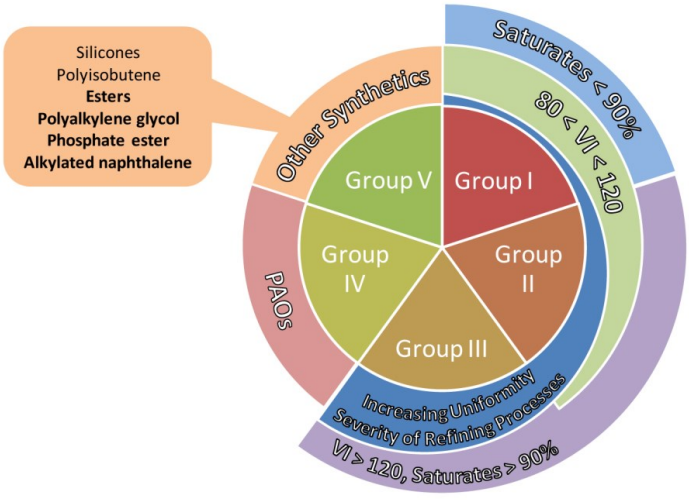

Figure 2.1 API Automotive Lubricant Base Stock Groups [adapted from [259]]

As shown in Figure 2.1, American Petroleum Institute (API), provides a classification of base oils into groups. As the group they belong to, both the production process and their composition vary. Group I base oils are classified as less than 90 percent saturates, greater than 0.03 percent sulfur and with a viscosity-index range of 80 to 120. Group II base oils are defined as being more than 90 percent saturates, less than 0.03 percent sulfur and with a viscosity index of 80 to 120. Since all the

hydrocarbon molecules of these oils are saturated, Group II base oils have better antioxidation properties. Group III base oils are greater than 90 percent saturates, less than 0.03 percent sulfur and have a viscosity index above 120. These oils are refined even more than Group II base oils and generally are severely hydrocracked (higher pressure and heat). This longer process is designed to achieve a purer base oil. Group IV base oils are polyalphaolefins (PAOs). They have a much broader temperature range and are great for use in extreme cold conditions and high heat applications. Finally, Group V base oils are classified as all other base oils, including silicone, phosphate ester, polyalkylene glycol (PAG), polyolester, biolubes, etc. These base oils are at times mixed with other base stocks to enhance the oil's properties. Group V oils are of miscellaneous chemical compositions that fall outside of the Group I–IV trend. This classification suggests that, as the group to which they belong increases, the base oils in Groups I, II and III are more saturated and more paraffinic, i.e. less naphthenic and aromatic. Oils in Group IV are composed of synthetically-derived poly-alpha-olefins that are fully saturated and fully paraffinic.

It is widely accepted that the lubricant base oil and its chemical formulation could give rise to abnormal combustion events within modern gasoline engines. To fully understand the process underlying pre-ignition events, it is essential to investigate the influence of lubricant base stocks. This because different properties of the lubricating oil depend on it, such as the kinematic viscosity, volatility and oxidative stability, which influence the ignition delay time [148].

Kassai et al. [151] proposed that LSPI could be triggered earlier by the ignition of base oil with high ignitability able to increase local temperature of surrounding pre-mixed mixture. The subsequent gas phase reaction may be accelerated by temperature and additive catalytic effects and finally pre-ignition can occur which is strong enough to start flame propagation. Same results were showed in another work by Kassai et al. [176], in which the contribution of base oil and metallic additives to the ignitability of droplets was separately evaluated to understand the fundamental mechanism involved. Results showed that the base oil itself can promote the high ignitability of droplets and that metallic additives can also additionally promote or inhibit the ignitability of droplets in the premixed fuel-air mixture. High ignitability of the lubricant oil was presumed to be primarily dependent on the base oil. Further confirmations were provided by Amann et al. [259], who investigated a large number of common and unconventional engine lubricants and base stocks. It was recognized that most of the currently available engine lubricant exhibit a very high cetane number (are highly reactive) and therefore were expected to be prone to autoignition. Finally, they suggested unconventional base stocks such as certain esters or alkylated naphthalenes, showing a reactivity level much lower than common engine lubricant base stocks. Welling et al. [147], found that the ignition tendency was lower for less reactive base oils and for base oils mixed with certain additives. Consequently, it was suggested that low reactivity base oils could be used to reduce the occurrence of LSPI. Haas et al. [300] investigated the influences of lubricant oil calcium and magnesium concentrations in the additive package, oil viscosity, oil aging and base oil chemical structural properties on ignition propensity through their effects on DCN measurements, and hence on their potential importance to lead to LSPI phenomena. Results showed that no significant influence on DCN was observed with

respect to calcium or magnesium level, oil aging, or peroxide synergy, indicating that DCN is a strong function of the base oil Group classification. They stated that ignition propensity of the fuel-oil is primarily controlled by the original chemical properties of the base oil. Moreover, was pointed out that the Derivative Cetane Number (DCN) increases with increasing base oil API Group Number (I through IV). This conclusion arose from the observation that Group I–IV base oils had an increasing CH_2/CH_3 ratio, indicates that these oils are mainly composed of linear paraffinic structures which are known to promote ignition propensity through low/intermediate temperature chain branching reactions [252,301]. These observations are consistent with the results of several other studies [147,176,244,259,261] that show the chemical properties of the base oil hydrocarbon fraction significantly influence pre-ignition behavior.

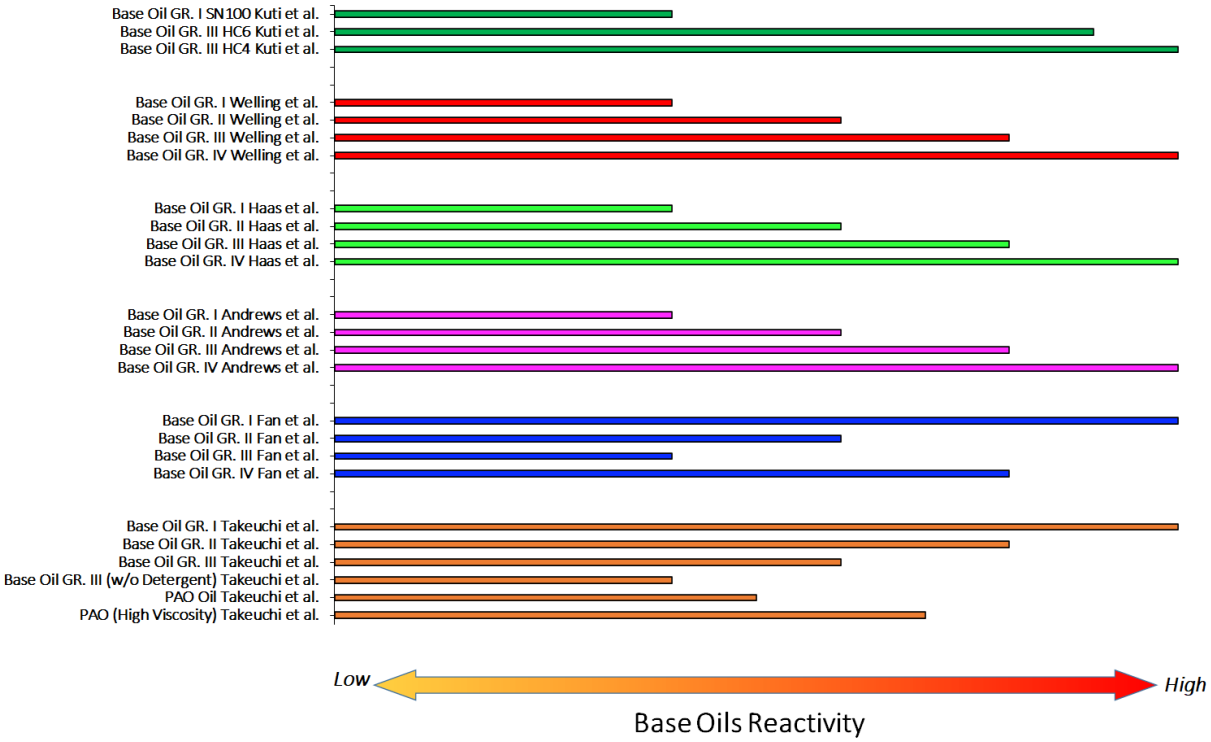

Figure 2.2. Base Oils Reactivity

Kuti et al. [261] conducted a fundamental investigation to elucidate the effects of lubricant oil composition which could lead to LSPI. In this experimental campaign, a mixture consisting of different percentage of iso-octane and base oils was injected in an IQT. It was found that the reduction of the ignition delay was to be attributed to the higher reactivity of the lubricant base oil constituents in the fuel mixtures, as the base stock oils are mainly composed of saturated alkanes. In particular, the mixtures with the Group III (i.e. HC4 and HC6) base oil are more reactive compared to iso-octane/SN100 (Group I) base oil mixtures. This was attributed to the high quantity of saturates (>95%) in the Group III base oils, which are mainly alkanes. Moreover, they suggested to use Group III base oils that could favor the formulation of engine lubricants in terms of corrosiveness and emission profiles since it contains less sulfur and aromatics compared to the Group I lubricants. However, the issue of its reactivity favoring pre-ignition processes in DISI engines needs to be taken into

consideration. This is in line with several works [302–304], in which Group III Base Oil was chosen as the basis for formulating performing engine oils capable of improving LSPI prevention performance, oxidative stability and detergency.

Takeuchi et al. [149], while agreeing that the chemical properties of the base oil hydrocarbon fraction significantly influence pre-ignition behavior, pointed out that the oxidative reactivity is high in the Group I and Group II base oils, with comparatively high component ratio of naphthene, relative to that for Group III or IV (PAO) base oils where the oxidative reactivity is low for the iso-paraffin. Finally, they observed that higher viscosity Group IV base stock produced more pre-ignition than a lower viscosity Group IV. Seeking a more detailed explanation for these observations, the authors found that the auto-ignition temperature of the base stocks at 10 atm pressure correlates well with pre-ignition event frequency. This led the authors to hypothesize that the engine oil effect on LSPI is a better described as a chemical (combustion-related) phenomenon than a physical one.

Andrews et al. [287], after having measured the effect of base oil quality on pre-ignition, showed that the base stocks that most influence the pre-ignition phenomena were the high quality Group III and IV base stocks and lower for Group I and II. Their results about the effect of base stock quality on pre-ignition are in according with Welling et al. [147], but disagree with Takeuchi et al. [149], who found less pre-ignition events for high quality Group III and IV base stocks.

While, Fan et al. [260], by comparing the reactivity between the different groups, determined that base stock type III has the shortest ignition delay time. More specifically, the ignition delay time of type III is slightly shorter than type II and much shorter type I and type IV. The similarity between type III and type II is due to the fact that they are base oils hydrogenation and refined and therefore their carbon chain lengths are close and perform close cetane number. Comparison between type I and type IV revealed that type IV had slightly shorter ignition delay time than type I, because are nearly the same except evaporation losses.

2.2. Role of Lubricant Oil Additives

In addition to being influenced by the type of base oil, the frequency of super-knock phenomena is also influenced by the content of additives. They might present a catalytic enhancement effect, leading to a reduction in the ignition delay which can favor the auto-ignition of the lubricant droplets in combustion chamber. Some works show that some types of additives lead to an increase in the frequency of pre-ignition events, while others act as inhibitors [304,305].

In general, additives are compounds used in the formulation of the lubricating oil and have the role of enhancement of the physico-chemical properties [306–310]. Depending on the application, various combinations of additives are used to meet the required performance level. The additives are different and play the fundamental role of guaranteeing lubrication performance over time. Additives

are divided into several categories. Among these, the most important are antioxidants, detergents, anti-wear, friction modifiers, viscosity modifiers and corrosion inhibitors.

Antioxidants are intended to inhibit the oxidation of hydrocarbons. This process can be inhibited by either of two pathways, specifically by converting peroxide radicals ($ROO^{\bullet}$) into an inactive state, or by destroying hydroperoxides (ROOH). The most widely used antioxidants include compounds of sulfur, phosphorus, and nitrogen. Detergent additives have the function of preventing contamination of engine surfaces and capturing any contaminants in the oil volume, where they meet dispersants. There are two major groups of compounds used as the active components of such additives, specifically alkyl sulfonates and alkyl salicylates. Their compositions are represented by cationic surfactants, ie, salts of second-group metals (eg, Mg, Ca, or Ba) and alkyl sulfonic acid or alkyl salicylic acid. Anti-wear additives have the function of preserving surfaces from wear, under high loads and temperatures. They are commonly used in oil to reduce the wear of boundary-lubricated contacts by forming a protective layer on the surface which prevents the direct asperity-asperity contact thus reducing wear. Friction modifiers additives are inserted in order to reduce friction losses, in order to ensure 2-8% fuel saving [311–313]. Finally, corrosion inhibitor additives must preserve the metal surface when exposed to the environment.

Due to the complexity of lubrication, the interactions between various additives are a key factor in developing a new formulation of lubricant oil [314–318]. It is well known that the addition of appropriate additives to the base oil can reduce friction and oxidation, enhancing the anti-wear performance and preventing the oxidation of lubricant oil and additives [319–325]. For this reason, multifunctional additives such as Molybdenum Dithio Carbamate (MoDTC) and Zind Dialkyl Dithio Phosphate (ZDDP) are employed in lubrication oil formulations, with the aim to improve lubricant performance [326–328]. The MoDTC is characterized by atoms of Molybdenum (Mo), Sulfur (S), Carbon (C) and Nitrogen (N), while ZDDP consisting of Zinc (Zn), Sulfur (S) and Phosphorus (P) atoms. Molybdenum Dithio Carbamate (MoDTC), as a typical friction modifier is known to provide effective reduction in friction by producing molybdenum disulfide MoS_2 [306–308,329,330]. The chemical structures allow ZDDP to act not just as an antiwear additive, but also to provide highly desirable antioxidant and/or metal passivating properties [309,310,331–334]. In fact, the MoDTC produces molybdenum trisulfide (MoS_3) which, by means of ZDDP, leads to the formation of the protective layer constituted by MoS_2 [335–339] that effectively reduces friction [340–344]. Subsequently, this protective layer made of MoS_2 can degrade and lead to the formation of an abrasive compound of MoO_3 which leads to increased wear [345–349]. Therefore, the ZDDP, in addition to favoring the formation of a protective layer, has the function of eliminating MoO_3 by preventing the oxidation of MoS_2 [316,318,350,351]. Indeed, it was showed that the combination of ZDDP and MoDTC leads to an improvement of their properties, demonstrating the phenomenon of synergy [352–356]. In confirmation of this, it was also observed that MoDTC alone is not as effective as compared to the mixture of ZDDP and MoDTC [357–361].

Such synergy is also reflected on the frequency of pre-ignition (LSPI) events. In several papers it is reported that increasing the amount of MoDTC and ZDDP, through the increase of Mo and P, leads

to a reduction of the LSPI frequency [149,152,156,304,305,362]. For this reason, in the existing literature both Mo and P are described as elements capable of suppressing the onset of LSPI and are sometimes considered interchangeable with MoDTC and ZDDP. Although Mo and P are present in the chemical structure of MoDTC and ZDPP, they actually represent different compounds characterized by different effects. Indeed, in literature, it is reported that pure elements such as Mo, Zn and P could lead directly or indirectly to an increase in the LSPI frequency [139,141,288].

2.3. Additives Influence on LSPI Frequency

By means of the figures proposed in the following discussion an analysis of the influence of different additives on the LSPI Frequency was carried out. The experimental measurements analyzed and presented in Figure 2.3, Figure 2.4, Figure 2.6 and Figure 2.6 derive from the works by Takeuchi et al. [149], Hirano et al. [152], Fujimoto et al. [156] and Onodera et al. [304] and were obtained adopting the same experimental procedure.

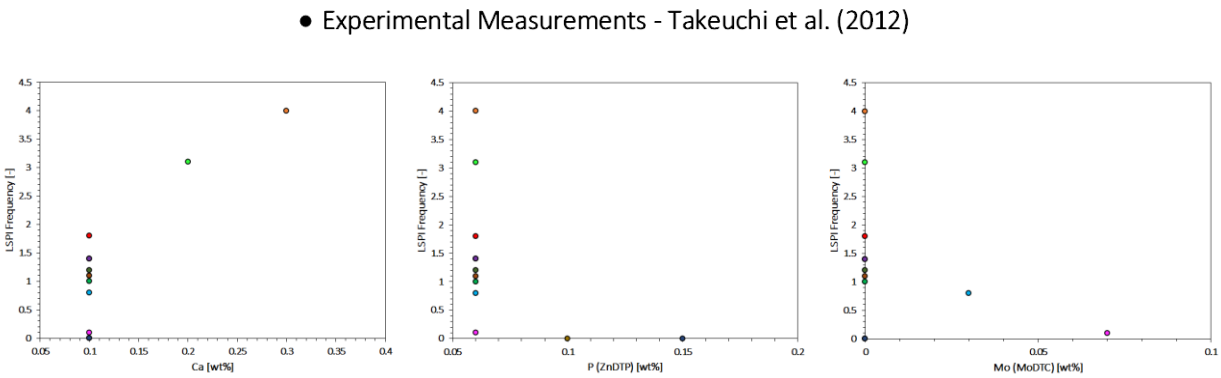

Figure 2.3. Analysis of the additive contents on LSPI frequency.

From the analysis it could be inferred that Calcium (Ca) is the element that most leads to an increases in the LSPI frequency. Several works showed that Calcium (Ca) detergent influenced the frequency and the severity of LSPI events [149,154,243,244,288,305,363]. In particular with the increase of the calcium content the ignition delay decreases drastically and had the tendency to promote auto ignition and abnormal combustion and can be ignited more easily [151,156,260,362,364]. In lubricant, calcium exists in a micelle state of $CaCO_3$, which will be thermally decompounded into CaO and CO_2 at high temperature. Thereafter, CaO particles convert into $CaCO_3$ again by absorbing CO_2 with an evolution of heat [140,176,304]. As this conversion is an exothermic reaction, the temperature of CaO particles increases. These hot particles can contact non-evaporated fuel and oxidize, thus generating heat that results in pre-ignition [74,140,142,262]. Furthermore, Fan et al. [260] showed how Ca-based elements, such as Ca-Salicylate and Ca-Sulfonate, can also influence the pre-ignition phenomena. In this study, these two elements were compared with each other, showing that Salicylate detergent has shorter ignition delay than Sulfonate. This is in line with the results provided by Miyasaka et al. [154], which highlight the influence of CaSa-based engine oil additive on

abnormal combustion, indicating that the addition of a CaSa-based detergent to engine oil tends to promote auto-ignition and abnormal combustion.

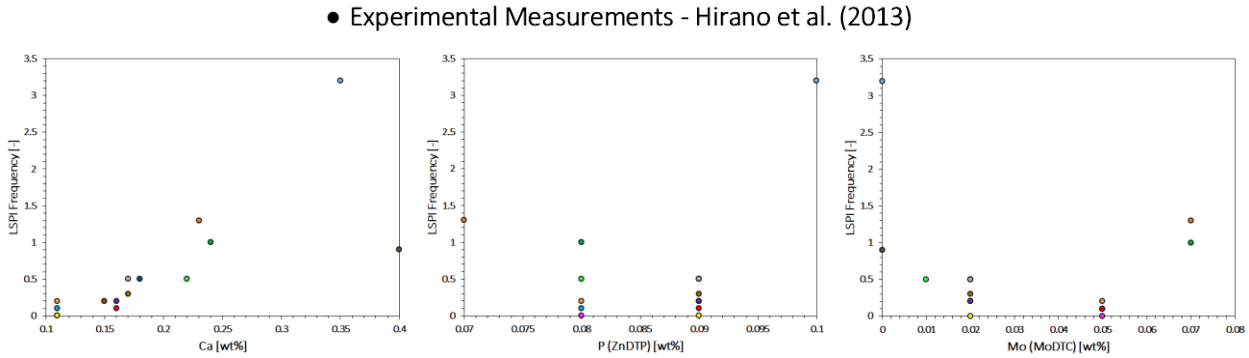

Figure 2.4. Analysis of the additive contents on LSPI frequency.

Several works suggested to increase the amount of elements capable of suppressing LSPI events such as ZDDP and MoDTC and to reduce the Ca detergent, considered an element capable of favoring these undesiderable phenomena [149,154,156]. Indeed, as can be inferred from the analysis, the increase in the LSPI frequency could be counteracted by the reduction of Calcium (Ca) or by the increase of elements such as MoDTC and ZnDTP [149,152,154,156,176,304]. This is in line with the work by Pan et al. [365], who highlighted that the increase of calcium content or the decrease of ZDDP content in lubricants promotes the auto-ignition. While Ritchie et al. [362], noted a test with a near-zero LSPI rates at the low calcium level. It was also highlighted that higher catalytic contents promote the oxidation process of the oil/ fuel mixture, leading to a higher LSPI rate, while Zinc dialkyldithiophosphates (ZDDP) and Molybdenum Dithiocarbamates (MoDTC) showed preventative effects on LSPI, inhibiting the oxidation process by decomposition of peroxides [366], changing radicals or peroxides into stable substances [232,367]. The beneficial influence of these attributes to the binding of free radicals during decomposition of hydroperoxides at the low-temperature regime [368]. Also Takeuchi et al. [149] and Miyasaka et al. [154] confirmed that MoDTC or ZDDP have a preventative effect on LSPI.

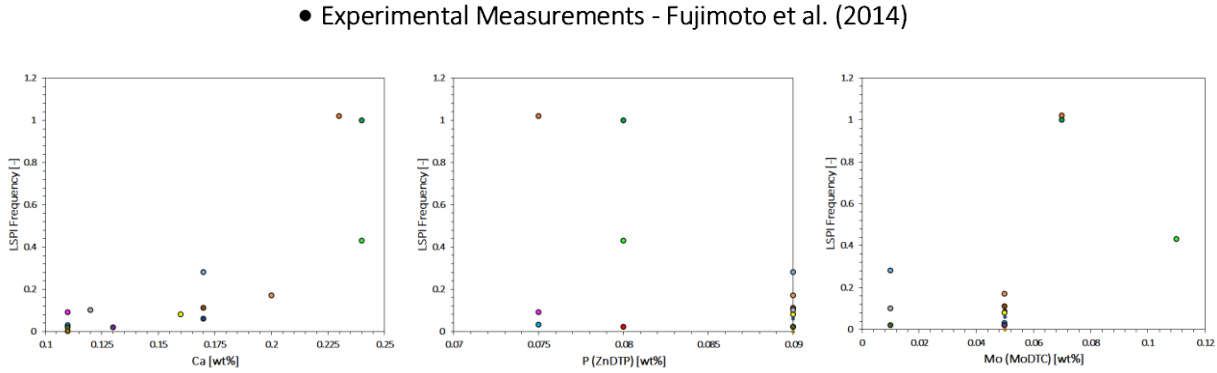

Figure 2.5. Analysis of the additive contents on LSPI frequency.

However, Calcium (Ca) cannot be reduced too much, because the detergent properties of the lubricating oil would be compromised, while ZDDP cannot be increased beyond a certain threshold,

because it can cause poisoning of the post-treatment system [156,302,304,369,370]. Furthermore, elements such as MoDTC and ZnDTP contain an amount of sulfur and phosphorus which, according to current regulations, must be limited. Therefore, the variation of MoDTC and ZDDP must comply with the limits imposed by regulations and functionality of the after-treatment system [371–373]. This beacause, ZDDP contains metal, phosphorus, and sulphur atoms, all of which can degrade exhaust after-treatment performance [369,370]. Kaneko et al. [302], studied the friction performance of engine oil, with a combined used of magnesium detergent and MoDTC, because is expected to become an essential technology for low viscosity engine oil with LSPI prevention performance. Results showed that Magnesium detergents were revealed to deteriorate low friction performance of oil with molybdenum-dithio-carbamate (MoDTC). They suggested to use borated dispersant reduces friction in oil with magnesium detergents, for improving oil performance. This is in line with the work by Martin et al. [374], who revealed that molybdenum-dithio-carbamate (MoDTC) reduces friction in the presence of borated calcium salicylate.

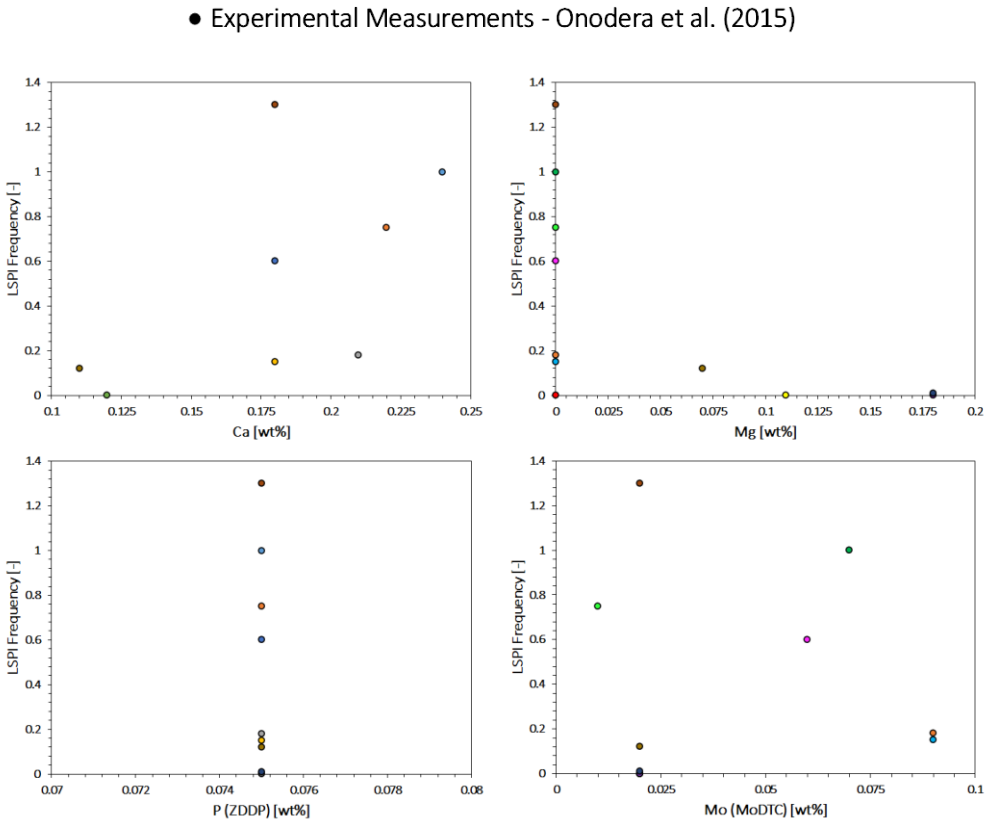

Figure 2.6. Analysis of the additive contents on LSPI frequency.

However, the replacement of Calcium (Ca) with less reactive elements and with adequate detergent properties such as Magnesium (Mg), can represent a solution capable of guaranteeing detergent properties and LSPI prevention. In fact, the analysis shows how the addition of Mg or the replacement of Ca with Mg does not lead to an increase in the LSPI Frequency. Kassai et al. [151], highlighted that, in addition to additives such as ZDDP and MoDTC, Magnesium (Mg) can also be considered as a component capable of reducing LSPI events. Onodera et al. [304] proposed to reduce the calcium content and increase that of MoDTC or, alternatively, to replace the Calcium (Ca) with a less reactive

detergent, such as Magnesium (Mg). The same conclusions were made by Ritchie et al. [362], who stated that Magnesium (Mg) detergents can reduce the occurrence of LSPI if it is used as a detergent in place of Calcium. This was in line with the results of Kocsis et al.[288], in which was highlighted that displacing some or all of the calcium with magnesium reduces the LSPI rate relative to an all-calcium lubricant. Same conclusions were made by Michlberger et al. [239]. However, Mg also has side effects. In fact, a high amount of Mg can lead to a rapid oxidation of the MoDTC and, therefore, compromise the antiwear lubricating properties. Kaneko et al. [302], studied the friction performances of MoDTC-doped engine oils formulated with magnesium detergent, which is necessary for good LSPI prevention performance. They found that Magnesium detergents were revealed to deteriorate low friction performance of oil with MoDTC, while borated dispersant reduces friction in oil with Magnesium detergents. Gupta et al. [375], argued that although a switch to an all-Magnesium formulation, or severely limiting the concentration of Calcium in the engine oil may help reduce LSPI, the perceived benefits may be outweighed by the significant penalty on fuel economy.

The analysis of the experimental measurements highlights an extremely interesting result. Specifically, comparing MoDTC and ZDDP, it appears that ZDDP may be more effective in preventing LSPI events than MoDTC. The chemical structures allow ZDDP to act not just as an antiwear additive, but also to provide highly desirable antioxidant and/or metal passivating properties [309,310,331–334]. Thus, the reason could be that ZnDTP is an effective antioxidant that inhibits both the formation and the effects of reactive radical species [367], preventing oxidation of the lubricant oil by changing radicals or peroxides into stable substances [232,368]. The effects of ZDDP additives were confirmed to be ignition destabilization, prolonging of the ignition delay time and inhibiting of flame kernel growth [176].

Several studies support the observation resulting from the analysis of the proposed experimental measurements. Fletcher et al. [305], observed that MoDTC did not provide statistically significant reduction in LSPI frequency, while zinc dithio-phosphate (ZDDP) dramatically reduced LSPI frequency. For further confirmation, in the work by Ritchie et al. [362] was found that increasing the concentration of zinc-dialkyl-dithio-phosphate (ZDDP) from 0.05% to 0.19% reduced the LSPI event count by more than 90%, essentially independent of the alkyl group used to formulate the ZDDP. However, the synergy between MoDTC and ZDDP is evident, leading to effective prevention of LSPI events and to an improvement of their properties [352–356]. Such a synergy becomes more effective if the balance between the two elements and the balance of the additive package are optimized [357–361]. In the literature there are several evidences that highlight the synergy between ZDDP and MoDTC. Kassai et al. [151] showed that calcium additives could promote LSPI under some conditions, while magnesium, ZDDP and molybdenum-dithio-carbamate (MoDTC) were found to inhibit LSPI. Hayakawa et al. [141] comparing the effects of ZDDP- and MoDTC-based engine oil additives on abnormal combustion, found that these additives showed no effect on auto-ignition.

Obviously, the prevention of LSPI events does not only involve balancing the package additively, but also the type of base oil and its chemical-physical characteristics, such as viscosity, volatility and thermo-oxidative stability, all properties that can be compromised by the interaction with the fuel

inside the combustion chamber. Due to the complexity of lubrication, the interactions between various additives are a key factor in developing a new formulation of lubricant oil [314–318]. It is well known that the addition of appropriate additives to the base oil can reduce friction and oxidation, enhancing the anti-wear performance and preventing the oxidation of lubricant oil and additives [319–325]. For this reason, multifunctional additives are employed in lubrication oil formulations, with the aim to improve lubricant performance [326–328].

2.4. Lack of knowledge on Additives

To this date, due to the poor knowledge of the effects of additives on pre-ignition phenomena there is no unanimous consensus on some types of additives, this because pre-ignition phenomena are random, and oil additive effects are only one of the possible pre-ignition sources.

For instance, there is no consensus on whether Zn and Mo have effects on pre-ignition. In the work by Kassai et al. [176], zinc additives were confirmed to be ignition destabilization, prolonging of the ignition delay time and inhibiting of flame kernel growth. On the contrary, in the work by Park et al. [139] was found that Calcium, Zinc and Molybdenum had the greatest effect on pre-ignition, while Boron, Phosphorus, and Magnesium indirectly affect preignition. Hayakawa et al. [141] found that Zinc and Molybdenum additives had little effect on pre-ignition. Kocsis et al. [288] showed that the impact of the Zinc, Magnesium and Molybdenum additives on LSPI were seen at the higher Calcium concentrations. Ritchie et al. [362] found that Magnesium (Mg) detergents have no effect on LSPI, and can reduce the occurrence of LSPI if it is used as a detergent in place of Calcium. This is in line with, Kassai et al. [151], who showed that calcium additives could promote LSPI , while magnesium, ZDDP and MoDTC were found to inhibit LSPI. In confirmation of this, Michlberger et al. [239], showed how a lubricating oil formulation containing a reduced Ca content with the addition of Mg exhibited a reduction in LSPI events and excellent LSPI durability. This is consistent with other works , in which overbased magnesium detergent system resulted in zero LSPI events [304,362]. On the contrary, Hayakawa et al. [141] comparing the effects of ZDDP- and MoDTC-based engine oil additives on abnormal combustion, found that these additives showed no effect on auto-ignition.

In addition, there are additives whose effects are not fully known. Ritchie et al. [362] and Kassai et al. [151], found that Sodium (Na) detergents act as LSPI promoter in the presence of Calcium. In confirmation of this, Fletcher et al. [305] found that for a mixed-metal detergent system, the introduction of Sodium can increase LSPI frequency. Moreover, Miura et al. [286], investigated the effects of Calcium (Ca), Magnesium (Mg) - and Sodium (Na) -based additives, mixed separately into the test fuel. It was highlighted that due to the separate mixing, the Mg- and Na-based additives did not show evident effects on promoting auto-ignition. Nomura et al. [376], found that higher Manganese (Mn) concentrations led to a greater frequency of LSPI occurrences, this because the sensitivity of volatility to the frequency of LSPI occurrences increased in conjunction with higher Manganese (Mn) concentrations. Moreover, high concentrations of Manganese (Mn) lead to

increased deposits in the cylinder, suggesting a correlation with LSPI events. In the work by Tamura et al. [80], was observed that CaSa-derived and ZDDP-derived deposits facilitated auto-ignition and increased knock intensity, whereas MoDTC-derived deposits did neither. Miyasaka et al. [154] found that the addition of a calcium salicylate based detergent to engine oil tended to promote pre-ignition.

Chapter 3

In this Chapter an overview focusing on recent experimental and numerical research efforts is presented. The first section focuses on the recent development in lubricant oil formulation, aimed at reducing its impact on undesired abnormal combustion event. The last section provides a brief overview on the results showed by different research group in the modeling of lubricant oil combustion. From the latter, useful indications can be derived which can be considered as a starting point for a more efficient and reliable modeling of the onset of pre-ignition triggered by the interaction between lubricant oil and fuel.

3.1. Research Direction on Oil Formulation

This represents a promising area for future research work, as developing inhibited additives could provide solutions for suppressing pre-ignition and super-knock. Several research groups have focused on the development of lubricating oils capable of guaranteeing excellent performance in terms of detergency, oxidation stability and reduction of LSPI events. Figure 3.1 summarizes the lubricant oil formulations proposed in various works.

Elliot et al. [377] tested the effect of Potassium (K) and Lithium (Li) substitutes for calcium in detergents, of which the former prevented LSPI very well. Furthermore, he compared several zirconium, zinc and cobalt boosters with varying ligands. The overall impact of Zirconium (Zr) and Zinc (Zn) on LSPI occurrence was preventive, but the effect of Cobalt (Co) varied heavily depending on the used ligand.

Fujimoto et al. [156] reported some guidelines in order to reduce the LSPI frequency caused by lubricant oil. It was proposed a high-quality base oil (Group III and Group IV) and optimized additive components in which the amount of calcium-based detergent was reduced to levels lower than general ILSAC oils, and a sufficient amount of anti-oxidants, such as ZDDP and MoDTC were added. Moreover, it was determined a specific map for the performance of the engine oil in accordance with the amount of Calcium detergent and ZDDP (Figure 3.2). Considering the proposed diagram, an optimum formulation was selected for satisfying all performance requirements, which consisted of an amount of Ca = 0.12 wt% and P = 0.09 wt%. In particular, the proposed formulation consisted of a level of Ca equal to 0.12 wt%, P equal to 0.09 wt% and Mo equal to 0.01% wt. Moreover, the developed oil achieved the target of reducing the LSPI frequency to 10% of that of a conventional oil (API SM, 0W-20).

Liu et al. [303] studied the formulation of two oils (A and B), consisting of Group III base oil, containing Ca-salicylate and Mg-sulfonate (Oil A) and Ca-salicylate and Mg-salicylate (Oil B). Furthermore, borated dispersant and MoDTC were present in both formulations. Investigation was emphatically conducted on the various effects of Mg-salicylate and Mg-sulfonate on the all-round performance of engine oil. They found that Mg-sulfonate showed a significant detrimental impact on silicone rubber, while the influence from Mg-salicylate remained acceptable. Both formulations provided good LSPI prevention property, as LSPI frequency was almost zero, and fuel economy improvement. They concluded that a 0W-16 oil adopting the same additive package could have achieved the same or even better LSPI prevention performance.

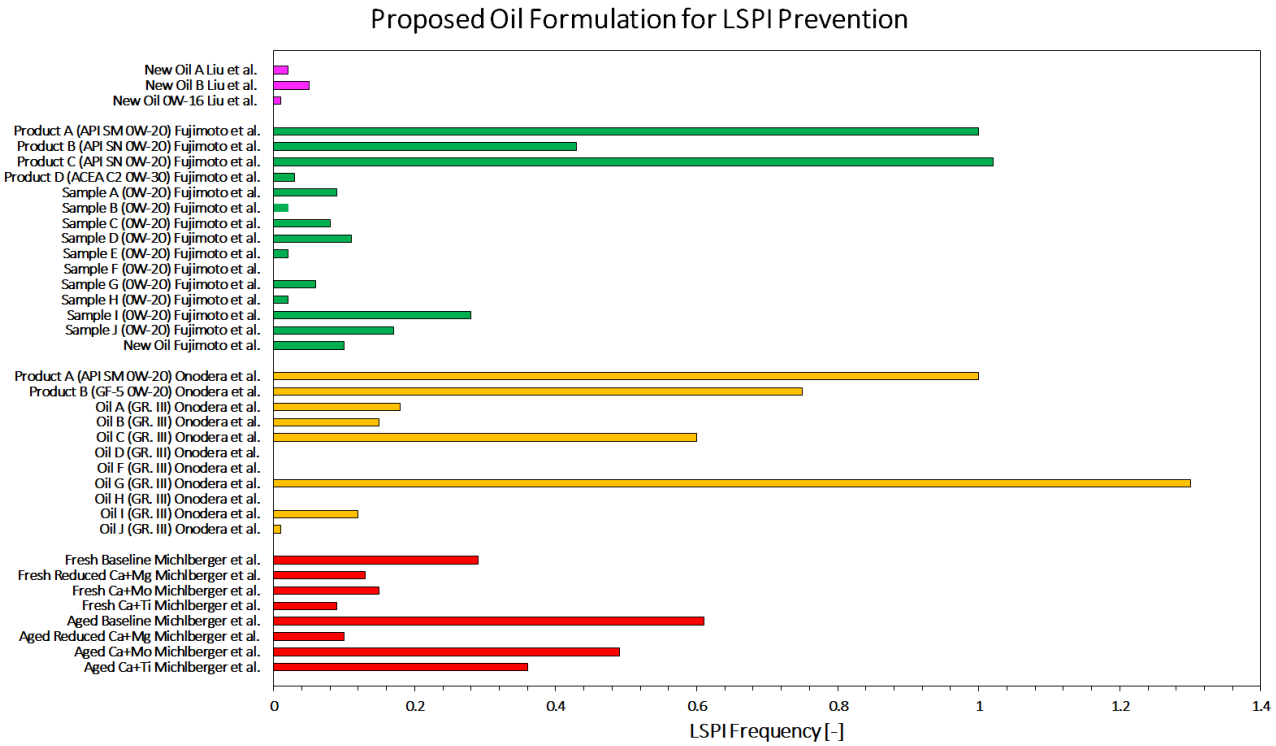

Figure 3.1. Proposed Lubricant Oil Formulations

Onodera et al. [304], focused on two approaches for formulating an engine oil for LSPI prevention, applicable for ILSAC GF-6 engine oil. The first approach consisted in fixing the amount of Phosphorus equal to 0.075% wt and varying the amount of Molybdenum and Calcium. Using this approach, a minimum amount of Calcium and Molybdenum was determined, as reported in Figure 3.3 (a). While the second approach consisted in fixing the amount of Molybdenum and Phosphorus respectively equal to 0.02% wt and 0.075% wt and varying the amount of Calcium and Magnesium, as shown in Figure 3.3 (b). In this way, it was found that calcium could be replaced with a less reactive component such as Magnesium. By means of this analysis, they determined an ideal formulation by increasing the Molybdenum content, used as a friction modifier, while calcium detergent was replaced with a Magnesium (Mg) detergent, improving the anti-rust performance, while it does not negatively impact LSPI prevention performance.

In the work by Michlberger et al. [239] four different oil formulations were evaluated, three of which formulated for the purpose of preventing LSPI events. Results show that some formulating strategies work well for LSPI prevention. In particular, the three LSPI mitigating formulation strategies consisted of reducing Calcium (Ca) content and added Magnesium (Mg) for LSPI mitigation, maintain high Ca but include MoDTC for LSPI mitigation, and maintain high Ca but include Ti (Titanium) for LSPI mitigation. But, after aging both Ca + Mo and Ca + Ti formulations were observed to have very high LSPI, while the reduced Ca + Mg formulation maintained strong LSPI mitigating performance, showing excellent LSPI durability.

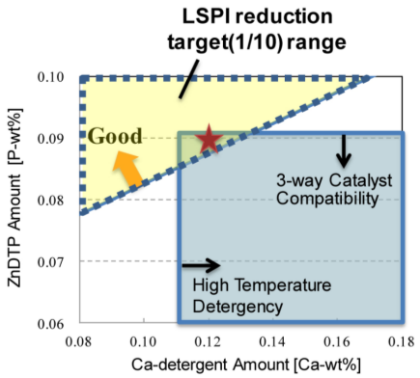

Figure 3.2. Maps the performance of the engine oil in accordance with the amount of Ca detergent and ZDDP. [156]

Kaneko et al. [302], studied the friction performances of MoDTC-doped engine oils formulated with magnesium detergent, which is necessary for good LSPI prevention performance. They found that Magnesium detergents were revealed to deteriorate low friction performance of oil with MoDTC, while borated dispersant reduces friction in oil with Magnesium detergents. In light of this results, GF-6 proto-type formulation was set with mixed calcium and magnesium detergents at 0.16 mass% of Ca and 0.07 mass% of Mg, respectively, to ensure LSPI prevention performance. Moreover, borated dispersant was formulated to promote formation of harder poly-borophosphate tribofilm which prevents itself from being scraped by magnesium detergent, causing low friction. This newly formulation technology of engine oil was applicable for ILSAC GF-6 engine oil and after, where LSPI prevention performance and low viscosity are required for excellent fuel economy.

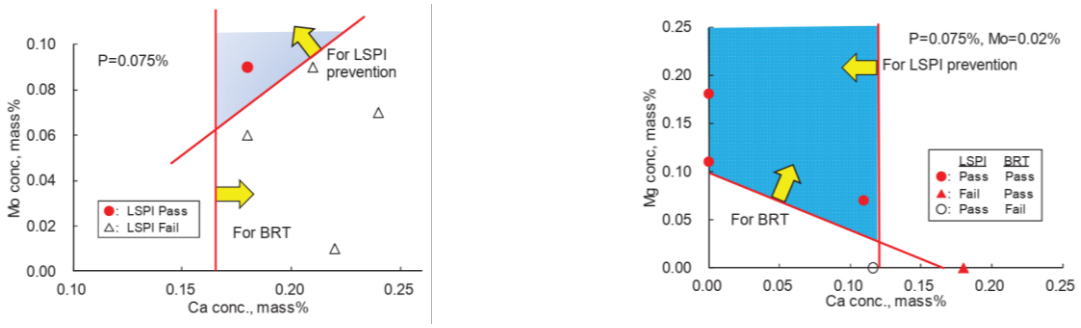

(a) (b)

Figure 3.3. Target area of Mo and Ca for LSPI prevention and BRT (a) and Target area of Ca and Mg for LSPI prevention and BRT (b) [304]

3.2. Lubricant Oil Combustion Modeling

In recent years, with improvement of computational capability more attention has been paid to numerical investigation of the onset of pre-ignition triggered by the interaction between lubricant oil and fuel.

Dahnz et al. [96,145], investigated the influence of oil droplets on the auto-ignition properties by means of simulations using a one-dimensional combustion model. In order to reduce computational effort a reduced mechanism developed by Andrae and Head [378], consisting of 142 species and 672 reactions, was employed. For the simulations, oil droplets were modeled with n-Heptane (n-C_7H_{16}) in an initially homogeneous stoichiometric mixture of iso-Octane (i-C_8H_{18}) and air. They pointed out that their approach was not an appropriate representation of the fuels and lubricants used in real engines. Palaveev et al. [155], carried out an investigation to support the understanding of the physical processes (evaporation and mixing with the surrounding gas phase) and chemical processes (ignition delay time) during droplet ignition. For this aim, data from n-hexadecane (n-$C_{16}H_{34}$) were used to describe the evaporation behavior of lubricant, while chemical kinetics were taken from n-heptane (n-C_7H_{16}). Specifically, the reduced reaction mechanism for the oxidation of n-heptane and iso-octane mixtures by Ahmed et al. [379] was used, consisting of 233 species and 2019 reactions. The required physical data for the liquid and the gaseous phase of n-hexadecane were taken from Polling et al. [380]. Moriyoshi et al. [74,140], numerically investigated the influence of an oil droplet on the pre-ignition, modeled by n-heptane (n-C_7H_{16}) . In their simulations a reduced Primary Reference Fuel (PRF) mechanism (33 species and 38 reactions) developed by Tsurushima [381] was employed. From their analysis they deduced that the mere presence of an oil droplet was unable to generate a pre-ignition, unless the ambient gas temperature, pressure and droplet's temperature were high enough that was a rare condition in an engine. Then, they identified Calcium (Ca) as the trigger for the pre-ignition. In light of this, they concluded that the droplets with $CaCO_3$, burning inside the cylinder, changed into CaO particles, and these CaO particles absorb CO_2 during the next cycle's compression stroke with an evolving heat, causing a pre-ignition of the ambient mixture. Similar results were obtained by Huang et al. [175]. In their work, by means of 3D simulation coupled with PRF mechanism (41 species and 125 reactions), n-Heptane (n-C_7H_{16}) was used as a substitute for the direct evaporation product of the lubricant oil droplet. They pointed out that the shortening of the ignition delay time for the air/ fuel mixture caused by lubricant oil evaporation was not enough to initiate pre-ignition, but they can promote the generation of stable and highly reactive intermediate radicals that are formed during the low temperature hydrocarbon oxidation process.

From the literature review conducted, it is evident that in order to adequately model the influence of the lubricant oil it is necessary to define a different surrogate species than n-Heptane (n-C_7H_{16}). This is in line with the work by Kalghatgi et al. [77], in which was highlighted that n-Heptane (n-C_7H_{16}) ignition delay time values were still too high for accomplishing this. The conclusion was that to satisfy ignition delay time and critical initiating flame size requirements, the oil would have to be somewhat more reactive than n-Heptane. Lubricant Oil is more ignitable than fuel because it has a larger cetane

number than the gasoline components, and the combustion delay of the oil are shorter than that of the fuel [151].

To accomplish this aim, several authors employed long-chain hydrocarbon species in order to adequately model the liquid phase and gas phase properties of the lubricant oil. Ohtomo et al. [168] employed a one-dimensional model was used for investigating the influence of a single droplets on the ignition delay fo fuel/air mixture. In this work, the physical properties of the droplet were represented as n-eicosane (n-$C_{20}H_{42}$), while the chemical kinetics of the fuel and droplet vapor were taken from those for iso-octane (i-C_8H_{18}) and n-heptane (n-C_7H_{16}), respectively. In the work by (2014)Lauer et al. [178] a detailed version of the Toluene Reference Fuel (TRF) was used (1121 species, 4959 reactions) in order to account for the long-chain hydrocarbon reactions during the low temperature oxidation, which play a key role for pre-ignition. They modeled the oil/fuel mixture using an adapted surrogate fuel consisted of 60 vol. % toluene, 21 vol. % iso-octane and 19 vol. % n-heptane. More recently, Ohtomo et al. [87], defined the composition of the droplet as a mixture of six hydrocarbons. This six hydrocarbons mixture consisted of n-Octane (n-C_8H_{18}), n-Decane (n-$C_{10}H_{22}$), n-Tetradecane (n-$C_{14}H_{30}$), n-Hexadecane (n-$C_{16}H_{34}$), n-Eicosane (n-$C_{20}H_{42}$) and n-Heptacosane (n-$C_{27}H_{56}$). Fei et al. [86], performed numerical simulations of droplet evaporation with different initial droplet radius. For this purpose, a one-dimensional transient model was used which described the energy balance between the droplet and its gas phase and the heat and mass transfer in the droplet and the phase change process. This model was previously developed by Zhang and Law [382]. In their analysis, a two-component mixture consisting of nonacosane ($C_{29}H_{60}$) and hexatriacontane ($C_{36}H_{74}$) was used as the surrogate of the lubricant oil.

Nevertheless, some progress in recent years, the chemical kinetic mechanism of long-chain alkanes requires unacceptable computational efforts, making them inadequate for pratical engine simulations [383–388]. In order to reduced computational costs, some authors proposed to employ only one chemical species for the modeling of the lubricant oil. In the work by Gupta et al. [84], iso-Octane (i-C_8H_{18}) was used to represent gasoline for the gas phase chemistry by means of Primary Reference Fuels (PRF) developed by Liu et al. [389], while sub-mechanism based on the kinetics published by Kawanabe et al. [390] was used for representing auto-ignition driven by gas-phase kinetics of n-Hexadecane, assumed as lubricant oil surrogate species. In this work, however, no bibliographic or experimental evidence was showed regarding the efficacy of using n-Hexadecane as a surrogate species to emulate the chemical-physical characteristics of the lubricating oil. Furthermore, no validation of the resulting reaction mechanism is showed. Ullal et al. [391], employed a reduced mechanism for $C_{21}H_{44}$, consisting of 129 species and 559 reaction, extracted from the mechanism developed by Ra and Reitz [392]. The reduced mechanism was optimized by adjusting the reaction rate constants in order to capture the reactivity of the lube oil. However, no validation of the resulting mechanism was showed after the reduction and optimization operation. Although they stated that according to Kuti et al. [261], surrogate species such as n-$C_{16}H_{34}$, n-$C_{17}H_{36}$ and n-$C_{18}H_{38}$ could be employed to emulate the chemical-physical characteristics of the oil, they did not explicitly indicate the species used to model the lubricating oil and did not show any litereture

evidence. It can probably be assumed that they used the $C_{21}H_{44}$ species, as they claim that a typical lubricating oil contains hydrocarbons heavier than C_{21}.

However, engine simulations are commonly computationally expensive. Analytical correlations are frequently implemented in Computational Fluid Dynamics (CFD) codes in order to save computational time. For instance, analytical correlations for the laminar flame speed are usually preferred in engine practical simulations [393–395] in the place of detailed chemical kinetics, avoiding the use of dedicated and computationally expensive reaction mechanisms. Fujimoto et al. [156] developed an empirical correlation in order to estimate the LSPI frequency as a function of the mass fraction of lubricant oil additives, such as Calcium, Ca, Phosphorus, P, and Molybdenum, Mo:

$$\mathrm{LSPI}_{\mathrm{frequency}} = 6.59 \cdot \mathrm{Ca} - 26.6 \cdot \mathrm{P} - 5.12 \cdot \mathrm{Mo} + 1.69.$$

However, the applicability of the correlation proposed by Fujimoto et al. [156] is quite limited, since its use was recommended only for the same engine type and operating conditions considered in their study. In addition, it requires the additive mass fractions to be determined as well as it does not consider the influence of temperature and lubricant oil amounts inside the combustion chamber.

It is evident that the modeling of the interaction between fuel and lubricant oil represents a really challenging task, that require to consider both the chemical and physical aspect. Nowadays, numerical simulations could play a key role towards the fast development of innovative engine technologies. Thus, the accurate chemical modeling of the fuel-lubricant oil interaction, by means of the development of reliable auxiliary tools, could provide information difficult or impossible to obtain solely through experiments, enabling the further development of the internal combustion engines.

Chapter 4

The Detailed "GasLube" Chemical Model

In this Chapter, a reaction mechanism, suitable for simulating the lubricant oil influence on the combustion process of gasoline-like fuels, is developed and presented. The proposed reaction mechanism is motivated by evidence reported in the literature highlighting that lubricant oil droplets can be the most likely inducer of pre-ignition phenomena, as well as the fact that lubricant oil can represent the main source of very fine soot particles emitted from the engine. In other words, the mixture of fuel and lubricant oil, through complex physical and chemical reactions involving long hydrocarbons chains, can auto-ignite before the spark timing or, if not the case, can become one of the major candidates in the generation of soot precursors. Therefore, developing a reliable reaction mechanism able to simulate the oil-fuel mixture behavior and contribution in terms of pre-ignition and soot formation is fundamental for predicting the onset of knocking phenomena and particle size distributions of soot emissions. In this study, surrogate components reproducing the lubricant oil propensity to ignition were first identified. A detailed reaction mechanism was then developed and validated starting from existing mechanisms proposed for the single species. In particular, alkanes ranging from C_{16} to C_{18} were selected as oil surrogates. Zero-dimensional numerical simulations were conducted in order to validate the proposed mechanism versus literature experimental data aimed at reproducing the effect of commercial lubricants on ignition propensity of gasoline-like fuels. From this analysis it was possible to define a suitable composition of the surrogate mixture proposed to model lubricant oil effects.

4.1. Introduction

The growing attention to climate change, to pollution in cities, and to saving energy requires that automotive industries pay attention to the design of internal combustion engines (ICEs). In fact, global demand for more efficient and cleaner ICEs is constantly increasing, and these characteristics have to be guaranteed in order to render these engines a sustainable alternative to electric engines.

It appears that gasoline fueled engines show great potential to further improve their efficiency and meet upcoming stringent emission regulations [16,35,38,51] in comparison to compression ignition (CI) engines. Technology development trends in gasoline Spark-Ignition (SI) engines have exploited high boosting, downsizing and direct injection strategies as common practice to enhance power density and reduce fuel consumption [33–35]. Furthermore, the idea of realizing Gasoline Compression Ignition (GCI) engines, relying on the Homogeneous Charge Compression Ignition (HCCI) combustion concept, has gained increasing attention over the last decades, due to the potential of

achieving diesel-like thermal efficiencies with significantly reduced NO_x and soot emissions [49–51]. However, the development of such technologies is far from being considered completely mature and is challenging for engine designers, especially concerning the direct injection technology at low-speed and high-load operating regimes. The occurrence of abnormal combustion modes represents the main obstacle, which prevents current engines from achieving optimized combustion phasing and higher compression ratios.

Highly-boosted Direct Injection Spark-Ignition (DISI) engines show their major weakness at low-speed and high-load operating regimes, which can present the onset of particularly violent detonation phenomena, known as super-knock or Low-Speed Pre-Ignition (LSPI) [94–96]. These phenomena prevents these engines from achieving optimized combustion phasing and higher boost pressures and compression ratios [67–69].

Such a phenomenon is significantly different from conventional knock, in which the end-gas auto-ignites ahead the spark-triggered propagating flame, because the pressure and temperature of the unburned mixture are excessively increased by the compression effect due to the thermal expansion of the burned zone (which can overlap that of the moving piston). Rapid Compression Machine (RCM) experiments [396–400] demonstrated that the mechanism of super-knock consists of hotspot-induced deflagration-to-detonation transition, followed by high-pressure oscillation. In other words, a local "hot-spot" in the combustion chamber can be the cause of a surface pre-ignition before top dead center. A pre-ignition-triggered deflagration (flame propagating at subsonic speed) starts the combustion. Then, the spark ignition occurs, and a second flame front may propagate if the spark ignition is in an unburned zone. The rapid expansion of the burned gas quickly compresses the unburned mixture to higher temperature and pressure. Finally, a second hot-spot in the end gas induces the detonation (supersonic propagating waves) of the unburned mixture at high temperature and high pressure. A single super-knock event is sufficient to severely and instantaneously damage an engine due to the extremely high peak pressure and the associated pressure oscillations involved [401]. Furthermore, super-knock events appear randomly and show little direct relationship to engine control parameters [402], so that the use of common knock suppression methods, such as retarding spark timing, cooling the intake charge, and enhancing heat transfer, are not effective ways for avoiding super-knock [403]. Therefore, super-knock is at present the major obstacle for further improving the boost level of turbo-charged SI engines.

It is generally accepted that super-knock is triggered by local pre-ignition events most likely related to lubricant-fuel interactions within the combustion chamber. In order to highlight the influence of lubricating oil in promoting early ignition, studies show that the reactivity of homogeneous stoichiometric air-fuel mixtures is too low to explain a spontaneous pre-ignition event before the timed spark event [244]. Thus, only local and stochastic heterogeneities within the air–fuel mixture or external contaminants like lubricant oil or deposits, could explain higher local reactivities for premature auto-ignition. Many studies rely on combustion visualization while the number of numerical simulations is still limited. The optical studies have highlighted that only local and stochastic heterogeneities within the air–fuel mixture, possibly induced by external contaminants,

such as oil or carbonaceous deposits, can explain the significatively higher local reactivity that causes premature auto-ignition. The long-chained hydrocarbons that compose lubricant oil have shorter Total Ignition Delay (TID), thus, their presence can locally enhance the mixture reactivity. Moreover, metal additives can also have a catalytic enhancement effect [362].

The auto-ignition tendency of engine lubricant oil received little attention in the past, because it was commonly assumed that engine lubricant effects on knock could be considered negligible due to the low amounts of lubricant oil that reach the combustion chamber. However, with modern DISI engines being developed to operate at higher loads and closer to knock limits, the reactivity of engine lubricants can significantly impact the knock behavior. Nowadays, research is making greater efforts to investigate the influence of lubricant oil on the onset of pre-ignition phenomena. However, there is still a lack of experimental data concerning fundamental characteristics of lubricant oil auto-ignition.

It must be also considered that oil contamination within the combustion chamber can represent a non-negligible source for soot particle generation, as highlighted by recent literature findings [107–110,112]. The presence of hydrocarbons with longer chains during the combustion event can enhance soot precursor formation in the reaction zone [113,114], including C_2 species, such as the ethyl radical (C_2H_5) and acetylene (C_2H_2), which are the most abundant gaseous hydrocarbon species in regions where soot is formed [59,115]. A strict correlation between soot levels and the occurrence frequency of super-knock has been observed [139–141]. Carbonaceous deposits and floating soot particles within the combustion chamber can serve as high temperature spots able to prematurely ignite the mixture. This points out a possible secondary way by which lubricant oil can promote pre-ignition phenomena. It has been demonstrated that a clean combustion chamber without carbon deposits clearly shifts to higher values the pressure level at which pre-ignition occurs [69]. Similarly, increasing spray-wall interaction strongly increases the probability of pre-ignition events [404].

Concerning GCI engines, although research has made a significant progress, the two main issues that have traditionally prevented HCCI from penetrating the automotive market still remain the difficulty in controlling combustion phasing and duration as well as the inability to achieve high loads [405]. Despite the fact that HCCI combustion is ideally described as an instantaneous and uniform autoignition event of the entire in-cylinder air-fuel mixture, in reality ignition occurs sequentially at different spatial locations throughout the mixture over a short time. The overall ignition event is initiated through "sensitive spots" randomly located throughout the combustion chamber. These spots can be either higher temperature or more reactive zones and chemical kinetics plays a crucial role in determining HCCI combustion characteristics, sensibly more than in SI or diesel engines [406–408]. Thus, local composition inhomogeneities within the in-cylinder mixture can drastically impact the extent of certain reactions within a given temperature range. Lubricant oil contamination can play a non-negligible role in affecting HCCI combustion controllability.

The creation of non-uniform high temperature combustion zones is the result of early uncontrolled local auto-ignition events [409]. The interaction between these high temperature zones can produce

excessive heat release rates and generate high-amplitude pressure waves [410,411]. Such a phenomenon is known as ringing. The ringing limit, analogously to knocking in SI engines, is one of the principal constraints to high load operation for HCCI engines. Delayed combustion timing can be used for avoiding ringing. However, misfire and cyclic variability become major constraints, curtailing its applicability [405]. Among the most promising strategies aimed at extending the high load limits of HCCI is Spark-Assisted Compression Ignition (SACI). Like in a conventional SI engine, the energy discharged by means of a spark plug initiates the process. Combustion advances by flame propagation until the unburned end gases are ignited through heating and compression from the advancing flame front in a way resembling HCCI combustion. Heat release occurs in a more controlled way than in a knock event, so that the final auto-ignition allows for long term engine operation [412,413]. In other words, SACI avoids excessive pressure-rise rates that lead to ringing, allowing to achieve higher load levels than HCCI for the same intake pressure. Local stochastic heterogeneities within the air–fuel mixture, possibly induced by lubricant oil contaminations, can lead, once again, to uncontrolled auto-ignition that renders the development of such a technology challenging.

For all the above-mentioned reasons, it is crucial to study the reaction paths involved in the combustion of lubricant oils. In the literature, there is an evident lack of dedicated research on autoignition delay times of lubricant oils. This is instead essential for developing reliable reaction mechanisms useful at predicting the onset of super-knocking phenomena, as well as soot formation in SI engines. In order to provide some tentative guidance, Kalghatgi et al. [77] analyzed the influence of the addition of n-heptane to iso-octane. It was observed that the ignition delay values were still too high for autoignition to occur at the measured pre-ignition pressures and estimated temperatures. The conclusion was that to satisfy ignition delay time and critical initiating flame size requirements, the oil would have to be somewhat more reactive than n-heptane.

This study defines a way for taking into account the presence of lubricant oil in the combustion process involving gasoline-like fuels. In particular, a detailed reaction mechanism, containing selected surrogate species for lubricant oil, is developed ad validated by means the comparison between 0D numerical simulations and experimental results reported in the literature.

4.2. Materials and Methods

An approach based both on the analysis of exiting experimental data and the accomplishment of numerical simulations was adopted. Namely, the analysis of experimental evidence available in the literature allowed the definition of hydrocarbon species suitable for reproducing oil's chemical properties in terms of ignition propensity. Once defined the surrogate species, a detailed reaction mechanism was developed and validated. In order to test the developed mechanism, 0D numerical simulations were conducted using the CHEMKIN PRO code. The closed homogeneous batch reactor model was employed for solving the time-dependent balance equations for the total mass, the gas-phase species and the energy [414]. The simulations aimed at reproducing experimental

measurements available in the literature, carried out to quantify the effect of commercial lubricants on the ignition delay time of iso-octane, selected as representative surrogate for commercial gasoline. The comparison between numerical results and experiments, allowed eventually the definition of a possible composition for a surrogate mixture of hydrocarbons that is suitable for modelling the influence of lubricant oil.

4.2.1. Surrogate Species Definition for modeling Lubricant Oil

All Chemical analyses indicate that base oils are mainly composed of C_{15}–C_{34} normal alkanes (n-paraffins) combined with other iso-alkanes and cycloalkanes [261,299]. Considering that it is known that alkanes larger than C_{14} exhibit nearly identical fuel/air gas-phase ignition delay times across a range of operating temperatures [415,416], surrogate components comprising linear or low-branched alkanes having the number of carbon atoms ranging from 15 to 20 can be considered good candidates at representing the ignition propensity and ignition kinetics of lubricant oils for engine applications.

In order to quantify the effects of oil addition on the ignition propensity of gasoline, Kuti et al. [261] carried out a fundamental experiment involving an Ignition Quality Tester (IQT), in which lubricant base oils, such as SN100 (Group I) and HC4 and HC6 (Group III), as well as a fully formulated lubricant (SAE20W50), were mixed, in the relative amounts of 1% and 10% by volume, with iso-octane (iC_8H_{18}). Successively, with the aim to provide some guidance about the choice of oil surrogate components, the same experiment was repeated by replacing the oils with $nC_{16}H_{34}$, $nC_{17}H_{36}$ and $nC_{18}H_{38}$. These species were mixed with iso-octane in the same proportions used for the oils. A comparison between the recorded trends is reported in Figure 4.1.

It is noteworthy that the addition of 1% by volume of base oils or fully formulated lubricants into 99 % by volume of iso-octane resulted in ignition delays being averagely shortened by 15%, compared to 100% iso-octane, as shown in Figure 4.1 (a) and (b), respectively. Further increase in their amount to 10% in the mixtures reduced the average total ignition delay time by up to 54%. Base oils and fully formulated lubricant highlighted a quite similar behaviour, suggesting that it is the hydrocarbon fraction that contributes primarily to enhance the reactivity, and not the inorganic or organometallic additives. This result implies that it is reasonable to neglect the additives' effect in the development of a reaction mechanism for lubricant oil. The experiments in which $nC_{16}H_{34}$, $nC_{17}H_{36}$ and $nC_{18}H_{38}$ were added to pure iso-octane showed trends that appeared to be really close to those obtained for oil lubricants. This result suggests that C_{16}–C_{18} hydrocarbons are adequate surrogates for capturing the ignition characteristics of commercial engine lubricants and thus a reaction mechanism for iso-octane, comprising such hydrocarbon species, is proposed in the present work. In particular, the model employed in the present works comprises n-$C_{16}H_{34}$ and $C_{18}H_{38-2}$ as surrogate hydrocarbon species for lubricant oil, for which accurate mechanisms are available in the literature.

4.2.2. Mechanism Development and Validation

The chemical kinetic model presented in this work aims to capture lubricant oil influence on pre-ignition occurrence in gasoline engines. It is developed starting from existing reaction mechanisms available in the literature, already validated for the species discussed in the previous section. In particular, the reduced Primary Reference Fuel (PRF) mechanism proposed by Wang et al. [384] based on 73 species and 296 reactions, was used to reproduce the behavior of iso-octane. The species and reactions involved in the mechanism developed by Sarathy et al. [416] for 2-methyl-alkanes up to C_{20} and n-alkanes up to C_{16}, containing approximately 7200 species and 31400 reactions, were added to the PRF mechanism. It must be highlighted that, unfortunately, to the authors' knowledge, no reduced mechanisms for alkanes up to C_{20} are available in the literature. Therefore, a detailed mechanism was used for those species and the resulting mechanism consists of 7182 species and 31721 reactions.

A thorough analysis of reactions and species involved in the two original mechanisms was performed in order to ensure that the merging process does not affect the agreement with the experimental data against which the starting mechanisms were originally validated. Therefore, the resulting reaction mechanism was validated against the literature data already used for validating the mechanisms by Wang et al. [384] for iso-octane and n-heptane and by Sarathy et al. [416] for 2-methylhexane, respectively.

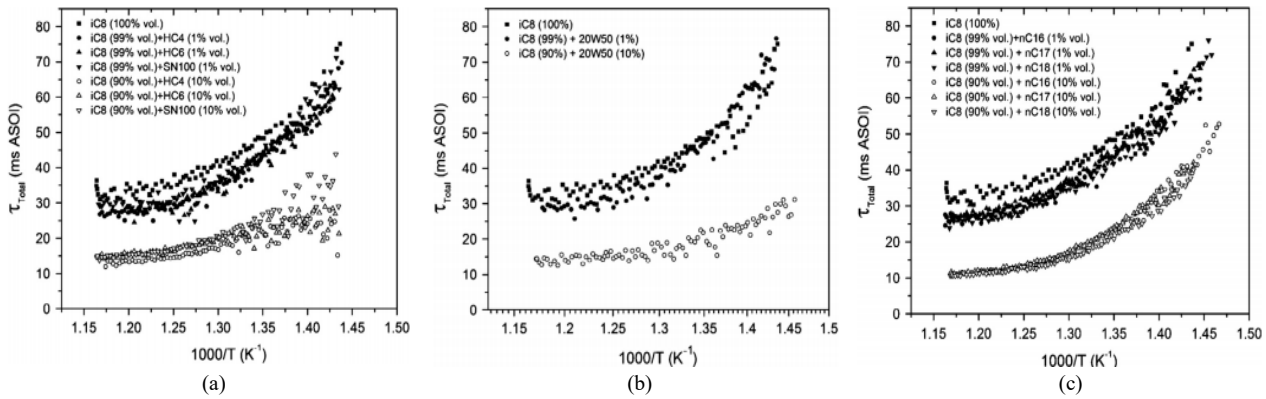

Figure 4.1. Variations of ignition delay with temperature for iso-octane and lubricant base oil mixtures, iso-octane and SAE20W50 lubricant mixtures and iso-octane and C_{16}–C_{18} n-alkanes adapted from Kuti et al. [261].

Figure 4.2 (a) shows the results in which 0D homogeneous constant-volume reactor simulations (solid lines) were performed to reproduce the shock-tube experiments carried out by Fieweger et al. [417] (marks) in the case of pure iso-octane and n-heptane. A pressure of 40 bar and stochiometric conditions were considered in this case, as it was in the experiments. Figure 4.2 (b) shows the results of 0D RCM kinetic modeling of the tests performed by Silke et al. [418], concerning 2-methylhexane. In the last case, the closed homogeneous batch reactor model was used to simulate the RCM experiments in a temperature range 600-900 K, considering a pressure of 15 atm and an equivalence ratio equal to 1. The onset of ignition was estimated as the point of maximum temperature rise (max dT/dt). In Figure 4.2 (a) and (b) the dashed lines refer to the numerical predictions obtained by using the reaction mechanisms developed by Wang et al. [384] and Sarathy et al. [416], respectively.

The results obtained by means of the proposed reaction mechanism are in good agreement with the experimental data and are close to those obtained by the numerical simulations employing the two original mechanisms. This result confirms that the merging process did not affect the ability of capturing the ignition delay trends of the pure species considered for the validation.

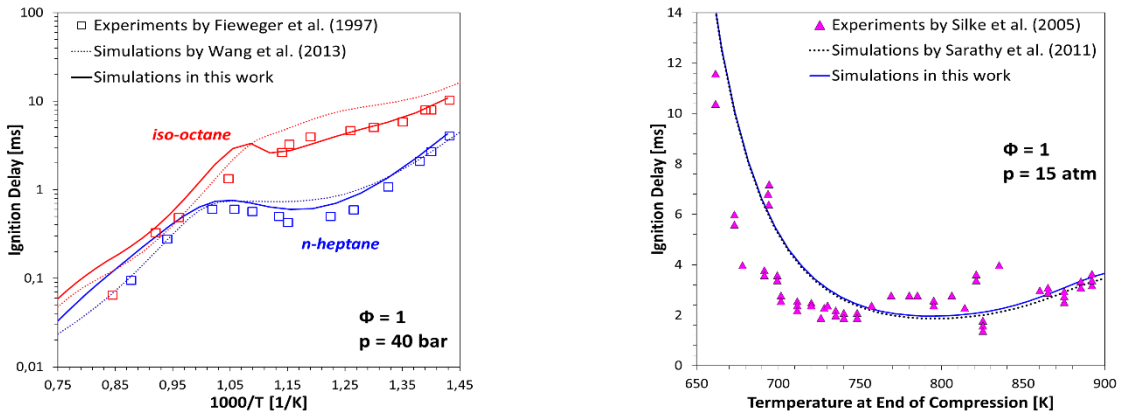

Figure 4.2. Simulations using the present mechanism (solid lines) and comparisons with literature experimental data (marks) and mechanisms (dashed lines). (a) shock-tube experiments by Fieweger et al. [417] using iso-octane and n-heptane and simulations by the PRF mechanism of Wang et al. [384]; (b) Galway RCM experiments by Silke et al. [418] using 2-methylhexane and simulations by the mechanism of Sarathy et al. [416].

4.3. Numerical Simulations

Using the proposed detailed reaction mechanism including lubricant oil surrogate components, numerical simulations were performed to test its capability of predicting the lubricant oil influence on ignition propensity of gasoline-like fuels. In order to pursue this goal, 0D simulations aimed at reproducing the experimental IQT tests, carried out by Kuti et al. [261], were performed. The same procedure used for estimating the ignition delay in the experiments was used in the numerical simulations, namely it was based on the time of maximum pressure rate rise (max dp/dt).

4.3.1. Operating Conditions

In the numerical simulations, the surrogate hydrocarbon species (n-$C_{16}H_{34}$ and $C_{18}H_{38\text{-}2}$) selected for modeling lubricant oil were mixed with iso-octane, in the amounts of 1 and 10% by volume. The ignition delay of the mixtures was calculated considering a closed homogeneous batch reactor model. In the experiments, an ambient pressure of 15 bar was maintained in an IQT with a volume of 210 cm^3. However, as the fuel was injected into the chamber vaporization took place, and the mixture temperature decreased accordingly. As a consequence, the chamber pressure decreased of about 1.5 bar [261]. Therefore, in order to reproduce the experimental conditions reached at the end of the injection process, a pressure of 13.5 bar was considered in the simulations. The fuel mass injected was kept constant and equal to 83 mg/inj. The initial temperature was varied from 650 to 900 K and

the initial mass of air in the chamber changed accordingly. As a result, the global equivalence ratio, Φ, varied from 0.82 to 1.14, as the temperature increased. For clarity, the operating conditions used in the numerical simulations are summarized in Figure 4.3. It must be highlighted that the different hydrocarbon mixture compositions are characterized by different stoichiometric air-to-fuel ratios. However, the relative amount of the species added to iso-octane was small, so that the variations of Φ with temperature for the seven considered cases coincide within plotting accuracy, as shown in Figure 4.3.

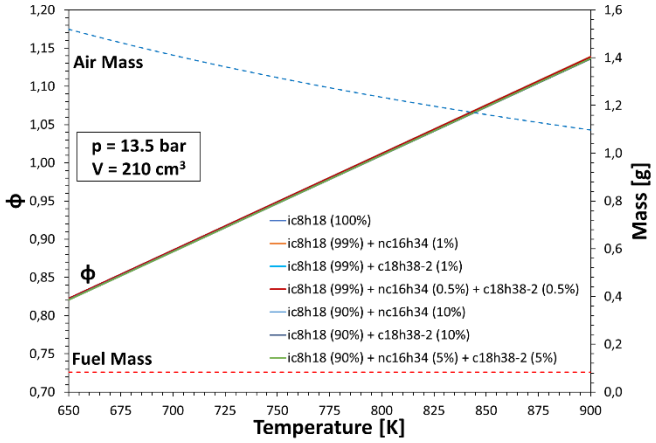

Figure 4.3. Operating conditions used in the simulations aimed at reproducing the experiments by Kuti et al. [261].

4.4. Results and Discussion

Numerical simulations were conducted to assess the accuracy of the present mechanism in predicting the percentage reduction of the ignition delay that gasoline experiences in the presence of lubricant oil contaminants. Figure 4.4 provides a comparison between the experimentally measured (marks) and the numerically predicted (lines) data about the reduction of ignition delay caused by an addition of 1 or 10% by volume of lubricant oil to iso-octane. The marks in Figure 4.4 (a) represent the average reduction measured for the different base oils employed in the experiments and previously described (see Figure 4.1 (a)). The experiments reported in Figure 4.4 (b) are related to the fully formulated lubricant oil SAE20W50 (previously shown in Figure 4.1 (b)).

Figure 4.4 shows that the averaged ignition delay reduction derived from the experiments by Kuti et al. [261] is between the values obtained by the two numerical simulations using n-$C_{16}H_{34}$ and $C_{18}H_{38-2}$ (dashed lines). This result was obtained for both the two considered volume fractions and for both base oils and the commercial lubricant oil, confirming the effectiveness of the developed mechanism in reproducing the lubricant oil effect on ignition propensity of iso-octane.

Only at low temperatures a discrepancy appears in the case of 1% volume fraction for the fully formulated lubricant oil, but one can notice that generally, the uncertainty of the experimental measurements increases at low temperatures, especially for temperatures lower than 750 K, as it is possible to infer from Figure 4.1 and from the error bars reported in Figure 4.4. Therefore, it is difficult

to ascribe the reason of such a discrepancy only to poor accuracy of the reaction mechanism in the low-temperature range. In addition, for all other cases the agreement can be considered more than satisfactory at the lower temperatures.

On the basis of these results, it was possible to determine a surrogate hydrocarbon mixture that could averagely reproduce the reactivity of lubricant oils. Namely, it was concluded that a surrogate binary mixture composed of n-$C_{16}H_{34}$ and $C_{18}H_{38\text{-}2}$, taken in the same proportions, can reproduce the higher reactivity of lubricant-fuel mixtures in comparison to that of pure iso-octane with good accuracy. Figure 4.4 also shows the results obtained from the simulations in which this surrogate mixture was mixed with pure iso-octane (red and blue solid lines). Such a mixture shows an intermediate behavior with respect to n-$C_{16}H_{34}$ and $C_{18}H_{38\text{-}2}$, in terms of ignition delay, and therefore can be reasonably assumed as a surrogate mixture capable of reproducing the effects of commercial lubricant oils on gasoline's ignitability.

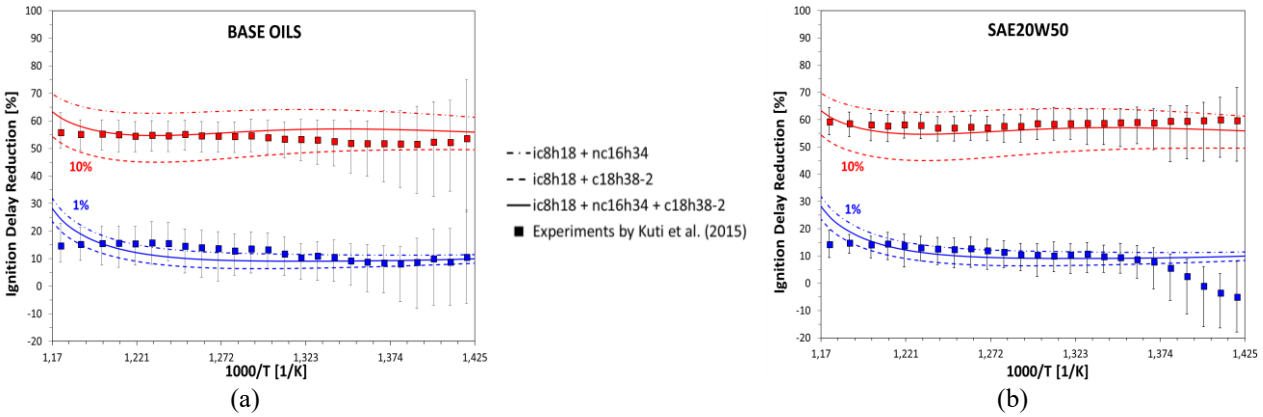

Figure 4.4. Percentage reduction in ignition delay measured by Kuti et al. [261] due to an addition to iso-octane of 1% (blue marks) and 10% by volume (red marks) of base oils (a) and fully formulated lubricant oil (b). Numerical simulations with n-$C_{16}H_{34}$ and $C_{18}H_{38\text{-}2}$ (dashed lines). Simulations with a binary surrogate mixture (50% n-$C_{16}H_{34}$ and 50% $C_{18}H_{38\text{-}2}$, by volume) added to iso-octane (solid lines).

4.5. Conclusions

The present work helps to define a way for taking into account lubricant oil presence within an engine's combustion chamber, in order to simulate its contribution to pre-ignition and soot formation processes. On the basis of experimental results available in the literature, hydrocarbons species suitable for reproducing oil's chemical reactivity were first identified. Specifically, it was found that C_{16}–C_{18} hydrocarbons can be considered adequate surrogates that are able to capture the ignition characteristics of commercial lubricant oils. Then, a detailed reaction mechanism containing the selected surrogate species was developed starting from existing mechanisms. The reduced PRF mechanism proposed by Wang et al. [384] was coupled with the mechanism developed by Sarathy et al. [416] for 2-methyl-alkanes up to C_{20} and n-alkanes up to C_{16}. The resulting mechanism consisted of 7182 species and 31721 reactions. It was validated against the same literature data used for

validating the two starting mechanisms. It was found that the merging process did not affect the ability of capturing ignition delay trends of the species considered for the validation. The results obtained by means of the proposed reaction mechanism were very close to those obtained by numerical simulations employing the two original mechanisms.

Once the surrogate species for lubricant oil were defined and the reaction mechanism validated, 0D numerical simulations were conducted in order to reproduce experimental measurements available in the literature, aimed at quantifying the effect of lubricant oils on the ignition delay of iso-octane (selected as surrogate for commercial gasoline). The simulated system was a closed homogeneous batch reactor in which n-$C_{16}H_{34}$ and $C_{18}H_{38-2}$ were mixed with iso-octane, with 1 or 10% by volume. The results showed that the percentage reduction of the ignition delay measured in the experiments was between the values obtained by the numerical simulations using n-$C_{16}H_{34}$ and $C_{18}H_{38-2}$. The results demonstrate the accuracy of the developed mechanism in reproducing lubricant oil effect on the ignition propensity of gasoline-like fuels.

Furthermore, by means of the numerical analysis, it was possible to determine a surrogate hydrocarbon mixture that could averagely reproduce the reactivity of both base oils and a fully formulated lubricant oil. In particular, it was observed that a mixture of n$C_{16}H_{34}$ and $C_{18}H_{38-2}$, in the same proportions, can emulate the chemical characteristics of a commercial lubricant oil in a satisfactory way. Future work will arrive at reducing the proposed mechanism to make it suitable for Three-Dimensional (3D) engine simulations.

Chapter 5

The Reduced "GasLube" Chemical Model

Recent research highlights the influence of the presence of lubricant oil droplets on the combustion process in Direct Injection Spark Ignition (DISI) engines. Lubricant oil is considered to be the main responsible agent for the onset of pre-ignition phenomena, which can escalate highly undesired super-knock events. Moreover, lubricant oil plays a primary role in the generation of very fine soot particle emissions. In this Chapter, a reduced reaction mechanism is developed for modeling the combustion of gasoline-oil mixtures, allowing one to simulate the variation in ignitability of gasoline-like fuels induced by the presence of lubricant oil. In this study, a single hydrocarbon species, namely n-Hexadecane (n-$C_{16}H_{34}$), is shown to reproduce lubricant oil chemical and physical characteristics. Great effort has been performed to identify the most significant reaction pathways to reduce the complexity of the chemistry mechanism and the number of variables, while maintaining the important features of detailed mechanisms, for the highest computational efficiency. The proposed reduced mechanism has been validated for a wide range of operating conditions. It is employed for 3D simulations of experimental measurements in which iso-Octane was blended with different percentages of lubricant oil and its surrogates. Operating conditions representative of those of a typical turbocharged DISI engine are considered. The very good agreement obtained in the comparison with the experimental data confirms the effectiveness of the proposed "GasLube" mechanism in reproducing lubricant oil's influence on ignition propensity of gasoline-like fuels. Furthermore, the 3D numerical simulations allowed a detailed analysis of the ignition phenomenon, providing more insight into the basic processes of lubricant oil induced pre-ignition events in DISI gasoline engines.

5.1. Introduction

Three-Dimensional (3D) Computational Fluid Dynamic (CFD) simulations play an important role towards fast development of innovative engine technologies. However, engine simulations are commonly computationally expensive. Moreover, there is an evident lack of knowledge of lubricant-oil-related auto-ignition processes in engines. In a previous work [419], a possible way for taking into account the presence of lubricant oil within the engine combustion chamber has been explored. Hydrocarbons species suitable for reproducing lubricant oil chemical reactivity were first identified. Namely, it was found that C_{16}–C_{18} hydrocarbons can be considered adequate as lubricant oil surrogates. A detailed reaction mechanism containing the selected surrogate species was developed,

which consisted of approximatively 7200 species and 32000 reactions. However, it is still prohibitive to employ such a detailed reaction mechanism in engine combustion simulations because of the unacceptably high computational resources required. Therefore, a prerequisite for studying the combustion process in engines is the availability of accurate reduced reaction mechanisms.

The aim is twofold: i) to develop a reduced reaction mechanism, including essential lubricant oil pathways, useful to predict the onset of pre-ignition phenomena in gasoline engine simulations; ii) to perform accurate 3D numerical simulations using the proposed reduced mechanism, providing a detailed study of the auto-ignition process of gasoline/oil mixtures. The proposed, so-called, "GasLube" mechanism is extensively validated in conditions representative of those of a typical turbocharged DISI engine. Namely, 3D CFD simulations aimed at reproducing the experimental study by Kuti et al. [261], in which iso-Octane (i-C_8H_{18}) was blended with different percentages of either fully formulated lubricant oil (SAE 20W50) or base oils or n-Hexadecane (n-$C_{16}H_{34}$) and injected in an Ignition Quality Tester (IQT). Finally, a thorough analysis of the 3D numerical results, with a particular focus on the study of the pressure traces and of the Heat Release Rate (HRR), is used to explain the role of lubricant oil on the reduction of the TID time of the mixture.

5.2. The Chemical Model

The proposed reduced reaction mechanism is based on the detailed reaction mechanism developed in a previous work [419], composed of 7182 species and 31721 reactions. Such a mechanism represents a first step in the development of a numerical tool able to model the chemical effects of lubricant oil involved in the combustion process of a gasoline engine.

Iso-Octane was selected as surrogate for gasoline. Considering that the ignitability of iso-Octane alone cannot explain the occurrence of pre-ignition phenomena, the need for surrogate species for lubricant oil represents a crucial aspect. Kalghatgi et al. [77] highlighted that n-Heptane (n-C_7H_{16}) TID values are still too high for accomplishing this. Therefore, in order to match TID times and critical flame start requirements of pre-ignition phenomena a "simple" Primary Reference Fuel (PRF) mechanism cannot produce satisfactory results. Lubricant oil is more reactive, and a dedicated analysis aimed at determining appropriate surrogate species is needed. Chemical analyses indicate that base oils are mainly composed of C_{15}–C_{34} normal alkanes (n-paraffins) combined with other iso-alkanes and cycloalkanes [261,299]. Considering that it is known from the literature that alkanes larger than C_{14} exhibit nearly identical fuel/air gas-phase TID times across a range of operating temperatures [415,416], surrogate components comprising linear or low-branched alkanes having the number of carbon atoms ranging from 15 to 20 were considered good candidates to represent the ignition propensity and ignition kinetics of lubricant oil.

The results of [419] showed that mixtures of n-Hexadecane (n-$C_{16}H_{34}$) and 2-methyl-Heptadecane ($C_{18}H_{38}$-2) can emulate the chemical characteristics of a commercial lubricant oil satisfactorily.

Although an optimal composition for such a mixture was obtained, the need to drastically reduce the mechanism size compelled the idea of using only one surrogate species for lubricant oil. The results obtained with this approach are still acceptable and the accuracy reduction negligible. This is possible because variation in the composition produced relatively small variations in the TID values, which were comparable to experimental uncertainties. Therefore, the selection of n-Hexadecane as a surrogate species for lubricant oil is considered to be a reasonable compromise in the present work.

As done in [419], the reduced PRF mechanism developed by Wang et al. [384], consisting of 73 species and 296 reactions, is selected for describing iso-Octane chemistry. This mechanism is merged with the detailed Lawrence Livermore National Laboratory (LLNL) mechanism, developed by Sarathy et al. [416] for 2-methylalkanes from C_7 to C_{20} and n-alkanes from C_8 to C_{16}, containing approximatively 7200 species and 31400 reactions, in order to include n-Hexadecane reaction paths for reproducing the lubricant oil contribution. The two mechanisms share a core composed of H_2/O_2 and H_2/CO sub-mechanisms, and they have in common the reaction paths for species with number of carbon atoms ranging from one to seven. A semi-automatic procedure was adopted in the merging process.

With the aim of rendering such a mechanism suitable for practical simulations, in the present work, a systematic reduction was performed. The unimportant species and reaction pathways were identified and eliminated, while the main features of the detailed scheme were preserved. The complexity of the mechanism, as well as the number of variables, were drastically reduced, so that a smaller computational cost is demanded. The Directed Relation Graph method with Error Propagation (DRGEP) and the Full Species Sensitivity Analysis (FSSA) were employed by means of the use of the CHEMKIN PRO software [420]. The DRGEP (a variant of the Directed Relation Graph (DRG) method), is considered the most effective skeletal mechanism reduction method among those operating through species removal. DRGEP not only uses a straightforward and effective treatment strategy but also requires significantly less computational cost [421]. Briefly, by fixing a group of target species, the method estimates the importance of the remaining species in contributing to their formation. The detailed mechanism was incrementally reduced and once the desired level of simplification was achieved, the FSSA allowed us to further reduce the mechanism. In this latter case, the most important species for iso-Octane, n-Heptane and n-Hexadecane (which were the main species in the original mechanisms) were retained. In all the performed reduction steps, a range of temperatures spanning from 500 to 1500 K, a range of pressures from 10 to 80 bar and a range of equivalence ratios from 0.5 to 3 were covered.

Once the reduction procedure was concluded, Zero-Dimensional (0D) simulations were performed to validate the obtained simplified mechanism. Namely, TID results obtained with the reduced mechanism were compared with those obtained by employing the two original mechanisms. The closed homogeneous batch reactor model was employed for solving the time-dependent balance equations for the total mass, the gas-phase species and the energy. The operating conditions for this validation considered the equivalence ratio ranging between 0.8 and 2.0, the pressure from 10 to

$25\ bar$ and the temperature from 650 to $870\ K$. The results of this simulations are discussed in detail in the Results section.

5.3. 3D Numerical Simulations

5.3.1. Governing Equations and Numerical Method

Numerical simulations were performed by solving the 3D Reynolds-Averaged Navier-Stokes (RANS) equations for compressible reacting flows, closed by the renormalization group (RNG) k-epsilon turbulence model [422] using the CONVERGE™ CFD v.2.4 software [423]. A second-order-accurate upwind finite-volume spatial discretization method is employed in conjunction with the pressure-implicit splitting of operators (PISO) algorithm. Second-order-accurate implicit time integration is used, with variable time step sizes determined on the basis of the Courant-Friedrichs-Lewy (CFL) number and other physical time step constraints for the spray, evaporation and combustion processes [424]. A Lagrangian particle tracking method, combined with standard spray breaking models, is employed to represent the spray dispersion and subsequent evaporation processes. The Eulerian gas-phase transport equations are solved in a fully coupled way with the Lagrangian droplet tracking technique [424].

The spray is modeled using the Kelvin-Helmholtz and Rayleigh-Taylor (KH-RT) model [425,426]. The Rayleigh-Taylor model without breakup length and without distribution is used for breakup of the liquid spray [427]. The breakup models are tuned to better represent the spray behavior (penetration and evaporation) of the injector; in particular, the Rayleigh-Taylor time-constant, C_τ, was decreased to adjust the liquid penetration length. At low values of C_τ, small drops evaporate quickly while larger drops coalesce together causing clumps that remain as liquid for a long period of time [428]. A value of 0.1 is therefore set for C_τ. Finally, the Frossling model including the boiling model is employed [429] for determining the rate of change of droplet radius due to vaporization of fuel.

Wall heat loss is accounted by the model proposed by O'Rourke and Amsden et al. [430]. The Rosin–Rammler injection size distribution models, applied to newly created child drops for improving the drop size distribution predictions, based on the Sauter Mean Diameter (SMD) set equal to $120\ \mu m$, is used with a distribution parameter of 3.5 for the modified KH-RT break-up models. Furthermore, the dynamic drag model was implemented by determining the droplet drag coefficient dynamically, accounting for variations in the drop shape through a drop distortion parameter. The effect of the turbulent flow on spray drops is modeled using O'Rourke's turbulent dispersion model [431].

Droplet collisions significantly affect the liquid spray penetration length. The O'Rourke collision model [431] and the No-Time-Counter method [432] are employed, together with the O'Rourke Collision Outcomes [432]. Infinite thermal conductivity is used, considering uniform temperature distribution inside the droplets and assuming the droplets impinging on the wall to rebound into the chamber [433].

The chemical reaction closure was implemented by a multi-zone combustion model based on the well-stirred reactor assumption that groups computational cells based on temperature and equivalence ratio of $5\ K$ and $0.05 \cdot \phi$ increments [434,435].

5.3.2. Computational Domain and Operating Conditions

The IQT is a bench-scale device, designed for the direct measurement of liquid fuel TID times, under thermodynamic conditions in DISI engines. It consists of a constant volume combustion chamber with external electrical heating elements. The experimental procedure follows the standard test of ASTM D6890-08.

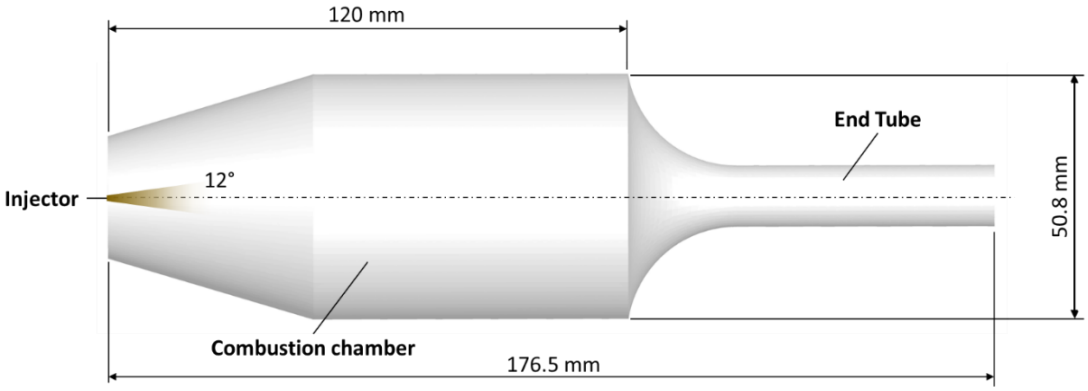

Figure 5.1. Computational domain employed in the simulations reproducing the experimental study by Kuti et al. [261] and used for the 3D validation of the reduced mechanism in engine-like conditions.

The computational domain considered in the present study to model the IQT device is shown in Figure 5.1. It reproduces the IQT facility employed by Kuti et al. [261]. The IQT has a total volume capacity of $0.213\ l$ and is composed of a constant volume combustion chamber, terminating with a narrow "end tube" region. The fuel is injected in the combustion chamber by means of a single-hole inward opening pintle nozzle injector.

The IQT was employed to evaluate the reduction of iso-Octane TID time due to the presence of lubricant oil. In the reference experiments, high molecular weight hydrocarbons such as n-Hexadecane, n-Heptadecane (n-$C_{17}H_{36}$), and n-Octadecane (n-$C_{18}H_{38}$) were selected as surrogates of lubricant base oil constituents and mixed with iso-Octane (gasoline surrogate) in proportions of 1 and 10% by volume. Alternatively, lubricant base oils such as SN100 (Group I) or HC4 or HC6 (Group III) or a fully formulated lubricant (SAE 20W50) were mixed with iso-octane in the same proportions. In our simulations, n-Hexadecane was mixed with iso-Octane in the same volume proportions considered in the work by Kuti et al. [261]. The comparisons with the experiments were performed concerning not only this pure species, but also lubricant base oils and fully formulated lubricant oil SAE 20W50.

Kuti et al. [261] measured TID times at an initial pressure of $15\ bar$, which is similar to the pressure at ignition in a typical turbocharged DISI engine. A temperature range of $680–873\ K$ was considered in those experiments [261]. The same initial pressure considered in the experiments by Kuti et al.

[261] and four different air temperatures, namely $730, 770,\ 800$ and $833\ K$, were considered in the simulations, as shown in Table 5.1, which summarizes the operating conditions used for the present simulations. A total fuel mass of $83\ mg$ was injected in $2\ ms$ with a square profile [436]. Following the approach used by Mubarak Ali et al. [436], the injector was modeled imposing: a nozzle diameter equal to $1.1\ mm$; a spray cone angle of $12°$; a sheet thickness of $0.27\ mm$; and a circular injection radius equal to $0.48\ mm$. The nozzle discharge coefficient, C_D, was set to 0.79 [436] and a correlation for the coefficient of velocity, C_V, was used as well. The global equivalence ratio varied according to the initial temperature as discussed in [419]. The TID time was evaluated from pressure data by means of the gradient method, following the procedure described in Appendix A.

Table 5.1 Operating conditions considered in the simulations used for the 3D validation of the reduced mechanism for reproducing the experiments by Kuti et al. [261].

Initial composition	$21\%\ O_2, 79\%\ N_2$
Initial pressure	$15\ bar$
Initial temperatures	$730, 770, 800, 833\ K$
Fuel surrogate species	Iso-Octane
Lubricant oil surrogate species	n-Hexadecane
Lubricant oil mixed with fuel	$0\%, 1\%, 10\%$
Fuel injection duration	$2\ ms$
Fuel mass	$83\ mg$

5.3.3. Model Validation

The IQT simulations involve the modeling of a liquid spray injection followed by evaporation and mixing processes. Simultaneously, chemical reactions take place. The associated TID time is strongly influenced by the spray-related phases because this influence the thermodynamic conditions and determine the equivalence ratio distribution within the chamber. Therefore, for reliable TID predictions, it is of fundamental importance to ensure a proper modeling of both physical and chemical phenomena involved in the IQT simulations. An accurate study for ensuring grid independency of the solution was conducted and it is reported in Appendix B. The overall numerical method was verified by preliminary simulations of an IQT experiment by Mubarak Ali et al. [436] employing an existing mechanism for pure iso-Octane, namely, the skeletal PRF mechanism (56 species and 169 reactions) developed by Liu et al. [386]. The resulting parameter set for both the dynamic mesh discretization and the spray models are summarized in Table 5.2. The mesh for the entire domain is shown in Figure 5.2 at $0.5\ ms$ after the start of the injection. The maximum number of cells before ignition was 274828 (obtained $2.3\ ms$ after the start of the injection).

Figure 5.3 reports the predicted pressure trace. In the same figure, the experimental pressure trace by Mubarak Ali et al. [436] used for the validation is shown for comparison (dashed black line). A TID of $34.4\ ms$ was obtained in the simulation which is comparable to the value derived from the experimental data, which was about $34.8\ ms$.

Table 5.2 List of the parameters set for both the dynamic discretization and the spray models.

Simulation Parameters	Values
KH-RT spray models	
KH Breakup model size constant (B_0)	0.61
KH Breakup model velocity constant (C_1)	0.188
KH Breakup model time constant (B_1)	7
RT model time constant (C_τ)	0.1
RT model size constant (C_{RT})	0.1
Shed factor	1.0
New parcel cutoff	0.05
Number of injected parcels (n_p)	50000
Dynamic discretization	
Base grid size (dx_{base})	1 mm
Local grid size with AMR (dx_{AMR})	0.5 mm
AMR velocity sub-criterion	0.5 m/s
AMR temperature sub-criterion	375 K

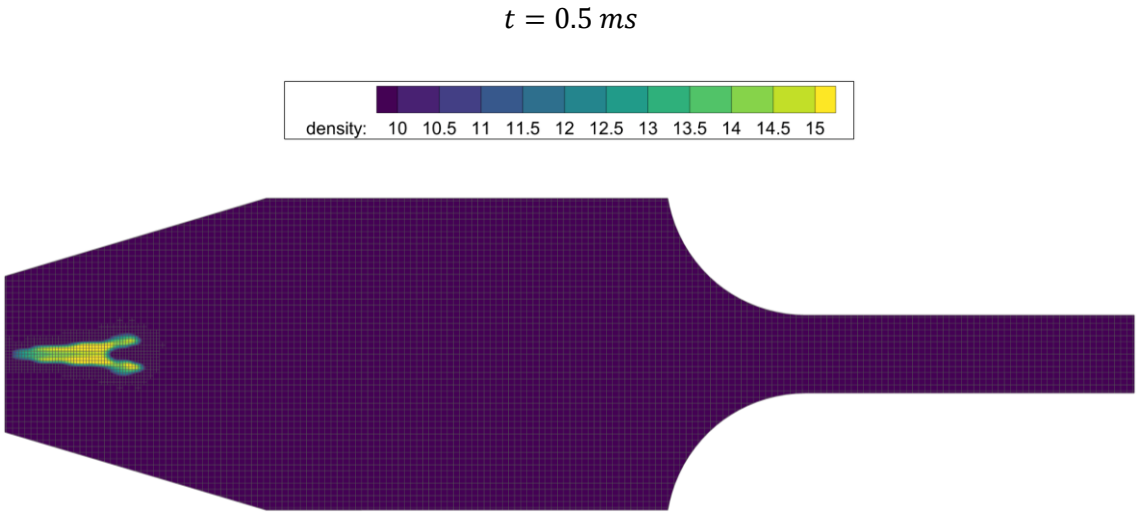

Figure 5.2. Dynamic discretization of the entire domain, depicted at $0.5\ ms$ after the start of the injection. A density contour plot is superimposed on the grid for spray comparisons.

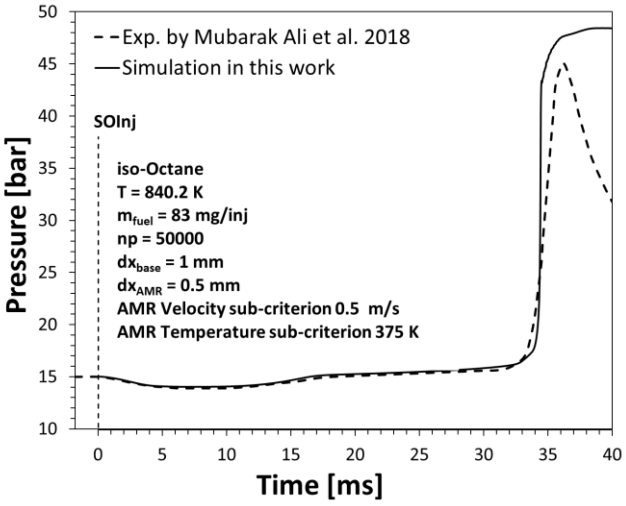

Figure 5.3. Comparison between the numerical pressure trace (solid black line) and the experimental one by Mubarak Ali et al. [436] (dashed black line).

The IQT facility is not equipped with optical access, thus there were not any spray images reported in the work by Kuti et al. [261]. However, a common practice for visualizing the spray consists in conducting open-air experiments, in which pressure and temperature ambient conditions are considered, while the injection pressure and the needle lift are kept in operating conditions similar to those used during the normal operation [436–438]. Therefore, in order to provide further validation of the iso-Octane spray modeling, a qualitative comparison with the optical images of the open-air experiments reported in the work by Mubarak Ali et al. [436] was performed.

In the analysis of these optical spray images, it is essential to consider the typical variability observable in the spray pattern, due to some intrinsic aspects of the experimental procedure. For instance, it is well known that needle oscillations during the injection event can affect in a non-negligible way the hollow cone angle of the spray [437]. In the spray images by Mubarak Ali et al. [436], it was observed that the spray axis resulted tilted downwards of about 7° with respect to the IQT symmetry axis. Thus, the optical images were rotated counterclockwise by 7° for aligning the spray axis with the IQT symmetry axis. The cone angle of the spray was found to be 12° in the images selected for the present comparison and this value was the same reported by Mubarak Ali et al. [436].

Figure 5.4 reports the comparison performed at ambient pressure and temperature with the post-processed spray images by Mubarak Ali et al. [436]. The numerical results are represented in the upper half planes by the density iso-surface at $1.18\ kg/m^3$, value that encloses the spray-related region. A satisfactory agreement was obtained in the comparison of the spray behavior, as it is also possible to observe in Figure 5.5, which depicts the measured and the predicted spray penetration length.

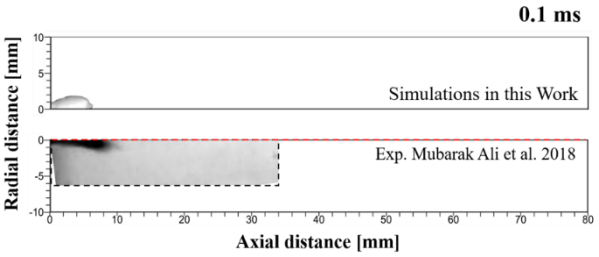

(a)

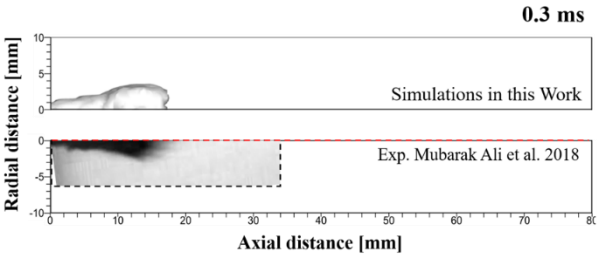

(b)

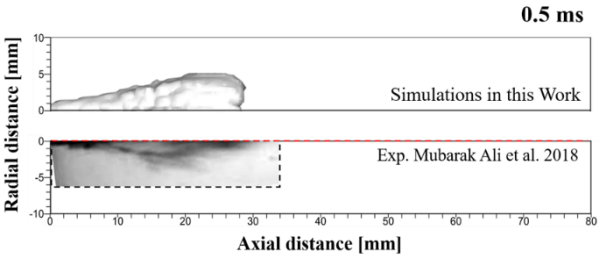

(c)

Figure 5.4 Comparison between the numerical simulations performed at ambient pressure and temperature initial conditions and the spray images from the experiments by Mubarak Ali et al. [436].

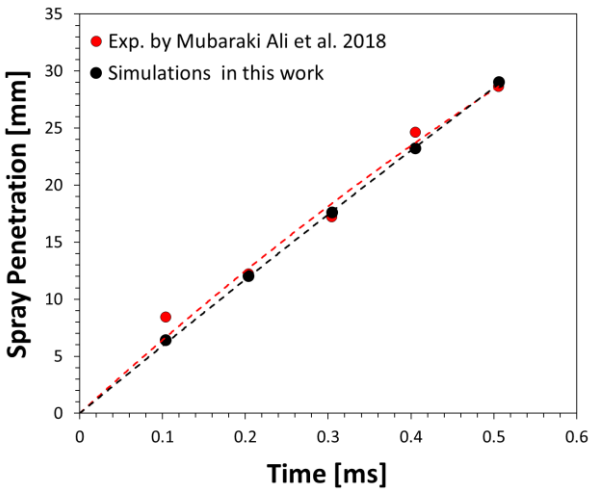

Figure 5.5 Measured (red markers) and predicted (blue markers) spray penetrations.

5.4. Results and Discussion

The reduced reaction mechanism is first presented and 0D simulations are performed to demonstrate its accuracy in comparison to the detailed mechanism in a wide range of conditions. Then, the results of 3D simulations that reproduce the IQT experiments by Kuti et al. [261] are discussed, demonstrating and explaining the reduction of iso-Octane TID time due to lubricant oil (or its surrogates) addition in engine-like conditions.

5.4.1. Reduced Chemical Mechanism Optimization and Validation

A first reduction step was performed considering the following target species in the DRGEP method: n-C_7H_{16}, n-$C_{16}H_{34}$, C_2H_2, CO, i-C_3H_7CHO, N_2, OH, CO_2, H_2O_2, HO_2, H_2O. The resulting reduced version of the mechanism consisted of 1740 species and approximatively 10000 reactions. For a further reduction, the FSSA was performed retaining the most important species for i-C_8H_{18}, n-C_7H_{16} and n-$C_{16}H_{34}$, which were the main species considered and a final reduced mechanism consisting of 522 species and 2277 reactions was obtained.

In order to guarantee that the reduction operation did not affect the mechanism accuracy, the results obtained with the present reduced version of the mechanism were directly compared with those obtained by the two original mechanisms. Figure 5.6 compares TID values for i-C_8H_{18} obtained with the present reduced mechanism with those obtained by using the PRF mechanism by Wang et al. [384]. Figure 5.7 compares the results of the present reduced mechanism with those of the detailed LLNL mechanism by Sarathy et al. [416] with respect to n-$C_{16}H_{34}$. The reduction procedure has non-negligible impacts on the results. Figure 5.6 shows that the (non-optimal) reduced mechanism (dashed black lines in Figure 5.6) tends to overestimate i-C_8H_{18} TID times in comparison to the PRF mechanism by Wang et al. [384] (dashed red lines in Figure 5.6), especially in the high-temperature range (temperatures higher than $775\ K$). Figure 5.7 shows that, although less pronounced, a generalized overestimation of the n-$C_{16}H_{34}$ TID is obtained as well with the (non-optimal) reduced mechanism (dashed black lines in Figure 5.7) in comparison to the detailed LLNL mechanism by Sarathy et al. [416] (dashed red lines in Figure 5.7).

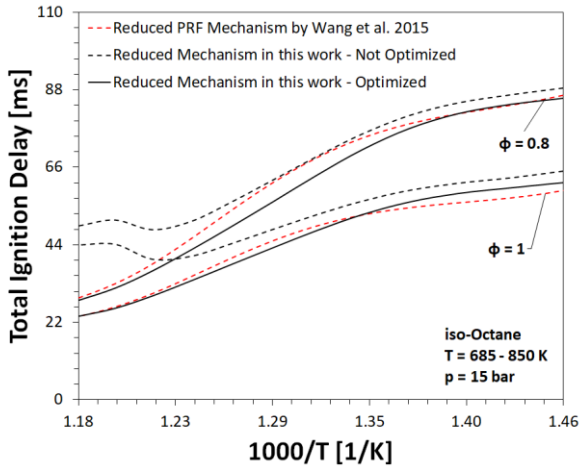

Figure 5.6 TID values for Iso-Octane (i-C_8H_{18}) obtained from 0D homogeneous batch reactor simulations employing the reduced mechanism before (dashed back lines) and after the optimization process (solid black lines) and the PRF mechanism by Wang et al. [384] (dashed red lines).

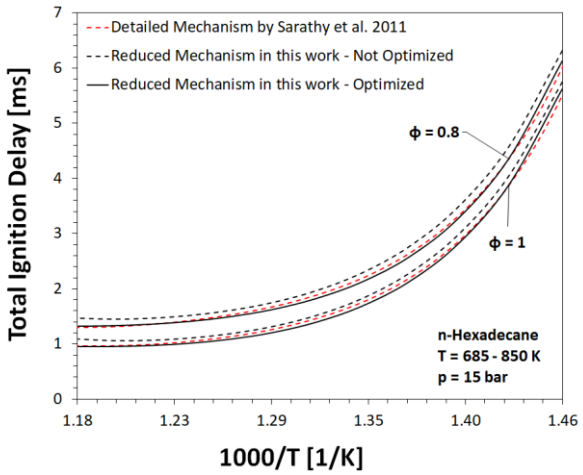

Figure 5.7 TID values for n-Hexadecane (n-$C_{16}H_{34}$) obtained from 0D homogeneous batch reactor simulations employing the reduced mechanism before (dashed back lines) and after the optimization process (solid black lines) and the mechanism by Sarathy et al. [416] (dashed red lines).

The operating conditions reported in Figure 5.6 and Figure 5.7 reproduce the IQT operating range considered in the experiments by Kuti et al. [261]. In Table 5.3 and Table 5.4 the main reactions considered for the tuning procedure are reported for i-C_8H_{18} and n-$C_{16}H_{34}$, respectively. Reaction R1 was used to tune the mechanism at high temperatures, while reaction R2 contributes to globally shift either downwards or upwards the TID curves, because it governs the initiation stages of i-C_8H_{18} oxidation due to OH radicals, which are highly reactive chemical intermediates. In this way it is possible to globally control the i-C_8H_{18} consumption rate. At low temperatures the a-C_8H_{17} radical undergoes the typical low temperature branching reaction pathways, and the reactions R3, R4, R5, R6 were used to tune the reactivity of i-C_8H_{18} at intermediate and low temperatures. The reactions R7, R8, R9 were used to tune the reactivity at the lowest temperatures. Moreover, the reaction rate constants of reaction R10 were adjusted to control the reactivity of i-C_8H_{18} at low temperature as

well, because the a-C_8H_{17} radical decomposition competes with the low temperature branching reactions as the temperature increases.

Table 5.3 Reaction Rate Constants optimized for iso-Octane. The Arrhenius temperature dependence $\left(k = AT^b e^{-\frac{E_a}{RT}}\right)$ is considered.

	Reaction	A	b	E_a
R1	i-C_8H_{18} = t-C_4H_9 + i-C_4H_9	4.828 e^{20}	-3.925	8.415 e^{04}
R2	i-C_8H_{18} + OH = a-C_8H_{17} + H_2O	0.625 e^{07}	1.800	1.431 e^{03}
R3	a-$C_8H_{17}O_2$ = a-$C_8H_{16}OOH_{-b}$	2.000 e^{11}	0.000	2.045 e^{04}
R4	i-C_8eter_{ab} + OH = i-C_4H_8 + i-C_3H_7CO + H_2O	1.250 e^{25}	0.000	0.000 e^{00}
R5	a-$C_8H_{16}OOH_{-b}O_2$ = a-$C_8H_{16}OOH_{-b}$ + O_2	1.200 e^{23}	-2.357	3.728 e^{04}
R6	a-$C_8H_{16}OOH_{-b}O_2$ = i-C_8ket_{ab} + OH	2.350 e^{10}	0.000	2.100 e^{04}
R7	i-C_8ket_{ab} = i-C_3H_7CHO + t-C_3H_6CHO + OH	4.000 e^{15}	0.000	3.900 e^{04}
R8	i-C_8ket_{ab} = $C_6H_{13}CO$ + CH_2O + OH	3.980 e^{10}	0.000	4.300 e^{04}
R9	a-C_8H_{17} = C_3H_7 + C_3H_6 + C_2H_4	1.117 e^{14}	-1.270	2.970 e^{04}
R10	a-C_8H_{17} = i-C_4H_8 + i-C_4H_9	6.090 e^{02}	2.480	8.520 e^{03}

Table 5.4 Reaction Rate Constants optimized for n-Hexadecane. The Arrhenius temperature dependence $\left(k = AT^b e^{-\frac{E_a}{RT}}\right)$ is considered.

	Reaction	A	b	E_a
R11	n-$C_{16}H_{34}$ + OH = $C_{16}H_{33-5}$ + H_2O	7.000 e^{10}	1.61	-3.500 e^{1}
R12	n-$C_{16}H_{34}$ + HO_2 = $C_{16}H_{33-5}$ + H_2O_2	2.800 e^{2}	3.37	1.372 e^{4}
R13	$C_{16}H_{33}O_{2-5}$ = $C_{16}OOH_{5-7}$	4.500 e^{14}	0.00	2.045 e^{4}
R14	$C_{16}ket_{5-7}$ = OH + n-$C_4H_9COCH_2$ + n-$C_9H_{19}CHO$	1.250 e^{15}	0.00	3.900 e^{4}

The A-Factor values for reactions R11 and R12 were modified in order to regulate H_2O and H_2O_2 formation due to H-atom abstraction from n-$C_{16}H_{34}$ by HO_2 and OH radicals. It is worth mentioning that H-atom abstraction reactions due to these two radicals occur at both low and high temperatures. Moreover, the reaction rate constants of the reactions R13 and R14 were modified to improve the TID timing prediction at intermediate and low temperatures.

The improvements achieved with the optimization procedure are seen in Figure 5.6 and Figure 5.7. The curves related to the optimized reduced mechanism (solid black lines) appear much closer to the targeted ones (dashed red lines). The final results obtained after the reduction and the tuning procedures are shown in Figure 5.8 and Figure 5.9 for iso-Octane and n-Hexadecane, respectively. The results can be considered satisfactory considering that the number of species was reduced by about 93%, while accuracy was preserved in a wide range of operating conditions, in terms of temperature, pressure and equivalence ratio.

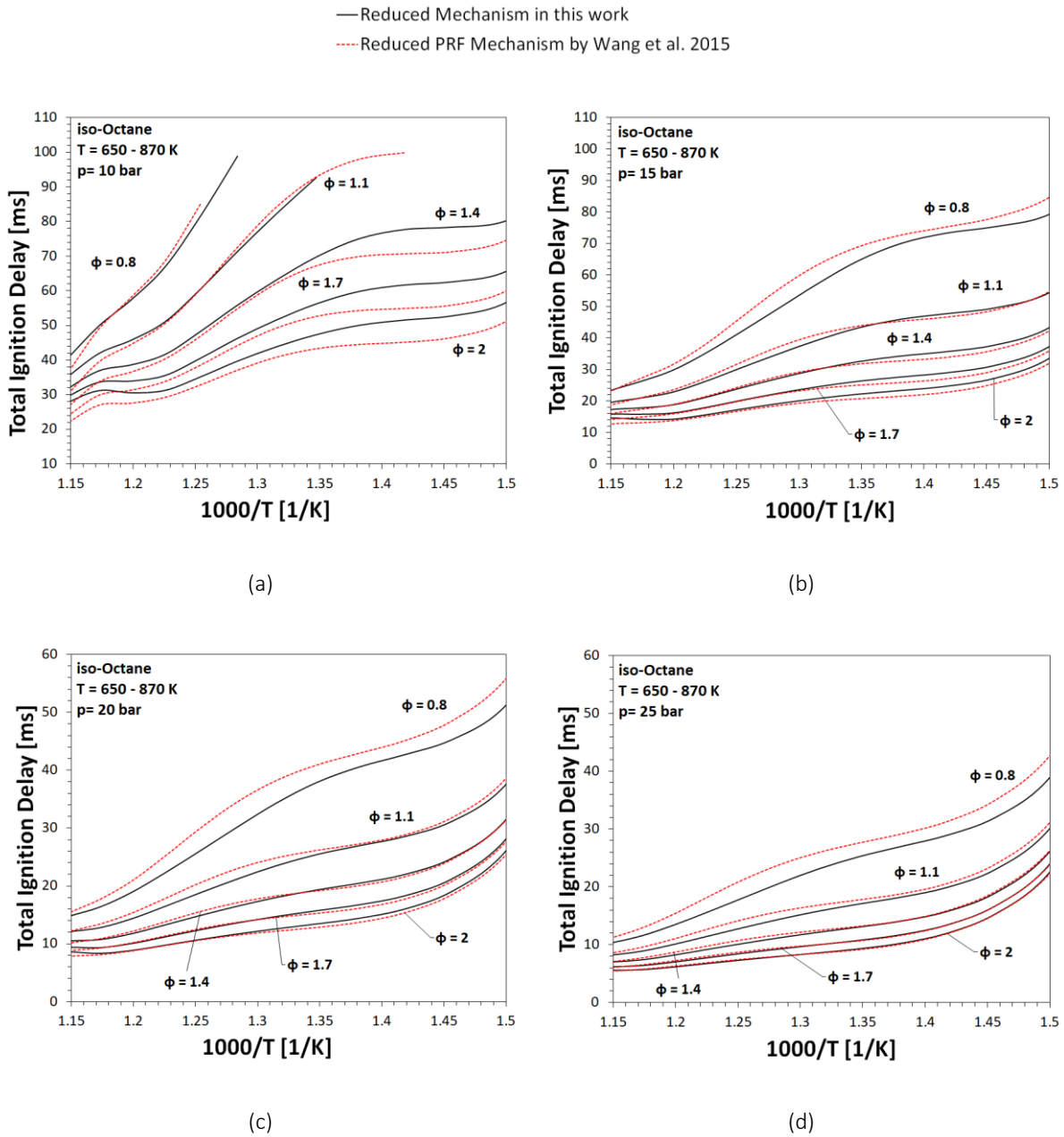

Figure 5.8 TID values for Iso-Octane obtained from the 0D homogeneous batch reactor simulations performed to validate the present reduced mechanism (solid black lines) against the PRF mechanism by Wang et al. [384] (dashed red lines), over a wide range of operating conditions.

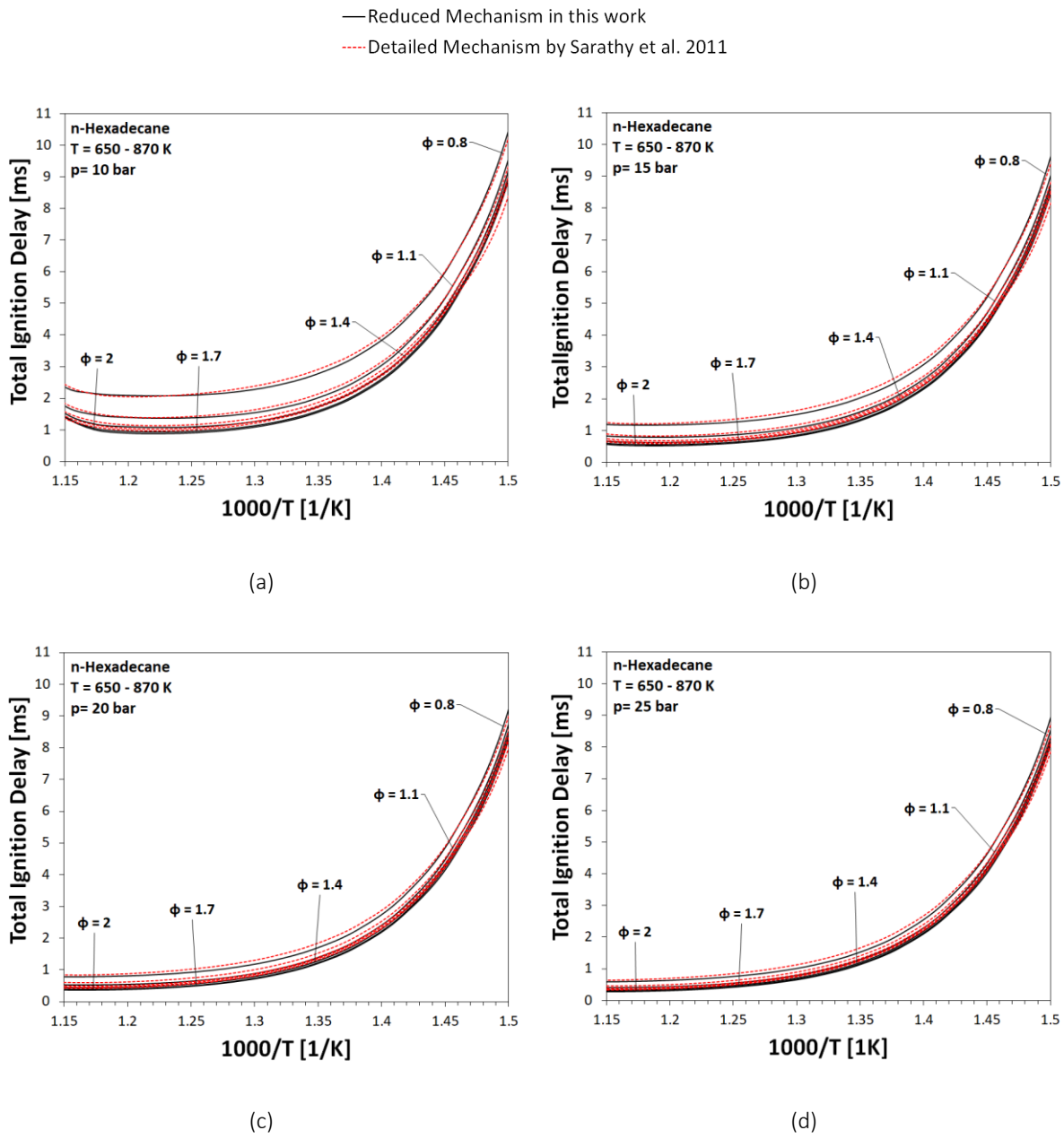

Figure 5.9 TID values for Iso-Octane obtained from the 0D homogeneous batch reactor simulations performed to validate the present reduced mechanism (solid black lines) against the mechanism by Sarathy et al. [416] (dashed red line), over a wide range of operating conditions.

5.4.2. Results Three-Dimensional Simulations in Engine-like Conditions

The obtained reduced mechanism makes it possible to predict the occurrence of lubricant oil induced pre-ignition phenomena in SI engines. This happens especially in the case of high boost GDI engines, in which the highly undesirable super-knock events are related to lubricant oil in the combustion chamber. Therefore, it was of interest to test and validate such a mechanism in conditions that can be considered relevant for a practical engine application. 3D CFD simulations, involving spray formation and mixing processes were performed to this purpose. This was possible due to the

reduced size of the mechanism obtained in this work. In previous work [419], only 0D simulations were carried out. In the present work, the numerical results are directly compared with the measured TID values obtained by varying the lubricant oil (or rather the selected surrogate species) amount added to iso-Octane in IQT tests with the operating conditions of Table 5.1.

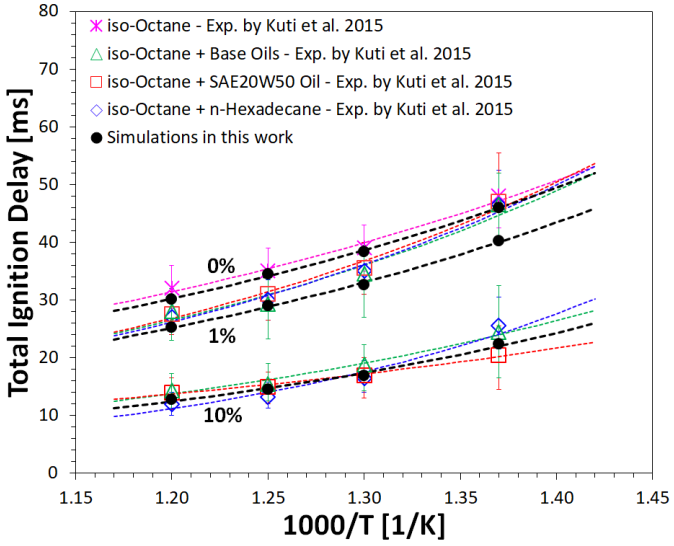

Figure 5.10 Comparison between the experimental data by Kuti et al. [261] and the results obtained from the 3D simulations. The plot reports the effect on the iso-Octane TID due to the percentage of lubricant oil (or an its surrogate species).

The comparison between the 3D simulations and the experimental data by Kuti et al. [261] is reported in Figure 5.10 for the three different levels of either lubricant oil or it surrogates, namely 0, 1 and 10% by volume in iso-Octane. The open symbols represent the average values of the TID measured for pure iso-Octane (purple stars), for mixtures of iso-Octane and base oils (green triangles), for mixtures of iso-Octane and fully-formulated oil SAE20W50 (red squares), and for mixtures of iso-Octane and pure n-Hexadecane (blue diamonds), respectively. The error bars reported on the same graph provide the range of uncertainty of the experimental data. A single average value for the three base oils investigated in the experiments was considered in this analysis, because no significative differences were highlighted in the experimental work. The results obtained from the IQT simulations employing n-Hexadecane as oil surrogate are reported also in Figure 5.10 as solid black circles. A more than satisfactory agreement with the experimental data is obtained, and not only with reference to the pure species. In fact, the experiments with n-Hexadecane appeared to be really close to those obtained with base and fully formulated oils. These findings imply that it is reasonable to neglect the additives' effect in the development of the reaction mechanism for lubricant oil. Namely, it is the hydrocarbon fraction that contributes primarily to enhance the reactivity, and not the inorganic or organometallic additives. And the hydrocarbon fraction can be modeled with a single surrogate species, namely the n-Hexadecane.

In the comparison, only for the case of 1% by volume of the added chemical compound, does a discrepancy appear at the lower temperatures. However, it must be highlighted that the uncertainty of the experimental measurements increased as the temperature decreased [261,419], and this was

especially true for temperatures lower than 750 K in the case of the measurements by Kuti et al. [261]. Furthermore, the low amount itself of lubricant to be added to iso-Octane might also have represented an additional uncertainty source, when only 1% by volume was considered. With 10% by volume, the variability observed in the data reported by Kuti et al. [261] was generally lower. Therefore, it is difficult to ascribe the reason of such a discrepancy to the reaction mechanism in the low-temperature range.

A more detailed analysis of the variation of the TID with the volume percentage of lubricant added to iso-Octane is reported in Figure 5.11 for each of the temperatures considered. For the cases at 833, 800 and $770\ K$ (Figure 5.11 (a), (b) and (c), respectively), all the trend lines are very close to each other and thus the numerical results are in good agreement not only with the pure n-Hexadecane case, but also with those relative to the base and the fully formulated lubricant oils. For the case at $730\ K$ (Figure 5.11 (d)), a larger variability in the obtained trend lines is observed. Furthermore, the points relative to the case with 1% concentration show the largest distance from the corresponding exponential trend lines.

As observed by Kuti et al. [261], adding 1% by volume of lubricant oil to iso-Octane reduces the iso-Octane TID by averagely 15%. An increase of lubricant oil amount to 10% further reduces the average TID time by up to 54%. Figure 5.11 points out that, independently of the temperature, the TID reduction due to lubricant oil addition follows an exponential behavior. Small amounts of lubricant oil significantly reduce the iso-Octane TID, while increasingly larger amounts lead to a plateau value, tending to the n-Hexadecane TID value in those conditions. These results highlighted that even trace amounts of lubricant oil can drastically affect iso-Octane ignitability propensity. This confirms the main role that lubricant oil might play in triggering pre-ignition events in the engine combustion chamber, especially at high-boost conditions.
Figure 5.10 and 4 highlight that a single pure species, n-Hexadecane, can be employed as surrogate species in engine simulations involving the modeling of lubricant oil, and confirm the effectiveness of the present "GasLube" mechanism, developed for iso-Octane/n-Hexadecane mixtures, in reproducing lubricant oil influence on the ignition propensity of gasoline-like fuels.

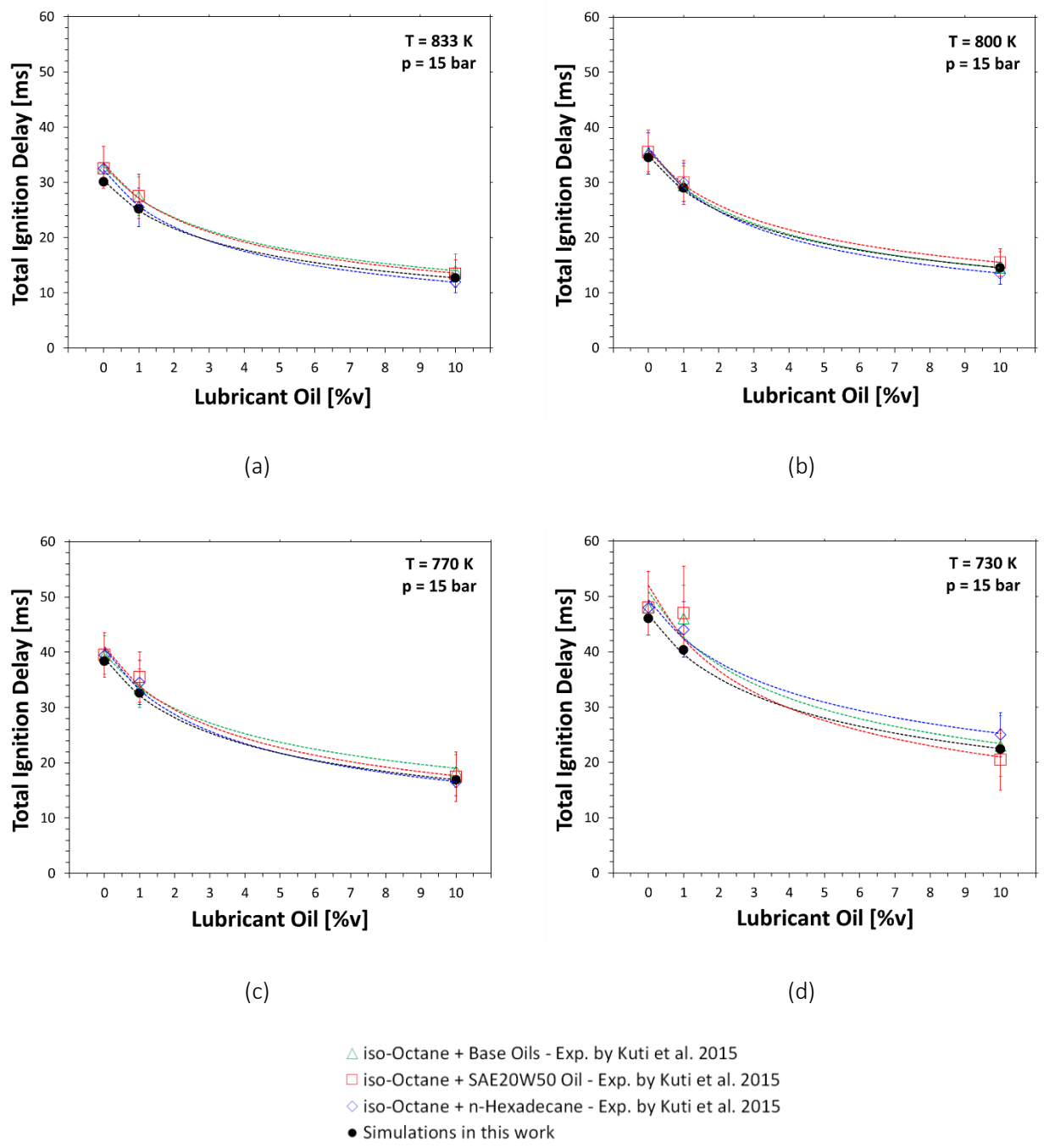

Figure 5.11 Variation of TID with volume percentage of either lubricant oil or its surrogate species, added to iso-Octane, for each of the initial temperatures considered.

Figure 5.12 shows the TID partition into Physical Ignition Delay (PID) and Chemical Ignition Delay (CID), according to the procedure explained in Appendix A and depicted in Figure A-2. Conventionally, the PID identifies the first instants of the TID, i.e., the time interval in which the fluid-dynamic aspects are dominant and wherein spray atomization, vaporization and mixing of air occur. The CID is the remaining part of the TID, during which chemical reactions take place and pressure and temperature rise until the start of ignition occurs. The results in Figure 5.12, together with the data of Figure 5.11, show that the final reduction of the TID is mainly due to the PID reduction when the lubricant oil surrogate species is added to iso-Octane. And this was more evident at the highest temperature, i.e.,

at $833\ K$ (last three columns at the right-hand-side of Figure 5.12), under which the increase in the lubricant surrogate amount produced a decrease of the PID from 30% to roughly 15%, highlighting the progressively reduced importance of the physical aspects that contributed to determine the TID value. As the temperature decreases, it is possible to notice that the PID fraction did not follow a monotonic trend with respect to the lubricant surrogate percentage. At temperatures lower than $800\ K$, after a significant reduction of the PID fraction with the 1% of lubricant surrogate, it rises again when 10% lubricant surrogate was considered. This result suggests that the thermodynamic conditions have great importance in determining the different impact that the same amount of lubricant oil might have on the iso-Octane ignition process.

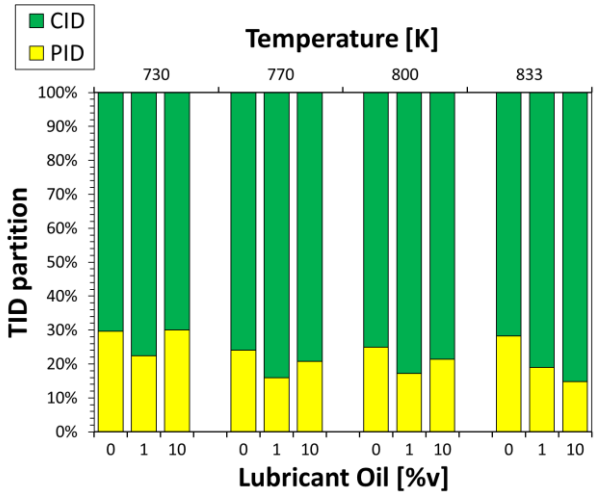

Figure 5.12 TID partition into PID and CID, according to the procedure exposed in Appendix A. Variations with both initial temperature and volume percentage of either lubricant oil or its surrogate species.

Figure 5.13 reports the pressure traces (blue lines) together with the corresponding HRR traces (red lines) obtained by varying the lubricant surrogate amount, for each of the temperatures considered. The Point of Inflection (PoI) (cf. Appendix A) is reported as a yellow circle on the corresponding pressure trace. Generally, the analysis of the HRR traces points out that the typical two-stage process characterizing the iso-Octane auto-ignition (solid lines in Figure 5.13) was drastically affected by the addition of the lubricant oil surrogate species. The reduction of the TID corresponds to a progressive transformation of the ignition event in a "quasi" one-stage process (cf. dash-dotted lines in Figure 5.13, referring to 10% by volume of lubricant oil surrogate species). With larger amounts of lubricant oil surrogate species mixed with iso-Octane, exothermic reactions started to take place early, inducing an early heat release. Therefore, a larger amount of heat is released in a shorter time in the first stage of the ignition processes, which in turn accelerates the second ignition stage.

The first ignition stage, responsible for the Low Temperature Heat Release (LTHR), is the most fuel-type-dependent ignition stage. Above $850\ K$ the hydrogen-oxygen system starts to dominate the fuel oxidation (the branching reactions involving hydrogen peroxide became the most important ones), so that the intermediate and hot ignition stages are relatively independent of the fuel type [40]. The initiation hydrogen abstraction and the subsequent alkylperoxy radical isomerization reactions govern the LTHR stage [418,439]. A lubricant oil molecule, modeled as a n-Hexadecane, is sensibly

more conducive to LTHR than iso-Octane, because of its large number of secondary bonds, its longer chain length, and its greater internal flexibility [418,439–441]. Secondary carbon-hydrogen bonds have lower activation and thus allow faster hydrogen abstraction reactions. In a long and flexible molecule, the process of an O_2 chain abstracting a nearby hydrogen atom is facilitated. As a consequence, the formation and decomposition of highly oxygenated intermediates (e.g., ketohydroperoxides) associated with LTHR are speeded up by the presence of larger amount of long straight-chained n-Hexadecane [442]. An increasingly faster vaporization event is induced by an increasingly larger and anticipated LTHR in the first stage of the ignition. As a result, the PoI was progressively anticipated by the addition of n-Hexadecane to iso-Octane, for each of the cases shown in Figure 5.13.

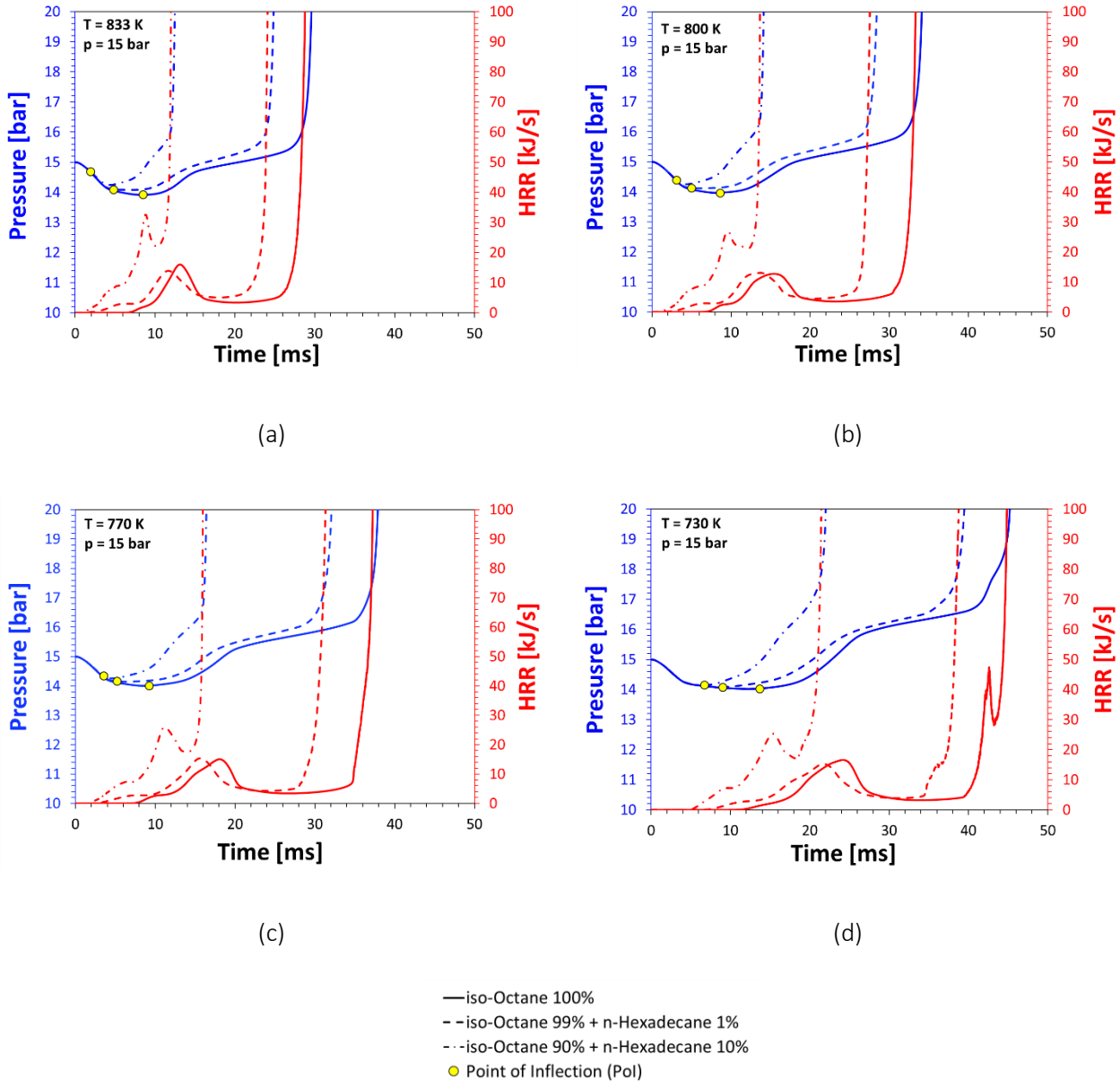

Figure 5.13 Pressure traces (blue lines) and corresponding HRR traces (red lines) obtained in the 3D simulations by varying the n-Hexadecane percentage fraction in iso-Octane, for each of the temperatures considered. The PoI (yellow marker) was reported for each of the corresponding pressure trace.

It was previously observed that 1% by volume of n-Hexadecane produced a generalized reduction of the PID percentage fraction, while a further increase from 1 to 10% produced contrasting effects, depending on the initial temperature. The PoI and HRR analysis can explain the results showed in Figure 5.12. Firstly, it must be considered that the reactions of alkyl radicals with oxygen molecules in the first ignition stage are highly temperature dependent [61]. Secondly, n-Hexadecane has higher molecular weight and is less volatile than iso-Octane, so that the spray vaporization proceeds less fast when a larger amount of lubricant surrogate is mixed with iso-Octane. At intermediate-low temperatures (below $800\ K$), the temperature was not sufficiently high to significatively accelerate the spray vaporization process when n-Hexadecane was present in larger amounts (i.e., 10%). In these cases, the chemical processes were accelerated more than the physical ones. Namely, the time needed to release enough energy to bring the temperature of the first stage to a value that cause auto-ignition was reduced more than the time needed to complete the vaporization process. However, with increasingly higher temperatures, an increasing faster and larger LTHR significantly accelerated the vaporization process more than the chemistry involved during the Negative Temperature Coefficient (NTC) phase that followed the LTHR. As a result, at $833\ K$, the PID fraction with 10% by volume of n-Hexadecane in iso-Octane was lower than that with 1%. This explains why, the chemical-related processes assumed more importance with respect to the physical-related ones, becoming the controlling processes in determining the final TID at the highest temperature. The reduced importance of the physical aspects is also inferable by noting that, at $833\ K$, the PoI was shifted by a larger time interval (Figure 5.13 (a)) with respect to what happened with lower temperatures with the increase of the n-Hexadecane amount from 1 to 10% by volume.

Figure 5.13 (c) shows an additional important aspect that can further underline the significant effects that lubricant oil can have on the iso-Octane combustion process. At the lowest temperature, i.e., $730\ K$, the iso-Octane auto-ignition presented a three-stage heat release, namely an Intermediate Temperature Heat Release (ITHR), close to the High Temperature Heat Release (HTHR) is visible at the end of the second ignition stage. ITHR has been observed in engines [443,444] and auto-ignition phenomena with more than two stages have been documented in the literature for surrogate species used for distillate-type fuels [445–447]. The controlling chemistry is attributed to competition between Alkyl Peroxy radical chain branching, propagation, and termination pathways [446]. With the presence of 1% by volume of lubricant in iso-Octane, the reduction in the TID is associated with a reduction of this intermediate stage. And with 10% by volume of n-Hexadecane such an intermediate stage was completely absorbed by the high temperature one, so that a two-stage process was restored. These findings highlight the large differences between the reactivity characteristics of iso-Octane and the lubricant oil surrogate species, namely n-Hexadecane. Thus, even very small amounts of lubricant oil can have a non-negligible impact on the iso-Octane ignitability propensity, especially when high-pressure and low temperature are considered, as it happens when low-speed pre-ignition events are observed in high-boost DISI engines.

5.5. Conclusions

A reduced reaction mechanism suitable for practical engine simulations has been developed. This, so-called "GasLube" mechanism accurately predicts the reduction of gasoline Total Ignition Delay (TID) time due to lubricant oil contamination occurring within the combustion chamber of an internal combustion engine. Being able to emulate fuel-lubricant interactions inside the combustion chamber is crucial for developing high boost Direct Injection Spark-ignition (DISI) engines, as well as for controlling Gasoline Compression Ignition (GCI) engines.

The reduced GasLube mechanism was obtained by merging two existing mechanisms and operating various reduction and optimization steps, by which the number of species was reduced of about 93%, while accuracy was preserved. In its final version it includes 522 species and 2277 reactions, representing a significant step forward compared to the previous detailed versions.

Three-Dimensional Computational Fluid Dynamic simulations were performed to reproduce the experimental study by Kuti et al., in which iso-Octane was blended with either fully formulated lubricant (SAE 20W50) or its surrogate species and injected in an Ignition Quality Tester (IQT). An initial pressure of $15\ bar$ and four different temperatures, namely $730, 770,\ 800$ and $833\ K$, were considered. n-Hexadecane was selected as the unique surrogate species and was able to reproduce the chemical-physical properties of engine lubricant oil. It was possible to reproduce that 1% by volume of lubricant shortens the iso-Octane TID by an average 15% and 10% by volume can produce a reduction of about 54%. It was also pointed out that the TID reduction due to lubricant oil addition followed an exponential behavior, confirming that even trace amounts of lubricant oil can drastically affect iso-Octane ignitability propensity.

The results showed that the final reduction of the TID was mainly ascribable to the Physical Ignition Delay (PID) reduction when the lubricant oil surrogate species was added to iso-Octane. An increasingly faster vaporization event was induced by an increasingly larger heat released in the first stage of the ignition. This was evident at the highest temperature. As the temperature decreased, the percentage fraction of the PID did not follow a monotonic trend with respect to the lubricant surrogate percentage. The lower volatility of n-Hexadecane induced less fast spray vaporization when it was in larger amounts (i.e., 10% by volume) and the temperatures were lower. These results suggest that the thermodynamic conditions have great importance in determining the different impact that the same amount of lubricant oil might have on the iso-Octane ignition process.

Heat Release Rate (HRR) traces pointed out that the typical two-stage process characterizing iso-Octane auto-ignition progressively transformed into an almost one-stage process with the increase of the n-Hexadecane amount. At the lowest temperature, i.e., $730\ K$, the iso-Octane auto-ignition presented a three-stages heat release. With 1% by volume of n-Hexadecane in iso-Octane, the reduction in the TID was associated with a significative reduction of the intermediate stage. And with 10% by volume of n-Hexadecane such an intermediate stage was completely absorbed by the high temperature one.

In conclusion, it was verified that a single pure species, n-Hexadecane, can be employed as surrogate species for emulating lubricant oil and that the proposed reduced "GasLube" mechanism can be employed to predict lubricant oil induced abnormal combustion modes for modern gasoline engines.

Chapter 6

The "GasLube" Analytical Correlation

In this Chapter, a simple analytical correlation is presented and proposed to predict variations of gasoline ignition delay induced by the presence of lubricant oil, at different temperatures. Such a correlation was developed by taking into account both experimental data available in the literature and numerical simulations employing the "GasLube" reaction mechanism, developed for iso-Octane/n-Hexadecane mixtures. Operating conditions representative of those of typical turbocharged DISI engines were considered for the validation. The proposed correlation makes possible to accurately derive the ignition delay of gasoline/lubricant oil mixtures directly from the values related to pure iso-Octane (gasoline surrogate), avoiding the use of dedicated reaction mechanisms, and thus saving computational time.

6.1. Introduction

Numerical simulations can represent an auxiliary tool in the investigation of new challenging problems. However, engine simulations are commonly computationally expensive. Analytical correlations are frequently implemented in Computational Fluid Dynamics (CFD) codes in order to save computational time. For instance, analytical correlations for the laminar flame speed are usually preferred in engine practical simulations [393–395] in the place of detailed chemical kinetics. Emulating the chemical behavior of lubricant oil has become essential for performing numerical simulations of the combustion process occurring in a modern DISI engine and thus for predicting LSPI events and further improve these engines. Dedicated reaction mechanisms are being developed for this very purpose, but these can result very computationally demanding [419].

Fujimoto et al. [156] developed an empirical correlation in order to estimate the LSPI frequency as a function of the mass fraction of lubricant oil additives, such as Calcium, Ca, Phosphorus, P, and Molybdenum, Mo:

$$\mathrm{LSPI}_{\mathrm{frequency}} = 6.59 \cdot \mathrm{Ca} - 26.6 \cdot \mathrm{P} - 5.12 \cdot \mathrm{Mo} + 1.69.$$

However, the applicability of the correlation proposed by Fujimoto et al. [156] is quite limited, since its use was recommended only for the same engine type and operating conditions considered in their study [156]. In addition, it requires the additive mass fractions to be determined as well as it does not consider the influence of temperature and lubricant oil amounts inside the combustion chamber.

The aim of this Chapter is to show the development of an analytical correlation able to predict the variations of gasoline ignition delay induced by the presence of lubricant oil at different temperatures. Operating conditions representative of those reigning in the combustion chamber of a modern DISI engine were considered. In order to generate an appropriate dataset on which the correlation could be developed, both experimental data available in the literature and Zero-Dimensional (0D) numerical simulations employing the "GasLube" reaction mechanism [448] – developed for iso-Octane/n-Hexadecane mixtures – were considered. By means of the proposed correlation, the ignition delay of gasoline/lubricant oil mixtures can be derived directly from the values related to pure iso-Octane. Therefore, the implementation of the proposed correlation in numerical codes allows the use of much simpler and already known mechanisms, saving computational time.

6.2. Methodology

An empirical correlation must be validated against an appropriate number of experimental data in order to be considered reliable. Therefore, the experimental data available in the literature that quantified the reactivity of mixtures of gasoline and lubricant oil were first analyzed.

However, the number of available data is still rather small, because the interest in this topic is increased only recently. In addition, due to the physical properties of lubricant oil, a rigorous procedure to assess its chemical ignition delay has not been already well defined. In fact, the experimental facilities employed in the available studies must deal with spray-related phenomena that make challenging the correct interpretation of the derived measurements [437,449,450].

In this study, numerical chemistry was used as auxiliary tool to overcome these limitations. In order to perform successful numerical simulations able to predict the chemical behavior of lubricant oil, it is essential to dispose of a reliable approach for modeling lubricant oil. Therefore, the most appropriate surrogate species and the related reaction mechanism were selected in accordance with the most recent numerical studies.

0D numerical simulations were carried out using Ansys Chemkin PRO code. The closed homogeneous batch reactor model was employed for solving the time-dependent balance equations for the total mass, the gas-phase species and the energy [414]. The ignition delay was derived by the pressure time history by employing the gradients method. The procedure was the same used in previous experimental and numerical studies [261,448], thus a direct comparison with the results reported in these studies was possible.

As a first step, the numerical simulations were used to critically analyze the available data with the aim to isolate the chemical-related information. After that, additional simulations were performed in order to generate a more appropriate dataset for the correlation development. The operating ranges

within which the analytical correlation was developed were extended in comparison to that related to the experimental data. This aspect was crucial in order to better highlight the dependence upon the selected variables. The volume fraction of lubricant oil in gasoline was varied from 0 to 1. A range of initial temperatures of the charge varying from 700 to 850 K was considered. Stochiometric conditions, as it is typical of a modern DISI engines, were considered. An initial pressure of 15 bar was selected, because it represents the only value at which experimental data were produced, and consequently the reaction mechanism validated. Nevertheless, this value can be considered representative of the conditions reigning in a modern DISI when pre-ignition events might occur [261].

An analytical expression was proposed to capture the dependence of gasoline ignition delay upon lubricant oil volume fraction and temperature, in the above-mentioned operating ranges. An iterative non-linear least-squares regression was performed for the parameters estimation. The bi-square algorithm was adopted, in combination with the trust region algorithm [451]. Although the correlation was validated for a lubricant oil volume fraction varying from 0 to 1, its utilization is suggested for lubricant oil amounts not larger than 10% by volume, namely in a range that might resemble more realistic conditions findable in practical engine applications.

6.2.1. Experimental Data

The most significative experimental investigation is represented by the work carried out by Kuti et al. [261]. This work provided both indications about surrogate species suitable to mimic the physicochemical characteristics of lubricant oil and quantitative data about the influence of lubricant oil on gasoline reactivity.

In this fundamental research, an Ignition Quality Tester (IQT), whose schematic representation is reported in Figure 6.1, was employed to measure the ignition delay time of mixtures of iso-Octane (i-C_8H_{18}) and lubricant oils having different formulations. Different base oils - such as SN100 (Group I) and HC4 and HC6 (Group III) - and a fully formulated lubricant oil (SAE 20W50) were considered. The results are reported in Figure 6.2. It was found that adding 1% by volume of lubricant oil to iso-Octane reduced the iso-Octane ignition delay by averagely 15%. An increase of lubricant oil amount to 10% further reduced the average ignition delay time by up to 54%.

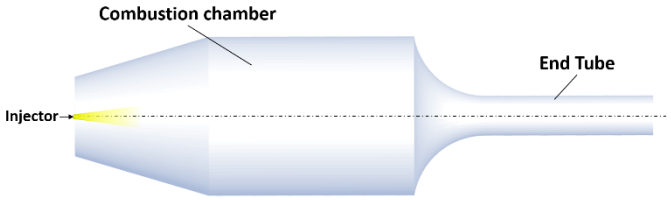

Figure 6.1. Schematic representation of the Ignition Quality Tester (IQT) facility.

Base oils and fully formulated lubricant showed a quite similar behaviour, suggesting that it is the hydrocarbon fraction that contributes primarily to enhance the reactivity, and not the inorganic or

organometallic additives. Furthermore, it was highlighted that the same effects obtained by adding lubricant oils to iso-Octane was obtained by adding a pure hydrocarbon species. Namely it was shown that the addition of either n-$C_{16}H_{34}$ or n-$C_{17}H_{36}$ or n-$C_{18}H_{38}$ - with no appreciable differences among them - produced trends really close to those obtained with base or fully formulated lubricant oils, as it is shown in Figure 6.2. The latter finding represents an empirical proof that C_{16}–C_{18} normal alkanes can be considered adequate surrogates for commercial engine lubricants.

However, the data reported by Kuti et al. [261] cannot be directly used to develop an analytical model. In the experiments employing an IQT facility, the mixture whose reactivity need to be measured is injected as a liquid in a constant volume chamber. This implies that spray breakup, vaporization and mixing take place before the start of the ignition. In these experiments, the ignition delay is indirectly derived from in-chamber pressure records, as the time interval between the start of injection and the start of ignition [261,437,452]. The unavoidably consequence is that the measured ignition delay times unproperly enclose physically related aspects. The ignition delay values should instead provide information exclusively related to chemical aspects. To this regard, the data reported by Kuti et al. [261] as ignition delay should be identified as total ignition delay, τ_{tot}, [453,454], as reported in Figure 6.2. The first instants after the injection, in which the fluid-dynamic aspects are dominant, are conventionally known as physical ignition delay, τ_{phys}. The remaining part of τ_{tot} represents the chemical ignition delay, τ_{chem}, namely the time interval of actual interest, in which chemical reactions take place.

There are additional drawbacks intrinsically related to the derivation of ignition delay values from experiments carried out with an IQT facility that should be taken into account when the interest is focused only on the chemical-related aspects, as in the present study. There are, for instance, issues related to inhomogeneities of the charge within the chamber due to the physical properties of lubricant oil and the limited time available for mixing. The formation of reactivity gradients due to local charge stratification can significantly alter the measured value of the ignition delay in comparison to that expected in homogeneous conditions [449,450,455].

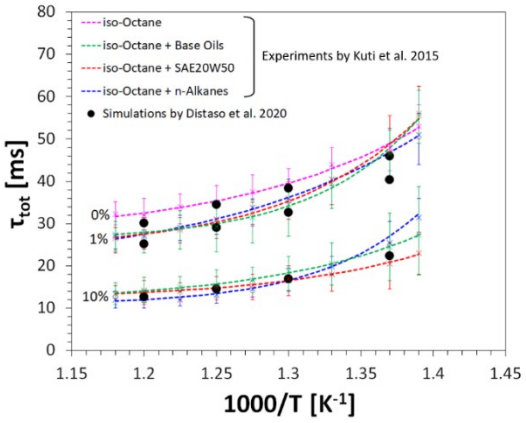

Figure 6.2. Experimental measurements carried out by Kuti et al. [261] of the total ignition delay, τ_{tot}, of mixtures of iso-Octane with either base oils or a fully-formulated lubricant oil or its surrogate species. Comparison with the 3D numerical simulations performed by Distaso et al. [448].

Furthermore, in the experiments by Kuti et al. [261] reported in Figure 6.2, the global equivalence ratio (ϕ) was not kept constant, but rather it was varied with the initial temperature. The variation of the initial temperature was obtained by regulating the heat supplied to the outer walls of the combustion chamber by means of electrical heaters. The mass of the ignitable mixture injected in the IQT was kept constant, while the air mass within the chamber varied according to the variation of its density induced by the imposed temperature changes. Consequently, the global equivalence ratio varied according to the temperature variations (with no appreciable differences among the different mixtures considered) as it is shown in Figure 6.3. The global equivalence ratio increased by about 0.15 points in correspondence of an increase of the temperature from the lowest to the highest value considered in the experiments by Kuti et al. [261]. It is well known that the equivalence ratio has a strong effect on ignition delay [450]. Thus, such a variation cannot be considered negligible, and its effects surely had a significative impact in determining the trends reported in Figure 6.2.

The data reported in Figure 6.2 show a double dependence: an evident one on the temperature and a hidden one on the mixture strength. This aspect is of extremely importance and must be taken into consideration for developing a reliable correlation. From this analysis it derived that to perform numerical analysis was essential to better analyze the available experimental data.

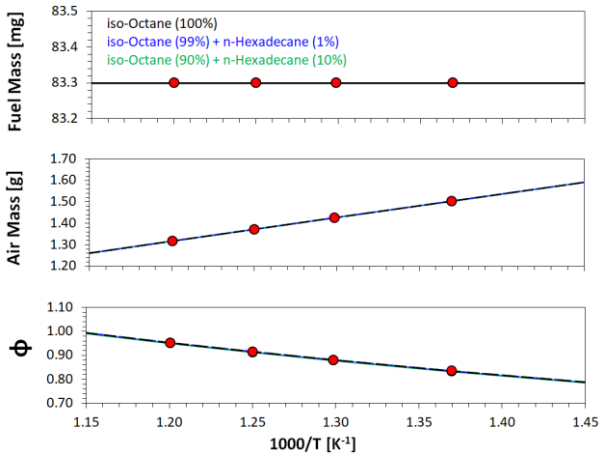

Figure 6.3. Variation of the global equivalence ratio, ϕ, according to the air mass and the fuel mass in the experiments by Kuti et al. [261]. Red points: operating conditions considered in the 3D numerical simulations by Distaso et al. [448].

6.2.2. Lubricant Oil Oxidation Modeling

To properly simulate the oxidation process of lubricant oil, it is necessary to select a surrogate species able to emulate its chemical characteristics and to dispose of a reaction mechanism that can predict the most significative reaction paths in a wide range of operating conditions. The literature on this topic is quite young and more efforts should be putted in the future for the definition of reaction mechanisms of practical use. This might encourage experimentalists to design more advanced

experimental equipment. In turn, disposing of a larger number of experimental data can result useful to improve accuracy and predictive capabilities of the numerical models.

Chemical analyses indicate that base oils are mainly composed of C_{15}–C_{54} normal alkanes [261,299]. Searching for a structural formula containing all the required information related to physical, chemical, and biological properties of the compound cannot be considered a viable solution, at the moment. Such an approach would probably result in a molecule having an average number of carbon atoms around 35 [456]. Chemical kinetic mechanisms for long-chain alkanes require unacceptable computational efforts [415,416,457]. Furthermore, molecules with heavy molecular weight along with large molecular structure represent a challenge for experimental studies and require special treatments.

A common approach is to consider the simplest molecule that can reproduce the reactivity of lubricant oil. The findings of different research groups converge towards a single n-alkane molecule, namely n-Hexadecane (n-$C_{16}H_{34}$). This is in accordance with the well-known fact that alkanes larger than C_{14} exhibit nearly identical fuel/air gas-phase ignition delay times across a range of operating temperatures [415,416]. In addition, it is in line with the experimental results provided by Kuti et al. [261]. Some attempts were also made to further simplify this result by considering n-Heptane (n-C_7H_{16}) – a well-known and largely studied molecule - but with poor results. Both Dahnz et al. [96,145] and Kalghatgi et al. [146] observed ignition delay values still too high in comparison to lubricant oil, which resulted to be more reactive than n-Heptane.

Gupta et al. [84] proposed to use the mechanism based on the kinetics developed by Kawanabe et at. [390] for n-Hexadecane combined with the PRF reduced mechanism by Liu et al. [389] in order to investigate pre-ignition events triggered by the presence of oil droplets in turbo-charged gasoline engines. Wang et al. [458] employed a reduced chemical mechanism for iso-Octane, n-Heptane and n-Hexadecane, derived form that developed by Kawanabe et al. [390] to study the auto-ignition and detonation induced by surrogate lubricating oil in stoichiometric iso-Octane/air mixture. However, in these studies no validations against experimental data were provided for the mechanism developed by Kawanabe et al. [390] in order to prove that it is able to emulate the auto-ignition propensity of gasoline/oil mixtures in the thermodynamic conditions considered for the simulations.

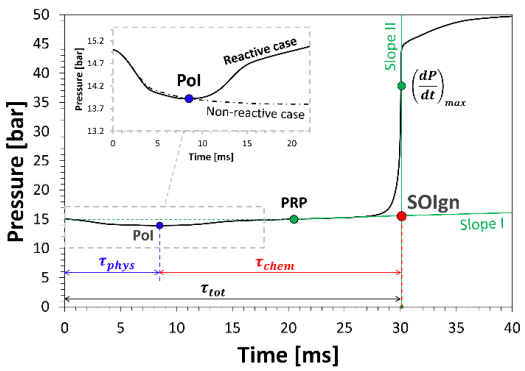

Figure 6.4. Point of Inflection (PoI) method for the determination of the physical (τ_{phys}) and chemical (τ_{chem}) components of the total ignition delay (τ_{tot}) from the numerical pressure history. More details can be found in [448].

To the authors' knowledge the "GasLube" reaction mechanism developed by Distaso et al. [448] for iso-Octane/n-Hexadecane mixtures is the only reaction mechanism fully validated against experimental data. It was tested in Three-Dimensional (3D) numerical CFD simulations that successfully replicated the experiments by Kuti et al. [261], as shown in Figure 6.2. The predicted τ_{tot} values were very close to those recorded in the experiments for the pure species - thus for the fully formulated lubricant oil - added to iso-Octane.

From the numerical simulations it is possible to infer additional information, difficult or impossible to obtain from the experiments. The analysis of the numerical pressure history performed in [448] allowed τ_{phys} and τ_{chem} to be determined by means of the Point of Inflection (PoI) method. Reactive and non-reactive cases were compared in order to distinguish between chemical- and physical-related processes, as it is shown in Figure 6.4. For the sake of brevity, the procedure is not here reported, but its detailed description can be found in [448], together with the definition of the other points reported in Figure 6.4. The results of this analysis are depicted in Figure 6.5, which shows that τ_{phys} represented a non-negligible fraction of τ_{tot}, varying from 15 to 30%, according to the thermodynamic conditions and the lubricant amount added to iso-Octane. In addition, it must be emphasized that the percentage fraction of τ_{phys} does not follow a monotonic trend with respect neither to the lubricant surrogate percentage nor the initial temperature, highlighting that the trends are the effects of several complex phenomena occurring simultaneously within the combustion chamber. These results underline that it is essential to enucleate the chemical component from τ_{tot} values obtained in the experiments by Kuti et al. [261] in order to develop an analytical expression able to predict the effects on the chemical ignition delay of gasoline (iso-Octane) due to the presence of lubricant oil (n-Hexadecane).

In addition, by means of the 3D numerical simulations it was possible to analyze the mixing process inside the IQT combustion chamber, with the aim to highlight the presence of inhomogeneities in the charge distribution. Figure 6.6 – which was not shown in [448] because beyond the scope of that work – reports the contour plots of the equivalence ratio at the start of ignition for a low-temperature case (i.e., 730 K). This case was selected because representative of the operating conditions that showed the largest sensitivity to equivalence ratio variations, as it will be pointed out later on. Figure 6.6 shows a stratification of the charge, with the creation of leaner zones near the injector nozzle and richer zones in correspondence of the end-tube entrance. This happens for all the iso-Octane/n-Hexadecane mixtures considered. The presence of more reactive zones, with local equivalence ratio values up to 3, can significantly deviate the measured value of the ignition delay from the actual one, corresponding to homogeneous conditions. In fact, it was found that in the simulations the ignition started developing from those richer zones, for all the cases considered. These results confirm what was already pointed out by previous numerical studies [449,450,455]. This aspect needs also to be carefully taken into account in the development of the proposed correlation.

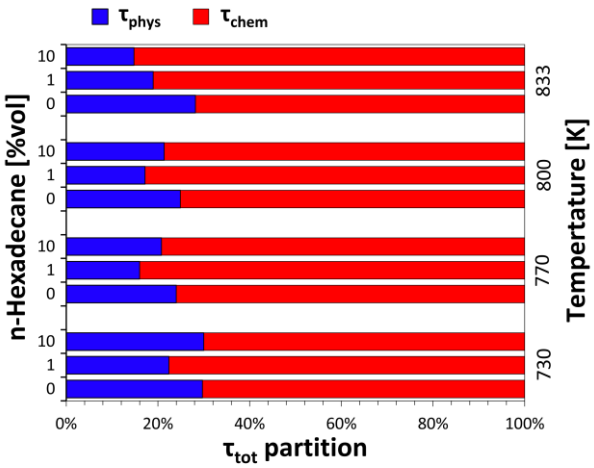

Figure 6.5. Results reported by Distaso et al. [448] about the partition of the total ignition delay (τ_{tot}) into the physical (τ_{phys}) and chemical (τ_{chem}) components.

In addition, by means of the 3D numerical simulations it was possible to analyze the mixing process inside the IQT combustion chamber, with the aim to highlight the presence of inhomogeneities in the charge distribution. Figure 6.6 – which was not shown in [448] because beyond the scope of that work – reports the contour plots of the equivalence ratio at the start of ignition for a low-temperature case (i.e., 730 K). This case was selected because representative of the operating conditions that showed the largest sensitivity to equivalence ratio variations, as it will be pointed out later on. Figure 6.6 shows a stratification of the charge, with the creation of leaner zones near the injector nozzle and richer zones in correspondence of the end-tube entrance. This happens for all the iso-Octane/n-Hexadecane mixtures considered. The presence of more reactive zones, with local equivalence ratio values up to 3, can significantly deviate the measured value of the ignition delay from the actual one, corresponding to homogeneous conditions. In fact, it was found that in the simulations the ignition started developing from those richer zones, for all the cases considered. These results confirm what was already pointed out by previous numerical studies [449,450,455]. This aspect needs also to be carefully taken into account in the development of the proposed correlation.

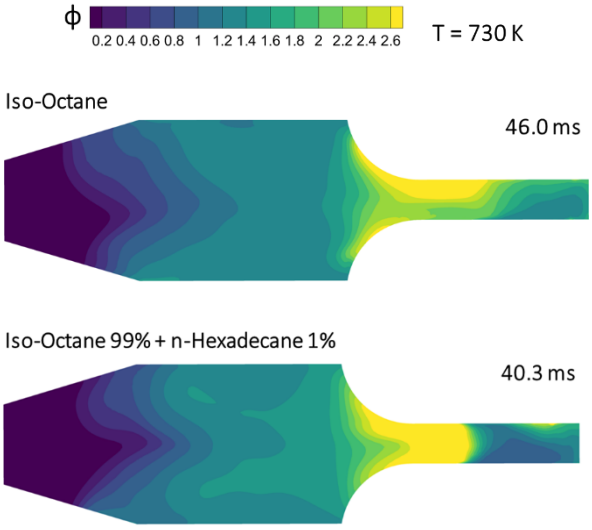

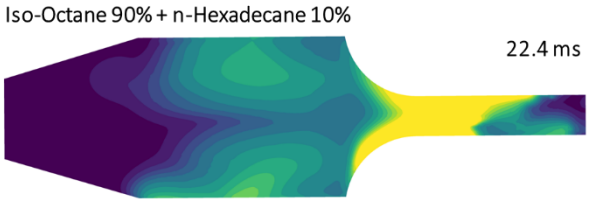

Figure 6.6. Contour plots of the equivalence ratio, ϕ, at the start of ignition for an initial temperature of 730 K. Results deriving from the 3D simulations performed by Distaso et. al [448].

6.3. Results and Discussion

0D simulations employing the "GasLube" reaction mechanism [448] and n-Hexadecane as surrogate species for lubricant oil were performed in order to derive a more appropriate dataset on the basis of which the analytical correlation could be derived.

Figure 6.7 reports the results in terms of $\boldsymbol{\tau_{chem}}$ variation with respect to the temperature obtained from the 0D simulations performed at constant equivalence ratio, for pure iso-Octane (a), for mixtures with 1% (b) and 10% (c) of n-Hexadecane in iso-Octane and for pure n-Hexadecane (d). The red points reported in the graphs correspond to those of Figure 6.3, namely they were drawn in correspondence of the initial temperatures at which the 3D simulations reported in [448] were performed. These results show that variations in equivalence ratio produce more significative effects when the temperature is lower, as well as when n-Hexadecane is present in smaller volumes. Namely, at lower temperatures (i.e., 730 K), a variation of the equivalence ratio from 0.83 to 0.95 produces a reduction of iso-Octane $\boldsymbol{\tau_{chem}}$ of about 30% (Figure 6.7 (a)). The effects are less marked as the n-Hexadecane fraction increases (Figure 6.7 (c)) and become negligible in the case of pure n-Hexadecane (Figure 6.7 (d)). At higher temperatures, a variation of the equivalence ratio produces less evident effects even in the case of pure iso-Octane (Figure 6.7 (a)), thus independently from the chemical species composing the mixture.

Figure 6.8 reports a comparison between the 3D simulations reported in [448] (black points) and the 0D simulations performed in the present work (red points – corresponding to the red points in Figure 6.7). Where the effects induced by an equivalence ratio variation are less pronounced (i.e., at high temperatures and with large n-Hexadecane fractions) the difference can be exclusively attributed to the presence of physical processes. This because the spray-related processes were reproduced in the 3D simulations while they were not modeled in the 0D simulations. In these cases, the ignition delay values obtained from the 3D simulations enclosed the τ_{phys} component and thus result higher than those obtained from the 0D simulations. This explains why the 3D simulations overestimates the ignition delay in the case of 10% of n-Hexadecane regardless of temperature and at 833 K regardless of mixture composition. The n-Hexadecane volume fraction in the former case and the temperature

in the latter case were sufficiently high to make negligible the effects of the equivalence ratio variation.

At lower temperatures and for smaller n-Hexadecane volume fractions, the effects of the inhomogeneities become dominant. In the richer zones that are locally formed within the chamber at the ignition time (cf. Figure 6.6) the local equivalence ratio is significantly higher than the overall value and the start of ignition is consequently anticipated. Therefore, Figure 6.8 shows that the 3D simulations underestimated the ignition delay values in the low-temperature range and in correspondence of small amounts of n-Hexadecane.

Moreover, it must be noted that in the experiments the chemical reactions start to take place when the pressure has been reduced due to the mixture evaporation. Albeit less markedly, a pressure reduction results in longer ignition delay values. This effect overlaps with the others already describes.

The results obtained from the 0D simulations highlight that for mixtures having low fractions of n-Hexadecane, the chemical ignition delay, τ_{chem}, show a stronger dependence upon temperature in comparison to what was observed in the 3D simulations. Therefore, the reduction of the τ_{chem} of iso-Octane induced by the presence of n-Hexadecane cannot be considered totally independent from the temperature, as resulted from the experiments by Kuti et al. [261]. With 1% of n-Hexadecane, the purely chemical part of the iso-Octane ignition delay is reduced by a value that ranges from 27% to 43%, in correspondence of a variation of the temperature from 730 to 833 K. Increasing the n-Hexadecane volume fraction the effects of the temperature become less significative. Namely, in the case of 10%, the percentage reduction varies from 80% to 82%.

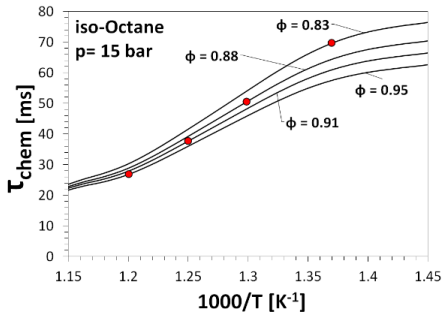

(a)

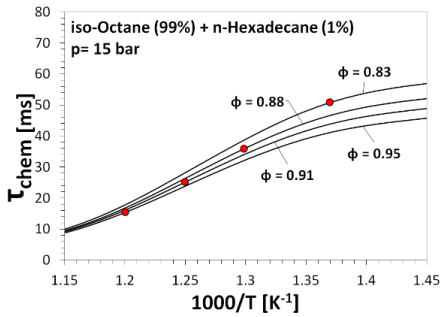

(b)

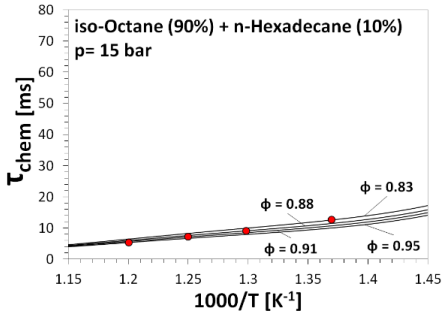

(c)

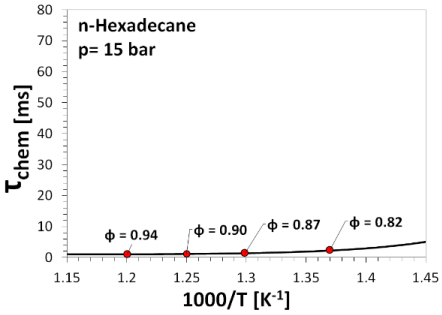

(d)

Figure 6.7. Variation of the chemical ignition delay, τ_{chem}, with respect to the temperature, obtained from 0D simulations. Pure iso-Octane (a); mixtures with 1% (b) and 10% (c) of n-Hexadecane in iso-Octane; pure n-Hexadecane (d). Red points: operating conditions considered in the 3D simulations performed by Distaso et al. [448].

The data obtained from the 0D simulations also point out that the effects of lubricant oil on gasoline reactivity are actually more relevant than those reported by Kuti et al. [261], who estimated a percentage reduction about 15% and 54%, with 1% and 10% by volume of lubricant oil, respectively. Such a discrepancy is mainly attributable to inhomogeneities of the charge formed inside the IQT combustion chamber, which produce different effects depending on lubricant concentration and thermodynamic conditions.

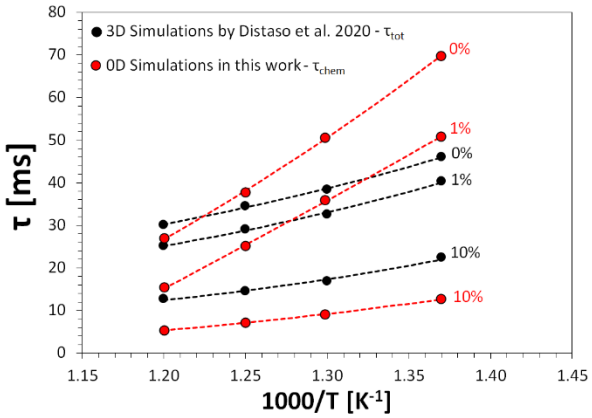

Figure 6.8. Comparison between 3D simulations performed by Distaso et al [448] and 0D simulations performed in this work.

6.3.1. Definition of the Dataset for the Correlation

The previous analysis showed that the available experimental data cannot be directly used in the development of an analytical correlation conceived to capture exclusively the variations in the chemical behavior of gasoline induced by the presence of lubricant oil. Thus, additional 0D numerical simulations employing the "GasLube" mechanism [448] were performed in order to generate a dataset more appropriate for this purpose.

The range of operating conditions of the experiments by Kuti et al. [261] was enlarged in order to better capture the dependence of iso-Octane (gasoline surrogate) ignition delay upon n-Hexadecane (lubricant oil surrogate) volume fraction and temperature. Namely, the n-Hexadecane fraction was varied from 0 to 1, and the temperature from 700 to 850 K. Stoichiometric conditions and a pressure of 15 bar were considered. The selected points used in the development of the correlation are reported in Figure 6.9.

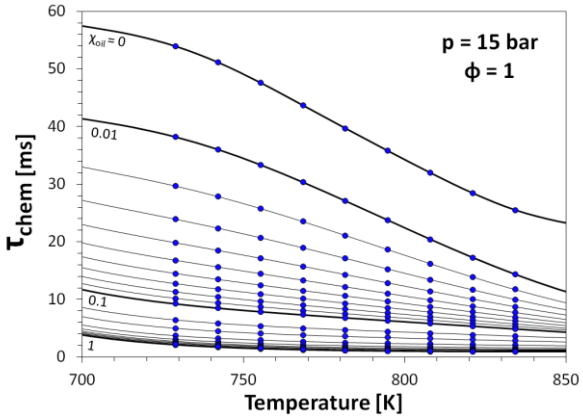

Figure 6.9. Dataset used in the development of the correlation and generated by performing 0D numerical simulations employing the "GasLube" mechanism [448].

The relative change of iso-Octane chemical ignition delay, $\Delta\tau_R$, due to the addition of n-Hexadecane can be defined as:

$$\Delta\tau_r = \frac{\tau_{Gas} - \tau_{GasLube}}{\tau_{Gas}}, \qquad (1)$$

where τ_{Gas} represents the chemical ignition delay of pure iso-Octane and $\tau_{GasLube}$ the chemical ignition delay of the considered gasoline/lubricant mixture, namely the chemical ignition delay of the iso-Octane/n-Hexadecane mixture evaluated by means of the "GasLube" reaction mechanism in the 0D simulations. It must be noticed that $\Delta\tau_R$ has been defined to be always a positive quantity since the presence of n-Hexadecane always produces a reduction of the chemical ignition delay of iso-Octane and thus $\tau_{Gas} > \tau_{GasLube}$.

Knowing the chemical ignition delay of pure iso-Octane, τ_{Gas} – which can be calculated by means of one of the mechanisms developed for this well-studied species - it is possible to correct such a value to factor in the presence of lubricant oil, as it follows:

$$\tau_{GasLube} = \tau_{Gas}(1 - \Delta\tau_r). \qquad (2)$$

6.3.2. Development of the Correlation

Disposing of a correlation for $\Delta\tau_r$ allows the chemical ignition delay of iso-Octane/n-Hexadecane mixtures to be calculated starting from the values relative to pure iso-Octane. For this purpose, it is needed to study how $\Delta\tau_R$ varies according to the variation of the volume fraction of n-Hexadecane in iso-Octane, χ_{oil}, in the considered temperature range. This is shown in Figure 6.10.

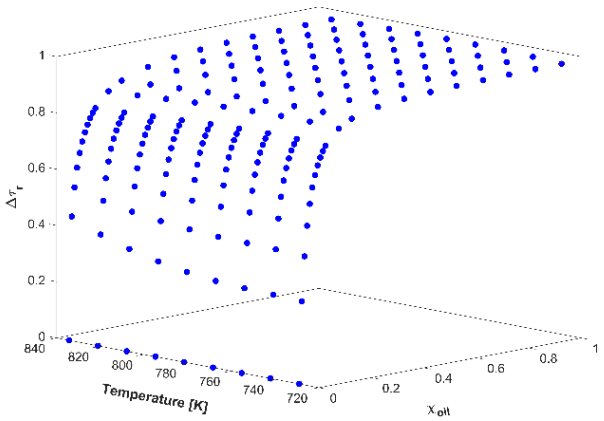

Figure 6.10. Relative change of iso-Octane chemical ignition delay, $\Delta\tau_R$, as a function of the volume fraction of n-Hexadecane in iso-Octane, χ_{oil}, and the temperature.

The volume fraction of the lubricant surrogate species, χ_{oil}, has a more relevant influence than temperature. The value of $\Delta\tau_r$ quickly increases with the increase of χ_{oil} and reaches values comparable to the maximum ones ($\Delta\tau_r = 0.96$) already at $\chi_{oil} = 0.3$. Namely, a mixture with about 30% by volume of n-Hexadecane already shows a reactivity comparable to that of pure n-Hexadecane. The relative change of the chemical ignition delay induced by a variation of the temperature is significative only when small amounts of n-Hexadecane are considered. For concentrations of n-Hexadecane larger than 4% by volume, the value of $\Delta\tau_r$ can be considered to be independent from the temperature.

However, with small amounts of n-Hexadecane – as it is most likely the case of the combustion chamber of a DISI engine – the mixtures show a higher sensitivity with respect to a variation of the thermodynamic conditions. At higher temperatures, the increase of iso-Octane reactivity induced by small amounts of n-Hexadecane is more significative. For instance, at 833 K, 1% by volume of n-Hexadecane is sufficient to shorten the iso-Octane ignition delay by about 45%. It must be noted that this value is slightly higher than that reported previously (i.e., 43%) because this represents the actual variation calculated in stoichiometric conditions.

It was found that a "bi-exponential" function can adequately capture these trends. Namely, the fitting of the data reported in Figure 6.10 was performed considering the follow expressions:

$$\Delta\tau_R = a \cdot \left[1 - e^{c(T)\cdot\chi_{oil}}\right] + b \cdot \left[1 - e^{d(T)\cdot\chi_{oil}}\right], \qquad (3)$$

in which a and b are constant to be determined. The dependence upon the temperature is described by means of the functions $c(T)$ and $d(T)$, present in the exponential terms of Equation (3). A polynomial expression was proposed for these functions:

$$c(T) = c_0 + c_1 T + c_2 T^2 + c_3 T^3 \qquad (4)$$
$$d(T) = d_0 + d_1 T + d_2 T^2$$

The surface reported in Figure 6.11 represents the result deriving from the non-linear regression performed on the dataset reported in Figure 6.10 by employing Equations (3) and (4). The corresponding coefficients are reported in Table 6.1.

Figure 6.11 shows that the proposed "bi-exponential" formulation fits the data in a satisfactory way. The exponential influence of the volume fraction of the lubricant surrogate is well caught in the entire range of temperatures considered in the analysis.

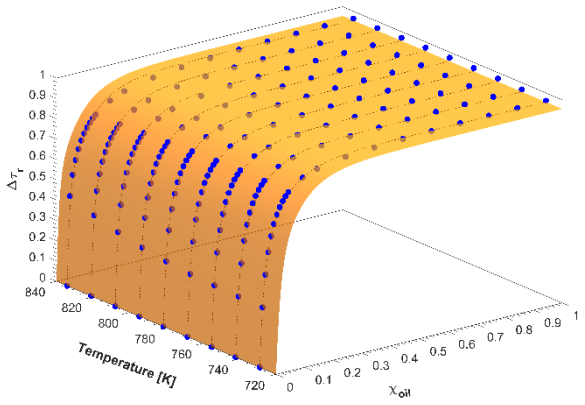

Figure 6.11. Visualization in the entire validation range of the correlation - Equations (3) and (4) - developed to capture the relative change of iso-Octane chemical ignition delay, $\Delta\tau_R$, as a function of the volume fraction of n-Hexadecane in iso-Octane, χ_{oil}, and the temperature.

Figure 6.12 reports the results by considering a narrowed range of operating conditions that might result closer to the conditions reigning in the combustion chamber of a modern DISI engine. Namely, it was considered the volume fraction of the lubricant surrogate species varying from 0 to 0.1. For a more exhaustive analysis, the comparisons between the predicted values and data deriving from the 0D numerical simulations are proposed in Figure 6.13 for two cases representative of low- and the high-temperature conditions. Figure 6.12 and Figure 6.13 confirm the good results obtained by employing Equations (3) and (4) for predicting the relative change of iso-Octane reactivity due to the addition of n-Hexadecane.

Table 6.1. Coefficient of Equations (3) and (4) obtained from the non-linear regression.

a	4.911
b	4.639
c_0	2.631
c_1	−5.685
c_2	8.610
c_3	−4.377
d_0	6.797
d_1	1.704
d_2	−3.703

Figure 6.12 reports the results by considering a narrowed range of operating conditions that might result closer to the conditions reigning in the combustion chamber of a modern DISI engine. Namely,

it was considered the volume fraction of the lubricant surrogate species varying from 0 to 0.1. For a more exhaustive analysis, the comparisons between the predicted values and data deriving from the 0D numerical simulations are proposed in Figure 6.13 for two cases representative of low- and the high-temperature conditions. Figure 6.12 and Figure 6.13 confirm the good results obtained by employing Equations (3) and (4) for predicting the relative change of iso-Octane reactivity due to the addition of n-Hexadecane.

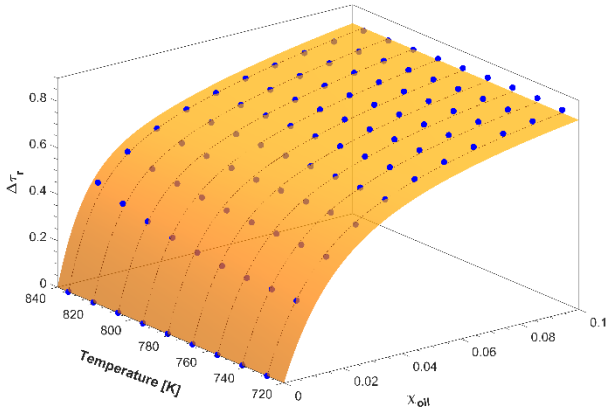

Figure 6.12. Detail of the correlation - Equations (3) and (4) – developed to capture the relative change of iso-Octane chemical ignition delay, $\Delta\tau_R$, as a function of the volume fraction of n-Hexadecane in iso-Octane, χ_{oil}, and the temperature.

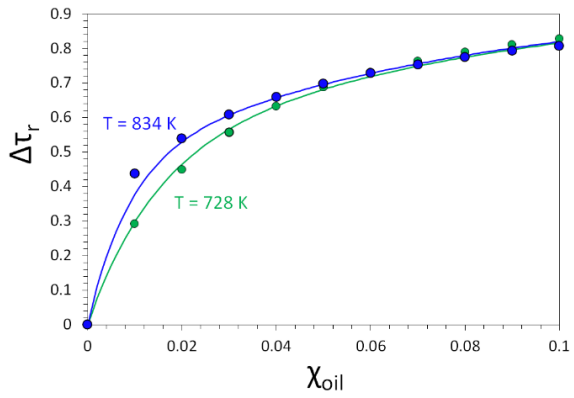

Figure 6.13. Comparison between the results obtained employing Equations (3) and (4) and the data obtained from the 0D simulations at 728 and 834 K.

6.4. Conclusions

An analytical correlation was developed in order to predict the variations of iso-Octane (gasoline surrogate) chemical ignition delay induced by the presence of n-Hexadecane (lubricant oil surrogate) in a range of operating conditions representative of those reigning in the combustion chamber of a

modern Direct Injection Spark-Ignition (DISI) engine. For this purpose, both experimental data available in the literature and numerical chemistry were considered.

Zero-dimensional numerical simulations employing the "GasLube" reaction mechanism were used to critically analyze existing experimental data and then to generate a dataset related to the chemical ignition delay of iso-Octane/n-Hexadecane mixtures. On the basis of the obtained data, an expression able to capture the relative change of iso-Octane chemical ignition delay, $\Delta\tau_R$, as a function of n-Hexadecane volume fraction and temperature was proposed. It was found that a "bi-exponential" function suits the purpose. Two polynomial expressions for the coefficients of the two exponential terms were used to capture the dependence upon the temperature.

A range of initial temperatures of the charge varying from 700 to 850 K was considered. Stochiometric conditions were considered. An initial pressure of 15 bar was selected. The correlation was validated considering the value of the fraction of lubricant oil in gasoline varying from 0 to 1. Very good results were obtained in the entire range of operating conditions considered, comprised the most likely conditions for the combustion chamber of a DISI engine, namely for lubricant oil up to 10% by volume. By means of the proposed correlation, the ignition delay of gasoline/lubricant oil mixtures can be derived directly from the values related to pure iso-Octane, avoiding the use of dedicated and computationally expensive reaction mechanisms.

Chapter 7

Lubricant Oil Influence on Hydrogen Reactivity

In this Chapter, a characterization of the effects caused by the interaction of hydrogen with lubricant oil in the combustion chamber of Hydrogen Internal Combustion Engines (HICEs) is presented. The analysis aims at ascertaining whether lubricant oil can vary the charge reactivity in a significant way so that it can promote its premature ignition. This investigation is motivated by the impelling needs to reduce the environmental impact of the mobility. Hydrogen represents one of the most attractive alternatives to replace fossil fuels in Internal Combustion Engines (ICEs), offering a strategically sound approach towards a sustainable transition to a carbon-free mobility. However, there are still criticalities that inhibit the development of efficient and reliable Hydrogen Internal Combustion Engines (HICEs), preventing such engines from penetrate the marketplace. Lubricant oil is considered the main responsible at the basis of many of these, especially for the onset of abnormal combustion modes. The unavoidable in-cylinder lubricant oil contamination has the ability to negatively affect the combustion process, representing one of the main enigmatic elements which need to be deal and resolved for delivering reliable and ready to market HICEs.

To unravel the role of lubricant oil in altering hydrogen auto-ignition tendency a reduced reaction mechanism was developed, selecting n-Hexadecane (n-$C_{16}H_{34}$) as a surrogate species to mimic lubricant oil chemical behavior. The detailed CRECK chemical model (Version 2003) was selected as a reference, from which the reduced reaction mechanism was derived. The resulting reduced kinetic mechanism is suitable for the use in practical CFD engine simulations, as it is very small in size (169 species and 2796 reactions). By employing the reduced kinetic model, Zero-Dimensional numerical simulations were performed to quantify the variation of hydrogen ignition delay time induced by different amounts of lubricant oil, considering a wide range of operating conditions consistent with those achievable in the engine combustion chamber during the compression stroke.

The results show that lubricant oil can have a significant impact on the charge reactivity, especially in the low-temperature range, which are considered safe if the analysis is restricted on the hydrogen combustion alone, with consequences that can potentially hamper the development of HICEs.

7.1. Introduction

The negative impacts of climate change are mounting very fast and bold actions are required. Greenhouse Gas (GHG) emissions from transport are major contributors to both climate change and air pollution, so that significant efforts are needed to improve the current technologies for mobility.

The most significant contribution to the GHG emissions abatement relies on the exploitation of carbon-neutral and low emission fuels. Hydrogen represents one of the most attractive alternatives to current fossil fuels. However, the development of efficient and reliable Hydrogen Internal Combustion Engines (HICEs) still faces some criticalities that prevent such engines from penetrate the marketplace. Among these, there is the spontaneous and premature ignition of the charge, with consequent loss of combustion phasing control that leads to knocking and possibly mechanical engine failure. This problem limits the engine power output by forcing a very lean operation [459].

These undesired events were initially ascribed to the presence of richer regions in the chamber. This might be the case for the Direct Injection (DI) mode, for which the achievement of a proper mixing is a really challenging tasks, but it appears unlikely for port fuel injection mode, for which a much better mixing is expected. Presumably, the explanation for the occurrence of premature autoignitions should be sought elsewhere. Hydrogen has a higher auto-ignition temperature compared to petroleum fuels [104], thus its resistance to knocking is expectedly higher. However, its lower ignition energy (one tenth that of gasoline) makes hydrogen easily ignitable by hot spots or residues in combustion chamber. Many recent works have linked the onset of abnormal combustions in HICEs to the presence of "sensitive spots" and lubricant oil, with an extremely low autoignition resistance can play a primary role in their generation [97,105,106].

It is crucial to study the reaction paths involved in lubricant oil oxidation and to understand how this indispensable element interacts with hydrogen. Unfortunately, all past research dedicated to lubricant oil chemical modelling has been focused on gasoline engines [84,87,155,175,448,460]. However, some general indication about lubricant oil chemical characteristics can be inferred from those studies and directly transferred to the case of HICEs.

For the sake of completeness, it must be mentioned that lubricant oil can produce additional deleterious effects that still need to be understood. Oil contamination can represent a non-negligible source for soot particles. The formation of lubricant-oil-derived particles in the finest and most dangerous range size (lower than 30 nm) was demonstrated independently from the fuel feeding the engine [107,109,115,461]. The long-chained hydrocarbons constituting lubricant oil enhance soot precursor formation [59,113]. Moreover, in-cylinder carbonaceous deposits and floating particles can serve as hot spots able to prematurely ignite the mixture [94], highlighting a possible secondary way by which lubricant oil can promote pre-ignition events.

The aim of this work is to shed light on lubricant oil potential of altering the charge reactivity in HICEs. A reduced kinetic mechanism was developed to this very purpose, selecting n-$C_{16}H_{34}$ as lubricant oil surrogate species. The detailed CRECK model (Version 2003) was used as the reference kinetic model for deriving a reduced mechanism having a small size, so that it can be also used in practical CFD engine simulations. The mechanism was employed in Zero-Dimensional (0D) simulations with the aim to quantify the effects that lubricant oil can have on hydrogen IDT in engine-like conditions. All the simulations were conducted considering the closed homogeneous batch reactor model with constant volume assumption for solving the time-dependent balance equations for the total mass, the gas-phase species mass, and the energy. A criterion for the IDT evaluation based on the maximum OH and/or CH increase was used.

7.2. Materials and Methods

7.2.1. Chemical Model Development

As a first step the selection of the most suitable lubricant oil surrogate species is needed. Unfortunately, all the research dedicated to lubricant oil combustion modeling has been focused on gasoline turbocharged DISI engines. However, these works provide some general indications that can be transferred to the case of HICEs. A common approach is to consider the simplest molecule that can reproduce the reactivity of lubricant oil. The findings of different research groups converge towards a single n-alkane molecule, namely n-Hexadecane $(n - C_{16}H_{34})$ [1,2]. This is in accordance with the well-known evidence that alkanes larger than C_{14} exhibit nearly identical fuel/air gas-phase ignition delay times across a range of operating temperatures [3,4].

Such an approach was successfully followed in a recent work by Distaso et al. [5], in which the so-called "GasLube" reduced chemical model was developed, starting from the detailed version developed in a previous work [6]. The reduced model was employed to reproduce the experimental data provided by Kuti et al. [7], about the reduction of the ignition delay times of iso-octane $(i - C_8H_{18})$ induced by different amount (i.e., 1% and 10%) of base oils and fully formulated oil in the mixtures.

The detailed CRECK model (Version 2003) was selected for the development of the reduced mechanism. The detailed model consists of 492 species and 17790 reactions for high and low temperature oxidation reactions. It is composed of several hierarchically organized and self-consistent sub-models, including a hydrogen sub-mechanism from Kèromnes et al. [8], a C1-C2 sub-mechanism from Metcalfe et al. [9], a C3 and molecular growth pathways from Burke et al. [10] and Ranzi et al. [11,12], recently updated by Bagheri et al. [13]. It is noteworthy that each sub-mechanism, as well as the detailed model have been thoroughly validated against experimental data covering a wide range of operating conditions and different facilities, such as shock tube, flow and jet stirred reactors.

The mechanism reduction was conducted employing DoctorSMOKE++, a numerical code based on the open-source software OpenSMOKE++ [14]. Further details about the reduction methodology and the software are available at the references [15,16]. For the reduction process, a range of temperatures spanning from 500 K to 2500 K, a pressure values from 1 bar to 50 bar and equivalence ratio from 0.5 to 4 were considered. The resulting reduced mechanism is small in size, as it consists of 169 species and 2796 reactions, with a reduction in the number of species of about 70%, which makes it suitable in practical CFD engine simulations with reduced computational costs.

To verify that the reduction process did not affect the effectiveness in predicting ignition delay values, the reduced model was tested and validated against experimental data. Furthermore, ignition delay time predictions of the starting detailed model were compared with those provided by the reduced model, covering a wide range of operating conditions.

7.2.2. 0D Numerical Simulations Setup

The proposed reduced chemical model was employed in zero-dimensional (0D) numerical simulations, to shed light on lubricant oil capability to alter hydrogen reactivity in HICEs-like conditions.

All the simulations were performed assuming the closed homogeneous batch reactor model with constant volume assumption for solving the time dependent balance equations for the total mass, the gas-phase species mass and energy. A maximum time interval of 500 ms was imposed, because longer time are not of interest for engines analysis. A criterion for the 44ignition delay time evaluation based on the maximum OH and/or CH increase was used.

The simulations were performed considering a wide range of operating conditions, in order to cover typical conditions achievable in Spark-Ignition (SI) and Compression Ignition (CI) engines during the compression stroke. The temperature was varied from 500 K to 1300 K, the pressure range covers values from 1 bar to 100 bar, three equivalence ratio were considered, namely 0.25, 0.50 and 0.75 and the lubricant oil fraction, χ_{oil}, was varied from 0 to 0.1.

7.2.3. Analysis Procedure Methodology

The results obtained were firstly analyzed comparing the ignition behavior of the two pure species to highlight the existing difference in reactivities, secondly to unravel the effects of the addition of lubricant oil surrogate species on the H_2 reactivity, as such an approach is more resembling of the conditions that can arise in the combustion chamber.

To highlight the lubricant oil induced change in reactivity a parameter able to quantify the order of magnitude of the variation in ignition delay time was defined as follow:

$$\Delta\tau = log_{10}\frac{\tau_{H_2}}{\tau_{H_2/Oil}} \quad (1)$$

The $\Delta\tau$ parameter can assume both positive and negative values, pointing out that the addition of lubricant oil surrogate species can results in an increase or decrease in reactivity (in shorter or longer IDTs), respectively.

In highlighting the role played by lubricant oil, an analysis focused on mixture reactivities is not sufficient alone to investigate which in-cylinder conditions can promote the onset of premature auto-ignition of the charge. When the piston travel from the bottom dead center (BDC) to the top dead center (TDC), the charge experienced an increase in temperature and pressure, reaching the suitable conditions for the trigger of the combustion. However, during the compression stroke, in-cylinder oil contamination could occur randomly, potentially resulting in undesired auto-ignition of the charge. Thus, it is more useful to conduct an analysis having the aim to elucidate the influence of in-cylinder thermodynamic conditions on the ignition delay time, in order to compare it with the typical residence time of the charge in the combustion chamber. Furthermore, such an approach allows to determine which instant of the compression stroke could be more prone to premature auto-ignition.

For this very purpose, different analyses were conducted, considering different mixtures, compression ratio (CR) and equivalence ratio (ϕ) values. The first analysis highlights the variation of the ignition delay times due to the thermodynamic conditions that may establish in the combustion chamber at half compression stroke (HCS) and at top dead center (TDC).

The second analysis shows which in-cylinder thermodynamic conditions at HCS and TDC and which lubricant oil fraction, χ_{oil}, could lead to ignition delay times resulting potentially in a safe or unsafe engine operating condition in terms of premature ignitions.

In this analysis the effective compression ratio (ECR) was also considered. This because, the compression process does not effectively start when the piston is at the BDC, but rather when the inlet valve is effectively closed (IVC_{eff}), namely a few crank angle degrees (CADs) after the bottom dead center (ABDC). Thus, a merely geometric definition of the CR may not be faithfully representative of the compression stroke. Based on the experimental data provided by Modiyani et al. [17], a parameter ε that allowed to correct the geometric compression ratio (GCR) was defined as follow:

$$\varepsilon = \frac{ECR}{GCR} \; with \; \varepsilon \; \epsilon \; [0.7, 1.1]$$

For a more in-depth analysis, the compression lines are reported, considering different initial conditions for the modeling of the compression stroke, as listed in Table 7.1:

Table 7.1. Different initial conditions for the modeling of the compression stroke

Case	Temperature [K]	Pressure [bar]
A	310	1.2
B	310	1.0
C	350	1.2
D	350	1.0

Using different compression ratio values and different initial conditions, two areas were defined, which enclose the thermodynamic conditions that can arise in the cylinder at half compression stroke (HCS) and at top dead center (TDC), with the aim to elucidate which phase of the compression stroke could be more prone to undesired auto-ignition. This allowed to directly compare the ignition delay times of the H_2/Air and $H_2/n-C_{16}H_{34}/Air$ mixtures with the time needed by the piston to complete the compression stroke.

7.3. Results and Discussion

7.3.1. Reduced Chemical Model Validation

The reduced chemical model was tested against experimental data in order to ensure that the reduction process did not affect its effectiveness in predicting IDT values. Figure 7.1 and Figure 7.2 show the comparison between the numerical results (solid lines) and shock tube experiments carried out by Zhang et al. [18] and Hu et al. [19] (symbols), involving pure hydrogen at different pressure and equivalence ratio values.

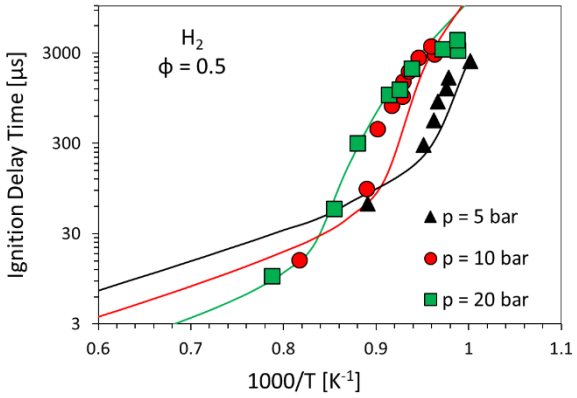

Figure 7.1. Comparison between Hydrogen experimental data provided by Zhang et al. [18] (symbols) and numerical simulations in this work obtained by means of the reduced kinetic model (solid lines).

Considering the range of temperatures investigated in this work, it was necessary to validate/test/verify the reduced chemical model against $n-C_{16}H_{34}$ experimental IDT values, paying attention to the low-to-intermediate temperature reactivity. Unfortunately, all the experimental studies involving $n-C_{16}H_{34}$ have been focused in the high temperature range. This is mainly due to the lower vapor pressure of large n-alkanes which complicates gas phase auto-ignition experiments in the low-to-intermediate temperature. To the authors knowledge there is only one experimental investigation available in the literature, concerning $n-C_{16}H_{34}$ auto-ignition in the low-to-intermediate temperature.

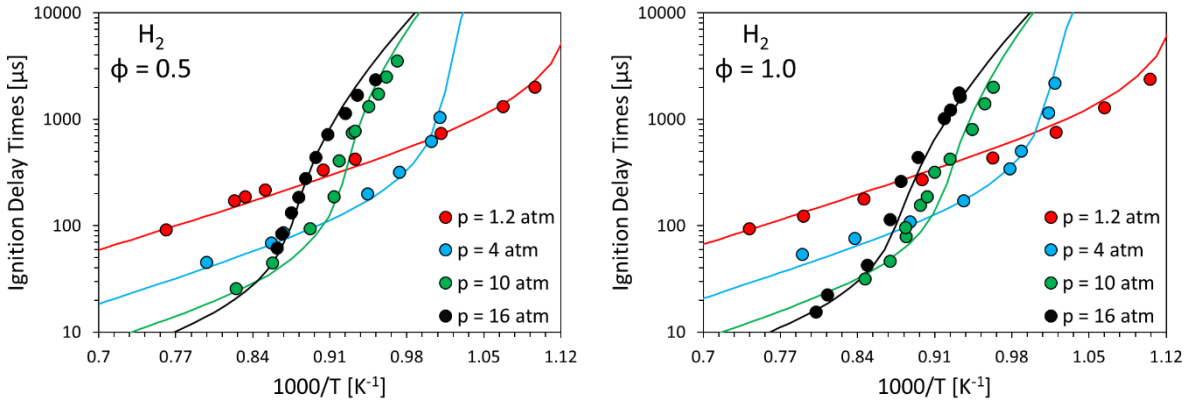

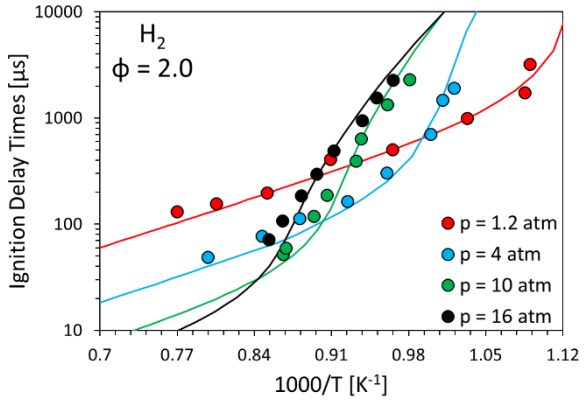

Figure 7.2. Comparison between Hydrogen experimental data provided by Hu et al. [19] (symbols) and numerical simulations in this work obtained by means of the reduced kinetic model (solid lines).

Figure 7.3 depict experimental IDT results provided by Yu et al. [20] (symbols) employing a heated rapid compression machine (HRCM). In the same figures the numerical results (solid lines) are also reported. It is worth mentioning that Yu et al. [20] provided the validation of several kinetic mechanism available in the literature, including the detailed chemical model employed for the development of the reduced model proposed in this work.

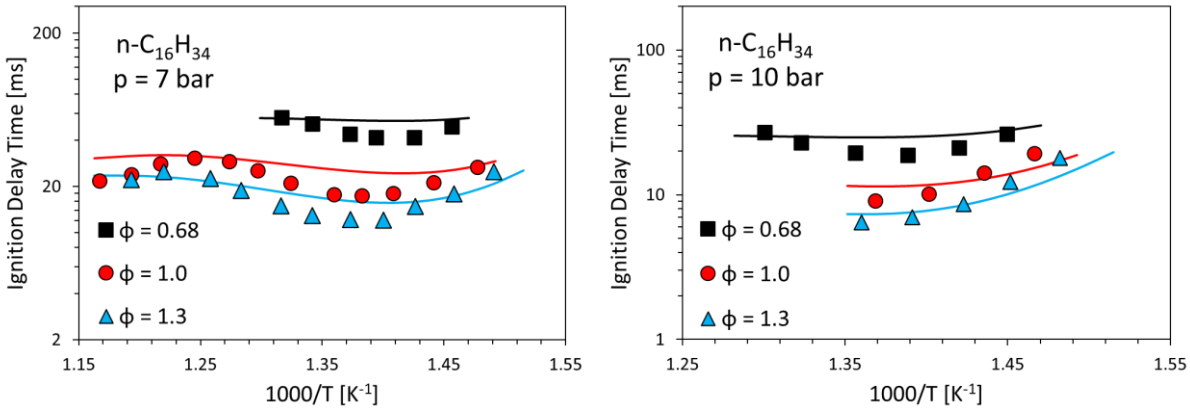

Figure 7.3. Comparison between n-Hexadecane experimental data provided by Yu et al. [20] (symbols) and numerical simulations in this work obtained by means of the reduced kinetic model (solid lines).

In order to ascertain the capability of the reduced model to capture the typical ignition behavior of mixtures composed by H_2 and n-alkanes, namely cool flame and Negative Temperature Coefficient (NTC) chemistry, the reduced mechanism was further tested against experimental data. Unfortunately, in the literature there is no availability of experimental data focusing on the ignition behavior of $H_2/n-C_{16}H_{34}$ mixtures in the low-to-intermediate temperature range. Thus, the reduced reaction mechanism was tested against experimental data provided by Comandini et al. [21]. The results concerned mixtures consisting of n-Heptane, $n-C_7H_{16}$ and H_2 in different proportion, with a constant pressure of 20 bar and different equivalence ratio values (i.e. 0.832, 1 and 1.248). the comparison between experiment (symbols) and numerical (solid lines) results are depicted in Figure 7.4.

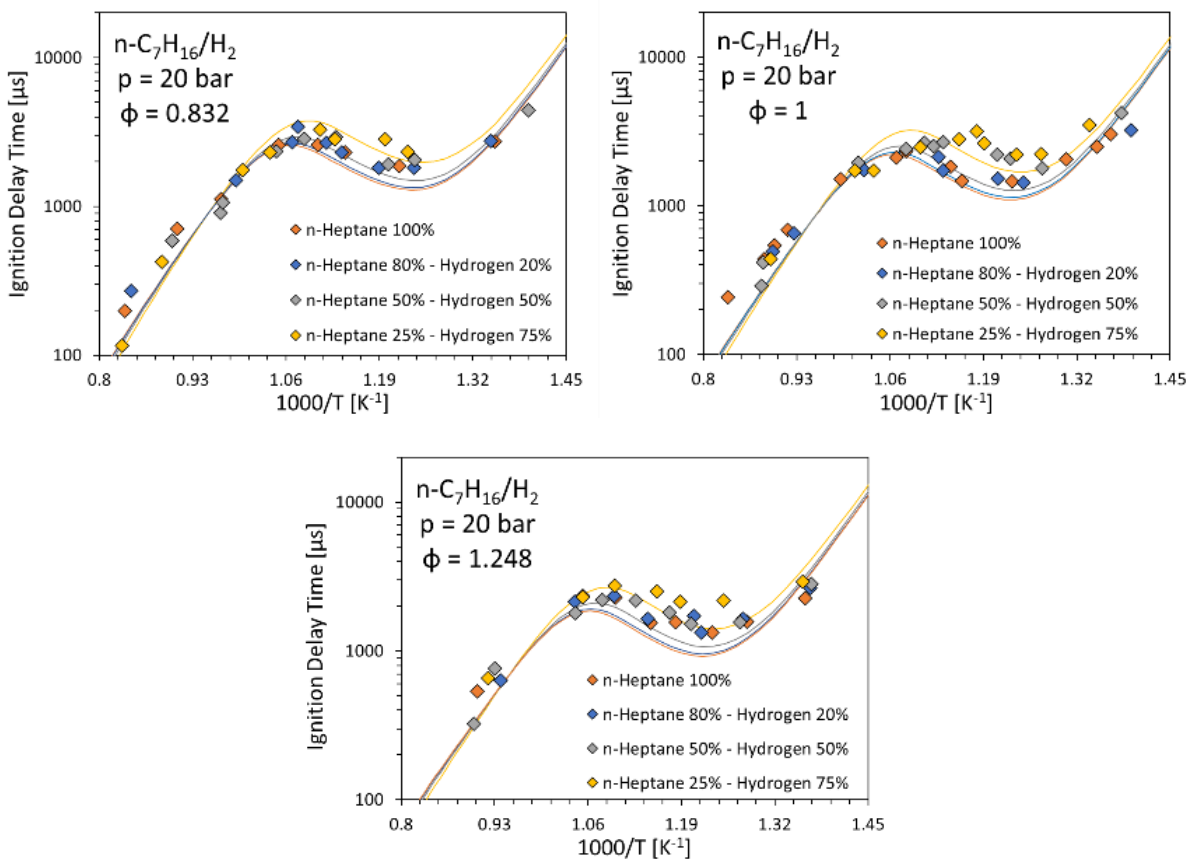

Figure 7.4. Comparison between n-C_7H_{16}/ H_2 experimental data provided *by Comandini et al.* [21] (symbols) and numerical simulations in this work obtained by means of the reduced kinetic model (solid lines).

As a further test, the results of the reduced mechanism were compared with those of the reference detailed model used in this work. The comparison involved H_2 and $n-C_{16}H_{34}$ pure species, considering a wide range of operating conditions. Namely the temperature was varied from 500 K to 1300 K, the pressure from 5 bar to 50 bar and the equivalence ratio from 0.5 to 2.0 as can be inferred from the Figure 7.5 and Figure 7.6, the IDT results provided by the reduced mechanism perfectly overlap those of the reference detailed model.

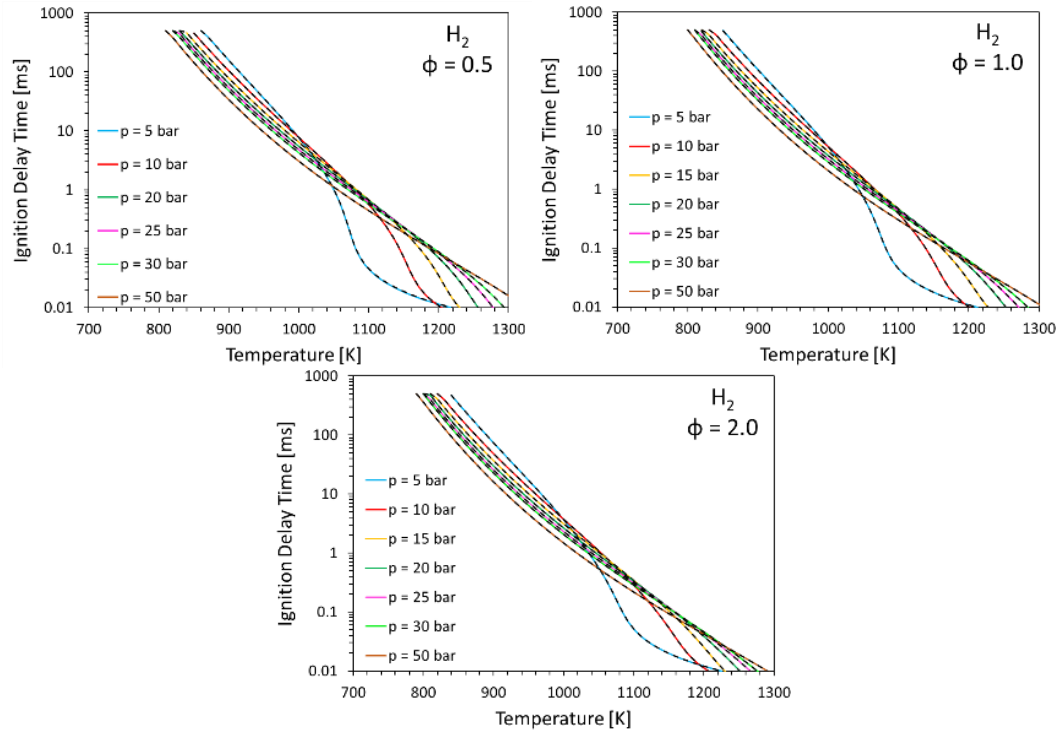

Figure 7.5. Comparison between the predictions in ignition delay times provided by the starting detailed model (solid lines) and the reduced model (dashed lines), for pure species Hydrogen and n-Hexadecane at different pressure and equivalence ratio.

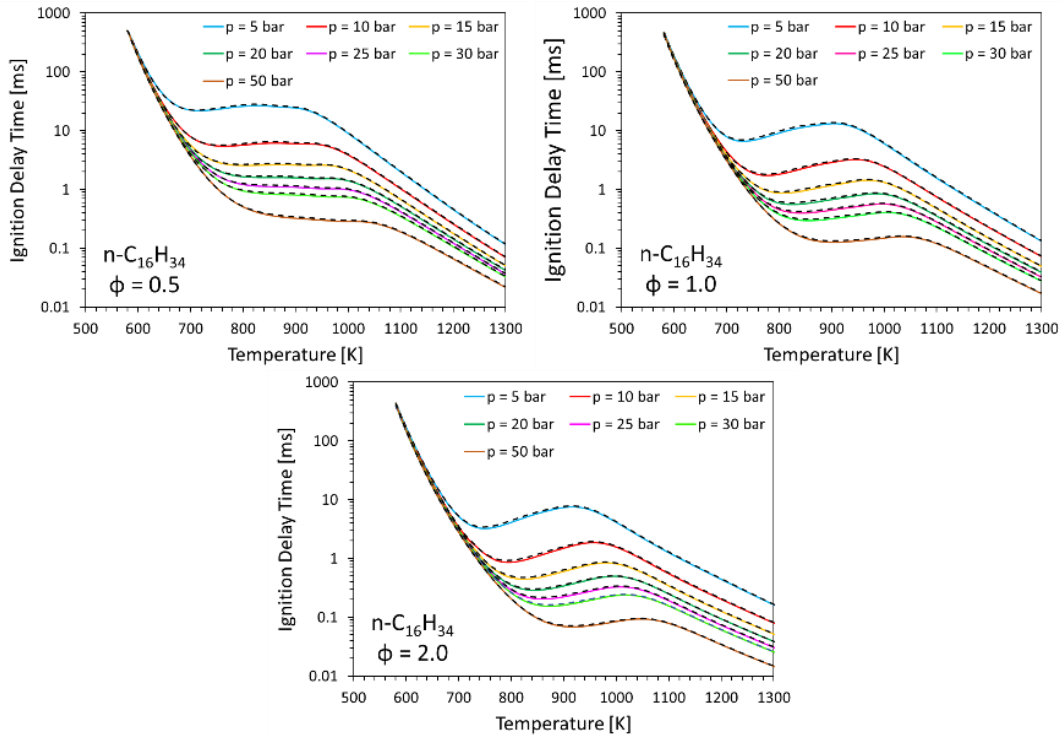

Figure 7.6. Comparison between the predictions in ignition delay times provided by the starting detailed model (solid lines) and the reduced model (dashed lines), for pure species Hydrogen and n-Hexadecane at different pressure and equivalence ratio.

The tests conducted have shown that the reduction process did not affect the reliability of the chemical model in predicting IDT values.

7.3.2. Pure Species Ignition Behavior Analysis

Figure 7.7 and Figure 7.8 show a comparison between H_2/Air (light blue solid line) and $n-C_{16}H_{34}/Air$ (gold solid line) mixtures in terms of HRR traces and IDTs at different equivalence ratios and pressures.

It is noticeable that H_2/Air and $n-C_{16}H_{34}/Air$ mixtures show a deeply different ignition behavior, mainly due to the extremely different molecular structure. This is evident especially in the low-to-intermediate temperature regime, in which lubricant oil surrogate species reactivity extends to the temperatures significatively lower and with higher reactivity than H_2. This is attributable to the typical chemistry of the long straight-chained hydrocarbon species associated with the so-called cool flames and NTC regime [4,20,22,23]. Only at very high temperatures the H_2/Air mixture shows shorter IDT values.

The analysis of HRR trace points out the different auto-ignition process characterizing the two pure species. When a long straight-chained hydrocarbon species is involved in the combustion process, the exothermic reactions started to take place early, leading to a Low Temperature Heat Release (LTHR) during the first ignition stage. As a result, an early HR is released in a shorter time in the first ignition stage, which in turn promotes the second ignition stage. The first ignition stage, in which LTHR occurs, is the most fuel-type-dependent ignition stage and it is governed by the initiation hydrogen abstraction and the subsequent alkylperoxy radical isomerization reactions [24–26].

A lubricant oil molecule modeled as a long straight chained $n-C_{16}H_{34}$, presents a large number of secondary bonds with lower activation energy, allowing a faster and simpler hydrogen abstraction. The large number of secondary C-H bonds in $n-C_{16}H_{34}$ molecule promotes the initial H-abstraction step, by which the related alkyl-radicals are produced. After multiple oxygen addition and isomerization steps, ketohydroperoxide species are formed and readily decomposed in a degenerate chain branching pathways that are at the basis of the low-temperature heat release (LTHR) in the cool flame regime, also involved in engine knock phenomena [27]. Instead, the second ignition stage is relatively fuel-independent, because at higher temperatures the H_2/O_2 system starts to dominate the oxidation process, in which the branching reactions involving H_2O_2 decomposition became progressively most important [28].

On the contrary, the H_2 IDT curves show a single ignition stage. The effect of the single ignition stage is also appreciable in Figure 7.8, which depict a clear monotonic trend over the whole temperature range. In the high temperature regime, it is observed a steeper decrease of the IDT curve. Such a change in slope is attributable to the transition from weakly to strongly explosive behavior observed for H_2/Air mixtures [29]. It is worth to mention that the pressure range of interest for engine applications is that associated with the third explosion limit of the H_2/O_2 chemistry. In this range, for temperatures slightly above the third limit, the HO_2 chemistry dominates, while for significatively higher temperatures the $H+O_2$ chain branched mechanism speeds up the H_2 oxidation process.

The transition in explosivity is delimited by the extended second explosion limit and it is visible at around 1050/1100 K in Figure 7.8.

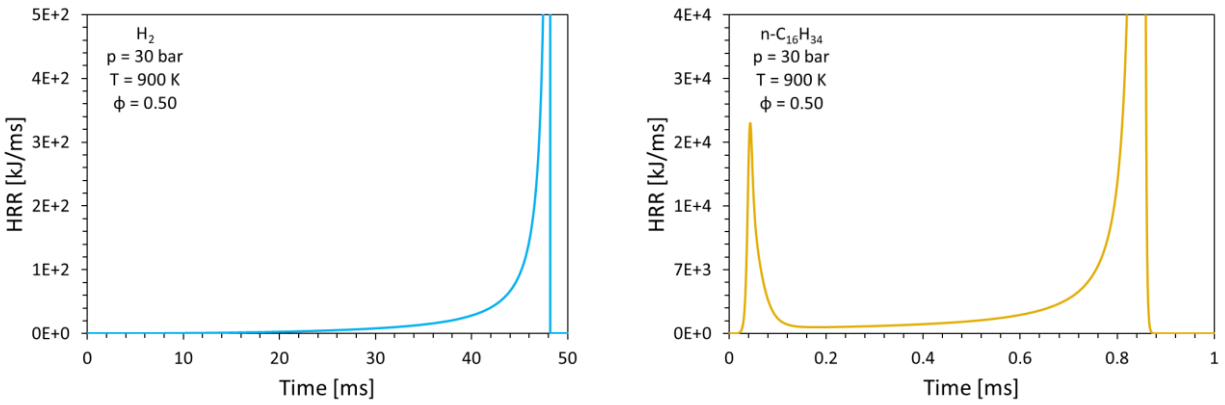

(a) (b)

Figure 7.7. Comparison between HRR traces H_2/Air (light blue solid line) and $n-C_{16}H_{34}/Air$ (gold solid line).

As a consequence of the quite different behavior showed by the two species, four region can be identified, as highlighted in Figure 7.8. The lowest $\mathrm{n-C_{16}H_{34}}$ auto-ignition temperature at a given pressure, defines the extension of Region 1, in which neither $\mathrm{n-C_{16}H_{34}}/Air$ nor $\mathrm{H_2/Air}$ mixtures can be ignited, due to excessively low temperatures. In Region 2, $\mathrm{n-C_{16}H_{34}}$ shows explosive behavior, while the temperatures are still too low for promoting $\mathrm{H_2}$ ignition. The extension of the Region 2 is given by the lowest $\mathrm{H_2}$ auto-ignition temperature, which also defined the lower boundary of the Region 3. In Region 3, the temperatures are quite high to ignite $\mathrm{H_2}$, even if the related IDT values are longer than those of $\mathrm{n-C_{16}H_{34}}$. Near the lower limit of Region 3, the difference between the IDT values of $\mathrm{n-C_{16}H_{34}}$ and $\mathrm{H_2}$ is larger than two orders of magnitude, which suggests that at least the first half of this region needs to be taken under consideration. Finally, Region 4 identified the high temperature region, in which $\mathrm{H_2}$ is more reactive than $\mathrm{n-C_{16}H_{34}}$, showing shorter IDT values. The boundary that separates Region 3 from Region 4 is located at temperature slightly lower than that at which $\mathrm{H_2/O_2}$ system starts to show a strongly explosive behavior and dominates the oxidation process.

The existence of the Region 2 and 3 is a first clear indication that lubricant oil can represent a potential issue for the normal HICEs operating conditions. From the analysis of these regions some important indications can be derived.

The temperature values in Region 2 are well below the $\mathrm{H_2}$ auto-ignition temperature, thus not considered potentially dangerous if the analysis is restricted to the $\mathrm{H_2}$ ignition. However, it is evident that in-cylinder oil contamination can extend the range of dangerous temperatures. Most importantly, these low temperatures are comparable with in-cylinder values achievable during the compression stroke before combustion. In Region 3, although the temperature values start to be relatively high, there might be some chances to the onset of undesired charge auto-ignition around the top dead center (TDC) or even latter. This because, $\mathrm{n-C_{16}H_{34}}$ shows a significatively higher reactivity than $\mathrm{H_2}$. From this analysis can be inferred that in-cylinder oil contamination can be

potentially dangerous for the regular operation of HICEs in a temperature range spanning from Region 2 to Region 3.

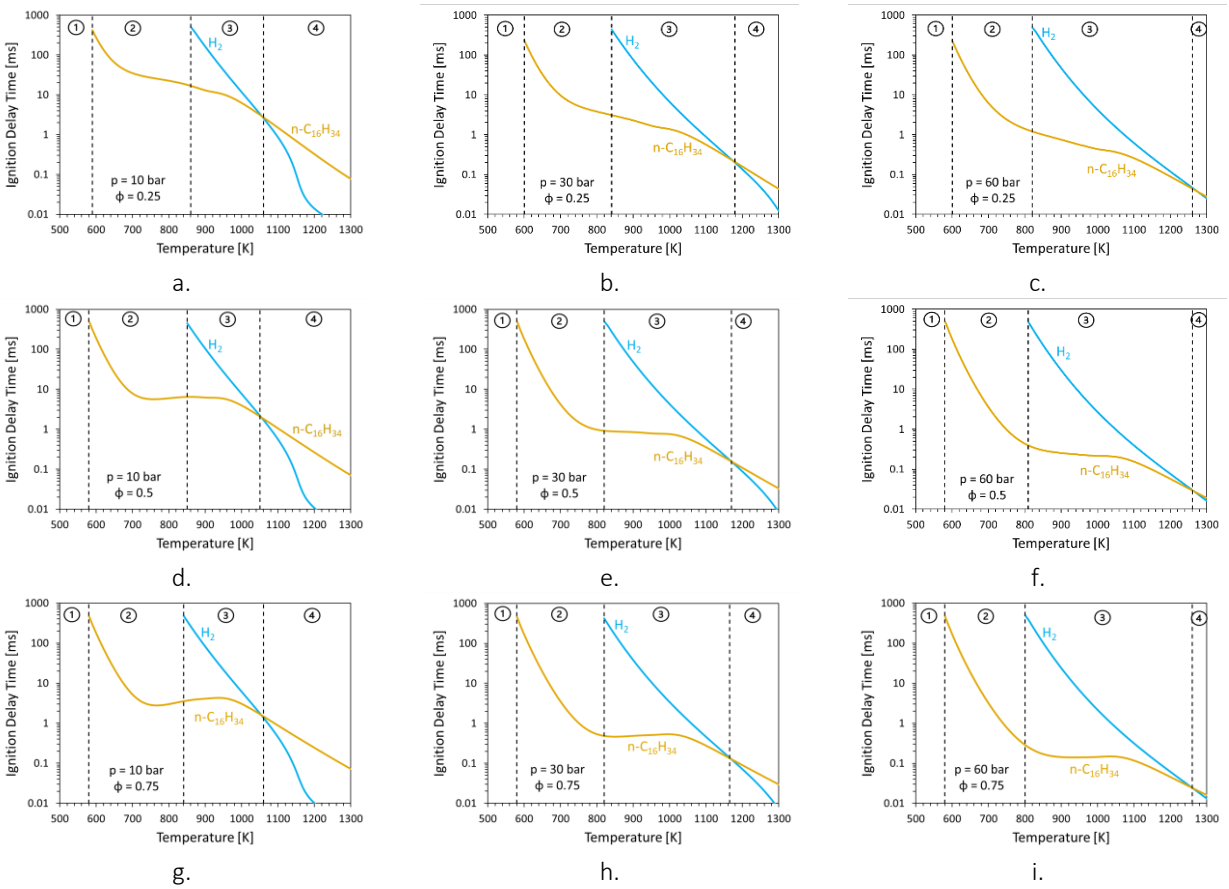

Figure 7.8. Comparison between H_2/Air and $n-C_{16}H_{34}/Air$ mixtures ignition behavior at different pressure and equivalence ratio values

Figure 7.8 show that a pressure increases drastically affect the $\mathrm{n-C_{16}H_{34}}$ IDT curves. As a consequence, the $\mathrm{n-C_{16}H_{34}}$ curves move down to significatively shorter times. In addition, NTC regime is shifted towards higher temperatures, and it becomes progressively less pronounced with the pressure increases. As an example, for an equivalence ratio ϕ of 0.25 at 10 bar (Figure 7.8-a), $\mathrm{n-C_{16}H_{34}}$ shows an IDT equal to 10 ms at 960 K, while $\mathrm{H_2}$ shows the same IDT at 1000 K. At 60 bar (Figure 7.8-c), $\mathrm{n-C_{16}H_{34}}$ ignites in 10 ms at 680 K, while $\mathrm{H_2}$ require 10 ms at 960 K.

However, the pressure increases not only affect IDT values, but also the relative extension (extent) of the four regions. As a result of the pressure increase, the temperature range defining the extent of the Region 2 is slightly narrowed. The lower limit seems to be not very sensitive, remaining stable at around 580 K, while the upper limit shifted from about 850 K at 10 bar to about 810 K at 60 bar, due to the slightly lower $\mathrm{H_2}$ auto-ignition temperature. These modifications determine that Region 2 is almost entirely occupied by the cool flame regime at higher pressure, while includes both cool flames and NTC regimes at lower pressures.

During the last part of the compression stroke, the in-cylinder pressure can reach values comparable with 30 bar and 60 bar. Therefore, if thermodynamic conditions suitable for a premature auto-ignition of the charge are established, such pre-ignition event is surely the consequence of the low-

temperature heat release involved in the cool flame chemistry, typical of the long-chained hydrocarbon species that composing lubricant oil.

On the contrary, the extent of the Region 3 increases, because the reactivity crossing point between H_2 and $n-C_{16}H_{34}$, which defines the upper limit of the Region 2, is shifted toward higher temperatures. As a result, the temperature range in which the lubricant oil surrogate species remains more reactive than hydrogen is extended by the pressure increases. This is linked to the shifting of the transition from weakly to strongly explosive behavior of the H_2/O_2 system to higher temperatures with the pressure increase, in accordance with what has been previously observed [29,30].

An increase in equivalence ratio affects the shape of the $n-C_{16}H_{34}$ related IDT curves but does not affect the relative extension of the four regions. In the Region 2 it is noticeable a greater reactivity of the lubricant oil surrogate species as the equivalence ratio increases. At 30 bar and ϕ=0.25 (Figure 7.8-b) $n-C_{16}H_{34}$ shows an IDT value equal to 1 ms at 1040 K, while this time is reached at 750 K at ϕ=0.75 and 30 bar (Figure 7.8-h). This is due to the higher amount of long straight-chained $n-C_{16}H_{34}$ in the mixture, which increase the formation and decomposition of highly oxygenated intermediates (i.e., ketohydroperoxides) [27]. Furthermore, the NTC regime becomes more pronounced as the equivalence ratio increase, leading to a clear non-monotonic trend. This behavior is attributable to the interaction between the alkyl-radical and O_2 and the consequent formation of the conjugate alkene and HO_2 radical, which does not contribute to chain branching, but rather tends to produce the metastable H_2O_2. The olefins formation and the interruption of the chain branching pathway determine the entrance into NTC regime, leading to an increase in IDT with the temperature. For the sake of completeness, as the temperature is further increased, the H_2/O_2 system starts to dominate the oxidation process, by which the H_2O_2 decomposition becomes increasingly important. As a consequence, the $n-C_{16}H_{34}$ IDT curve resumes its rapid decrease with temperature.

7.3.3. H_2/n-$C_{16}H_{34}$/Air Mixtures Ignition Behavior Analysis

The results showed in the above analysis highlight the difference in reactivity existing between the two pure species. However, such an approach is not sufficient to thoroughly analyze the thermochemical conditions that may arise in the combustion chamber where lubricant oil contamination occurs. When oil droplets are released, a gaseous mixture of oil and fuel can form and reacts with the available air. As a result, the charge experiences a local increase of the fuel-to-air ratio where oil is entrained. This because, the two species require a different amount of air for obtaining the same equivalence ratio value. This effect on the fuel-to-air ratio is depicted in Figure 7.9.

Considering a H_2/Air mixture having an initial equivalence ratio, ϕ_{H2}, of 0.25, a lubricant oil volume fraction, χ_{oil}, equal to 0.01 produces a global equivalence ratio, ϕ_g, of 0.4. For χ_{oil} equal to 0.05 and 0.10 the global equivalence ratio, ϕ_g, reaches values of 0.9 and 1.6 respectively. For an initial ϕ_{H2} = 0.5, a volume fraction of 0.02 is sufficient to establish locally stoichiometric conditions (i.e., ϕ_g = 1.0). For $\chi_{oil} = 0.05$ the global equivalence ratio stands at 1.8 and for $\chi_{oil} = 0.10$ reaches a value of 3.2.

For the richer ϕ_{H2} (i.e., 0.75), a volume fraction of $\chi_{oil} = 0.01$, $\chi_{oil} = 0.05$ and $\chi_{oil} = 0.10$ leads to a global equivalence ratio of 1.7, 2.7 and 4.8 respectively.

This points out that lubricant oil contamination can lead to a non-negligible local enrichment of the charge, which in turn increases local reactivity, due to its higher reactivity in the low-temperature regime. These two competing effects were investigated by performing simulations in which the volume fraction, χ_{oil}, in $\mathrm{H_2}/Air$ mixture was varied from 0 to 0.10, with the global equivalence ratio, ϕg, varied accordingly to the trend showed in Figure 7.9.

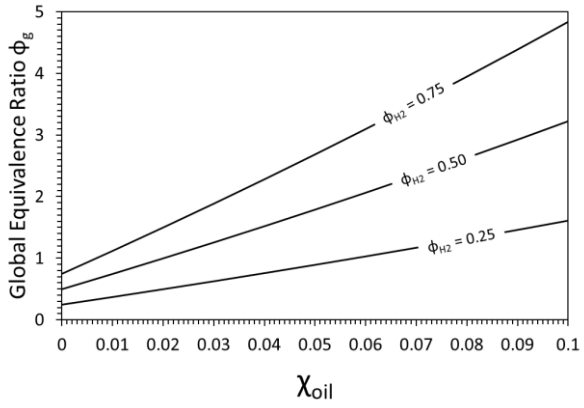

Figure 7.9. Global equivalence ratio (ϕ_g) variation with lubricant oil surrogate volume fraction (χ_{oil}) in H_2/Air mixtures.

Figure 7.10 report the IDT curves of the $\mathrm{H_2}/\mathrm{n}-\mathrm{C_{16}H_{34}}/Air$ mixtures at the same pressures and equivalence ratios considered in the previous analysis related to the pure species. As a reference, the IDT curves of $\mathrm{H_2}/Air$ (light blue solid lines) and $\mathrm{n}-\mathrm{C_{16}H_{34}}/Air$ (gold solid lines) mixtures are also reported. Figure 7.11 depict the order of magnitude of the IDT variation due to the addition of lubricant oil surrogate species in $\mathrm{H_2}/Air$ mixtures.

Figure 7.10 point out a common trend across all the considered operating conditions. For an oil fraction, χ_{oil}, ranging from 0.01 and 0.03, the IDT curves are comprised between those of $\mathrm{H_2}/Air$ and $\mathrm{n}-\mathrm{C_{16}H_{34}}/Air$ mixtures. Values of χ_{oil} comprised between 0.03 and 0.04 are sufficient to obtain IDT curves close to that of $\mathrm{n}-\mathrm{C_{16}H_{34}}/Air$ mixtures. For χ_{oil} greater than 0.04, the $\mathrm{H_2}/\mathrm{n}-\mathrm{C_{16}H_{34}}/Air$ related IDT curves show a reactivity even higher than that of $\mathrm{n}-\mathrm{C_{16}H_{34}}/Air$ mixtures, due to the increased fuel-to-air ratio. As a consequence, the portion of the IDT curves associated with the NTC regime are shifted down toward increasingly shorter IDT values as χ_{oil} is progressively increased.

In-cylinder lubricant oil contamination significantly alters hydrogen reactivity and even trace amounts could result in IDT variation of several order of magnitude. The order of magnitude variation of the reactivity of the H_2/n-$C_{16}H_{34}$ mixtures is shown in Figure 7.11. For the sake of brevity, only the results concerning ϕ_{H2} = 0.50 are reported, as the trend across all the considered operating conditions are very close to each other.

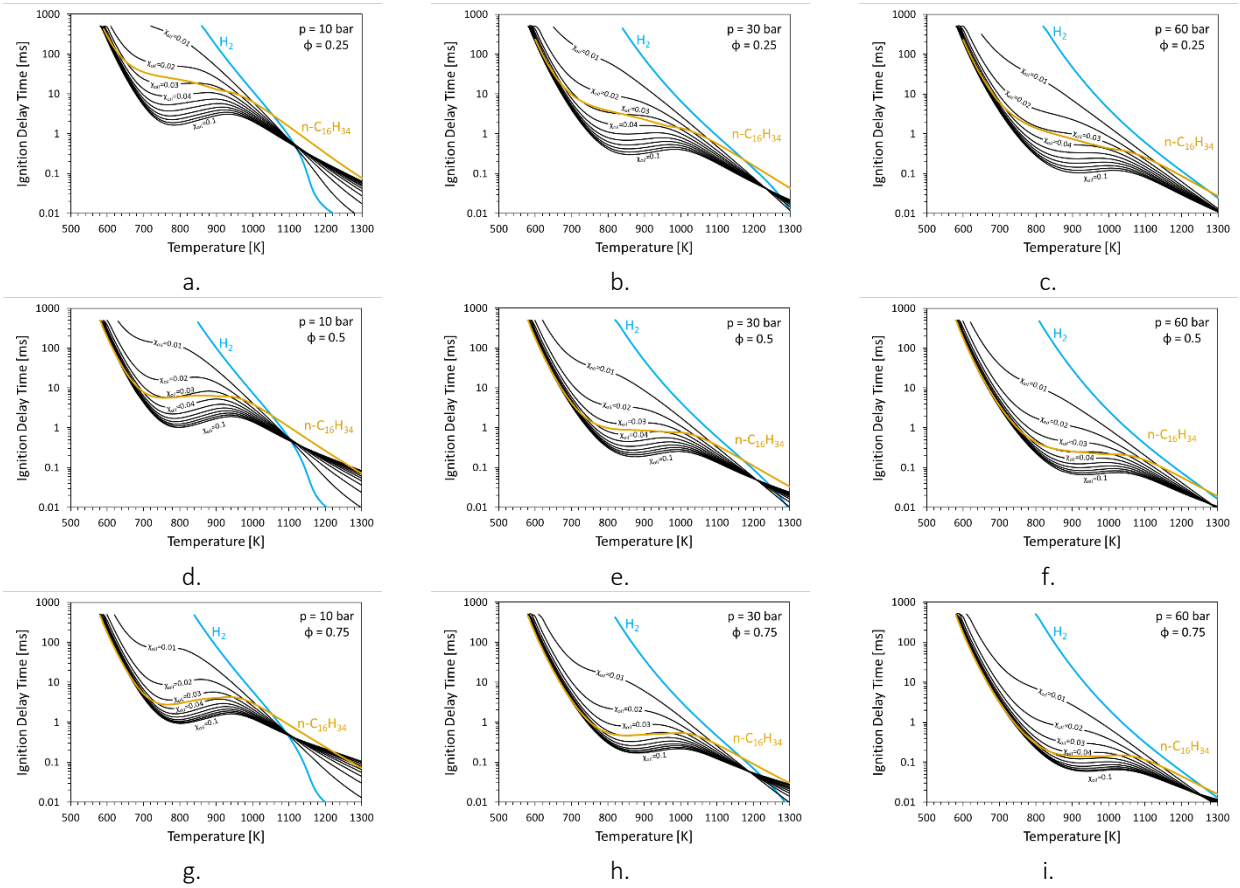

Figure 7.10. Effects of lubricant oil surrogate (n-$C_{16}H_{34}$) addition on H_2 IDT at different pressures and equivalence ratios. Light blue solid lines and gold solid lines refer to H_2/air mixtures and n-$C_{16}H_{34}$/air mixtures.

At ϕ_{H2} = 0.50 and 10 bar (Figure 7.11-a), the order of magnitude of the IDT variation goes from 0.8 to 1.8 for the IDT curves between $\mathbf{H_2/Air}$ and $\mathbf{n-C_{16}H_{34}/Air}$ mixtures. An increase in pressure leads to a greater IDT variation. For instance, at 30 bar (Figure 7.11-b), the order of magnitude varies from 1.3 to 2.6, while at 60 bar (Figure 7.11-c) reaches values between 1.6 and 2.8. For the same equivalence ratio and pressure values, the IDT curves close to that of $\mathbf{n-C_{16}H_{34}/Air}$ mixtures show a higher order of magnitude. The order of magnitude increases for the IDT curves close to that of $\mathbf{n-C_{16}H_{34}/Air}$ mixtures, namely are observed values of about 2.0 at 10 bar, 2.6 at 30 bar and 2.9 at 60 bar. Larger values of χ_{oil} could lead to orders of magnitude even greater than 3.

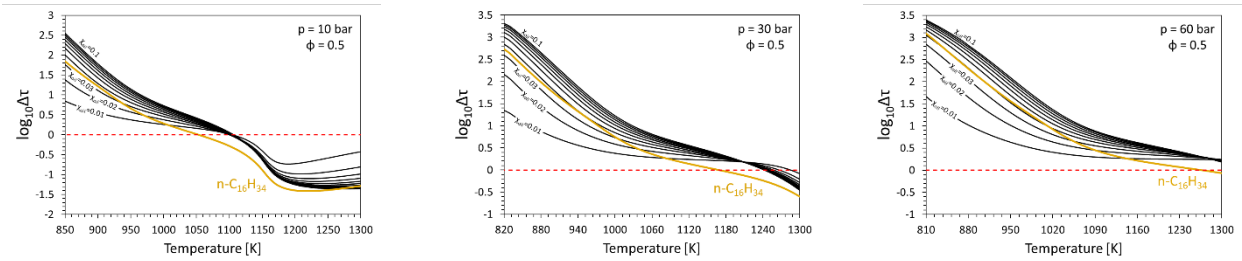

Figure 7.11. Order of magnitude of the IDT variation due to the lubricant oil surrogate (n-$C_{16}H_{34}$) addition in H_2/Air mixtures at different pressures and equivalence ratios. Black solid lines and gold solid lines refer to H_2/ n-$C_{16}H_{34}$/Air mixtures and n-$C_{16}H_{34}$/air mixtures.

7.3.4. H_2/n-$C_{16}H_{34}$/Air Mixtures Analysis in HICEs Operating Conditions

Figure 7.12 and Figure 7.13 show the variation of ignition delay times of $\mathrm{H_2/Air}$ and $\mathrm{H_2/n-C_{16}H_{34}/Air}$ mixtures due to the in-cylinder temperatures and pressures that may arise at half compression stroke (HCS, red area) and at top dead center (TDC, green area) at different compression ratios (i.e., 10 and 16). The analysis was conducted considering several constant IDTs with temperatures and pressures for different starting equivalence ratios ϕ_{H2} (i.e., 0.25, 0.50 and 0.75).

Each of the curves shown represent a curve with constant ignition delay time with temperature and pressure. In addition, each curve identifies two regions with lower (at the right side) and higher (at the left side) IDTs with respect to the reference constant IDT curve. As an example, considering the reference curve denoted with 10 ms, it encloses the points with constant IDT of 10 ms for each value of temperature and pressure. On the right side there are thermodynamic conditions that could lead to IDTs increasingly shorter than 10 ms, while on the left side there are IDTs increasingly longer than 10 ms.

An increase in equivalence ratio results in a shift of the curves toward lower temperatures, due to the higher mixture reactivities. The increase in reactivity especially affects $\mathrm{H_2/n-C_{16}H_{34}/Air}$, due to the presence of long-chained hydrocarbon species that leads to an increase of the fuel-to-air ratio. As a consequence of compression ratio increase, the HCS and TDC areas move along the isentropic compression lines, toward higher temperatures and pressures, establishing more conducive auto-ignition conditions at HCS and TDC.

For $\mathrm{H_2/Air}$ mixtures, for all the compression and equivalence ratio values considered, the thermodynamic conditions that can arise at **HCS** always result in IDTs considerably longer than 100 ms (Figure 7.12) On the other hand, the most severe and conducive conditions could occur at **TDC**. At $\mathrm{CR} = 10$, an increase in equivalence ratio results in shorter IDTs at **TDC**. For instance, at ϕ_{H2} = 0.25 (Figure 7.12-a) the iso-τ curves ranging from 50 ms to 100 ms are included in the TDC area. This means that at **TDC** could arise thermodynamic conditions resulting in IDTs starting from 50 ms up to significantly longer than 100 ms. At ϕ_{H2} = 0.75 (Figure 7.12-e), could result in IDT values starting from 20 ms up to higher than 100 ms at TDC.

As can be inferred, an increase in CR could have a greater impact (Figure 7.12 b, d, f). At $\mathrm{CR} = 16$, at **TDC** could reign thermodynamic conditions resulting in IDTs even shorter than 1 ms. As a result, when the piston is about to complete the compression stroke, at **TDC** could arise thermodynamic conditions for which also $\mathrm{H_2/Air}$ mixtures could result in unsafe engine operating conditions.

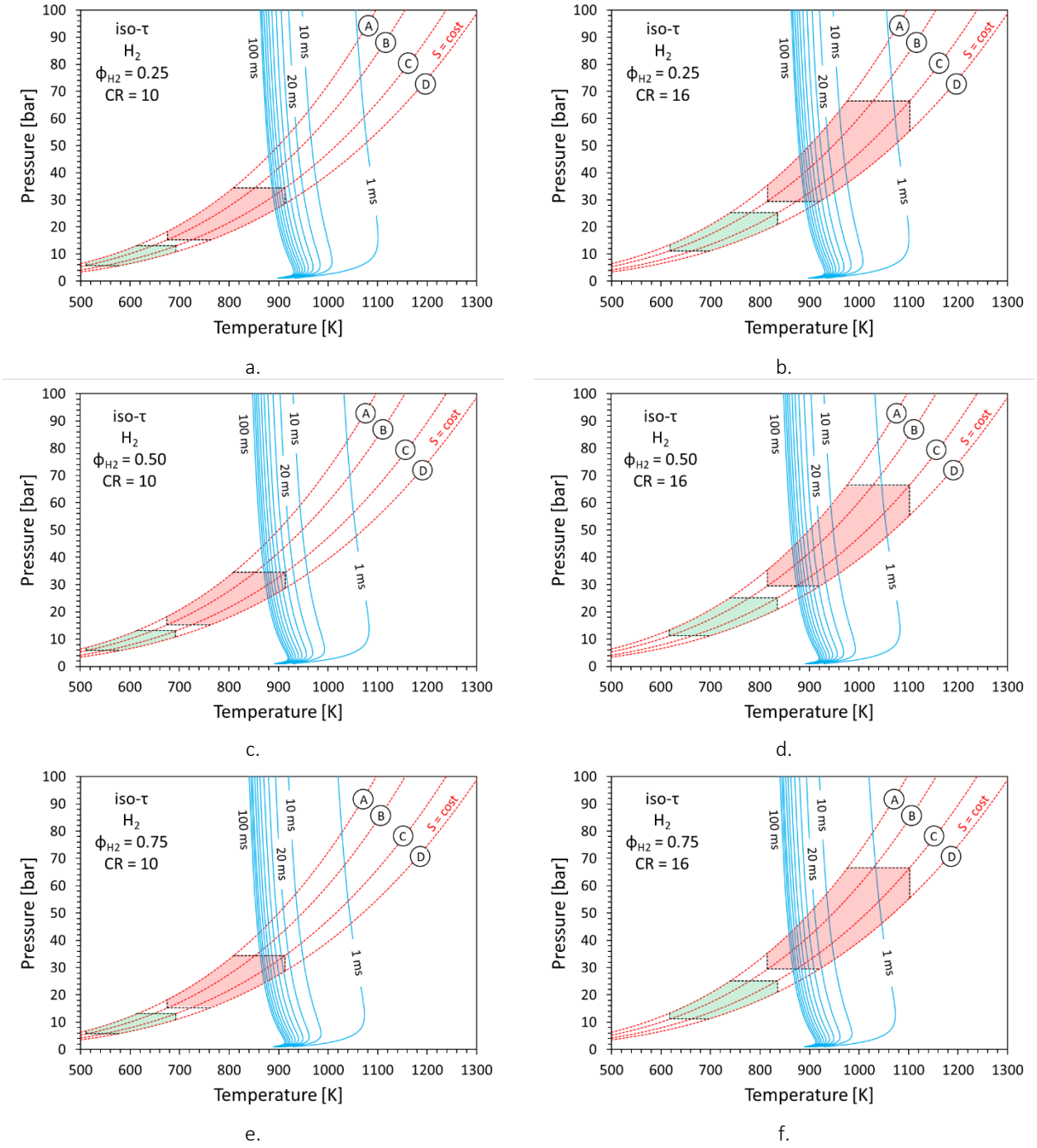

Figure 7.12. Variation of the IDTs of H_2/Air mixtures due to the in-cylinder temperature and pressure values, considering different equivalence ratio (i.e., 0.25, 0.50 and 0.75) and compression ratio (i.e., 10 and 16) values.

It is immediately noticeable that the lubricant oil addition dramatically affects the H_2/Air mixture reactivities. Differently from what was observed for H_2/Air mixtures, a lubricant oil fraction, χ_{oil}, equal to 0.05 could generate IDT values starting from 10 ms at **HCS**, for a $CR = 10$ and for all the equivalence ratio values considered in the analysis (Figure 7.13-a-c-e). At $CR = 16$, the in-cylinder temperatures and pressures at **HCS** result in IDTs significantly shorter than 10 ms for ϕ_{H2} = 0.25 (Figure 7.13-b) and even shorter than 1 ms for ϕ_{H2} = 0.50 (Figure 7.13-d) and ϕ_{H2} = 0.75 (Figure 7.13-f).

For $CR = 10$, at **TDC** could reign thermodynamic conditions resulting in IDT values considerably shorter than 10 ms, and for higher temperature and pressure values even significantly shorter than 1 ms (Figure 7.13-a-c-e). At $CR = 16$, the **TDC** area encloses temperature and pressure values resulting in IDTs always significantly shorter than 1 ms (Figure 7.13-b-d-f). The analysis carried out highlighted that undesired ignitions could be triggered by competing effects, in which lubricant oil contamination can contribute to determine even more conducive conditions.

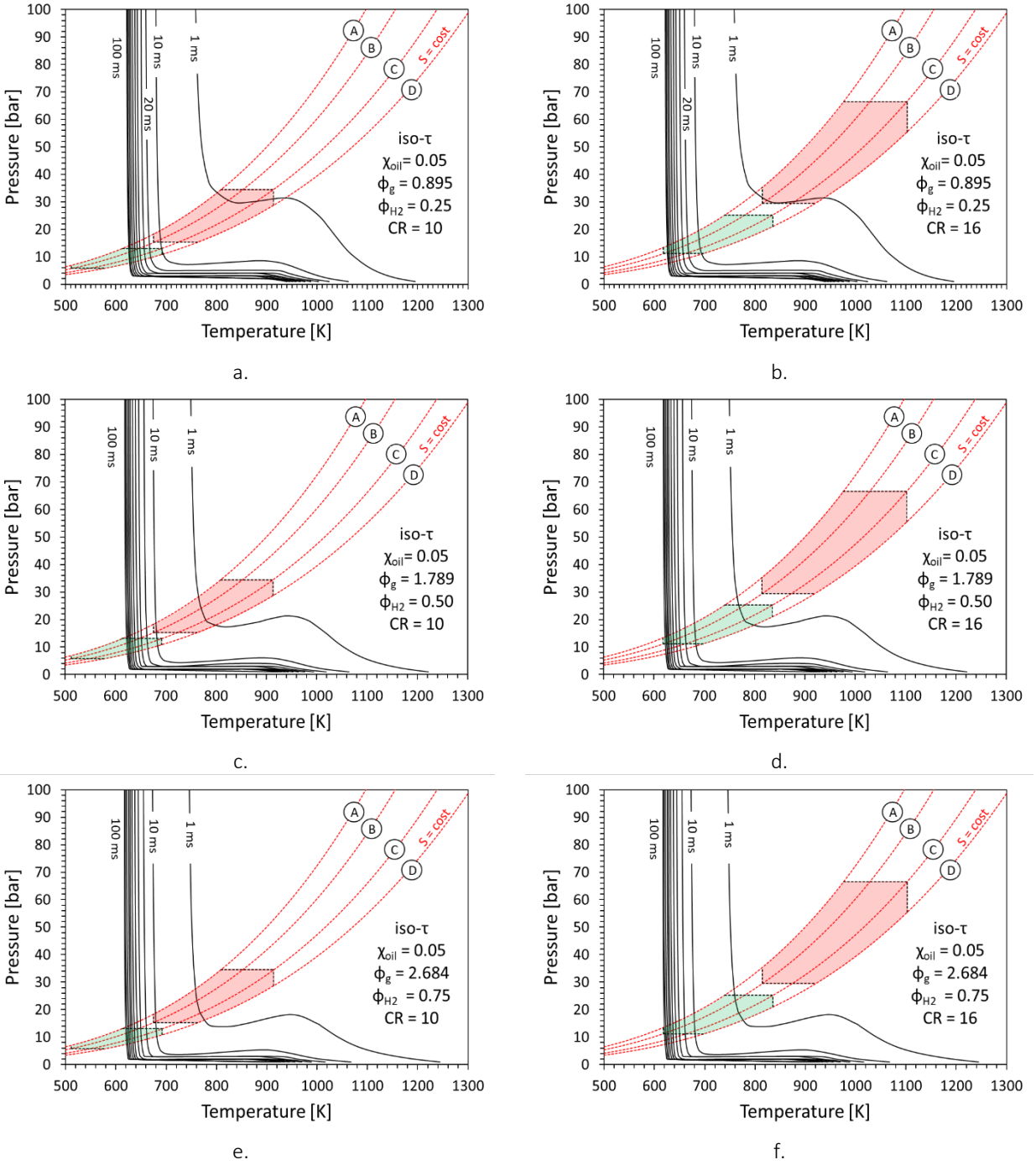

Figure 7.13. Variation of the IDTs of H_2/ n-$C_{16}H_{34}$/Air (i.e., χ_{oil} = 0.05) mixtures due to the in-cylinder temperature and pressure values, considering different equivalence ratio (i.e., 0.25, 0.50 and 0.75) and compression ratio (i.e., 10 and 16) values.

Figure 7.14 and Figure 7.15 allow a first comparison between the chemical IDTs of different mixtures with the residence time of the charge in the cylinder, for different equivalence ratio and compression ratio values. As for the previous analysis, each of the curves reported in Figure 7.14 and Figure 7.15 identifies two regions, with lower and higher IDTs than 10 ms and 1 ms at the left side and right side respectively. For the analysis times of 1 ms and 10 ms were chosen. The time of 10 ms is comparable with the time needed by the piston to cover half compression stroke, allowing to determine if the thermodynamic conditions in HCS (green area) can result potentially in a safe or unsafe engine operating condition for premature auto-ignition. To avoid undesired pre-ignition, the engine must run with a sufficient speed, in order to complete the latter half of the compression stroke in less time than the IDT of the considered mixture. The time of 1 ms is comparable with the time at which the combustion process starts when the piston is in the vicinity of the TDC. Most importantly, this time (i.e., 1 ms) is comparable with the typical ignition times of the mixtures. If the IDTs of the mixtures are lower than 1 ms, pre-ignition could occur, and it is more likely that a super-knock could arise.

For all the equivalence and compression ratio considered, uncontaminated hydrogen does not auto-ignited, because the temperatures established at HCS are well below to its auto-ignition temperature.

As in the previous analyses, in-cylinder lubricant oil contamination could strongly contribute to the onset of undesired premature auto-ignition of the charge. For ultra-lean operating condition (i.e., ϕ_{H2} = 0.25) at $\mathrm{CR} = 10$ (Figure 7.14-a), a temperature of 690 K and a pressure of 13 bar could arise at HCS. Under these thermodynamic values, an IDT of 9.6 ms can be obtained with a mixture of $\chi_{oil} = 0.05$. This time decrease to 5.8 ms with a mixture of $\chi_{oil} = 0.10$. For higher equivalence ratio values, at the same temperatures and pressures, the mixtures with $\chi_{oil} = 0.05$ and $\chi_{oil} = 0.10$ show IDTs of 7.4 ms and 5.2 ms for ϕ_{H2} = 0.50 (Figure 7.14-c), while these time decrease to 6.8 ms and 5 ms for ϕ_{H2} = 0.75 (Figure 7.14-e). As expected, an increase in equivalence ratio leads to shorter IDTs, due to the local enrichment of the charge induced by lubricant oil contamination.

Considering that the piston continues compressing the charge, there might be high probability of auto-ignition. For an engine speed equal to 1000 RPM, the piston needs 30 ms to travel from the BDC to the TDC, while 15 ms are needed to cover the latter half of the compression stroke. Comparing the IDTs with the time required by the piston to cover the latter half of the compression stroke, it is evident that for an engine speed of 1000 RPM, premature auto-ignition could occur long before the compression stroke is complete. Thus, to escape uncontrolled ignitions, the engine should increase its speed.

For ϕ_{H2} = 0.25 the engine should run at 1700 RPM and 2750 RPM to complete the latter half of the compression stroke in about 9 ms and 5.4 ms, before auto-ignition occurs, for $\chi_{oil} = 0.05$ and $\chi_{oil} = 0.10$, respectively. At ϕ_{H2} = 0.50, for the same mixture compositions, the engine should increase the speed at 2200 RPM (latter HCS in about 7 ms) and 3000 RPM (latter HCS in about 5 ms). For the richer operating condition (i.e., ϕ_{H2} = 0.75), the engine should further increase the speed. To escape auto-ignition, the engine needs to run at 2500 RPM for $\chi_{oil} = 0.05$ (latter HCS in about 6 ms) and 3750 RPM (latter HCS in about 4 ms).

As a further example, at ϕ_{H2} = 0.75 and $\mathbf{CR = 10}$ (Figure 7.14-e) for a temperature of 610 K and pressure of 11 bar at HCS, IDTs of 140 ms and 100 ms could be reached for mixtures of for $\chi_{oil} = 0.05$ and $\chi_{oil} = 0.10$, respectively. These IDT values might result critical for engine working at low speed (i.e., 100 RPM).

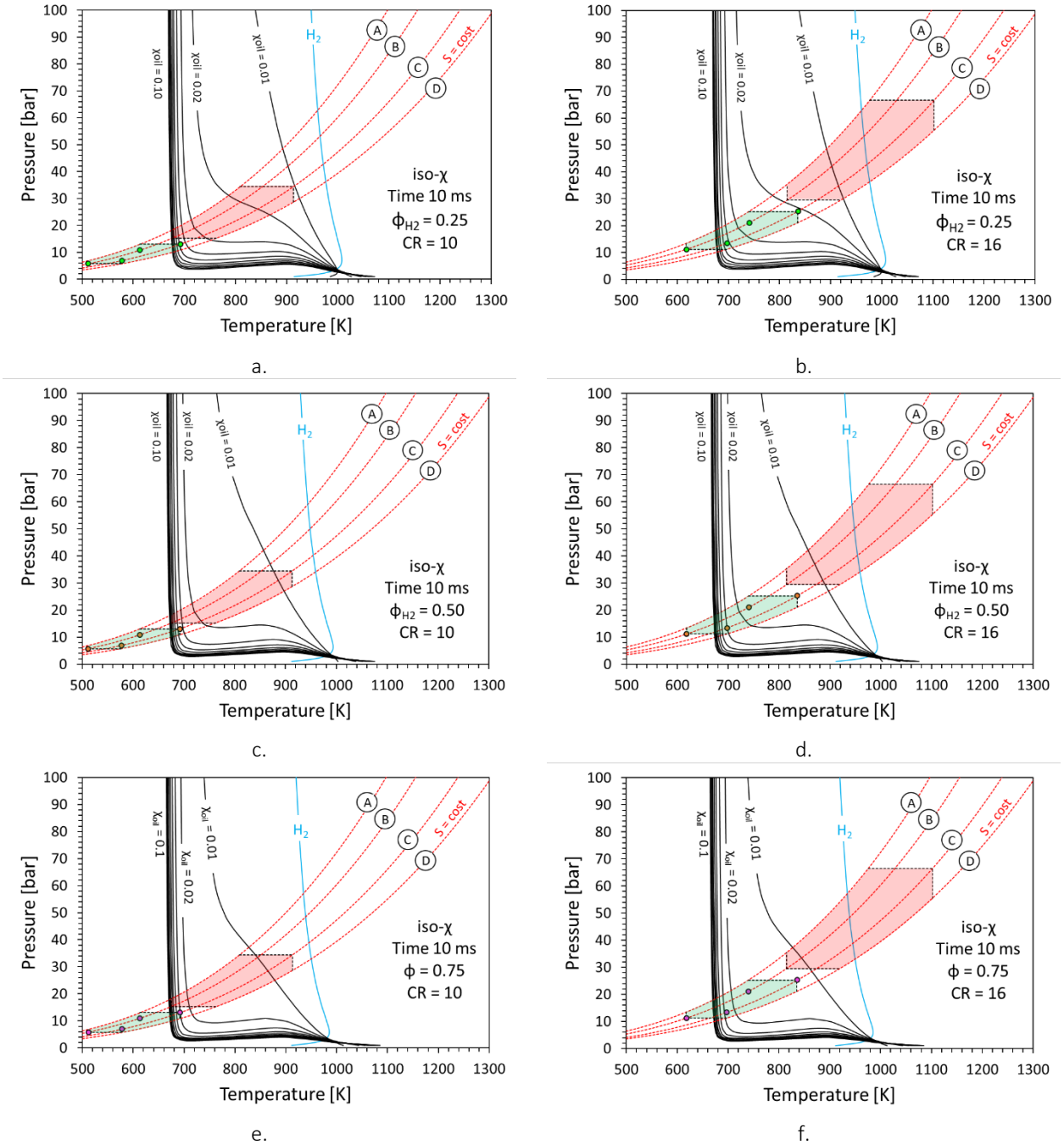

Figure 7.14. Variation of the IDTs of H_2/ n-$C_{16}H_{34}$/Air mixtures due to the in-cylinder temperature and pressure values, considering different equivalence ratio (i.e., 0.25, 0.50 and 0.75) and compression ratio (i.e., 10 and 16) values.

As a consequence of a compression ratio increase, higher temperatures and pressures could arise in the HCS. These more severe thermodynamic conditions lead to a shorter IDTs, thus requiring higher engine speeds to escape pre-ignition. In addition, more mixtures might result critical for the normal engine operation. For a $\mathbf{CR = 16}$, a mixture composition between $\chi_{oil} = 0.02$ and $\chi_{oil} = 0.03$ could already trigger premature auto-ignition. At ϕ_{H2} = 0.25 (Figure 7.14-b), the mixture with $\chi_{oil} =$

0.03 shows an IDT value of 4 ms, at temperature of 840 K and pressure of 25 bar reached at HCS. For the same lubricant oil fraction, temperature and pressure values, this time decrease to 1.6 ms and 1 ms at ϕ_{H2} = 0.50 (Figure 7.14-d) and ϕ_{H2} = 0.75 (Figure 7.14-f), respectively. For these IDT values, the engine should run at 4000 (ϕ_{H2} = 0.25) RPM, 10000 RPM (ϕ_{H2} = 0.50) and 16000 RPM (ϕ_{H2} = 0.75) to escape undesired auto-ignition of the charge. Larger lubricant oil fraction, χ_{oil}, drastically worsen the normal engine operation already for ultra-lean operating condition (i.e., ϕ_{H2} = 0.25). For instance, IDT values of 1.3 ms and 0.4 ms can be obtained for $\chi_{oil} = 0.05$ and $\chi_{oil} = 0.10$. These times required engine speeds equal to 15000 RPM and 50000 RPM to complete the latter half of the compression stroke before auto-ignition occurs.

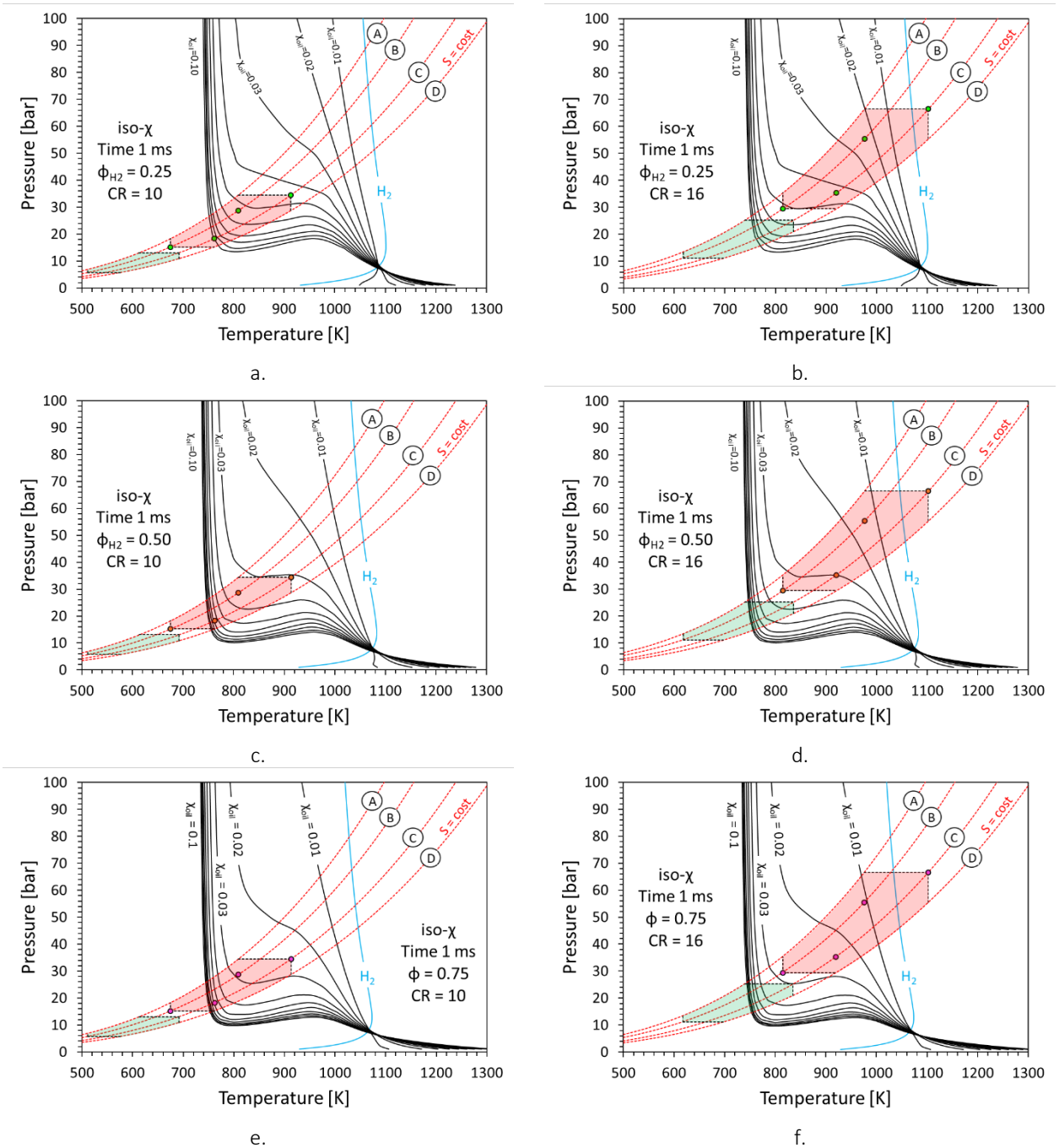

Figure 7.15. Variation of the IDTs of H_2/ n-$C_{16}H_{34}$/Air mixtures due to the in-cylinder temperature and pressure values, considering different equivalence ratio (i.e., 0.25, 0.50 and 0.75) and compression ratio (i.e., 10 and 16) values.

When the piston approaches the TDC, the suitable thermodynamic conditions for the trigger of the combustion process are established. However, these conditions could also favor the onset of uncontrolled auto-ignition of the charge. The mechanism involved in premature auto-ignition could be further favored by in-cylinder lubricant oil contamination.

At ϕ_{H2} = 0.25 and $\mathrm{CR} = 10$ (Figure 7.15-a), mixtures with χ_{oil} between 0 and 0.04 show IDTs always higher than 1 ms, thus not resulting in pre-ignition at TDC. Increasing the equivalence ratio tends to tighten the range of lubricant oil fraction, χ_{oil}, which does not result in uncontrolled auto-ignition of the charge. For instance, for ϕ_{H2} = 0.50 and $\mathrm{CR} = 10$ (Figure 7.15-c), mixtures with χ_{oil} between 0 and 0.03 are exempted from pre-ignition. This range is further reduced for ϕ_{H2} = 0.75 (Figure 7.15-f), in which only χ_{oil} ranging from 0 to 0.02 show no premature auto-ignition.

For a $\mathrm{CR} = 10$, the thermodynamic conditions that could arise at TDC cover a range of temperature between 910 K and 680 K and a pressure range spanning from 34 bar to 15 bar. For all the equivalence ratios considered (Figure 7.15-a, c and f) and for the lowest temperature and pressure values at TDC, no mixtures result in premature auto-ignition, as their IDTs are always longer than 1 ms. On the contrary, for the highest values, some mixtures show IDTs shorter than 1 ms, thus resulting in unsafe engine operating conditions. For ϕ_{H2} = 0.25, $\mathrm{H_2/n-C_{16}H_{34}/Air}$ mixtures with χ_{oil} between 0.05 and 0.10 show IDTs shorter than 1 ms (Figure 7.15-a). In the case of ϕ_{H2} = 0.50, the mixtures that could potentially result in premature auto-ignition are comprised between χ_{oil} 0.04 and 0.10 (Figure 7.15-c). In the last case, ϕ_{H2} = 0.75, mixtures with $\chi_{oil} = 0.03$ could be already considered unsafe for the normal engine operation.

For $\mathrm{CR} = 16$, the in-cylinder temperatures at TDC sweep from 815 K to 1100 K and pressures from 30 bar to 66 bar. Differently from what was observed for $\mathrm{CR} = 10$, at the highest temperature and pressure values (i.e., 1100 K and 66 bar) even uncontaminated hydrogen may auto-ignited undesirably, as it shows an IDT shorter than 1 ms.

At ϕ_{H2} = 0.25 (Figure 7.15-b), pure hydrogen auto-ignited in 0.53 ms. This time decrease to 0.46 ms ϕ_{H2} = 0.50 (Figure 7.15-d) and 0.28 ms for the richer conditions of ϕ_{H2} = 0.75 (Figure 7.15-f). As the oil fraction, χ_{oil}, in H_2/Air increases, the mixtures are considerably more reactive, showing an IDT significantly shorter than 1 ms. For instance, at 1100 K and 66 bar, the mixture with $\chi_{oil} = 0.05$ and $\chi_{oil} = 0.10$ auto-ignited in 0.12 ms and 0.072 ms in the ultra-lean operating conditions (i.e., ϕ_{H2} = 0.25). These times decrease to 0.08 ms and 0.05 ms for ϕ_{H2} = 0.50, up to 0.06 ms and 0.04 ms for the richer case (i.e., ϕ_{H2} = 0.75). For the lowest temperature and pressure values, 815 K and 30 bar, χ_{oil} between 0 and 0.05 could be considered potentially safe for ϕ_{H2} = 0.25, as their IDTs are longer than 1 ms (Figure 7.15-b). This potentially safe range is reduced by the increase in equivalence ratio. For instance, at ϕ_{H2} = 0.50, this range is narrowed to χ_{oil} between 0 and 0.03, and further limited to χ_{oil} ranging from 0 to 0.02 at ϕ_{H2} = 0.75. This trend is attributable to the competing effects due to the increase in the starting equivalence ratio (i.e., ϕ_{H2}) and to the local enrichment induced by lubricant oil contamination.

7.4. Conclusions

The present work provides for the first time a thoroughly characterization on the role of lubricant oil in altering hydrogen ignition behavior in the combustion chamber of Hydrogen Internal Combustion Engines (HICEs). The analysis aims to shed light whether trace amounts of lubricant oil can vary the charge reactivity in a significant way so that it can promote its premature ignition.

To meet this aim, a reduced reaction mechanism was developed from the detailed CRECK kinetic model (Version 2003), selecting $\mathrm{n-C_{16}H_{34}}$ (n-Hexadecane) as lubricant oil surrogate species. The reduced chemical model was tested against experimental data in order to ensure that the reduction process did not affect its effectiveness in predicting IDT values. The tests conducted have shown that the reduction process did not affect the reliability of the chemical model in predicting IDT values.

The reduced mechanism was employed in Zero-Dimensional (0D) numerical simulations in order to quantify the lubricant oil induced variations in hydrogen Ignition Delay Time (IDT). A wide range of operating conditions were considered, in terms of equivalence ratios, range of temperatures and pressures, and compression ratios, in order to cover engine operations spanning from Spark-Ignition (SI) to Compression Ignition (CI) engines.

The comparison between the ignition behavior of $\mathrm{H_2/Air}$ and $\mathrm{n-C_{16}H_{34}/Air}$, provide the first evidence that lubricant oil can represent a potential issue for the normal HICEs operation, especially in the low-to-intermediate temperature regime, in which lubricant oil surrogate species reactivity extends to the temperatures significatively lower and with higher reactivity than $\mathrm{H_2}$. This first result reveals that in-cylinder oil contamination can facilitate the mixture ignition at temperatures considerably lower than the $\mathrm{H_2}$ auto-ignition temperature. Thus, temperatures considered safe for pure $\mathrm{H_2}$ might be potentially prone to the onset of uncontrolled auto-ignition.

It was also highlighted that due to the lubricant oil addition, the charge locally experience an increase in reactivity, not only because of its chemical properties, but also because it produces a local enrichment. As a result, the $\mathrm{H_2/n-C_{16}H_{34}}/Air$ mixtures show reactivities even higher than $\mathrm{n-C_{16}H_{34}}/Air$. Trace amounts of lubricant oil could result in IDT variations of several order of magnitude, thus potentially resulting in unsafe HICEs operating conditions.

The analysis of the variation of ignition delay time of $\mathrm{H_2/Air}$ and $\mathrm{H_2/n-C_{16}H_{34}}/Air$ mixtures due to the thermodynamic conditions consistent with those achievable at half compression stroke (HCS) and at top dead center (TDC), highlighted that the lubricant oil addition results in a drastic shortening of the IDTs, for all the operating conditions considered. For the higher compression ratio, at TDC can be established thermodynamic conditions for which even $\mathrm{H_2/Air}$ mixtures show IDTs significantly shorter than 1 ms. The comparison between the IDTs and the residence time of the charge in the cylinder during the compression stroke again highlighted that traces amount of lubricant oil can promote the onset of uncontrolled ignitions. When these premature auto-ignition occurs at TDC, it is more likely that a super-knock could arise.

The present work provides several evidence about lubricant oil capability in altering the reactivity of H_2/Air mixtures in HICEs-like conditions, highlighting that the accurate chemical modelling of the fuel-lubricant interaction could be a "trump card" for enabling the further development of the internal combustion engine. Due to the small size, the reduced reaction model presented in this work can be directly implemented in CFD simulations for providing information difficult or impossible to obtain solely through experiments.

Summary and Outlook

The present study aims to shed light on the criticalities arising from the interaction between fuel and lubricant oil in modern internal combustion engines, through rigorous numerical investigations. A variety of fuels, including traditional fossil fuels (gasoline) as well as carbon-free alternatives (hydrogen), were considered. Chemical models were developed and validated to isolate the lubricant oil's contribution to abnormal combustion events. In Chapter 1, a brief overview is given on the mechanisms by which lubricant oil can induce abnormal combustion. Chapter 2 provides a comprehensive analysis of the current literature on the lubricant oil chemical formulations that have been found to promote premature auto-ignition of the charge. Finally, in Chapter 3, an overview of ongoing research efforts to improve the understanding and mitigate the complexities arising from the fuel/lubricant oil interaction is presented. This includes the development of new lubricant oil formulations to reduce their impact on fuel reactivity and the use of numerical simulations to model lubricant oil oxidation.

The analysis conducted in the first three chapters highlights that in-cylinder lubricant oil contamination is at the basis for the onset of several criticalities that strongly hinder the further development of efficient and cleaner internal combustion engines. In a scenario where immediate implementation of sustainable and innovative solutions is required, numerical simulations have the potential to significantly contribute in the understanding of the complexities arising from the fuel/lubricant oil interaction, enabling the exploration of previously unexplored solutions. Chapter 4 outlines the first effort to account for lubricant oil contamination in the engine's combustion chamber and its impact on pre-ignition and soot formation. Through a comprehensive literature review, C_{16}-C_{18} hydrocarbons were identified as suitable surrogates for reproducing the chemical reactivity of commercial lubricant oils. A detailed reaction mechanism was developed from existing mechanisms and validated against literature data. 0D numerical simulations were then conducted to quantify the effect of lubricant oils on the ignition delay of iso-octane (as a surrogate for gasoline). The results showed that a mixture of n-$C_{16}H_{34}$ and $C_{18}H_{38}$-2, in the same proportions, can adequately emulate the chemical characteristics of a commercial lubricant oil.

In Chapter 5, the detailed mechanism presented in the previous chapter was reduced to be implemented in 3D CFD engine simulations with reduced computational costs. The reduced "GasLube" mechanism was developed through merging two existing mechanisms and applying reduction and optimization steps, reducing the number of species by 93% while preserving accuracy. n-Hexadecane was chosen as the sole lubricant oil surrogate and accurately predicts the reduction of gasoline's Total Ignition Delay (TID) time due to lubricant oil contamination in the engine's

combustion chamber. This is crucial for developing high boost Direct Injection Spark-ignition (DISI) engines and controlling Gasoline Compression Ignition (GCI) engines. The results showed that lubricant oil addition caused an exponential decrease in TID time, proving that even trace amounts of lubricant oil can greatly affect iso-Octane's ignitability. The reduction in TID time was attributed to the Physical Ignition Delay (PID) reduction caused by faster vaporization from increased heat release in the first stage of ignition. The results also showed that n-Hexadecane can be used as a surrogate for lubricant oil and the reduced "GasLube" mechanism can predict lubricant oil-induced abnormal combustion modes in modern gasoline engines.

In order to predict with reduced computational costs, the variations of iso-Octane chemical ignition delay induced by the presence of lubricant oil, a simple and workable expressions were derived and validated against experimental data. For this very purpose, in Chapter 6 zero-dimensional numerical simulations were used to analyze existing experimental data and generate a new dataset related to the chemical ignition delay of iso-Octane/n-Hexadecane mixtures. A "bi-exponential" expression was proposed, useful to capture the relative change in iso-Octane chemical ignition delay as a function of n-Hexadecane volume fraction and temperature. The results were very good for operating conditions considered, up to 10% lubricant oil by volume, in the range most likely for the combustion chamber of a DISI engine. The proposed correlation allowed the ignition delay of gasoline/lubricant oil mixtures to be derived directly from pure iso-Octane values, avoiding the use of computationally expensive reaction mechanisms.

As a response to the climate emergency, the transport sector has embraced a paradigm shift towards the utilization of carbon-neutral technologies. This scenario has not only catalyzed the development of electric-based technologies but has also re-ignited the interest toward hydrogen. Hydrogen opens the way to its utilization in the mobility sector in internal combustion engines (ICEs), replacing fossil fuels in those applications for which battery electric vehicle and fuel cell electric vehicle technologies are not suitable or are still not mature. HICEs represents a sustainable and clean alternative to fossil fuels offering a strategically sound approach towards a rapid transition to a carbon-free mobility. Nevertheless, there are still criticalities that need to be assessed for accelerating the development of this technology. Many of these are related to a single component that has been too often neglected in the study of engine combustion, namely lubricant oil. Chapter 7 focuses on the impact of lubricant oil on hydrogen ignition behavior in Hydrogen Internal Combustion Engines (HICEs). The study aims to investigate the potential of trace amounts of lubricant oil to alter the hydrogen ignition behavior and lead to premature ignition in HICEs. A reduced reaction mechanism was developed and validated with experimental data. The reduced mechanism was used in Zero-Dimensional numerical simulations to analyze the lubricant oil's effect on hydrogen Ignition Delay Time (IDT) under a range of operating conditions covering both Spark-Ignition (SI) and Compression-Ignition (CI) engines. The results showed that lubricant oil can reduce the IDT significantly, leading to premature auto-ignition

and potentially to super-knock. The study highlights the importance of considering the fuel-lubricant interaction in the chemical modeling of HICEs for enabling their further development. Due to the small size, the reduced reaction model presented in this work can be directly implemented in CFD simulations for providing information difficult or impossible to obtain solely through experiments, achieving still unexplored potentialities of such technology.

The mechanisms of lubricant oil-induced abnormal combustion still need to be explored further. Experimental investigations aimed at defining more suitable surrogate chemical species to mimic chemical and physical characteristics of lubricant oil could be extremely useful. This could lead to the development of more reliable numerical tools and chemical models. Indeed, developing specialized numerical models able to emulate fuel-lubricant interactions from both the physical and chemical point of views will open the way toward achieving still unexplored potentialities of modern ICEs. Further advancements in understanding the underlying mechanisms and models that can predict these phenomena are crucial for the development of ICEs technology and the decarbonization of mobility.

Investigations of different lubricant composition could provide important insights on the influence of oil characteristics on soot emissions. This could give useful indications for elucidating the mechanisms of oil-derived soot formation, which may be very important in reducing soot emissions in modern engines and in developing new lubricant oil formulations. This assumes a significant relevance in the scenario of decarbonization of mobility. Considering the HICEs, they potentially represent a carbon-free technology. Although HICEs have the potential to be carbon-free, they can still produce particulate emissions. Proper lubrication is essential for their operation, but lubricant oil can also be a significant source of solid carbonaceous emissions, in the finest and most dangerous range size (lower than 30 nm). This is a significant concern that should be addressed to ensure the success of HICEs.

Appendix

Appendix A. Ignition delay definition

In order to accurately evaluate the effect of lubricant oil on the Total Ignition Delay (TID) time of the mixture it is necessary to define a standard procedure to derive TID values from pressure data. In fact, several methods have been proposed in the literature for evaluating the TID time, which differ remarkably from one case to another, so that the definition is not unique, and consistent procedures are needed when numerical simulations are compared with experimental data.

The TID measurement starts with the start of the fuel injection (SOInj). However, it must be pointed out that in an IQT facility the time conventionally indicated as Start of Injection (SOInj) does not necessarily match the start of data acquisition, but rather it occurs about 1.8 ms after [261,450,462]. Such a value is obtained from the analysis of a typical needle lift profile recorded during an IQT experiment [450]. This aspect was also highlighted in the work by Kuti et. al [261] in which such a value was taken into account for the TID evaluation.

Larger discrepancies exist about the definition of the TID end, namely about the definition of the Start of the Ignition (SOIgn) [450,462,463]. In the present study, the TID time was evaluated following a procedure based on the gradient method, which allows one to correctly capture the final ignition event for cases characterized by a two-stage process [450].This method is based on the evaluation of the pressure derivative with respect to time at two functional points by drawing two tangent lines to the pressure trace. The first tangent line (Slope I) is evaluated at the so-called Pressure Recovery Point (PRP), defined as the time instant at which the initial pressure is restored after the drop due to the heat absorbed from the charge during the fuel evaporation. The second tangent line (Slope II) is evaluated using the maximum value of the pressure gradient, $(dP/dt)_{max}$, associated with the thermal runaway. The Start of Ignition (SOIgn) is defined as the time at which the two tangent lines intersect each other. The procedure is depicted in Figure A-1 for a typical smoothened pressure trace recorded during an IQT experimental data acquisition.

The present procedure was employed by Kuti et. al [261] as well. The in-chamber pressure trace reported in Figure A-1 refers to experiments performed by Mubarak Ali et al. [436], which were used in the present study for the numerical model validation, viz., for the grid independency analysis and the spray model tuning in the 3D numerical simulations. The gradient method was employed in the work by Mubarak Ali et al. [436] for the TID evaluation as well, but the distinction between the SOInj and the start of the data acquisition was not considered in this case. Therefore, the averaged value of the TID reported by Mubarak Ali et al. [436] included temporal shifting and the numerical pressure traces were aligned according to the SOInj definition reported in Figure A-1. (cf. Figure 5.3).

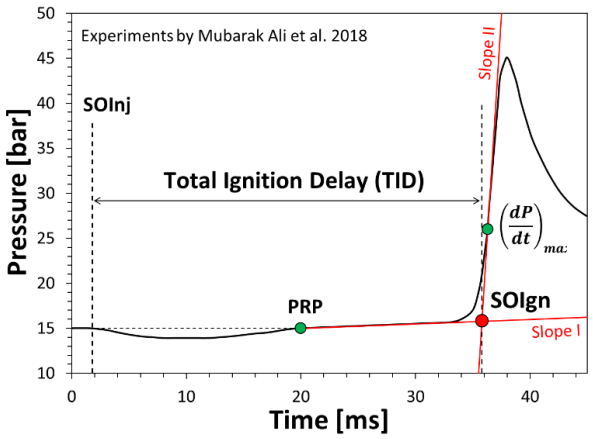

Figure A-1 Graphical representation of the gradients method employed for the evaluation of the Total Ignition Delay (TID) from the chamber pressure history for both the experiments and the simulations.

It is also of interest to evaluate the relative importance of the physical- and the chemical-related events on the observed TID value. For this purpose, the TID is partitioned into two parts, representing the Physical Ignition Delay (PID) and the Chemical Ignition Delay (CID), respectively. Conventionally, the PID identifies the first instants of the TID, i.e., the time interval in which the fluid-dynamic aspects are dominant and wherein spray atomization, vaporization and mixing of air fuel occur. The CID is the remaining part of the TID, during which chemical reactions take place and pressure and temperature rise until the SOIgn occurs. The method based on the determination of the Point of Inflections (PoI) was employed for their determination. The end of the PID (namely, the start of the CID) is defined as the point where the pressure traces of the reactive and non-reactive cases start to diverge from each other. The method is depicted in Figure A-2. and it was applied to the numerical results of the present work. The determination of the PoI was obtained by performing non-reactive simulations for each of the considered cases.

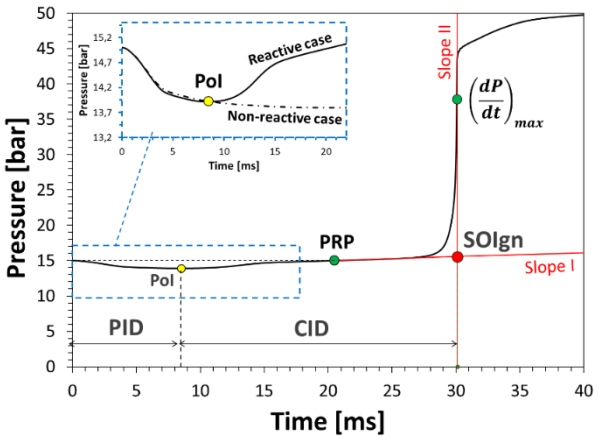

Figure A-2 Graphical representation of the Point of Inflection (PoI) method employed for the evaluation of the Physical Ignition Delay (PID) and Chemical Ignition Delay (CID) partition of the Total Ignition Delay (TID) from the numerical pressure history.

Appendix B. Grid independency analysis

The numerical method was verified by preliminary simulations employing the skeletal PRF mechanism (56 species and 169 reactions) developed by Liu et al. [386] and employed by Mubarak Ali et al. [436]. Mubarak Ali et al. [436] provide the pressure traces for pure iso-Octane, measured at high-pressure and temperature (initial air conditions of $15\ bar$ and $840.2\ K$). Moreover, they reported the results of open-air experiments ($1.10325\ bar$ and $300\ K$) in order to provide an optical characterization of the iso-Octane spray in the IQT. In both tests, a total fuel mass of $83\ mg$ was injected at $225\ bar$ for approximately $2\ ms$ in calm air.

Adaptive Mesh Resolution (AMR), both with respect to fluid velocity and temperature was used and in Table B-1, four different grids considered in this preliminary analysis are reported. For each level of refinement (i) the table provides the cell edge size (dx), the ratio between the injector nozzle diameter and the cell edge size (D_{nozzle}/dx) and the total number of cells (N_{cells}). A base-level edge size, dx_0, of 4 mm was considered. The edge size corresponding to the specific level of refinement (dx_i) was defined as follows:

$$dx_i = \frac{dx_0}{2^i}. \tag{1}$$

Figure B-1 shows the comparison between the experimental pressure trace (dashed black line) by Mubarak Ali et al. [436] and the present simulations by varying the grid level of refinement (i), maintaining a number of injected particles (n_p) equal to 50000. It is noteworthy that the cell size cannot be arbitrarily varied, but it is related to both the injector nozzle diameter and the number of injected parcels (set in the spray model). An under-resolved velocity field leads to an underprediction of the near nozzle penetration because the liquid-gas relative velocity is overestimated, resulting in an excessive drag and drop breakup. For accurate predictions of near-nozzle liquid penetration at least one cell should be included inside the nozzle diameter [424]. However, even though this constraint is fulfilled, when the number of injected parcels is too low in comparison to the local grid refinement level, there would be minimal or no drag on the parcel's drops outside of the core of the spray, resulting in excessive penetration [424]. Therefore, it is crucial to select a proper level of grid refinement and, in accordance, an adequate number of injected parcels.

Table B-1 Base-grids considered in the gird-sensitivity analysis, expressed in terms of level of refinement (i), cell edge size (dx), ratio between the injector nozzle diameter and the cell edge size (D_{nozzle}/dx) and overall number of cells (N_{cells}).

i	$dx\ [mm]$	D_{nozzle}/dx	N_{cells}
1	2	0.55	28965
2	1	1.1	215367
3	0.5	2.2	1658313
4	0.25	4.4	13047406

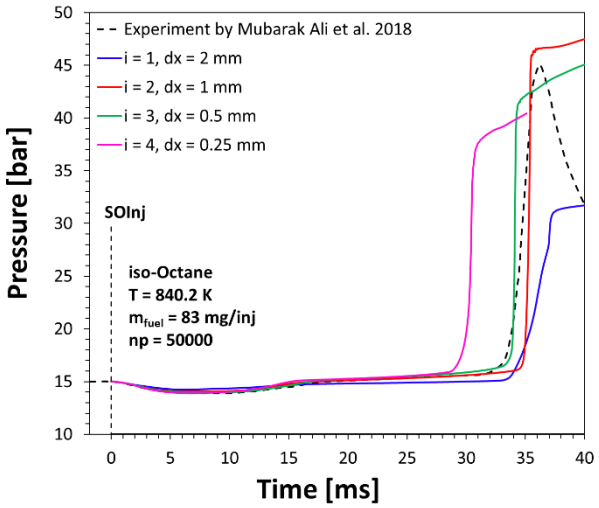

Figure B-1 Comparison between the experimental pressure trace (dashed black line) reported in the work by Mubarak Ali et al. [436] and the present simulations, colored according to the mesh refinement level (i).

Figure B-2 reports the time evolution of the spray penetration with the various levels of mesh refinement described in Table B-1. In the initial stages of the injection, the coarser grids show a slower penetration, while the situation is reversed when the spray approaches the IQT end tube length, after having traversed 120 mm. In the early injection stages, the calculated spray penetration decreases with i and when the ratio D_{nozzle}/dx is lower than 1, such as in the case of $i = 1$ (blue line in Figure B-2), the spray velocity was significantly underestimated. This aspect is also visible in Figure B-3, in which density contour plots are reported for the four meshes after $0.5\ ms$ from the start of the injection. The solution evaluated with the coarsest mesh (Figure B-3 (a)) appears clearly under-resolved, showing a smaller spray penetration. Although the penetration values corresponding to a refinement level ranging from 2 to 4 are comparable, the structure of the spray for the case $i = 2$ (Figure B-3 (b)) differs greatly from the cases $i = 3$ and $i = 4$ (Figure B-3 (c) and (d), respectively).

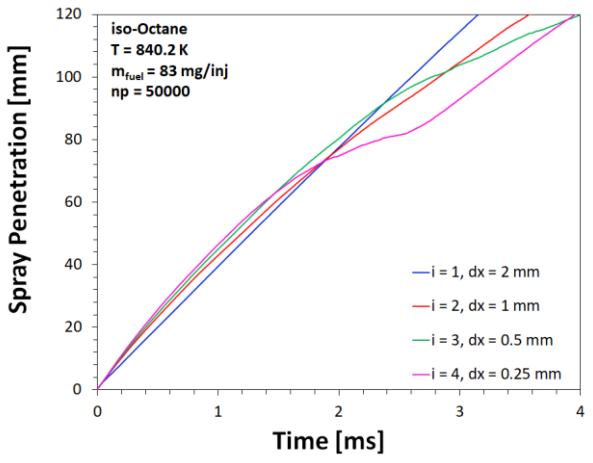

Figure B-2 Time evolution of the spray penetration, colored according to the mesh refinement level (i).

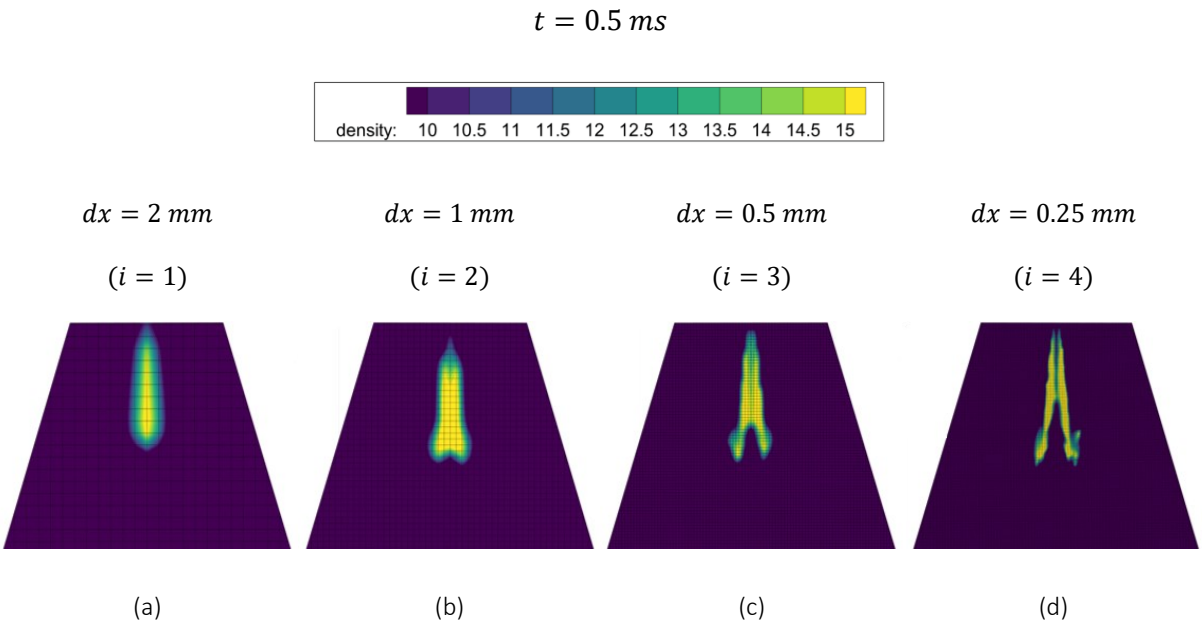

Figure B-3 Density contour plots after $0.5\ ms$ from the start of the injection for the four mesh refinement levels ($i = 1 \div 4$) considered.

After about $1\ ms$, the spray starts to lose its hollow-cone structure, and decelerates accordingly. The drops that have traversed a distance greater than the break-up length experience a secondary break-up phase. At about $2.5\ ms$ this phase becames dominant for the case $i = 4$ (magenta line in Figure B-2). Considering that in these simulations n_p was kept constant and equal to 50000, it follows that the parcel size becames too large in comparison to the cell size for the cases with $i > 3$. Therefore, for $i = 4$ the drag acting on the parcel's drops outside of the core of the spray was underestimated. This led to an overestimation of the spray velocity in the final stages, as it possible to infer from the higher slope that the case $i = 4$ (magenta line in Figure B-2) presented in comparison to the case $i = 3$ (green line in Figure B-2) between 3 and $4\ ms$. Therefore, with $i = 4$, the number of injected parcels was not sufficiently high. This explains the result of Figure B-1, which shows a considerably underestimated TID with the finest mesh. Based on these results, the final refinement level was chosen with an edge cell size of $0.5\ mm$ $(i = 3)$ and $n_p = 50000$.

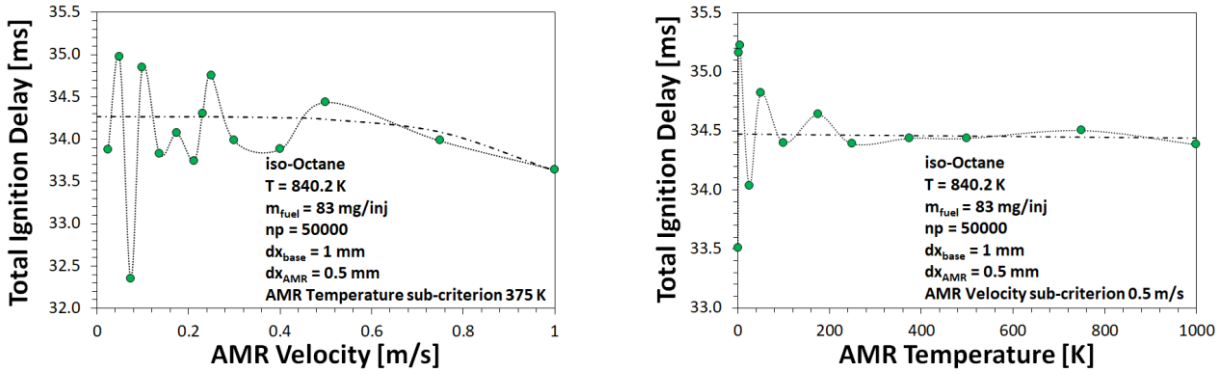

a) b)

Figure B-4 Influence on the predicted TID of the velocity (a) and temperature (b) AMR threshold values.

To minimize computational costs, while preserving accuracy, the grid resolution was locally increased only in high-gradient regions of the domain during the simulation. A base-grid edge size (dx_{base}) of 1 mm (corresponding to $i = 2$) was adopted and an additional level of dynamic refinement based on the AMR method was applied for ensuring a local grid size (dx_{AMR}) of $0.5\ mm$ ($i = 3$) in those regions where the estimated solution error on velocity and temperature is higher. The mesh is refined if the absolute value of the error is greater than the specified threshold value. Conversely, the mesh is coarsened if the absolute value of the error is below 1/5th of the specified threshold value [423]. Figure B-4 shows the influence on the predicted TID of the AMR threshold values for the error on velocity (a) and temperature (b). Threshold values of 0.5 m/s and 375 K were considered for the simulations, respectively. The velocity criterion had a stronger influence on the predicted TID than the temperature criterion. However, the latter had some influence in determining the pressure increase rate in the initial stages of the ignition, explaining the oscillations observed with the selection of a too small threshold value (cf. Figure B-4 (b)).

Figure B-5 shows the influence of the number of injected parcels, n_p, on the jet penetration and on the TID time. Figure B-5 (a) depicts the variation of the time required by the spray to traverse 120 mm (i.e., to reach the IQT end tube). A further increase of n_p over 50000 did not produce any variations in the spray behavior, demonstrating that 50000 represented reliable modeling of the secondary-breakup phase. Figure B-5 (b) shows that this trend was directly mirrored by the TID, as additional validation.

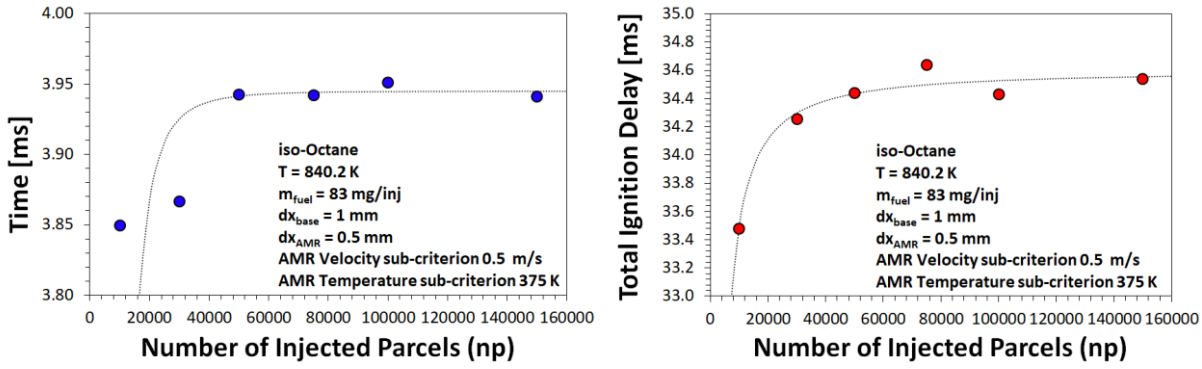

(a) (b)

Figure B-5 Influence of the number of injected parcels (n_p) on the time required by the spray to traverse 120 mm (i.e., to reach the IQT end tube) (a) and on the predicted TID (b).

Bibliography

[1] Kalghatgi G. Is it really the end of internal combustion engines and petroleum in transport? Appl Energy 2018;225:965–74.

[2] Reitz RD. Directions in internal combustion engine research. Combust Flame 2013;160:1–8.

[3] Lenton TM, Rockström J, Gaffney O, Rahmstorf S, Richardson K, Steffen W, et al. Climate tipping points—too risky to bet against. Nature 2019;575:592–5.

[4] Lin W-Y, Hsiao M-C, Wu P-C, Fu JS, Lai L-W, Lai H-C. Analysis of air quality and health co-benefits regarding electric vehicle promotion coupled with power plant emissions. J Clean Prod 2020;247:119152.

[5] Verma S, Dwivedi G, Verma P. Life cycle assessment of electric vehicles in comparison to combustion engine vehicles: A review. Mater Today Proc 2021.

[6] Bicer Y, Dincer I. Life cycle environmental impact assessments and comparisons of alternative fuels for clean vehicles. Resour Conserv Recycl 2018;132:141–57.

[7] Kawamoto R, Mochizuki H, Moriguchi Y, Nakano T, Motohashi M, Sakai Y, et al. Estimation of CO2 Emissions of internal combustion engine vehicle and battery electric vehicle using LCA. Sustainability 2019;11:2690.

[8] Electricity Statistics, IEA. https://www.iea.org/statistics/electricity/ 2019. Electricity Statistics, International Energy Agency (IEA). n.d.

[9] Qiao Q, Zhao F, Liu Z, Jiang S, Hao H. Cradle-to-gate greenhouse gas emissions of battery electric and internal combustion engine vehicles in China. Appl Energy 2017;204:1399–411.

[10] Hao H, Mu Z, Jiang S, Liu Z, Zhao F. GHG Emissions from the production of lithium-ion batteries for electric vehicles in China. Sustainability 2017;9:504.

[11] Del Pero F, Delogu M, Pierini M. Life Cycle Assessment in the automotive sector: A comparative case study of Internal Combustion Engine (ICE) and electric car. Procedia Struct Integr 2018;12:521–37.

[12] Hawkins TR, Singh B, Majeau-Bettez G, Strømman AH. Comparative environmental life cycle assessment of conventional and electric vehicles. J Ind Ecol 2013;17:53–64.

[13] Lombardi L, Tribioli L, Cozzolino R, Bella G. Comparative environmental assessment of conventional, electric, hybrid, and fuel cell powertrains based on LCA. Int J Life Cycle Assess 2017;22:1989–2006.

[14] Hernandez M, Messagie M, De Gennaro M, Van Mierlo J. Resource depletion in an electric vehicle powertrain using different LCA impact methods. Resour Conserv Recycl 2017;120:119–30.

[15] Gan Y, Wang M, Lu Z, Kelly J. Taking into account greenhouse gas emissions of electric vehicles for transportation de-carbonization. Energy Policy 2021;155:112353.

[16] Duronio F, De Vita A, Montanaro A, Villante C. Gasoline direct injection engines--A review of latest technologies and trends. Part 2. Fuel 2020;265:116947.

[17] Stanton DW. Systematic development of highly efficient and clean engines to meet future commercial vehicle greenhouse gas regulations. SAE Int J Engines 2013;6:1395–480.

[18] Kalghatgi GT. Developments in internal combustion engines and implications for combustion science and future transport fuels. Proc Combust Inst 2015;35:101–15.

[19] Reitz RD, Ogawa H, Payri R, Fansler T, Kokjohn S, Moriyoshi Y, et al. IJER editorial: the future of the internal combustion engine. Int J Engine Res 2020.

[20] Eckerle W, Sujan V, Salemme G. Future Challenges for engine manufacturers in view of future emissions legislation. SAE Tech Pap 2017-01-1923 2017. doi:https://doi.org/10.4271/2017-01-1923.

[21] Joshi A. Review of vehicle engine efficiency and emissions. SAE Int J Adv Curr Pract Mobil 2019;1:734–61.

[22] Di Mauro A, Chen H, Sick V. Neural network prediction of cycle-to-cycle power variability in a spark-ignited internal combustion engine. Proc Combust Inst 2019;37:4937–44.

[23] Ravaglioli V, Ponti F, De Cesare M, Stola F, Carra F, Corti E. Combustion Indexes for Innovative Combustion Control. SAE Int J Engines 2017;10:2371–81.

[24] Kuronita T, Sakai T, Queck D, Puts R, Visser S, Herrmann O, et al. A Study of Dynamic Combustion Control for High Efficiency Diesel Engine. SAE Tech Pap 2020-01-0297 2020.

[25] Distaso E, Amirante R, Cassone E, De Palma P, Sementa P, Tamburrano P, et al. Analysis of the Combustion Process in a Lean-Burning Turbulent Jet Ignition Engine Fueled with Methane. Energy Convers Manag 2020;In Press.

[26] Distaso E, Amirante R, Cassone E, Catapano F, De Palma P, Sementa P, et al. Experimental and numerical analysis of a pre-chamber turbulent jet ignition combustion system. 2019.

[27] Amirante R, Casavola C, Distaso E, Tamburrano P. Towards the Development of the In-Cylinder Pressure Measurement Based on the Strain Gauge Technique for Internal Combustion Engines. SAE Tech Pap 2015-24-2419 2015. doi:https://doi.org/10.4271/2015-24-2419.

[28] Ashok B, Ashok SD, Kumar CR. A review on control system architecture of a SI engine management system. Annu Rev Control 2016;41:94–118.

[29] Amirante R, Coratella C, Distaso E, Rossini G, Tamburrano P. Optical device for measuring the injectors opening in common rail systems. Int J Automot Technol 2017;18. doi:10.1007/s12239-017-0072-y.

[30] Patel PD, Lakdawala A, Chourasia S, Patel RN. Bio fuels for compression ignition engine: A review on engine performance, emission and life cycle analysis. Renew Sustain Energy Rev 2016;65:24–43.

[31] Rakopoulos DC, Rakopoulos CD, Giakoumis EG, Papagiannakis RG, Kyritsis DC. Influence of properties of various common bio-fuels on the combustion and emission characteristics of high-speed DI (direct injection) diesel engine: Vegetable oil, bio-diesel, ethanol, n-butanol, diethyl ether. Energy 2014;73:354–66.

[32] Yerrennagoudaru H, Manjunatha K, Raza A, Kantharaj BR, Mujahed A, Irshad K. Analysis and comparison of performance and emissions of compression ignition engine fuelled with diesel and different bio-fuels blended with Methanol. Mater Today Proc 2018;5:5175–85.

[33] Yi J, Wooldridge S, Coulson G, Hilditch J, Iyer CO, Moilanen P, et al. Development and optimization of the Ford 3.5 L V6 EcoBoost combustion system. SAE Int J Engines 2009;2:1388–407.

[34] Piock W, Hoffmann G, Berndorfer A, Salemi P, Fusshoeller B. Strategies towards meeting future particulate matter emission requirements in homogeneous gasoline direct injection engines. SAE Int J Engines 2011;4:1455–68.

[35] Leach F, Stone R, Richardson D, Lewis A, Akehurst S, Turner J, et al. Particulate emissions from a highly boosted gasoline direct injection engine. Int J Engine Res 2018;19:347–59.

[36] Pan M, Qian W, Wei H, Feng D, Pan J. Effects on performance and emissions of gasoline compression ignition engine over a wide range of internal exhaust gas recirculation rates under lean conditions. Fuel 2020;265:116881.

[37] Jiang C, Huang G, Liu G, Qian Y, Lu X. Optimizing gasoline compression ignition engine performance and emissions: Combined effects of exhaust gas recirculation and fuel octane number. Appl Therm Eng 2019;153:669–77.

[38] Kalghatgi G, Johansson B. Gasoline compression ignition approach to efficient, clean and affordable future engines. Proc Inst Mech Eng Part D J Automob Eng 2018;232:118–38.

[39] Robertson D, Prucka R. A Review of Spark-Assisted Compression Ignition (SACI) Research in the Context of Realizing Production Control Strategies. SAE Tech Pap 2019-24-0027 2019.

[40] Saxena S, Bedoya ID. Fundamental phenomena affecting low temperature combustion and HCCI engines, high load limits and strategies for extending these limits. Prog Energy Combust Sci 2013;39:457–88.

[41] Hunicz J, Mikulski M, Koszałka G, Ignaciuk P. Detailed analysis of combustion stability in a spark-assisted compression ignition engine under nearly stoichiometric and heavy EGR conditions. Appl Energy 2020;280:115955.

[42] Paykani A, Kakaee A-H, Rahnama P, Reitz RD. Progress and recent trends in reactivity-controlled compression ignition engines. Int J Engine Res 2016;17:481–524.

[43] Kokjohn SL, Hanson RM, Splitter DA, Reitz RD. Fuel reactivity controlled compression ignition (RCCI): a pathway to controlled high-efficiency clean combustion. Int J Engine Res 2011;12:209–26.

[44] Paykani A, Garcia A, Shahbakhti M, Rahnama P, Reitz RD. Reactivity controlled compression ignition engine: Pathways towards commercial viability. Appl Energy 2021;282:116174.

[45] Yao M, Zheng Z, Liu H. Progress and recent trends in homogeneous charge compression ignition (HCCI) engines. Prog Energy Combust Sci 2009;35:398–437.

[46] Duan X, Lai M-C, Jansons M, Guo G, Liu J. A review of controlling strategies of the ignition timing and combustion phase in homogeneous charge compression ignition (HCCI) engine. Fuel 2021;285:119142.

[47] Khandal S V, Banapurmath NR, Gaitonde VN. Performance studies on homogeneous charge compression ignition (HCCI) engine powered with alternative fuels. Renew Energy 2019;132:683–93.

[48] Saiteja P, Ashok B. A critical insight review on homogeneous charge compression ignition engine characteristics powered by biofuels. Fuel 2021;285:119202.

[49] Sellnau MC, Sinnamon J, Hoyer K, Husted H. Full-time gasoline direct-injection compression ignition (GDCI) for high efficiency and low NOx and PM. SAE Int J Engines 2012;5:300–14.

[50] Ra Y, Loeper P, Andrie M, Krieger R, Foster D, Reitz R, et al. Gasoline DICI engine operation in the LTC regime using triple-pulse injection. SAE Int J Engines 2012;5:1109–32.

[51] Solanki VS, Mustafi NN, Agarwal AK. Prospects of Gasoline Compression Ignition (GCI) Engine Technology in Transport Sector. Adv. Combust. Tech. Engine Technol. Automot. Sect., Springer; 2020, p. 77–110.

[52] Manente V, Johansson B, Cannella Wjij. Gasoline partially premixed combustion, the future of internal combustion engines? Int J Engine Res 2011;12:194–208.

[53] Liu Y, Li L, Lu H, Schmitt S, Deng J, Rao L. SI/HCCI Mode Switching Optimization in a Gasoline Direct Injection Engine Employing Dual Univalve System. J Eng Gas Turbines Power 2019;141.

[54] Kalghatgi G. Development of fuel/engine systems—the way forward to sustainable transport. Engineering 2019;5:510–8.

[55] Yang Q, Grill M, Bargende M. The Application of E-Fuel Oxymethylene Ether OME1 in a Virtual Heavy-Duty Diesel Engine for Ultra-Low Emissions. 2020.

[56] Christodoulou F, Sechenyh V, Zhao H, Garner CP, Clarke H. Performance of a novel liquid nitrogen power system. Appl Therm Eng 2021;191:116896.

[57] Martins J, Brito FP. Alternative fuels for internal combustion engines. Energies 2020;13:4086.

[58] Hosseini SE, Butler B. An overview of development and challenges in hydrogen powered vehicles. Int J Green Energy 2020;17:13–37.

[59] Distaso E, Amirante R, Tamburrano P, Reitz RD. Understanding the role of soot oxidation in gasoline combustion: A numerical study on the effects of oxygen enrichment on particulate mass and number emissions in a spark-ignition engine. Energy Convers Manag 2019;184:24–39.

[60] Gschwend D, Soltic P, Wokaun A, Vogel F. Review and performance evaluation of fifty alternative liquid fuels for spark-ignition engines. Energy \& Fuels 2019;33:2186–96.

[61] Larsson T, Stenlaas O, Erlandsson A. Future fuels for DISI engines: a review on oxygenated, liquid biofuels 2019.

[62] Elgowainy A, Han J, Ward J, Joseck F, Gohlke D, Lindauer A, et al. Current and future United States light-duty vehicle pathways: Cradle-to-grave lifecycle greenhouse gas emissions and economic assessment. Environ Sci \& Technol 2018;52:2392–9.

[63] Powell N, Hill N, Bates J, Bottrell N, Biedka M, White B, et al. Impact analysis of mass EV adoption and low carbon intensity fuels scenarios--summary report 2018.

[64] Senecal PK, Leach F. Diversity in transportation: Why a mix of propulsion technologies is the way forward for the future fleet. Results Eng 2019;4:100060. doi:10.1016/j.rineng.2019.100060.

[65] Lešnik L, Kegl B, Torres-Jiménez E, Cruz-Peragón F. Why we should invest further in the development of internal combustion engines for road applications. Oil \& Gas Sci Technol d'IFP Energies Nouv 2020;75:56.

[66] Leach F, Kalghatgi G, Stone R, Miles P. The scope for improving the efficiency and environmental impact of internal combustion engines. Transp Eng 2020:100005.

[67] Willand J, Daniel M, Montefrancesco E, Geringer B, Hofmann P, Kieberger M. Limits on downsizing in spark ignition engines due to pre-ignition. MTZ Worldw 2009;70:56–61.

[68] Inoue T, Inoue Y, Ishikawa M. Abnormal combustion in a highly boosted SI engine-the occurrence of super knock. SAE Tech Pap 2012. doi:10.4271/2012-01-1141.

[69] Haenel P, Seyfried P, Kleeberg H, Tomazic D. Systematic approach to analyze and characterize pre-ignition events in turbocharged direct-injected gasoline engines. SAE 2011 World Congr Exhib 2011. doi:10.4271/2011-01-0343.

[70] Zaccardi J-M, Escudié D. Overview of the main mechanisms triggering low-speed pre-ignition in spark-ignition engines. Int J Engine Res 2015;16:152–65.

[71] Splitter D, Kaul B, Szybist J, Speed L, Zigler B, Luecke J. Fuel-Lubricant Interactions on the Propensity for Stochastic Pre-Ignition. SAE Tech Pap 2019-24-0103 2019.

[72] Kubach H, Weidenlener A, Pfeil J, Koch T, Kittel H, Roisman I V., et al. Investigations on the Influence of Fuel Oil Film Interaction on Pre-ignition Events in Highly Boosted di Gasoline Engines. SAE Tech Pap 2018;2018-April:1–15. doi:10.4271/2018-01-1454.

[73] Teng H, Miao R, Cao L, Luo X, Hu T, Wu M. Characteristics of Abnormal Combustion in the Scavenging Zone for a Highly-Boosted Gasoline Direct Injection Engine. SAE Tech Pap 2017-01-1721 2017.

[74] Moriyoshi Y, Kuboyama T, Morikawa K, Yamada T, Imai Y, Hatamura K, et al. A Study of Low Speed Preignition Mechanism in Highly Boosted SI Gasoline Engines. SAE Int J Engines 2015;9:98–106. doi:10.4271/2015-01-1865.

[75] Wang Z, Qi Y, Liu H, Long Y, Wang JX. Experimental Study on Pre-Ignition and Super-Knock in Gasoline Engine Combustion with Carbon Particle at Elevated Temperatures and Pressures. SAE Tech Pap 2015;2015-April. doi:10.4271/2015-01-0752.

[76] Dahnz C, Spicher U. Irregular combustion in supercharged spark ignition engines - Pre-ignition and other phenomena. Int J Engine Res 2010;11:485–98. doi:10.1243/14680874JER609.

[77] Kalghatgi GT, Bradley D. Pre-ignition and 'super-knock'in turbo-charged spark-ignition engines. Int J Engine Res 2012;13:399–414.

[78] Mubarak Ali MJ, Hernandez Perez F, Vedharaj S, Vallinayagam R, Dibble R, Im H. Effect of Timing and Location of Hotspot on Super Knock during Pre-ignition. SAE Tech Pap 2017;2017-March. doi:10.4271/2017-01-0686.

[79] Ra Y, Reitz RD, Jarrett MW, Shyu TP. Effects of piston crevice flows and lubricant oil vaporization on diesel engine deposits. SAE Tech Pap 2006.

[80] Tamura K, Utaka T, Kamano H, Hayakawa N, Miyasaka T, Ishino T, et al. Abnormal Combustion Induced by Combustion Chamber Deposits Derived from Engine Oil Additives in a Spark-Ignited Engine. SAE Int J Engines 2014;8:200–5. doi:10.4271/2014-32-0091.

[81] Wang Z, Xu Y, Wang J. Suppression of super-knock in TC-GDI engine using two-stage injection in intake stroke (TSII). Sci China Technol Sci 2014;57:80–5. doi:10.1007/s11431-013-5374-3.

[82] Gupta A, Seeley R, Shao H, Remias J, Roos J, Wang Z, et al. Impact of Particle Characteristics and Engine Conditions on Deposit-Induced Pre-Ignition and Superknock in Turbocharged Gasoline Engines. SAE Int J Fuels Lubr 2017;10:830–41. doi:10.4271/2017-01-2345.

[83] Okada Y, Miyashita S, Izumi Y, Hayakawa Y. Study of Low-Speed Pre-Ignition in Boosted Spark Ignition Engine. SAE Int J Engines 2014;7:584–94. doi:10.4271/2014-01-1218.

[84] Gupta A, Shao H, Remias J, Roos J, Wang Y, Long Y, et al. Relative Impact of Chemical and Physical Properties of the Oil-Fuel Droplet on Pre-Ignition and Super-Knock in Turbocharged Gasoline Engines. SAE Tech Pap 2016;2016-Octob. doi:10.4271/2016-01-2278.

[85] Yi P, Long W, Feng L, Chen L, Cui J, Gong W. Investigation of evaporation and auto-ignition of isolated lubricating oil droplets in natural gas engine in-cylinder conditions. Fuel 2019;235:1172–83. doi:10.1016/j.fuel.2018.08.084.

[86] Fei S, Wang Z, Qi Y, Wang Y, Zhang H. Ignition of a Single Lubricating Oil Droplet in Combustible Ambient Gaseous Mixture under High-Temperature and High-Pressure Conditions. Combust Sci Technol 2019;191:2033–52. doi:10.1080/00102202.2018.1542382.

[87] Ohtomo M, Suzuoki T, Miyagawa H, Koike M, Yokoo N, Nakata K. Fundamental analysis on auto-ignition condition of a lubricant oil droplet for understanding a mechanism of low-speed pre-ignition in highly charged spark-ignition engines. Int J Engine Res 2019;20:292–303. doi:10.1177/1468087417751240.

[88] Qi Y, Xu Y, Wang Z, Wang J. The effect of oil intrusion on super knock in gasoline engine. SAE Tech Pap 2014;1. doi:10.4271/2014-01-1224.

[89] Mitsudharmadi H, Maharjan S, Elbaz AM, Qahtani YA, Roberts WL. Auto-Ignition of a Hexadecane Droplet Mixed with Different Octane Number Fuels at Elevated Pressures to Investigate the Pre-Ignition Behavior. Energy and Fuels 2020;34:806–16. doi:10.1021/acs.energyfuels.9b02540.

[90] Mayer M, Hofmann P, Geringer B, Williams J, Moss J. Influence of different fuel properties and gasoline-ethanol blends on low-speed pre-ignition in turbocharged direct injection spark ignition engines. SAE Int J Engines 2016;9:841–8.

[91] Jatana GS, Splitter DA, Kaul B, Szybist JP. Fuel property effects on low-speed pre-ignition. Fuel 2018;230:474–82. doi:10.1016/j.fuel.2018.05.060.

[92] Yue Z, Som S. Fuel property effects on knock propensity and thermal efficiency in a direct-injection spark-ignition engine. Appl Energy 2019:114221.

[93] Ruichen L, Boyan X, Yunliang Q, Weiyang X. Numerical Analysis of Low Speed Pre-Ignition and Knock Process in Downsized Turbocharged Direct Injection Engines with Ethanol-Gasoline Blends. Int J Automot Technol 2020;21:13–22.

[94] Wang Z, Liu H, Reitz RD. Knocking combustion in spark-ignition engines. Prog Energy Combust Sci 2017;61:78–112. doi:10.1016/j.pecs.2017.03.004.

[95] Vangraefschepe F, Zaccardi JM. Analysis of destructive abnormal combustions appearing at high load and low engine speed on high performance gasoline engines. Spark Ignition Engine Futur. SIA Congr., 2007.

[96] Dahnz C, Spicher U. Irregular combustion in supercharged spark ignition engines--pre-ignition and other phenomena. Int J Engine Res 2010;11:485–98.

[97] Gao J, Wang X, Song P, Tian G, Ma C. Review of the backfire occurrences and control strategies for port hydrogen injection internal combustion engines. Fuel 2022;307:121553. doi:10.1016/j.fuel.2021.121553.

[98] Li Y, Gao W, Li Y, Fu Z, Zou J. Numerical investigation on combustion and knock formation mechanism of hydrogen direct injection engine. Fuel 2022;316:123302.

[99] Shinde BJ, Karunamurthy K. Recent progress in hydrogen fuelled internal combustion engine (H2ICE)--A comprehensive outlook. Mater Today Proc 2022;51:1568–79.

[100] Lai F, Sun B, Wang X, Zhang D, Luo Q, Bao L. Research on the inducing factors and characteristics of knock combustion in a DI hydrogen internal combustion engine in the process of improving performance and thermal efficiency. Int J Hydrogen Energy 2022.

[101] Luo Q, Sun B. Inducing factors and frequency of combustion knock in hydrogen internal combustion engines. Int J Hydrogen Energy 2016;41:16296–305.

[102] Faizal M, Chuah LS, Lee C, Hameed A, Lee J, Shankar M, et al. Review of hydrogen fuel for internal combustion engines. J Mech Eng Res Dev 2019;42:35–46.

[103] Yip HL, Srna A, Yuen ACY, Kook S, Taylor RA, Yeoh GH, et al. A review of hydrogen direct injection for internal combustion engines: towards carbon-free combustion. Appl Sci 2019;9:4842.

[104] Aleiferis PG, Rosati MF. Controlled autoignition of hydrogen in a direct-injection optical engine. Combust Flame 2012;159:2500–15. doi:10.1016/j.combustflame.2012.02.021.

[105] Rouleau L, Duffour F, Walter B, Kumar R, Nowak L. Experimental and Numerical Investigation on Hydrogen Internal Combustion Engine. SAE TechPapers 2021. doi:10.4271/2021-24-0060.

[106] Xu H, Ni X, Su X, Xiao B, Luo Y, Zhang F, et al. Experimental and numerical investigation on effects of pre-ignition positions on knock intensity of hydrogen fuel. Int J Hydrogen Energy 2021;46:26631–45. doi:10.1016/j.ijhydene.2021.05.154.

[107] Amirante R, Distaso E, Napolitano M, Tamburrano P, Iorio SD, Sementa P, et al. Effects of lubricant oil on particulate emissions from port-fuel and direct-injection spark-ignition engines. Int J Engine Res 2017;18:606--620. doi:10.1177/1468087417706602.

[108] Premnath V, Khalek I, Morgan P, Michlberger A, Sutton M, Vincent P. Effect of Lubricant Oil on Particle Emissions from a Gasoline Direct Injection Light-Duty Vehicle. SAE Tech Pap 2018-01-1708 2018.

[109] Amirante R, Distaso E, Di Iorio S, Pettinicchio D, Sementa P, Tamburrano P, et al. Experimental Investigations on the Sources of Particulate Emission within a Natural Gas Spark-Ignition Engine. SAE Tech Pap 2017-24-0141 2017. doi:10.4271/2017-24-0141.

[110] Eisazadeh H, Ehteram MA, Khazaee I. Diffusion charging measurements on exhaust solid particle number and lung deposited surface area of compressed natural gas and diesel buses. Environ Sci Pollut Res 2020:16929–39.

[111] Singh AP, Pal A, Agarwal AK. Comparative particulate characteristics of hydrogen, CNG, HCNG, gasoline and diesel fueled engines. Fuel 2016;185:491–9.

[112] Distaso E, Amirante R, Tamburrano P, Reitz RD. Steady-state Characterization of Particle Number Emissions from a Heavy-Duty Euro VI Engine Fueled with Compressed Natural Gas. Energy Procedia 2018;148:671–8.

[113] Amirante R, Distaso E, Di Iorio S, Sementa P, Tamburrano P, Vaglieco BM, et al. Effects of natural gas composition on performance and regulated, greenhouse gas and particulate emissions in spark-ignition engines. Energy Convers Manag 2017;143. doi:10.1016/j.enconman.2017.04.016.

[114] El-Sherif a. S. Effects of natural gas composition on the nitrogen oxide, flame structure and burning velocity under laminar

premixed flame conditions. Fuel 1998;77:1539–47. doi:10.1016/S0016-2361(98)00083-0.

[115] Amirante R, Distaso E, Tamburrano P, Reitz RD. Measured and predicted soot particle emissions from natural gas engines. SAE Tech Pap 2015-24-2518 2015. doi:10.4271/2015-24-2518.

[116] Maier A, Klaus U, Dreizler A, Rottengruber H. Fuel-Independent Particulate Emissions in an SIDI Engine. SAE Int J Engines 2015;8:1334–41.

[117] Zhao H, Stone R, Zhou L. Analysis of the particulate emissions and combustion performance of a direct injection spark ignition engine using hydrogen and gasoline mixtures. Int J Hydrogen Energy 2010;35:4676–86.

[118] Miller AL, Stipe CB, Habjan MC, Ahlstrand GG. Role of lubrication oil in particulate emissions from a hydrogen-powered internal combustion engine. Environ Sci Technol 2007;41:6828–35.

[119] Thiruvengadam A, Besch MC, Yoon S, Collins J, Kappanna H, Carder DK, et al. Characterization of particulate matter emissions from a current technology natural gas engine. Environ Sci Technol 2014;48:8235–42. doi:10.1021/es5005973.

[120] Distaso E, Amirante R, Calò G, De Palma P, Tamburrano P. Evolution of soot particle number, mass and size distribution along the exhaust line of a heavy-duty engine fueled with compressed natural gas. Energies 2020;13. doi:10.3390/en13153993.

[121] Pirjola L, Karjalainen P, Heikkilä J, Saari S, Tzamkiozis T, Ntziachristos L, et al. Effects of fresh lubricant oils on particle emissions emitted by a modern gasoline direct injection passenger car. Environ Sci Technol 2015;49:3644–52.

[122] Qin J, Li X, Pei Y. Effects of Combustion Parameters and Lubricating Oil on Particulate Matter Emissions from a Turbo-Charged GDI Engine Fueled with Methanol/Gasoline Blends. SAE Tech Pap 2014;2014-Octob. doi:10.4271/2014-01-2841.

[123] Jang J, Lee Y-J, Kwon O, Lee M, Kim J. The effect of engine oil on particulate matter, emissions and fuel economy in gasoline and diesel vehicle. 2014.

[124] Bock N, Jeon J, Kittelson D, Northrop WF. Solid particle number and mass emissions from lean and stoichiometric gasoline direct injection engine operation. 2018.

[125] Choi S, Seong H. Lube oil-dependent ash chemistry on soot oxidation reactivity in a gasoline direct-injection engine. Combust Flame 2016;174:68–76.

[126] Kittelson DB, Watts WF, Johnson JP. Nanoparticle emissions on Minnesota highways. Atmos Environ 2004;38:9–19.

[127] Rönkkö T, Pirjola L, Ntziachristos L, Heikkilä J, Karjalainen P, Hillamo R, et al. Vehicle engines produce exhaust nanoparticles even when not fueled. Environ Sci Technol 2014;48:2043–50.

[128] Virtanen A, Rönkkö T, Kannosto J, Ristimäki J, Mäkelä JM, Keskinen J, et al. Winter and summer time size distributions and densities of traffic-related aerosol particles at a busy highway in Helsinki. Atmos Chem Phys 2006;6:2411–21.

[129] Alföldy B, Giechaskiel B, Hofmann W, Drossinos Y. Size-distribution dependent lung deposition of diesel exhaust particles. J Aerosol Sci 2009;40:652–63.

[130] Oberdörster G, Oberdörster E, Oberdörster J. Nanotoxicology: an emerging discipline evolving from studies of ultrafine particles. Environ Health Perspect 2005;113:823.

[131] Paur H-R, Cassee FR, Teeguarden J, Fissan H, Diabate S, Aufderheide M, et al. In-vitro cell exposure studies for the assessment of nanoparticle toxicity in the lung—A dialog between aerosol science and biology. J Aerosol Sci 2011;42:668–92.

[132] Manisalidis I, Stavropoulou E, Stavropoulos A, Bezirtzoglou E. Environmental and health impacts of air pollution: a review. Front Public Heal 2020;8:14.

[133] Brandenberger S, Mohr M, Grob K, Neukom HP. Contribution of unburned lubricating oil and diesel fuel to particulate emission from passenger cars. Atmos Environ 2005;39:6985–94.

[134] Eastwood P. Particulate emissions from vehicles. vol. 20. John Wiley & Sons; 2008.

[135] Jung H, Kittelson DB, Zachariah MR. The influence of engine lubricating oil on Diesel nanoparticle emissions and kinetics of oxidation. SAE Tech Pap 2003. doi:10.4271/2003-01-3179.

[136] La Rocca A, Shayler PJ, Fay MW. Nanoparticle characteristics of exhaust and soot-in-oil from a light duty diesel engine. 17th ETH Conf. Combust Gener Nanoparticles 2013.

[137] Liati A, Eggenschwiler PD. Characterization of particulate matter deposited in diesel particulate filters: Visual and analytical approach in macro-, micro-and nano-scales. Combust Flame 2010;157:1658–70.

[138] Shim B-J, Park K-S, Koo J-M, Nguyen MS, Jin SH. Estimation of soot oxidation rate in DPF under carbon and non-carbon based particulate matter accumulated condition. Int J Automot Technol 2013;14:207–12.

[139] Park S, Woo S, Oh H, Lee K. Effects of Various Lubricants and Fuels on Pre-Ignition in a Turbocharged Direct-Injection Spark-Ignition Engine. Energy and Fuels 2017;31:12701–11. doi:10.1021/acs.energyfuels.7b01052.

[140] Moriyoshi Y, Yamada T, Tsunoda D, Xie M, Kuboyama T, Morikawa K. Numerical Simulation to Understand the Cause and Sequence of LSPI Phenomena and Suggestion of CaO Mechanism in Highly Boosted SI Combustion in Low Speed Range. SAE Tech Pap 2015;2015-April. doi:10.4271/2015-01-0755.

[141] Hayakawa N, Miura K, Miyasaka T, Ishino T, Iijima A, Shoji H, et al. A Study on the Effect of Zn- and Mo-Based Engine Oil Additives on Abnormal SI Engine Combustion using In-Cylinder Combustion Visualization. SAE Int J Engines 2014;8:214–20. doi:10.4271/2014-32-0096.

[142] Kuboyama T, Moriyoshi Y, Morikawa K. Visualization and Analysis of LSPI Mechanism Caused by Oil Droplet, Particle and Deposit in Highly Boosted SI Combustion in Low Speed Range. SAE Int J Engines 2015;8:529–37. doi:10.4271/2015-01-0761.

[143] Magar M, Spicher U, Palaveev S, Gohl M, Müller G, Lensch-Franzen C, et al. Experimental Studies on the Occurrence of Low-Speed Pre-Ignition in Turbocharged GDI Engines. SAE Int J Engines 2015;8:495–504. doi:10.4271/2015-01-0753.

[144] Yilmaz E, Tian T, Wong VW, Heywood JB. The contribution of different oil consumption sources to total oil consumption in a spark ignition engine. SAE TechPapers 2004. doi:10.4271/2004-01-2909.

[145] Dahnz C, Han K-M, Spicher U, Magar M, Schießl R, Maas U. Investigations on pre-ignition in highly supercharged SI engines. SAE Int J Engines 2010;3:214–24.

[146] Kalghatgi GT, Bradley D. Pre-ignition and "super-knock" in turbo-charged spark-ignition engines. Int J Engine Res 2012;13:399–414. doi:10.1177/1468087411431890.

[147] Welling O, Collings N, Williams J, Moss J. Impact of lubricant composition on low-speed pre-ignition. SAE Tech Pap 2014;1. doi:10.4271/2014-01-1213.

[148] Welling O, Moss J, Williams J, Collings N. Measuring the Impact of Engine Oils and Fuels on Low-Speed Pre-Ignition in Downsized Engines. SAE Int J Fuels Lubr 2014;7:1–8. doi:10.4271/2014-01-1219.

[149] Takeuchi K, Fujimoto K, Hirano S, Yamashita M. Investigation of Engine Oil Effect on Abnormal Combustion in Turbocharged Direct Injection - Spark Ignition Engines. SAE Int J Fuels Lubr 2012;5:1017–24. doi:10.4271/2012-01-1615.

[150] Dingle SF, Cairns A, Zhao H, Williams J, Williams O, Ali R. Lubricant induced pre-ignition in an optical SI engine. SAE Tech Pap 2014;1. doi:10.4271/2014-01-1222.

[151] Kassai M, Torii K, Shiraishi T, Noda T, Goh TK, Wilbrand K, et al. Research on the Effect of Lubricant Oil and Fuel Properties on LSPI Occurrence in Boosted S. I. Engines. SAE Tech Pap 2016;2016-Octob. doi:10.4271/2016-01-2292.

[152] Hirano S, Yamashita M, Fujimoto K, Kato K. Investigation of engine oil effect on abnormal combustion in turbocharged direct injection - Spark ignition engines (Part 2). SAE Tech Pap 2013;11. doi:10.4271/2013-01-2569.

[153] Luo X, Teng H, Hu T, Miao R, Cao L. Mitigating Intensities of Super Knocks Encountered in Highly Boosted Gasoline Direct Injection Engines. SAE Tech Pap 2015;2015-March. doi:10.4271/2015-01-0084.

[154] Miyasaka T, Miura K, Hayakawa N, Ishino T, Iijima A, Shoji H, et al. A Study on the Effect of a Calcium-Based Engine Oil Additive on Abnormal SI Engine Combustion. SAE Int J Engines 2014;8:206–13. doi:10.4271/2014-32-0092.

[155] Palaveev S, Magar M, Kubach H, Schiessl R, Spicher U, Maas U. Premature flame initiation in a Turbocharged DISI engine - Numerical and experimental investigations. SAE Int J Engines 2013;6:54–66. doi:10.4271/2013-01-0252.

[156] Fujimoto K, Yamashita M, Hirano S, Kato K, Watanabe I, Ito K. Engine Oil Development for Preventing Pre-Ignition in Turbocharged Gasoline Engine. SAE Int J Fuels Lubr 2014;7:869–74. doi:10.4271/2014-01-2785.

[157] Suzuki R, Shoji H, Yoshida K, Iijima A. Analysis of Knocking in an SI Engine based on In-cylinder: Spectroscopic Measurements and Visualization. 2010.

[158] Merola SS, Vaglieco BM. Knock investigation by flame and radical species detection in spark ignition engine for different fuels. Energy Convers Manag 2007;48:2897–910.

[159] Ma X, Wang Z, Jiang C, Jiang Y, Xu H, Wang J. An optical study of in-cylinder CH2O and OH chemiluminescence in flame-induced reaction front propagation using high speed imaging. Fuel 2014;134:603–10.

[160] Graf N, Gronki J, Schulz C, Baritaud T, Cherel J, Duret P, et al. In-cylinder combustion visualization in an auto-igniting gasoline engine using fuel tracer-and formaldehyde-LIF imaging. SAE Trans 2001:1771–8.

[161] Bäuerle B, Hoffmann F, Behrendt F, Warnatz J. Detection of hot spots in the end gas of an internal combustion engine using two-dimensional LIF of formaldehyde. Symp. Combust., vol. 25, 1994, p. 135–41.

[162] Schießl R, Maas U. Analysis of endgas temperature fluctuations in an SI engine by laser-induced fluorescence. Combust Flame 2003;133:19–27.

[163] Huang Y, Li Y, Zhang W, Meng F, Guo Z. 3D simulation study on the influence of lubricant oil droplets on pre-ignition in turbocharged DISI engines. Proc Inst Mech Eng Part D J Automob Eng 2017:0954407017734695.

[164] Zaccardi J-M, Lecompte M, Duval L, Pagot A. Pre-ignition in highly charged spark ignition engines—visualisation and analysis. MTZ Worldw 2009;70:40–7.

[165] Heiss M, Lauer T. Analysis of Pre-ignition Initiation Mechanisms using a Multi-Cycle CFD-Simulation. Int. Multidimens. Engine Model. User's Gr. Meet., 2014.

[166] Heiss M, Lauer T. Analysis of Particle Separation With Respect to Pre-Igniton in An Si-Engine. 11th World Congr. Comput. Mech. (WCCM XI), Barcelona, Spain, 2014.

[167] Günther M, Uygun Y, Kremer F, Pischinger S. Pre-ignition and glow-ignition of gasoline biofuels. MTZ Worldw 2013;74:46–53.

[168] Ohtomo M, Miyagawa H, Koike M, Yokoo N, Nakata K. Pre-Ignition of Gasoline-Air Mixture Triggered by a Lubricant Oil Droplet. SAE Int J Fuels Lubr 2014;7:673–82. doi:10.4271/2014-01-2627.

[169] Hirose T, Masuda Y, Yamada T, Umemoto Y, Furutani H. Technical challenge for the 2-stroke premixed combustion gas engine (pre-ignition behavior and overcoming technique). CIMAC Pap 2013.

[170] Long Y, Wang Z, Qi Y, Xiang S, Zeng G, Zhang P, et al. Effect of Oil and Gasoline Properties on Pre-Ignition and Super-Knock in a Thermal Research Engine (TRE) and an Optical Rapid Compression Machine (RCM). SAE Tech Pap 2016;2016-April. doi:10.4271/2016-01-0720.

[171] Maharjan S, Qahtani Y, Roberts W, Elbaz A. The Effect of Pressure, Temperature and Additives on Droplet Ignition of Lubricant Oil and Its Surrogate. SAE Tech Pap 2018;2018-Septe:1–6. doi:10.4271/2018-01-1673.

[172] Yi P, Long W, Feng L, Wang W, Liu C. An experimental and numerical study of the evaporation and pyrolysis characteristics of lubricating oil droplets in the natural gas engine conditions. Int J Heat Mass Transf 2016;103:646–60.

[173] Ohtomo M, Suzuoki T, Miyagawa H, Koike M, Yokoo N, Nakata K. Fundamental analysis on auto-ignition condition of a lubricant oil droplet for understanding a mechanism of low-speed pre-ignition in highly charged spark-ignition engines. Int J Engine Res 2018:1468087417751240.

[174] Deng J, Wu Z, Feng W, Huang C, Li L. Research into autoignition characteristics of diesel fuel in a controllable active thermo-atmosphere. 2006.

[175] Huang Y, Li Y, Zhang W, Meng F, Guo Z. 3D simulation study on the influence of lubricant oil droplets on pre-ignition in turbocharged DISI engines. Proc Inst Mech Eng Part D J Automob Eng 2018;232:1677–93. doi:10.1177/0954407017734695.

[176] Kassai M, Shiraishi T, Noda T, Hirabe M, Wakabayashi Y, Kusaka J, et al. An Investigation on the Ignition Characteristics of Lubricant Component Containing Fuel Droplets Using Rapid Compression and Expansion Machine. SAE Int J Fuels Lubr 2016;9:469–80. doi:10.4271/2016-01-2168.

[177] Feng D, Buresheid K, Zhao H, Wei H, Chen C. Investigation of lubricant induced pre-ignition and knocking combustion in an optical spark ignition engine. Proc Combust Inst 2019;37:4901–10. doi:10.1016/j.proci.2018.07.061.

[178] Lauer T, Heiss M, Bobicic N, Holly W, Pritze S. A comprehensive simulation approach to irregular combustion. SAE Tech Pap 2014;1. doi:10.4271/2014-01-1214.

[179] Kalghatgi GT. Fuel and Additive Effects on the Rates of Growth of Combustion Chamber Deposits in a Spark Ignition Engine. 1997.

[180] Cheng SS. The impacts of engine operating conditions and fuel compositions on the formation of combustion chamber deposits. 2000.

[181] Stępień Z. Intake valve and combustion chamber deposits formation – the engine and fuel related factors that impacts their growth. Nafta-Gaz 2014;R. 70, nr:236–42.

[182] Nishiwaki K, Hafnan M. The determination of thermal properties of engine combustion chamber deposits. SAE Trans 2000:1400–13.

[183] Kalghatgi GT. Combustion chamber deposits in spark-ignition engines: a literature review. SAE Trans 1995:1349–63.

[184] Shu G, Dong L, Liang X. A review of experimental studies on deposits in the combustion chambers of internal combustion engines. Int J Engine Res 2012;13:357–69.

[185] Sandquist H, Denbratt I, Owrang F, Olsson J. Influence of fuel parameters on deposit formation and emissions in a direct injection stratified charge SI engine. SAE Trans 2001:1537–48.

[186] da Costa P, Cerqueira JM. Structural characterization of carbonaceous engine deposits 2010.

[187] Güralp O, Hoffman M, Assanis D, Filipi Z, Kuo T-W, Najt P, et al. Characterizing the effect of combustion chamber deposits on a gasoline HCCI engine. SAE Trans 2006:824–35.

[188] Güralp OA. The effect of combustion chamber deposits on heat transfer and combustion in a homogeneous charge compression ignition engine 2008.

[189] Güralp O, Hoffman M, Assanis DN, Filipi Z, Kuo T-W, Najt P, et al. Thermal Characterization of Combustion Chamber Deposits on the HCCI Engine Piston and Cylinder Head Using Instantaneous Temperature Measurements. 2009.

[190] Palaveev S, Magar M, Disch C, Schießl R, Kubach H, Spicher U, et al. Simulations and experimental investigations of intermittent pre-ignition series in a turbocharged DISI engine. 4th Int. Conf. Knocking Gasol. Engines, 2013, p. 414–42.

[191] Schünemann E, Witt A, Selder M, Schwarz C. Pre-ignition analysis on a turbocharged gasoline engine with direct injection. 4th Int. Conf. Knocking Gasol. Engines, 2013, p. 380–93.

[192] Kalghatgi GT, Price RJ. Combustion chamber deposit flaking. 2000.

[193] Kalghatgi GT. Combustion chamber deposit flaking--Studies using a road test procedure. SAE Trans 2002:2626–34.

[194] Kalghatgi GT. Combustion chamber deposit flaking and startability problems in three different engines. 2003.

[195] Hänichen P, Bender A, Voß B, Gambaryan-Roisman T, Stephan P. Drop evaporation of hydrocarbon fluids with deposit formation. Int J Heat Mass Transf 2019;128:115–24.

[196] Edney MK, Barker J, Reid J, Scurr DJ, Snape CE. Recent Advances in the Analysis of GDI and Diesel Fuel Injector Deposits. Fuel 2020;272:117682.

[197] Feng D, Buresheid K, Zhao H, Wei H, Chen C. Investigation of lubricant induced pre-ignition and knocking combustion in an optical spark ignition engine. Proc Combust Inst 2018.

[198] Slavchov RI, Mosbach S, Kraft M, Pearson R, Filip S V. An adsorption-precipitation model for the formation of injector external deposits in internal combustion engines. Appl Energy 2018;228:1423–38.

[199] Stepien Z, Krasodomski W. Investigation into Engine Deposit-Forming Tendency Due To Sulfate Salt Contamination of Gasoline--Ethanol Blends. Energy & Fuels 2019;33:4244–53.

[200] Xiao J, Song H, Yang X, Yu K, Huang Z, Yin Q, et al. Experimental study on the effects of nozzle temperature on internal deposits of a gasoline direct injector. Energy & Fuels 2018;32:8978–85.

[201] Pickl F, Russer M, Hauenstein M, Wensing M. Modelling and understanding deposit formation and reduction in combustion engines--Application to the concrete case of internal GDI injector deposit. Fuel 2019;236:284–96.

[202] Hänichen P, van Eyk M, Stephan P. Experimental investigations of fuel film evaporation with deposit formation. Int J Heat Fluid Flow 2018;70:125–30.

[203] Song H, Xiao J, Yang X, Yu K, Huang Z. The effects of surface temperature on the deposit behaviors of gasoline on a hot surface. Fuel 2018;215:111–22.

[204] Nikolakopoulos PG. Simulation of deposits effect on cylinder liner and influence on new and worn compression ring of a turbocharged DI engine. Simul Model Pract Theory n.d.;106:102195.

[205] Zhang Z, Zhang W, Ma X, Awad OI, Xu H, Shuai S. Effects of GDI injector deposits on spray and combustion characteristics under different injection conditions. Fuel 2020;278:118094.

[206] Venkataraman R, Eser S. Characterization of deposits formed on diesel injectors in field test and from thermal oxidative degradation of n-hexadecane in a laboratory reactor. Chem Cent J 2008;2:25.

[207] Barker J, Snape C, Scurr D. Information on the aromatic structure of internal diesel injector deposits from time of flight secondary ion mass spectrometry (ToF-SIMS). 2014.

[208] Kinoshita M, Saito A, Matsushita S, Shibata H, Niwa Y. A method for suppressing formation of deposits on fuel injector for direct injection gasoline engine. SAE Trans 1999:2177–84.

[209] Christensen E, Fioroni GM, Kim S, Fouts L, Gjersing E, Paton RS, et al. Experimental and theoretical study of oxidative stability of alkylated furans used as gasoline blend components. Fuel 2018;212:576–85.

[210] O'Brien CJ. Formation mechanisms of combustion chamber deposits. Massachusetts Institute of Technology, 2001.

[211] Altin O, Eser S. Carbon deposit formation from thermal stressing of petroleum fuels. Prepr Pap-Am Chem Soc, Div Fuel Chem 2004;49:764–6.

[212] Ahrenfeldt J, Henriksen U, Schramm J, Jensen TK, Egsgaard H. Combustion chamber deposits and PAH formation in SI engines fueled by producer gas from biomass gasification. 2003.

[213] Zerda TW, Yuan X, Moore SM, y Leon CAL. Surface area, pore size distribution and microstructure of combustion engine deposits. Carbon N Y 1999;37.

[214] Weidenlener A, Pfeil J, Kubach H, Koch T, Forooghi P, Frohnapfel B, et al. The influence of operating conditions on combustion chamber deposit surface structure, deposit thickness and thermal properties. Automot Engine Technol 2018;3:111–27. doi:10.1007/s41104-018-0030-3.

[215] Shimizu K, Takahata S, Miura K, Shoji H, Iijima A, Utaka T, et al. Influence of Calcium-Based Additives with Different Properties on Abnormal Combustion in an SI Engine. SAE Tech Pap 2016;2016-Novem. doi:10.4271/2016-32-0007.

[216] Smith GC, Hopwood AB, Titchener KJ. Microcharacterization of heavy-duty diesel engine piston deposits. Surf Interface Anal An Int J Devoted to Dev Appl Tech Anal Surfaces, Interfaces Thin Film 2002;33:259–68.

[217] Haji-Sulaiman MZ, Mat-Isa F. The effects of different gasoline blends doped with used engine oil on the forming tendency of simulated intake—valve deposits. Proc Inst Mech Eng Part D J Automob Eng 1999;213:47–51.

[218] Dearn K, Xu J, Ding H, Xu H, Weall A, Kirkby P, et al. An investigation into the characteristics of DISI injector deposits using advanced analytical methods. SAE Int J Fuels Lubr 2014;7:771–82.

[219] Salehi FM, Morina A, Neville A. Zinc dialkyldithiophosphate additive adsorption on carbon black particles. Tribol Lett 2018;66:1–7.

[220] Diaby M, Sablier M, Le Negrate A, El Fassi M, Bocquet J. Understanding carbonaceous deposit formation resulting from engine oil degradation. Carbon N Y 2009;47:355–66. doi:10.1016/j.carbon.2008.10.014.

[221] Hoang AT, Pham VV. A study of emission characteristic, deposits, and lubrication oil degradation of a diesel engine running on preheated vegetable oil and diesel oil. Energy Sources, Part A Recover Util Environ Eff 2019;41:611–25.

[222] Carlisle HW, Frew RW, Mills JR, Aradi AA, Avery NL. The effect of fuel composition and additive content on injector deposits and performance of an air-assisted direct injection spark ignition (DISI) research engine. SAE Trans 2001:1549–65.

[223] Von Bacho PS, Sofianek JK, Galante-Fox JM, McMahon CJ. Engine test for accelerated fuel deposit formation on injectors used in gasoline direct injection engines. 2009.

[224] Trobaugh C, Burbrink C, Zha Y, Whitacre S, Corsi C, Blizard N. Internal Diesel Injector Deposits: Theory and Investigations into Organic and Inorganic Based Deposits. SAE Int J Fuels Lubr 2013;6:772–84.

[225] Caceres D, Reisel JR, Sklyarov A, Poehlman A. Exhaust emission deterioration and combustion chamber deposit composition over the life cycle of small utility engines. J Eng Gas Turbines Power 2003;125:358–64.

[226] Owrang F, Mattsson H, Nordlund A, Olsson J, Pedersen J. Characterization of combustion chamber deposits from a gasoline direct injection SI engine. SAE Trans 2003:752–61.

[227] Fukui M, Sato T, Fujita N, Kitano M. Examination of lubricant oil components affecting the formation of combustion chamber deposit in a two-stroke engine. JSAE Rev 2001;22:281–5.

[228] Chapman EM, Costanzo VS. A Literature Review of Abnormal Ignition by Fuel and Lubricant Derivatives. SAE Int J Engines 2015;9:107–42. doi:10.4271/2015-01-1869.

[229] Wang J, Hu Z, Zhu D, Ding W, Li L, Yan W, et al. In Cycle Pre-Ignition Diagnosis and Super-Knock Suppression by Employing Ion Current in a GDI Boosted Engine. 2020.

[230] Liu H, Wang Z, Wooldridge M, Fatouraie M, Jia Z, Qi Y, et al. Highly Turbocharged Gasoline Engine and Rapid Compression Machine Studies of Super-Knock. SAE Int J Engines 2016;9:1475–85. doi:10.4271/2016-01-0686.

[231] Yang Y-W, Zhou Z, Liu H-M, Cheng C-H, Hu Y-H. Effect of engine oil on low-speed stochastic pre-ignition from turbocharged DI gasoline engine. Neiranji Gongcheng/Chinese Intern Combust Engine Eng 2015;36:58–61. doi:10.13949/j.cnki.nrjgc.2015.04.011.

[232] Mortier RM, Orszulik ST, Fox MF. Chemistry and technology of lubricants. vol. 107115. Springer; 2010.

[233] Stachowiak G, Batchelor AW. Engineering tribology. Butterworth-Heinemann; 2013.

[234] Lu R, Nanao H, Takiwatari K, Mori S, Fukushima Y, Murakami Y, et al. The effect of the chemical structures of synthetic hydrocarbon oils on their tribochemical decomposition. Tribol Lett 2015;60:27.

[235] Michlberger A, Sutton M. LSPI Durability, a Study of LSPI over the Life of a Vehicle. SAE Int J Engines 2018;11:3–11. doi:10.4271/03-11-01-0002.

[236] Zhang X, Murrenhoff H, Weckes P, Hölderich W. Effect of temperature on the ageing behaviour of unsaturated ester-based lubricants. J Synth Lubr 2004;21:1–11.

[237] Perryman MS, Tessier J, Wiher T, O'Donoghue H, McCracken AN, Kim SM, et al. Effects of stereochemistry, saturation, and hydrocarbon chain length on the ability of synthetic constrained azacyclic sphingolipids to trigger nutrient transporter down-regulation, vacuolation, and cell death. Bioorg Med Chem 2016;24:4390–7.

[238] Kalaskar VB, Swarts A, Alger T. Impact of Engine Age and Engine Hardware on Low-Speed Pre-Ignition. SAE Tech Pap 2018;2018-Septe:1–9. doi:10.4271/2018-01-1663.

[239] Michlberger A, Sutton M, Dohner B. Low Speed Pre-Ignition (LSPI) Durability â€" A Study of LSPI in Fresh and Aged Engine Oils. SAE Tech Pap 2018;2018-April:1–12. doi:10.4271/2018-01-0934.

[240] Gur'yanov YA. Criteria for limiting contamination of motor oil by fuel. Chem Technol Fuels Oils 2007;43:30–6.

[241] Tripathi AK, Vinu R. Characterization of thermal stability of synthetic and semi-synthetic engine oils. Lubricants 2015;3:54–79. doi:10.3390/lubricants3010054.

[242] Mariani V, Bianchi GM, Cazzoli G, Falfari S. A one-dimensional model for the motor oil-fuel dilution under gasoline engine boundary conditions. E3S Web Conf., vol. 197, 2020, p. 6004.

[243] Mayer M, Hofmann P, Geringer B, Williams J, Moss J, Kapus P. Influence of Different Oil Properties on Low-Speed Pre-Ignition in Turbocharged Direct Injection Spark Ignition Engines. SAE Tech Pap 2016. doi:10.4271/2016-01-0718.

[244] Zahdeh A, Rothenberger P, Nguyen W, Anbarasu M, Schmuck-Soldan S, Schaefer J, et al. Fundamental Approach to Investigate Pre-Ignition in Boosted SI Engines. SAE Int J Engines 2011;4:246–73. doi:10.4271/2011-01-0340.

[245] Peters N, Kerschgens B, Paczko G. Super-knock prediction using a refined theory of turbulence. SAE Int J Engines 2013;6:953–67.

[246] Wang Z, Liu H, Song T, Xu Y, Wang JX, Li DS, et al. Investigation on pre-ignition and super-knock in highly boosted gasoline direct injection engines. SAE Tech Pap 2014;1. doi:10.4271/2014-01-1212.

[247] Hu T, Teng H, Luo X, Chen B. Impact of Fuel Injection on Dilution of Engine Crankcase Oil for Turbocharged Gasoline Direct-Injection Engines. SAE Int J Engines 2015;8:1107–16. doi:10.4271/2015-01-0967.

[248] Hu T, Teng H, Luo X, Lu C, Luo J. Influence of Fuel Dilution of Crankcase Oil on Ignitability of Oil Particles in a Highly Boosted Gasoline Direct Injection Engine. SAE Tech Pap 2015;2015-Septe. doi:10.4271/2015-01-2811.

[249] Wakiru J, Pintelon L, Chemweno P, Muchiri P. Analysis of lubrication oil contamination by fuel dilution with application of cluster analysis. XVII Int Sci Conf Ind Syst 2017:252–7.

[250] Song B-H, Choi Y-H. Investigation of variations of lubricating oil diluted by post-injected fuel for the regeneration of CDPF and its effects on engine wear. J Mech Sci Technol 2008;22:2526–33.

[251] Haas FM, Won SH, Dryer FL, Pera C. Lube oil chemistry influences on autoignition as measured in an Ignition Quality Tester 2017.

[252] Won SH, Haas FM, Dooley S, Edwards T, Dryer FL. Reconstruction of chemical structure of real fuel by surrogate formulation based upon combustion property targets. Combust Flame 2017;183:39–49.

[253] Shayler PJ, Winborn LD, Scarisbrick A. The build-up of oil dilution by gasoline and the influence of vehicle usage pattern. 2000.

[254] Alger T, Huang Y, Hall M, Matthews RD. Liquid film evaporation off the piston of a direct injection gasoline engine. SAE Trans 2001:1295–306.

[255] Sagawa T, Fujimoto H, Nakamura K. Study of fuel dilution in direct-injection and multipoint injection gasoline engines. 2002.

[256] Dresel W, others. Lubricants and lubrication. John Wiley & Sons; 2007.

[257] Tung SC, McMillan ML. Automotive tribology overview of current advances and challenges for the future. Tribol Int 2004;37:517–36. doi:10.1016/j.triboint.2004.01.013.

[258] Krpan H, Matanović I, Ljubas D. Influence of engine oils dilution by fuels on their viscosity, flash point and fire point. Nafta 2010;61:73–9.

[259] Amann M, Alger T. Lubricant Reactivity Effects on Gasoline Spark Ignition Engine Knock. SAE Int J Fuels Lubr 2012;5:760–71. doi:10.4271/2012-01-1140.

[260] Fan C, Tong S, Xu X, Li J, He XY, Deng J, et al. Characteristics of Lubricants on Auto-ignition under Controllable Active Thermo-Atmosphere. SAE Int J Fuels Lubr 2016;9:358–62. doi:10.4271/2016-01-0889.

[261] Kuti OA, Yang SY, Hourani N, Naser N, Roberts WL, Chung SH, et al. A fundamental investigation into the relationship between lubricant composition and fuel ignition quality. Fuel 2015;160:605–13. doi:10.1016/j.fuel.2015.08.026.

[262] Peters N, Paczko G, Pitsch H, Germany A. Wall Film Evaporation causing Pre-ignition in Turbocharged Gasoline Engines. 25th Int. Colloq. Dyn. Explos. React. Syst. Leeds, UK, 2015.

[263] Gohl M, Brandt S, Wittler M, Budde M, Knoll G, Krause S, et al. Influence of the mixture formation on the lubrication oil emission of combustion engines. SAE Int J Fuels Lubr 2010;3:733–44.

[264] Han L, Zhu T, Qiao H, Zhang D, Fu D, Zhang J. Investigation of Low-Speed Pre-Ignition in Boosted Spark Ignition Engine. SAE Tech Pap 2015;2015-April. doi:10.4271/2015-01-0751.

[265] Luo X, Teng H, Hu T, Miao R, Cao L. An Experimental Investigation on Low Speed Pre-Ignition in a Highly Boosted Gasoline Direct Injection Engine. SAE Int J Engines 2015;8:520–8. doi:10.4271/2015-01-0758.

[266] Swain MR, Blanco JA, Swain MN. Abnormal combustion in a methanol fueled engine. SAE Trans 1989:1311–9.

[267] Troyer D, Fitch JC. Oil analysis basics. Noria corporation; 2001.

[268] Li Y-P, Ping Y-S, Yin Q. Experimental study on preignition and megaknock in turbocharged DI gasoline engine. Neiranji Gongcheng(Chinese Intern Combust Engine Eng 2012;33:63–6.

[269] Chan EC, Evans RL, Davy MH, Cordiner S. Pre-ignition characterization of partially-stratified natural gas injection. 2007.

[270] Hamilton LJ, Rostedt MG, Caton PA, Cowart JS. Pre-ignition characteristics of ethanol and E85 in a spark ignition engine. SAE Int J Fuels Lubr 2009;1:145–54.

[271] Zheng J, Miller DL, Cernansky NP, Liu D, Zhang M. The Effect of Active Species in Internal EGR on Preignition Reactivity and on Reducing UHC and CO Emissions in Homogeneous Charge Engines. SAE Trans 2003:1246–54.

[272] Sasaki N, Nakata K. Effect of fuel components on engine abnormal combustion. 2012.

[273] WolAk A, ZAj\kac G. THE KINETICS OF CHANGES IN KINEMATIC VISCOSITY OF ENGINE OILS UNDER SIMILAR OPERATING CONDITIONS KINETYKA ZMIAN LEPKOŚCI KINEMATYCZNEJ OLEJÓW SILNIKOWYCH W WARUNKACH EKSPLOATACJI. Eksploat I Niezawodn 2017;19:260.

[274] Rahimi B, Semnani A, Nezamzadeh-Ejhieh A, Shakoori Langeroodi H, Hakim Davood M. Monitoring of the physical and chemical properties of a gasoline engine oil during its usage. J Anal Methods Chem 2012;1. doi:10.1155/2012/819524.

[275] Farng LO, Rudnick L. Ashless antiwear and extreme-pressure additives. Lubr Addit Chem Appl 2003:223–57.

[276] Santos JCO, Santos IMG, Souza AG. Thermal degradation of synthetic lubricating oils: Part II--Rheological study. Pet Sci Technol 2017;35:535–9.

[277] Santos JCO, Santos IMG, Souza AG. Thermal degradation process of synthetic lubricating oils: Part I—Spectroscopic study. Pet Sci Technol 2015;33:1238–45.

[278] Santos JCO, Oliveira AD, Silva CC, Silva JDS, Souza AG, Lima LN. Kinetic and activation thermodynamic parameters on thermal decomposition of synthetic lubricant oils. J Therm Anal Calorim 2007;87:823–9.

[279] Santos J, Lima L, Santos I, Souza A. Thermal, spectroscopic and rheological study of mineral base lubricating oils. J Therm Anal Calorim 2007;87:639–43.

[280] Bielmeier E, Camera F, Neveu CD. A new breed of viscosity index improvers. Croat. Soc. Fuels Lubr. Symp. Proceedings, Croat. Eng. Assoc. XXXVI Symp. Lubr., vol. 353, 2003, p. 13.

[281] Müller M, Fan J, Spikes H. Design of functionalized PAMA viscosity modifiers to reduce friction and wear in lubricating oils. Automot. Lubr. Test. Adv. Addit. Dev., ASTM International; 2008.

[282] Akhmedov AI. Copolymers of isobutylene and decyl methacrylate with various monomers as lube oil VI improvers. Chem Technol Fuels Oils 1987;23:147–51.

[283] Jukić A, Rogošić M, Vidović E. Thermal stability of lubricating oil additives based on styrene and n-alkyl methacrylate terpolymers. Polym Plast Technol Eng 2009;49:74–7.

[284] Stambaugh RL. Viscosity index improvers and thickeners. Chem. Technol. Lubr., Springer; 1994, p. 124–59.

[285] Verstrate G, Struglinski MJ. Polymers as lubricating-oil viscosity modifiers. ACS Symp. Ser., vol. 462, 1991, p. 256–72.

[286] Miura K, Shimizu K, Hayakawa N, Miyasaka T, Iijima A, Shoji H, et al. Influence of Ca-, Mg-and Na-based engine oil additives on abnormal combustion in a spark-ignition engine. SAE Int J Engines 2016;9:452–7.

[287] Andrews A, Burns R, Dougherty R, Deckman D, Patel M. Investigation of Engine Oil Base Stock Effects on Low Speed Pre-Ignition in a Turbocharged Direct Injection SI Engine. SAE Int J Fuels Lubr 2016;9. doi:10.4271/2016-01-9071.

[288] Kocsis MC, Briggs T, Anderson G. The Impact of Lubricant Volatility, Viscosity and Detergent Chemistry on Low Speed Pre-Ignition Behavior. SAE Int J Engines 2017;10. doi:10.4271/2017-01-0685.

[289] Spicher U, Gohl M, Magar M, Hadler J. The Role of Engine Oil in Low-speed Pre-ignition. MTZ Worldw 2016;77:60–3. doi:10.1007/s38313-015-0079-6.

[290] Tormos B, Garc\'\ia JM, Bastidas S, Dom\'\inguez B, Oliva F, Cárdenas D. Investigation on low-speed pre-ignition from the quantification and identification of engine oil droplets release under ambient pressure conditions. Measurement 2020:107961.

[291] Qian Y, Zhao P, Tao C, Meng S, Wei J, Cheng X. Experimental study on evaporation characteristics of lubricating oil/gasoline blended droplet. Exp Therm Fluid Sci 2019;103:99–107. doi:10.1016/j.expthermflusci.2019.01.010.

[292] Zhang Y, Huang R, Wang Z, Xu S, Huang S, Ma Y. Experimental study on puffing characteristics of biodiesel-butanol droplet. Fuel 2017;191:454–62.

[293] Zhang Y, Huang R, Huang Y, Huang S, Ma Y, Xu S, et al. Effect of ambient temperature on the puffing characteristics of single butanol-hexadecane droplet. Energy 2018;145:430–41.

[294] Ma X, Zhang F, Han K, Yang B, Song G. Evaporation characteristics of acetone--butanol--ethanol and diesel blends droplets at high ambient temperatures. Fuel 2015;160:43–9.

[295] Ma X, Zhang F, Han K, Song G. Numerical modeling of acetone--butanol--ethanol and diesel blends droplet evaporation process. Fuel 2016;174:206–15.

[296] Avulapati MM, Ganippa LC, Xia J, Megaritis A. Puffing and micro-explosion of diesel--biodiesel--ethanol blends. Fuel 2016;166:59–66.

[297] Hsieh W-D, Chen R-H, Chen C-W, Chiu S-L, Lin T-H. Micro-explosion of a water-in-hexadecane compound drop. J Chinese Inst Eng 2012;35:579–87.

[298] Basu S, Miglani A. Combustion and heat transfer characteristics of nanofluid fuel droplets: A short review. Int J Heat Mass Transf 2016;96:482–503.

[299] Wang FC-Y, Zhang L. Chemical composition of group II lubricant oil studied by high-resolution gas chromatography and comprehensive two-dimensional gas chromatography. Energy & Fuels 2007;21:3477–83.

[300] Haas FM, Won SH, Dryer FL, Pera C. Lube oil chemistry influences on autoignition as measured in an ignition quality tester. Proc Combust Inst 2019;37:4645–54. doi:10.1016/j.proci.2018.06.165.

[301] Dryer FL. Chemical kinetic and combustion characteristics of transportation fuels. Proc Combust Inst 2015;35:117–44.

[302] Kaneko T, Yamamori K, Suzuki H, Onodera K, Ogano S. Friction Reduction Technology for Low Viscosity Engine Oil Compatible with LSPI Prevention Performance. SAE Tech Pap 2016;2016-Octob. doi:10.4271/2016-01-2276.

[303] Liu H, Jin J, Li H, Yamamori K, Kaneko T, Yamashita M, et al. 0W-16 Fuel Economy Gasoline Engine Oil Compatible with Low Speed Pre-Ignition Performance. SAE Int J Fuels Lubr 2017;10:0–6. doi:10.4271/2017-01-2346.

[304] Onodera K, Kato T, Ogano S, Fujimoto K, Kato K, Kaneko T. Engine Oil Formulation Technology to Prevent Pre-ignition in Turbocharged Direct Injection Spark Ignition Engines. SAE Tech Pap 2015;2015-Septe. doi:10.4271/2015-01-2027.

[305] Fletcher KA, Dingwell L, Yang K, Lam WY, Styer JP. Engine Oil Additive Impacts on Low Speed Pre-Ignition. SAE Int J Fuels Lubr 2016;9:612–20. doi:10.4271/2016-01-2277.

[306] Komaba M, Kondo S, Suzuki A, Kurihara K, Mori S. Kinetic study on lubricity of MoDTC as a friction modifier. Tribol Online 2019;14:220–5.

[307] Huai W, Chen X, Lu F, Zhang C, Ma L, Wen S. Tribological properties of sulfur-and phosphorus-free organic molybdenum

compound as additive in oil. Tribol Int 2020;141:105944.

[308] Ratoi M, Niste VB, Alghawel H, Suen YF, Nelson K. The impact of organic friction modifiers on engine oil tribofilms. RSC Adv 2014;4:4278–85.

[309] Du D, Kim S-S, Moon W-S, Jin S-B, Kwon W-S. Oxidation performance of oils containing ZnDTC, ZnDDP and their mixture after oxidation test by PDSC. Thermochim Acta 2003;407:17–23.

[310] Dörr N, Brenner J, Ristić A, Ronai B, Besser C, Pejaković V, et al. Correlation between engine oil degradation, tribochemistry, and tribological behavior with focus on ZDDP deterioration. Tribol Lett 2019;67:1–17.

[311] Danilov AM, Bartko R V, Antonov SA. Current Advances in the Application and Development of Lubricating Oil Additives. Pet Chem 2020:1–8.

[312] Ishikawa M, Yamamori K, Hirano S, Kowalski T, Linden J. Introduction of Fuel Economy Engine Oil Performance Target with New SAE Viscosity Grade. SAE Int J Fuels Lubr 2016;9. doi:10.4271/2016-01-0896.

[313] Sagawa T, Okuda S, Takeuchi Y, Yamazaki T, Hidan S, Masuko M. Study on fuel-saving durability of ultra-low viscosity 0W-8 gasoline engine oil. 2021.

[314] Li Y, Liu T, Zhang Y, Zhang P, Zhang S. Study on the tribological behaviors of copper nanoparticles in three kinds of commercially available lubricants. Ind Lubr Tribol 2018.

[315] Tomala A, Ripoll MR, Gabler C, Remškar M, Kalin M. Interactions between MoS2 nanotubes and conventional additives in model oils. Tribol Int 2017;110:140–50.

[316] Tomala A, Ripoll MR, Kogovšek J, Kalin M, Bednarska A, Michalczewski R, et al. Synergisms and antagonisms between MoS2 nanotubes and representative oil additives under various contact conditions. Tribol Int 2019;129:137–50.

[317] Aldana PU, Dassenoy F, Vacher B, Le Mogne T, Thiebaut B. WS2 nanoparticles anti-wear and friction reducing properties on rough surfaces in the presence of ZDDP additive. Tribol Int 2016;102:213–21.

[318] Guo Z, Zhang Y, Wang J, Gao C, Zhang S, Zhang P, et al. Interactions of Cu nanoparticles with conventional lubricant additives on tribological performance and some physicochemical properties of an ester base oil. Tribol Int 2020;141:105941.

[319] Shu J, Harris K, Munavirov B, Westbroek R, Leckner J, Glavatskih S. Tribology of polypropylene and Li-complex greases with ZDDP and MoDTC additives. Tribol Int 2018;118:189–95.

[320] Khaemba DN, Neville A, Morina A. A methodology for Raman characterisation of MoDTC tribofilms and its application in investigating the influence of surface chemistry on friction performance of MoDTC lubricants. Tribol Lett 2015;59:1–17.

[321] Bouchet MIDB, Martin JM, Le Mogne T, Bilas P, Vacher B, Yamada Y. Mechanisms of MoS2 formation by MoDTC in presence of ZnDTP: effect of oxidative degradation. Wear 2005;258:1643–50.

[322] Kang F, Wang D, Pu Y, Zeng X-F, Wang J-X, Chen J-F. Efficient preparation of monodisperse CaCO3 nanoparticles as overbased nanodetergents in a high-gravity rotating packed bed reactor. Powder Technol 2018;325:405–11.

[323] Zhang D, Li Z, Wei X, Wang L, Xu J, Liu Y. Study tribological properties of MoDTC and its interactions with metal detergents. J Tribol 2020;142.

[324] Dörr N, Agocs A, Besser C, Ristić A, Frauscher M. Engine oils in the field: A comprehensive chemical assessment of engine oil degradation in a passenger car. Tribol Lett 2019;67:1–21.

[325] Morina A, Neville A. Understanding the composition and low friction tribofilm formation/removal in boundary lubrication. Tribol Int 2007;40:1696–704.

[326] Liu E, Kouame SD. An XPS study on the composition of zinc dialkyl dithiophosphate tribofilms and their effect on camshaft lobe wear. Tribol Trans 2014;57:18–27.

[327] McQueen JS, Gao H, Black ED, Gangopadhyay AK, Jensen RK. Friction and wear of tribofilms formed by zinc dialkyl dithiophosphate antiwear additive in low viscosity engine oils. Tribol Int 2005;38:289–97.

[328] Miklozic KT, Forbus TR, Spikes HA. Performance of friction modifiers on ZDDP-generated surfaces. Tribol Trans 2007;50:328–35.

[329] Grossiord C, Varlot K, Martin J-M, Le Mogne T, Esnouf C, Inoue K. MoS2 single sheet lubrication by molybdenum dithiocarbamate. Tribol Int 1998;31:737–43.

[330] Balarini R, Diniz GAS, Profito FJ, Souza RM. Comparison of unidirectional and reciprocating tribometers in tests with MoDTC-containing oils under boundary lubrication. Tribol Int 2020;149:105686.

[331] Okubo H, Yonehara M, Sasaki S. In situ Raman observations of the formation of MoDTC-derived tribofilms at steel/steel contact under boundary lubrication. Tribol Trans 2018;61:1040–7.

[332] De Feo M, Minfray C, Bouchet MIDB, Thiebaut B, Martin JM. MoDTC friction modifier additive degradation: Correlation between tribological performance and chemical changes. RSC Adv 2015;5:93786–96.

[333] Peeters S, Restuccia P, Loehlé S, Thiebaut B, Righi MC. Characterization of Molybdenum Dithiocarbamates by First-Principles Calculations. J Phys Chem A 2019;123:7007–15.

[334] Parsaeian P, Ghanbarzadeh A, Van Eijk MCP, Nedelcu I, Neville A, Morina A. A new insight into the interfacial mechanisms of the tribofilm formed by zinc dialkyl dithiophosphate. Appl Surf Sci 2017;403:472–86.

[335] Espejo C, Thiébaut B, Jarnias F, Wang C, Neville A, Morina A. MoDTC tribochemistry in steel/steel and steel/diamond-like-carbon systems lubricated with model lubricants and fully formulated engine oils. J Tribol 2019;141.

[336] Al-Jeboori Y, Kosarieh S, Morina A, Neville A. Investigation of pure sliding and sliding/rolling contacts in a DLC/Cast iron system when lubricated in oils containing MoDTC-Type friction modifier. Tribol Int 2018;122:23–37.

[337] Liu K, Kang J, Zhang G, Lu Z, Yue W. Effect of temperature and mating pair on tribological properties of DLC and GLC coatings under high pressure lubricated by MoDTC and ZDDP. Friction 2020:1–16.

[338] de Barros' Bouchet MI, Martin JM, Le-Mogne T, Vacher B. Boundary lubrication mechanisms of carbon coatings by MoDTC and ZDDP additives. Tribol Int 2005;38:257–64.

[339] Otsu T. Effect of phosphorus film on frictional properties of molybdenum dithiocarbamate. Proc Inst Mech Eng Part J J Eng Tribol 2018;232:369–79.

[340] YE J, KANO M, YASUDA Y. Friction properties of tribofilm formed from engine oil additives (Part 2): Frictional and mechanical properties in nm-scale and mechanisms of friction reduction. Japanese J Tribol 2003;48:69–81.

[341] Graham J, Spikes H, Korcek S. The friction reducing properties of molybdenum dialkyldithiocarbamate additives: part I—factors influencing friction reduction. Tribol Trans 2001;44:626–36.

[342] Graham J, Spikes H, Jensen R. The friction reducing properties of molybdenum dialkyldithiocarbamate additives: Part II-Durability of friction reducing capability. Tribol Trans 2001;44:637–47.

[343] Khaemba DN, Neville A, Morina A. New insights on the decomposition mechanism of Molybdenum DialkyldiThioCarbamate (MoDTC): a Raman spectroscopic study. RSC Adv 2016;6:38637–46.

[344] Parenago OP, Kuz'mina GN, Zaimovskaya TA. Sulfur-containing molybdenum compounds as high-performance lubricant additives. Pet Chem 2017;57:631–42.

[345] Yue W, Liu C, Fu Z, Wang C, Huang H, Liu J. Effects of molybdenum dithiocarbamate and zinc dialkyl dithiophosphate additives on tribological behaviors of hydrogenated diamond-like carbon coatings. Mater Des 2014;64:601–7.

[346] Kosarieh S, Morina A, Flemming J, Lainé E, Neville A. Wear mechanisms of hydrogenated DLC in oils containing MoDTC. Tribol Lett 2016;64:1–17.

[347] Okubo H, Tadokoro C, Sumi T, Tanaka N, Sasaki S. Wear acceleration mechanism of diamond-like carbon (DLC) films lubricated with MoDTC solution: Roles of tribofilm formation and structural transformation in wear acceleration of DLC films lubricated with MoDTC solution. Tribol Int 2019;133:271–87.

[348] De Feo M, Bouchet MIDB, Minfray C, Esnouf C, Le Mogne T, Meunier F, et al. Formation of interfacial molybdenum carbide for DLC lubricated by MoDTC: Origin of wear mechanism. Wear 2017;370:17–28.

[349] Yoshida Y, Kunitsugu S. Friction wear characteristics of diamond-like carbon coatings in oils containing molybdenum dialkyldithiocarbamate additive. Wear 2018;414:118–25.

[350] Morina A, Neville A, Priest M, Green JH. ZDDP and MoDTC interactions in boundary lubrication—the effect of temperature and ZDDP/MoDTC ratio. Tribol Int 2006;39:1545–57.

[351] Zhang J, Ewen JP, Ueda M, Wong JSS, Spikes HA. Mechanochemistry of zinc dialkyldithiophosphate on steel surfaces under elastohydrodynamic lubrication conditions. ACS Appl Mater Interfaces 2020;12:6662–76.

[352] Morina A, Neville A, Priest M, Green JH. ZDDP and MoDTC interactions and their effect on tribological performance--tribofilm characteristics and its evolution. Tribol Lett 2006;24:243–56.

[353] Lu R, Shiode S, Tani H, Tagawa N, Koganezawa S. A Study on the Tribofilm Growth and Tribological Properties of Tribofilms Formed from Zinc Dialkyl Dithiophosphate (ZDDP) and Molybdenum Dialkyl Dithiocarbamate (MoDTC). Tribol Online 2018;13:157–65.

[354] Muraki M, Wada H. Influence of the alkyl group of zinc dialkyldithiophosphate on the frictional characteristics of molybdenum dialkyldithiocarbamate under sliding conditions. Tribol Int 2002;35:857–63.

[355] Mittal P, Rai H, Gosvami NN. Microscopic Tribology of ADC12 Alloy Under Lubricant Containing ZDDP and MoDTC Using In Situ AFM. Tribol Lett 2021;69:1–10.

[356] Du D-C, Kim S-S, Chun J-S, Suh C-M, Kwon W-S. Antioxidation synergism between ZnDTC and ZnDDP in mineral oil. Tribol Lett 2002;13:21–7.

[357] Spikes H. Friction modifier additives. Tribol Lett 2015;60:1–26.

[358] Rai Y, Neville A, Morina A. Transient processes of MoS2 tribofilm formation under boundary lubrication. Lubr Sci 2016;28:449–71.

[359] Gorbatchev O, Bouchet MIDB, Martin JM, Léonard D, Le-Mogne T, Iovine R, et al. Friction reduction efficiency of organic Mo-containing FM additives associated to ZDDP for steel and carbon-based contacts. Tribol Int 2016;99:278–88.

[360] De Barros M-I, Bouchet J, Raoult I, Le Mogne T, Martin J-M, Kasrai M, et al. Friction reduction by metal sulfides in boundary lubrication studied by XPS and XANES analyses. Wear 2003;254:863–70.

[361] Masuko M, Ohkido T, Suzuki A, Ueno T. Fundamental study of changes in friction and wear characteristics due to ZnDTP deterioration in simulating engine oil degradation during use. Tribol. Ser., vol. 43, Elsevier; 2003, p. 359–66.

[362] Ritchie A, Boese D, Young AW. Controlling Low-Speed Pre-Ignition in Modern Automotive Equipment Part 3: Identification of Key Additive Component Types and Other Lubricant Composition Effects on Low-Speed Pre-Ignition. SAE Int J Engines 2016;9:832–40. doi:10.4271/2016-01-0717.

[363] Elliott I, Sztenderowicz M, Sinha K, Takeuchi Y, Ushioda N. Understanding Low Speed Pre-Ignition Phenomena across Turbo-Charged GDI Engines and Impact on Future Engine Oil Design. SAE Tech Pap 2015;2015-Septe. doi:10.4271/2015-01-2028.

[364] Morikawa K, Moriyoshi Y, Kuboyama T, Yamada T, Suzuki M. Investigation of Lubricating Oil Properties Effect on Low Speed Pre-Ignition. SAE Tech Pap 2015;2015-Septe. doi:10.4271/2015-01-1870.

[365] Pan K, Deng J, Chen Y, Zhang E, Xie W, Qin Q, et al. Auto-ignition Characteristics of Lubricant Droplets under Hot Co-Flow Atmosphere. SAE Tech Pap 2018;2018-Septe:1–8. doi:10.4271/2018-01-1807.

[366] He Y, Liu Z, Stahl I, Zhang G, Zheng Y. Comparison of Stochastic Pre-Ignition Behaviors on a Turbocharged Gasoline Engine with Various Fuels and Lubricants. SAE Tech Pap 2016;2016-Octob. doi:10.4271/2016-01-2291.

[367] Cen H, Morina A, Neville A. Effect of lubricant ageing on lubricants' physical and chemical properties and tribological performance; Part I: effect of lubricant chemistry. Ind Lubr Tribol 2018;70:385–92.

[368] Mayer M, Hofmann P, Williams J, Tong D. Influence of the Engine Oil on Pre-ignitions at Highly Supercharged Direct-injection Gasoline Engines. MTZ Worldw 2016;77:36–41. doi:10.1007/s38313-016-0044-z.

[369] Bodek KM, Wong V V. The effects of sulfated ash, phosphorus and sulfur on diesel aftertreatment systems-a review 2007.

[370] Spikes H. Low-and zero-sulphated ash, phosphorus and sulphur anti-wear additives for engine oils. Lubr Sci 2008;20:103–36.

[371] Li J, Theis J, Chun W, Goralski C, Kudla R, Ura J, et al. Sulfur poisoning and desulfation of the lean NOx trap. 2001.

[372] Asanuma T, Hirota S, Yanaka M, Tsukasaki Y, Tanaka T. Effect of sulfur-free and aromatics-free diesel fuel on vehicle exhaust emissions using simultaneous PM and NOx reduction system. SAE Trans 2003:1448–55.

[373] Rastogi RB, Maurya JL, Jaiswal V. Low sulfur, phosphorus and metal free antiwear additives: synergistic action of salicylaldehyde N (4)-phenylthiosemicarbazones and its different derivatives with Vanlube 289 additive. Wear 2013;297:849–59.

[374] Martin J-M, Grossiord C, Varlot K, Vacher B, Le Mogne T, Yamada Y. Friction-induced two-dimensional solid films from lubricant additives. Lubr Sci 2003;15:119–32.

[375] Gupta A, Devlin M. Impact of Engine Oil Detergent on Low Speed Pre-Ignition (LSPI) and Fuel Economy Performance. 2020.

[376] Nomura T, Ueura H, Tanaka Y, Iida Y, Yuan Z, Ando A. The Effect of Gasoline Metallic Additives on Low Speed Pre-Ignition. SAE Tech Pap 2018;2018-April:1–7. doi:10.4271/2018-01-0936.

[377] Elliott I, Cherpeck R, Maria A, Gunawan T. Alternative Engine Oil Formulating Solutions to Reduce Low Speed Pre-Ignition. 2019.

[378] Andrae JCG, Head RA. HCCI experiments with gasoline surrogate fuels modeled by a semidetailed chemical kinetic model. Combust Flame 2009;156:842–51.

[379] Ahmed SS, Moréac G, Zeuch T, Mauß F. Reduced Mechanism for the Oxidation of the Mixtures of n-Heptane and iso-Octane. Proc. Eur. Combust. Meet. Louvain-la-Neuve, Belgium, 2005, p. 3–6.

[380] Poling BE, Prausnitz JM, O'connell JP. Properties of gases and liquids. McGraw-Hill Education; 2001.

[381] Tsurushima T. A new skeletal PRF kinetic model for HCCI combustion. Proc Combust Inst 2009;32:2835–41.

[382] Zhang H, Law CK. Effects of temporally varying liquid-phase mass diffusivity in multicomponent droplet gasification. Combust Flame 2008;153:593–602.

[383] Muharam Y, Warnatz J. Kinetic modelling of the oxidation of large aliphatic hydrocarbons using an automatic mechanism generation. Phys Chem Chem Phys 2007;9:4218–29.

[384] Wang H, Yao M, Reitz RD. Development of a reduced primary reference fuel mechanism for internal combustion engine combustion simulations. Energy & Fuels 2013;27:7843–53.

[385] Ra Y, Reitz RD. A reduced chemical kinetic model for IC engine combustion simulations with primary reference fuels. Combust Flame 2008;155:713–38.

[386] Liu Y-D, Jia M, Xie M-Z, Pang B. Development of a new skeletal chemical kinetic model of toluene reference fuel with application to gasoline surrogate fuels for computational fluid dynamics engine simulation. Energy & Fuels 2013;27:4899–909.

[387] Pal P, Wu Y, Lu T, Som S, See YC, Le Moine A. Multidimensional numerical simulations of knocking combustion in a cooperative fuel research engine. J Energy Resour Technol Trans ASME 2018;140:1–8. doi:10.1115/1.4040063.

[388] Mubarak Ali MJ, Hernandez Perez F, Sow A, Im H. A Computational Study of Abnormal Combustion Characteristics in Spark Ignition Engines. SAE Tech Pap 2018;2018-April:1–11. doi:10.4271/2018-01-0179.

[389] Liu Y-D, Jia M, Xie M-Z, Pang B. Enhancement on a skeletal kinetic model for primary reference fuel oxidation by using a semidecoupling methodology. Energy & Fuels 2012;26:7069–83.

[390] Kawanabe H, Ishiyama T. A Study on a Reduced Kinetic Model for n-Cetane and Heptamethylnonane Based on a PRF Reduced Kinetic Model. 2012.

[391] Ullal A, Ra Y, Naber JD, Atkinson W, Yamada S, Oda Y, et al. Numerical investigation of oil droplet combustion using single particle ignition cell model. Int J Engine Res 2020. doi:10.1177/1468087419896939.

[392] Ra Y, Reitz RD. A combustion model for multi-component fuels using a physical surrogate group chemistry representation (PSGCR). Combust Flame 2015;162:3456–81.

[393] Amirante R, Distaso E, Tamburrano P, Reitz RD. Laminar Flame Speed Correlations for Methane, Ethane, Propane and their Mixtures, and Natural Gas and Gasoline for Spark-Ignition Engine Simulations. Int J Engine Res 2017;18:951–70.

[394] Amirante R, Distaso E, Tamburrano P, Reitz RD. Analytical correlations for modeling the laminar flame speed of natural gas surrogate mixtures. Energy Procedia 2017;126:850–7.

[395] Teodosio L, Bozza F, Tufano D, Giannattasio P, Distaso E, Amirante R. Impact of the laminar flame speed correlation on the results of a quasi-dimensional combustion model for Spark-Ignition engine. Energy Procedia 2018;148:631–8.

[396] Wang Z, Qi Y, He X, Wang J, Shuai S, Law CK. Analysis of pre-ignition to super-knock: Hotspot-induced deflagration to detonation. Fuel 2015;144:222–7.

[397] Qi Y, Wang Z, Wang J, He X. Effects of thermodynamic conditions on the end gas combustion mode associated with engine knock. Combust Flame 2015;162:4119–28.

[398] Zhang P, Ji W, He T, He X, Wang Z, Yang B, et al. First-stage ignition delay in the negative temperature coefficient behavior: Experiment and simulation. Combust Flame 2016;167:14–23.

[399] Di H, He X, Zhang P, Wang Z, Wooldridge MS, Law CK, et al. Effects of buffer gas composition on low temperature ignition of iso-octane and n-heptane. Combust Flame 2014;161:2531–8.

[400] Wang Z, Qi Y, Liu H, Zhang P, He X, Wang J. Shock wave reflection induced detonation (SWRID) under high pressure and temperature condition in closed cylinder. Shock Waves 2016;26:687–91.

[401] Winklhofer E, Hirsch A, Kapus P, Kortschak M, Philipp H. TC GDI engines at very high power density—irregular combustion and thermal risk. 2009.

[402] Chapman E, Davis R, Studzinski W, Geng P. Fuel octane and volatility effects on the stochastic pre-ignition behavior of a 2.0 L gasoline turbocharged DI engine. SAE Int J Fuels Lubr 2014;7:379–89.

[403] Amann M, Mehta D, Alger T. Engine operating condition and gasoline fuel composition effects on low-speed pre-ignition in high-performance spark ignited gasoline engines. SAE Int J Engines 2011;4:274–85.

[404] Palaveev S, Magar M, Kubach H, Schiessl R, Spicher U, Maas U. Premature flame initiation in a turbocharged DISI engine-numerical and experimental investigations. SAE Int J Engines 2013;6:54–66.

[405] Bhurat SS, Pandey S, Chintala V, Ranjit PS. Technical barriers and their solutions for deployment of HCCI engine technologies--a review. Int J Ambient Energy 2019:1–14.

[406] Kalghatgi GT. Auto-ignition quality of practical fuels and implications for fuel requirements of future SI and HCCI engines. SAE Tech Pap 2005-01-0239 2005.

[407] Shibata G, Oyama K, Urushihara T, Nakano T. The effect of fuel properties on low and high temperature heat release and resulting performance of an HCCI engine. SAE Tech Pap 2004-01-0553 2004.

[408] Bunce M, Bunting BG, Wang J, Crawford R. Experimental and statistical comparison of engine response as a function of fuel chemistry and properties in CI and HCCI engines. SAE Tech Pap 2012-01-0857 2012.

[409] Griffiths JF, Whitaker BJ. Thermokinetic interactions leading to knock during homogeneous charge compression ignition. Combust Flame 2002;131:386–99.

[410] Andreae MM, Cheng WK, Kenney T, Yang J. On HCCI engine knock. SAE Trans 2007:355–63.

[411] Maurya RK, Saxena MR. Characterization of ringing intensity in a hydrogen-fueled HCCI engine. Int J Hydrogen Energy 2018;43:9423–37.

[412] Manofsky L, Vavra J, Assanis DN, Babajimopoulos A. Bridging the gap between HCCI and SI: Spark-assisted compression ignition. SAE Tech Pap 2011-01-1179 2011.

[413] Wang Z, He X, Wang J-X, Shuai S, Xu F, Yang D. Combustion visualization and experimental study on spark induced compression ignition (SICI) in gasoline HCCI engines. Energy Convers Manag 2010;51:908–17.

[414] Chemkin-Pro A. 17.2. ANSYS React Des San Diego 2016.

[415] Westbrook CK, Pitz WJ, Herbinet O, Curran HJ, Silke EJ. A comprehensive detailed chemical kinetic reaction mechanism for combustion of n-alkane hydrocarbons from n-octane to n-hexadecane. Combust Flame 2009;156:181–99.

[416] Sarathy SM, Westbrook CK, Mehl M, Pitz WJ, Togbe C, Dagaut P, et al. Comprehensive chemical kinetic modeling of the oxidation of 2-methylalkanes from C 7 to C 20. Combust Flame 2011;158:2338–57.

[417] Fieweger K, Blumenthal R, Adomeit G. Self-ignition of SI engine model fuels: a shock tube investigation at high pressure. Combust Flame 1997;109:599–619.

[418] Silke EJ, Curran HJ, Simmie JM. The influence of fuel structure on combustion as demonstrated by the isomers of heptane: a rapid compression machine study. Proc Combust Inst 2005;30:2639–47.

[419] Distaso E, Amirante R, Calò G, De Palma P, Tamburrano P, Reitz RD. Investigation of Lubricant Oil influence on Ignition of Gasoline-like Fuels by a Detailed Reaction Mechanism. Energy Procedia 2018;148:663–70.

[420] CHEMKIN-PRO 15112, San Diego: Reaction Design; 2012. n.d.

[421] An J, Jiang Y. Differences between direct relation graph and error-propagation-based reduction methods for large hydrocarbons. Procedia Eng 2013;62:342–9.

[422] Han Z, Reitz RD. Turbulence modeling of internal combustion engines using RNG κ-ε models. Combust Sci Technol 1995;106:267–95.

[423] Richards KJ, Senecal PK, Pomraning E. CONVERGE Manual (Version 2.3). Converg Sci Inc, Madison, WI-USA 2016.

[424] Senecal PK, Pomraning E, Richards KJ, Som S. Grid-convergent spray models for internal combustion engine computational fluid dynamics simulations. J Energy Resour Technol 2014;136:12204.

[425] Reitz RD, Diwakar R. Effect of drop breakup on fuel sprays. SAE Trans 1986:218–27.

[426] Reitz RD, Diwakar R. Structure of high-pressure fuel sprays. SAE Trans 1987:492–509.

[427] Senecal PK, Richards KJ, Pomraning E, Yang T, Dai MZ, McDavid RM, et al. A new parallel cut-cell Cartesian CFD code for rapid grid generation applied to in-cylinder diesel engine simulations. SAE Tech Pap 2007-01-0159 2007.

[428] Reitz RD, Beale JC. Modeling Spray Atomization With the Kelvin-Helmholtz/Rayleigh-Taylor Hybrid Model. At Sprays 2014;9:623–50. doi:10.1615/atomizspr.v9.i6.40.

[429] Amsden AA, O'rourke PJ, Butler TD. KIVA-II: A computer program for chemically reactive flows with sprays. Los Alamos Natl Lab, NM 1989.

[430] O'Rourke PJ, Amsden AA. A spray/wall interaction submodel for the KIVA-3 wall film model. SAE Trans 2000:281–98.

[431] O'Rourke PJ. Collective drop effects on vaporizing liquid sprays. Tech Rep 1981;LA-9069-T.

[432] Schmidt DP, Rutland CJ. A new droplet collision algorithm. J Comput Phys 2000;164:62–80.

[433] Manuel A, Gonzalez D, Borman GL, Reitz RD. A Study of Diesel Cold Starting using both Cycle Analysis and Multidimensional Calculations. SAE Tech Pap Ser 2010;1. doi:10.4271/910180.

[434] Babajimopoulos A, Assanis DN, Flowers DL, Aceves SM, Hessel RP. A fully coupled computational fluid dynamics and multi-zone model with detailed chemical kinetics for the simulation of premixed charge compression ignition engines. Int J Engine Res 2005;6:497–512.

[435] Raju M, Wang M, Dai M, Piggott W, Flowers D. Acceleration of detailed chemical kinetics using multi-zone modeling for CFD in internal combustion engine simulations. SAE Tech Pap 2012-01-0135 2012.

[436] Jaasim M, Elhagrasy A, Sarathy M, Chung SH, Im HG. Auto-ignition and Spray Characteristics of n-heptane and iso-octane Fuels in Ignition Quality Tester 2018.

[437] Bogin G, Dean AM, Ratcliff MA, Luecke J, Zigler BT. Expanding the experimental capabilities of the ignition quality tester for autoigniting fuels. SAE Int J Fuels Lubr 2010;3:353–67.

[438] Sim J, Badra J, Elwardani AE, Im HG. Spray modeling for outwardly-opening hollow-cone injector 2016.

[439] Ribaucour M, Minetti R, Sochet LR, Curran HJ, Pitz WJ, Westbrook CK. Ignition of isomers of pentane: an experimental and kinetic modeling study. Proc Combust Inst 2000;28:1671–8.

[440] Buda F, Bounaceur R, Warth V, Glaude P-A, Fournet R, Battin-Leclerc F. Progress toward a unified detailed kinetic model for the autoignition of alkanes from C4 to C10 between 600 and 1200 K. Combust Flame 2005;142:170–86.

[441] Healy D, Donato NS, Aul CJ, Petersen EL, Zinner CM, Bourque G, et al. Isobutane ignition delay time measurements at high pressure and detailed chemical kinetic simulations. Combust Flame 2010;157:1540–51.

[442] Tingas E-A, Wang Z, Sarathy SM, Im HG, Goussis DA. Chemical kinetic insights into the ignition dynamics of n-hexane. Combust Flame 2018;188:28–40.

[443] Szybist JP, Splitter DA. Pressure and temperature effects on fuels with varying octane sensitivity at high load in SI engines. Combust Flame 2017;177:49–66.

[444] Hwang W, Dec J, Sjöberg M. Spectroscopic and chemical-kinetic analysis of the phases of HCCI autoignition and combustion for single-and two-stage ignition fuels. Combust Flame 2008;154:387–409.

[445] Cai L, Pitsch H. Optimized chemical mechanism for combustion of gasoline surrogate fuels. Combust Flame 2015;162:1623–37.

[446] Sarathy SM, Tingas E-A, Nasir EF, Detogni A, Wang Z, Farooq A, et al. Three-stage heat release in n-heptane auto-ignition. Proc Combust Inst 2019;37:485–92.

[447] Yamamoto A, Oshibe H, Nakamura H, Tezuka T, Hasegawa S, Maruta K. Stabilized three-stage oxidation of gaseous n-heptane/air mixture in a micro flow reactor with a controlled temperature profile. Proc Combust Inst 2011;33:3259–66.

[448] Distaso E, Amirante R, Calò G, De Palma P, Tamburrano P, Reitz RD. Predicting Lubricant Oil Induced Pre-Ignition Phenomena in Modern Gasoline Engines: the Reduced GasLube Reaction Mechanism. Fuel 2020;281:118709.

[449] Bogin GE, DeFilippo A, Chen JY, Chin G, Luecke J, Ratcliff MA, et al. Numerical and experimental investigation of n-heptane autoignition in the ignition quality tester (IQT). Energy and Fuels 2011;25:5562–72. doi:10.1021/ef201079g.

[450] Yang SY, Naser N, Chung SH, Cha J. Effect of Temperature, Pressure and Equivalence Ratio on Ignition Delay in Ignition Quality Tester (IQT) Diesel, n-Heptane, and iso-Octane Fuels under Low Temperature Conditions. SAE Int J Fuels Lubr 2015;8:537–48.

[451] Yuan Y. Trust region algorithms for nonlinear equations. Hong Kong Baptist University, Department of Mathematics; 1994.

[452] Taylor JD. Fuels Performance Technologies: Milestone FY06 9.1--Using IQT measurements, develop simplified kinetic expressions for ignition of fuels that could be used in HCCI engine models. 2006.

[453] Lyn WT, Valdmanis E. The effects of physical factors on ignition delay. 1968.

[454] Rosseel E, Sierens R. The physical and the chemical part of the ignition delay in diesel engines. 1996.

[455] Bogin Jr GE, Osecky E, Chen JY, Ratcliff MA, Luecke J, Zigler BT, et al. Experiments and computational fluid dynamics modeling analysis of large n-alkane ignition kinetics in the ignition quality tester. Energy & Fuels 2014;28:4781–94.

[456] Hourani N, Muller H, Adam FM, Panda SK, Witt M, Al-Hajji AA, et al. Structural level characterization of base oils using advanced analytical techniques. Energy & Fuels 2015;29:2962–70.

[457] Touchard S, Fournet R, Glaude P-A, Warth V, Battin-Leclerc F, Vanhove G, et al. Modeling of the oxidation of large alkenes at low temperature. Proc Combust Inst 2005;30:1073–81.

[458] Wang C, Zhang B, Tao C, Wei J, Wang C, Zhou T, et al. Auto-ignition and Detonation Induced by Density Gradient of Surrogate Lubricant under Boosted-Gasoline-Engine-Like Condition. SAE Int J Engines 2021;14.

[459] Li Y, Gao W, Zhang P, Fu Z, Cao X. Influence of the equivalence ratio on the knock and performance of a hydrogen direct injection internal combustion engine under different compression ratios. Int J Hydrogen Energy 2021;46:11982–93.

[460] Distaso E, Amirante R, Cal G, Palma P De, Tamburrano P. Lubricant-Oil-Induced Pre-ignition Phenomena in Modern Gasoline Engines: Using Experimental Data and Numerical Chemistry to Develop a Practical Correlation. SAE Tech Pap 2021-24-0052 2021. doi:10.4271/2021-24-0052.Abstract.

[461] Miller AL, Stipe CB, Habjan MC, Ahlstrand GG. Role of lubrication oil in particulate emissions from a hydrogen-powered internal combustion engine. Environ Sci Technol 2007;41:6828–35. doi:10.1021/es070999r.

[462] Zheng Z, Badawy T, Henein N, Sattler E. Investigation of physical and chemical delay periods of different fuels in the ignition quality tester. J Eng Gas Turbines Power 2013;135.

[463] Jayakumar C, Zheng Z, Joshi UM, Bryzik W, Henein NA, Sattler E. Effect of inlet air temperature on auto-ignition of fuels with different Cetane number and volatility. ASME 2011 Intern. Combust. Engine Div. Fall Tech. Conf., 2011, p. 261–72.